



# Physical principles of brain–computer interfaces and their applications for rehabilitation, robotics and control of human brain states



Alexander E. Hramov <sup>a,b,c</sup>, Vladimir A. Maksimenko <sup>a,c</sup>,  
Alexander N. Pisarchik <sup>a,d,\*</sup>

<sup>a</sup> Laboratory of Neuroscience and Cognitive Technology, Innopolis University, Universitetskaya Str. 1, 420500 Innopolis, Republic of Tatarstan, Russia

<sup>b</sup> Immanuel Kant Baltic Federal University, A. Nevskogo Str. 14, 236016 Kaliningrad, Russia

<sup>c</sup> Saratov State Medical University, Bolshaya Kazachia Str. 112, 410012 Saratov, Russia

<sup>d</sup> Center for Biomedical Technology, Universidad Politécnica de Madrid, Campus Montegancedo, 28223 Pozuelo de Alarcón, Spain

## ARTICLE INFO

### Article history:

Received 3 May 2019

Received in revised form 15 January 2021

Accepted 10 March 2021

Available online 24 March 2021

Editor: D.K. Campbell

### Keywords:

Brain–computer interface

Artificial intelligence

Biological feedback

EEG analysis

MEG analysis

Classification techniques

Wavelets

Brain dynamics

## ABSTRACT

Brain–computer interfaces (BCIs) development is closely related to physics. In this paper, we review the physical principles of BCIs, and underlying novel approaches for registration, analysis, and control of brain activity. We analyze recent advances in BCI studies focusing on their applications for (i) controlling the movement of robots and exoskeletons, (ii) revealing and preventing brain pathologies, (iii) assessing and controlling psychophysiological states, and (iv) monitoring and controlling normal and pathological cognitive activity.

We consider the BCI as a hardware/software communication system that allows interaction of humans or animals with their surroundings without the involvement of peripheral nerves and muscles, using control signals generated from brain cerebral activity. Classifying BCIs into three main types (active, reactive and passive), we describe their functional models and neuroimaging methods, as well as novel techniques for signal enhancement and artifact recognition and avoidance, to improve BCI performance in real time. We also review different BCI applications, including communications, external device control, movement control, neuroprostheses, and assessment of human psychophysiological states.

Then, we describe the most common techniques for the analysis and classification of electroencephalographic (EEG) and magnetoencephalographic (MEG) data. Special attention is paid to modern technology based on machine learning and reservoir computing. We discuss main results on the creation and application of BCIs based on invasive and noninvasive EEG recordings. First, we consider neurointerfaces for controlling the movement of robots and exoskeletons. Second, we describe BCIs for diagnosis and control of pathological brain activity, in particular, epilepsy. We also discuss the results on the development of invasive BCIs for predicting and mitigating absence epileptic seizures. After that, we focus on passive neurointerfaces for assessing and controlling a person's psychophysiological states and cognitive activity. Special attention is given to optogenetic brain interfaces using photostimulation to deliver intervention to specific

\* Corresponding author at: Center for Biomedical Technology, Universidad Politécnica de Madrid, Campus Montegancedo, 28223 Pozuelo de Alarcón, Spain.

E-mail address: [alexander.pisarchik@ctb.upm.es](mailto:alexander.pisarchik@ctb.upm.es) (A.N. Pisarchik).

cell types. We outline the basic principles of optogenetic neurocontrol and extracellular electrophysiology recording. We also describe the state-of-the-art of miniaturized closed-loop optogenetic devices to control normal and pathological brain activities.

Further, we discuss the new emerging technological trend in the BCI development which consists in using neurointerfaces to improve the interaction between people, so-called brain-to-brain interfaces (BBIs). Such interfaces can increase the efficiency of collaborative processes when working in a group. We propose a BBI which distributes a cognitive load among all team members working on a common task. This BBI allows sharing the workload among the participants according to their current cognitive performance, estimated from their electrical brain activity. The novel results of the brain-to-brain interaction are promising for the development of a new generation of communication systems based on the neurophysiological brain activity of interacting persons, where the BBI estimates physical conditions of each partner and adapts the assigned task accordingly.

Finally, we trace the main historical epochs in BCI development and applications and highlight possible future directions for this research area, including hybrid BCIs.

© 2021 Elsevier B.V. All rights reserved.

## Contents

1. Introduction.....	3
2. Neural interfaces overview .....	8
2.1. Classification of brain-computer interfaces .....	8
2.1.1. Control command based classification .....	8
2.1.2. Input data processing modality based classification .....	8
2.1.3. Invasive and noninvasive brain-computer interfaces and brain-machine interfaces.....	9
2.2. Neuroimaging methods for brain-computer interfaces.....	9
2.2.1. Electrocorticography .....	9
2.2.2. Electroencephalography.....	9
2.2.3. Cerebral cortical registration of neural activity.....	11
2.2.4. Magnetoencephalography .....	12
2.2.5. Functional magnetic resonance imaging .....	14
2.2.6. Functional near-infrared spectroscopy .....	14
2.3. Functional models of neurointerfaces .....	15
2.3.1. Active brain-computer interfaces .....	15
2.3.2. Reactive brain-computer interfaces.....	17
2.3.3. Passive brain-computer interfaces.....	17
2.4. Brain-computer interfaces applications.....	19
2.4.1. Communication .....	20
2.4.2. Assistive technologies.....	22
2.4.3. Movements.....	23
2.4.4. Neuroprosthetics .....	23
2.4.5. Neurorehabilitation .....	24
2.4.6. Assessment of human conditions using passive brain-computer interfaces.....	24
3. EEG preprocessing methods for brain-computer interfaces .....	25
3.1. Independent component analysis and its modifications .....	25
3.2. Removing artifacts using Gram-Schmidt transformation.....	29
3.3. Removing artifacts using empirical mode decomposition.....	29
4. Brain activity pattern recognition and classification in multichannel data .....	31
4.1. Brain activity patterns for control commands .....	32
4.1.1. Slow cortical potential.....	33
4.1.2. Event-related potential .....	33
4.1.3. Multiscale brain activity .....	37
4.1.4. Functional brain connectivity .....	39
4.2. Brain-computer interface as a system for real-time pattern recognition .....	40
4.2.1. Features extraction and selection .....	41
4.2.2. Nonstationary and multiscale features of brain activity .....	42
4.3. Time-frequency and spatial-temporal feature extraction.....	43
4.3.1. Common spatial pattern.....	44
4.3.2. Wavelet-based skeleton method .....	44
4.3.3. Wavelet-based coherence measure .....	48
4.4. Pattern recognition and classification approaches .....	50
4.4.1. Linear discriminant analysis .....	50

4.4.2.	Bayesian classification .....	51
4.4.3.	Cluster analysis.....	51
4.4.4.	Support vector machine .....	52
4.4.5.	Combinations of classification techniques .....	52
4.4.6.	Linear regression .....	53
4.5.	Machine learning and reservoir computing .....	54
4.5.1.	Basics strategies of machine learning application .....	54
4.5.2.	Deep learning.....	55
4.5.3.	From supervised to unsupervised strategies in BCI research .....	60
4.5.4.	Machine learning for physics .....	62
4.5.5.	Optimization techniques for machine learning .....	68
5.	Brain–computer interfaces for controlling exoskeletons and robots .....	70
5.1.	Invasive brain–computer interfaces for controlling limb movements .....	70
5.1.1.	Upper limb control.....	70
5.1.2.	Lower limb control .....	72
5.2.	Noninvasive brain–computer interfaces for controlling limb movements .....	74
5.2.1.	Upper limb control.....	74
5.2.2.	Lower limb control .....	76
5.2.3.	Brain–computer interfaces for untrained subjects .....	77
6.	Prediction and prevention of epileptic seizures .....	79
6.1.	Open-loop interfaces for brain stimulation .....	79
6.2.	Closed-loop devices for seizure detection and suppression .....	79
6.3.	Seizure prediction and prevention .....	80
6.4.	Current state and further direction .....	82
7.	Brain–computer interfaces for evaluation and control of cognitive states .....	83
7.1.	Monitoring of cognitive states: alertness and drowsiness .....	83
7.2.	Workload and mental fatigue detection .....	89
7.3.	Emotions recognition .....	91
8.	Optogenetic brain interfaces .....	92
8.1.	Basic principles .....	92
8.2.	Open-loop and closed-loop optogenetic interfaces .....	93
8.3.	Approaches for hybrid optoelectronic interfaces .....	98
8.4.	On-probe $\mu$ LED-based approaches .....	99
8.5.	From rodents to primates .....	99
9.	Brain-to-brain interfaces .....	101
9.1.	Brain-to-brain interfaces for animal–animal interaction .....	101
9.2.	Brain-to-brain interfaces for human-to-human interaction .....	102
9.3.	Brain-to-brain interfaces for human-animal interaction .....	104
9.4.	Brain-to-brain interfaces for increasing human cognitive performance .....	105
10.	Brain–computer interface from past to future .....	106
	Declaration of competing interest .....	111
	Acknowledgments .....	111
	References .....	112

## 1. Introduction

A brain–computer interface (BCI), or a brain–machine interface (BMI), or simply a neural interface is a hardware–software complex (HSC) for functional interconnection between a biological object and a machine, i.e., for direct connection of computing or other digital intelligent control systems with the brain. Unlike traditional control devices, such as keyboards, mice, joysticks, etc., which interact with computing systems, the BCI records brain activity in various areas and translates these signals into commands for controlling an external digital device. BCI is one of the most rapidly progressing topics in various fields of science and technology, including engineering, physics, neuroscience, medicine, hightech industries, communications, robotics, and defense complexes [1–8]. Moreover, BCI is of special interest for rehabilitation and improvement of the quality of life of people with disabilities [9–14]. The BCI applications include, but not limited to,

- diagnostics and control of brain pathological activity and neurodegenerative diseases;
- rehabilitation of people after brain damage, for example, restoration of motor skills after a stroke;
- analysis and training of human resistance to specific stress effects;
- improvement of self-control and psycho-physiological state quality;
- control of robotic devices, including exoskeletons, to increase human capabilities;
- provide social interactions by allowing social applications to accurately assess and convey person's emotions;

## List of acronyms

AA	Adaptive automation
AAV5	Adeno-associated virus type 5
ABSI	Asynchronous brain-computer interface
ALS	Amyotrophic lateral sclerosis
AN	Anterior nucleus
ANN	Artificial neuronal network
ANOVA	Analysis of variance
AR	Autoregressive
ARTMAP	Adaptive resonance theory map
asSWLDA	Automatic stop step-wise linear discriminant analysis
ATM	Air traffic management
AUC	Area under curve
BBI	Brain-to-brain interface
BC	Brain-computer
BCI	Brain-computer interface
BMI	Brain-machine interface
BWS	Body weight support
CB	Computer-brain
CCR	Cerebral cortical registration
CEC	Constant error carousel
CNN	Convolutional neural network
CNS	Central nervous system
CS	Comprehensive sensing
CSP	Common spatial pattern
CSSP	Common spatio-spectral pattern
CSSSP	Common sparse spectral spatial pattern
CWT	Continuous wavelet transform
DL	Deep learning
DPFC	Dorsolateral prefrontal cortex
DVA	Degree of visual attention
ECG	Electrocardiograms
ECoG	Electrocorticogram
EEG	Electroencephalogram
EES	Epidural electric stimulation
EMD	Empirical mode decomposition
EMG	Electromyography
EOG	Electrooculogram
EP	Evoked potential
ERD	Event-related desynchronization
ERP	Event-related potentials
ErrP	Error potential
ERS	Event-related synchronization
ESS	Epidural electrical stimulation
FBC	Functional brain connectivity
FCBF	Fast correlation-based filter
FES	Functional electrical stimulation
FIR	Finite impulse response
FIRNN	Finite impulse response neural network
FF	Feed-forward
FFT	Fast Fourier transform
fMRI	Functional magnetic resonance imaging

fNIRS	Functional near infrared spectroscopy
FUS	Focused ultrasound
GA	Genetic algorithm
GF	Guidance force
GoF	Goodness-of-Fit
GRAM	Gradient model
GS	Generalized synchronization
GST	Gram–Schmidt transformation
HBCI	Hybrid BCI
HCT	High complexity task
HMM	Hidden Markov model
HSC	Hardware–software complex
IBK	Imagined body kinematics
IC	Integrated circuit
ICA	Independent component analysis
ICMS	Intracortical microstimulation
IIR	Infinite impulse response
ILED	Inorganic light-emitting diode
ITO	Indium tin oxide
KI	Kinesthetic imagination
k-NN	$k$ -nearest neighbors
KSE	Kuramoto–Sivashinsky equation
LCT	Low complexity task
LDA	Linear discriminant analysis
LED	Light-emitting diode
LFP	Local field potential
LM	Levenberg–Marquardt
LN	Linear network
LR	Linear regression
LSTM	Long short-term memory network
LVQ	Learning vector quantization
MDI	Model deviation index
MEG	Magnetoencephalogram
MEP	Motor evoked potential
MHAT	Mexican hat wavelet
ML	Machine learning
MLP	Multilayer perceptron
MRI	Magnetic resonance imaging
MSE	mean square error
MUA	Multiple-unit activity
mVEP	Motion-onset visual evoked potential
NHP	Nonhuman primate
NIRS	Near infrared spectroscopy
NN	Nearest neighbor
NoP	Number of peaks
OMP	Optically-pumped magnetometer
pBCI	Pilot brain–computer interface
PCA	Principal component analysis
PDE	Partial differential equation
PeGNC	Probability estimating guarded neural classifier
PFC	Prefrontal cortex
PIR	Passive infrared registration

PMC	Premotor cortex
PNN	Probabilistic neural network
PPC	Posterior parietal cortex
PSD	Power spectral density
PSO	Particle swarm optimization
QDA	Quadratic discriminant analysis
QTFM	QuSpin's total-field magnetometer
RBF	Radial basis function
RBFN	Radial based function network
RC	Reservoir computing
RF	Random forests
RL	Reinforcement learning
RNN	Recurrent neural network
RNS	Responsive neurostimulator
RT	Reaction time
SBCI	Synchronous BCI
SCP	Slow cortical potential
SEF	Subject eye fixation
SER	Signal-to-error ratio
SMA	Supplementary motor area
SMR	Sensorimotor rhythm
SNR	Signal-to-noise ratio
SoP	Sum of peaks
SQUID	Superconducting quantum interference device
SS	Signal slope
SSVEF	Steady-state visual evoked field
SSVEP	Steady-state VEP
SVM	Support vector machine
SUR	Single-unit recordings
SWD	Spike-wave discharge
tES	Transcranial electrical stimulation
tMS	Transcranial magnetic stimulation
TREM	Thresholding model
TTD	Thought translation device
TTLS	Transistor-transistor logic signal
TVEP	Transient VEP
VEP	Visual evoked potentials
VI	Visual imagination
VNS	Vagus nerve stimulator
WAG/Rij	Wistar albino glaxo/Rijswijk
WCSP	Wavelet common spatial pattern
WEEG	Workload EEG
WI	Workload index
wICA	Wavelet independent components analysis
WMSPC	Wavelet method with superparamagnetic clustering

- help partially or completely paralyzed people to interact with various external devices, for example, neuro-chat technology which allows people with disabilities to communicate with themselves and other people<sup>1</sup>;
- gaming industry;
- deeper understanding of human and animal brain activity, for example, brain function mapping.

<sup>1</sup> <http://neuro.chat>

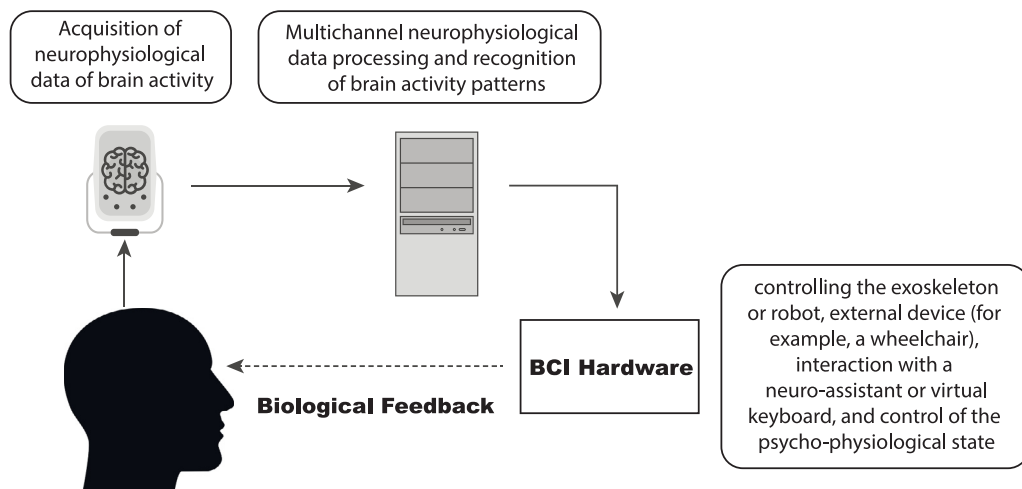


**Fig. 1.** General brain–computer neural interface scheme. Registration of multichannel data on brain activity. The electrical brain activity is most often used, but other types of neuroimaging are also explored (see Section 2.2). Intellectual processing of the obtained data and identification of characteristic patterns in real time, transfer of control commands to the interface hardware. Implementation of biological feedback to monitor the command execution of, training the operator to call necessary mental condition or exposure to it depending on his diagnosed condition.

The understanding of brain functions is very important for efficient BCI applications. In this respect, various methods are used for studying brain activity. In modern HSC BCIs, the brain macroactivity is recorded by electroencephalograms (EEG), magnetoencephalograms (MEG), near infrared spectroscopy (NIRS), etc., which to some extent reflect the functions of the central nervous system (CNS). One of the CNS tasks is to process and integrate incoming information from sensory stimuli received through peripheral nerves and send the signal back to actuators, for example, to muscles or glands, to cause an automatic or a conscious action. In addition, CNS and especially the brain, are responsible for higher integrative and cognitive abilities, such as thinking, learning, processing visual information, speech, memory, emotions, etc. These types of functional activity have their own signatures in the recorded brain activity. For instance, limb movements produce specific spatial-temporal patterns in EEGs [15,16]. Similar patterns associated with imaginary movements (so-called “motor imagery”) were also found and used in existing BCI prototypes to form up to four commands [17–19]. From the viewpoint of nonlinear physics, signal analysis, and artificial intelligence, the BCI system is a pattern recognition system in which different classification algorithms are used to identify “patterns” of brain activity [20,21].

A modern HSC BCI is a system based on artificial intelligence that can process brain activity in real time and recognize a certain final set of CNS activity patterns, as shown in Fig. 1. The processing CNS signals and the generation of control commands using a BCI include several successive phases, namely, data collection, their pre-processing (including the removal of recording artifacts) to prepare signals in a suitable form for further processing, forming a feature vector for identifying discriminant information in recorded signals, classification of signals based on the selected feature vector, and finally a control phase for transforming selected patterns of the brain activity into meaningful commands for any external connected device, such as, e.g., a wheelchair, or setting the direction of the cursor movement on a monitor screen.

It is important to note that the effective operation of a BCI is not possible without feedback between the HSC and the BCI operator, which is marked in Fig. 1 as “biological” feedback. This is necessary, first, to control the correctness of deciphering brain activity signals and interpreting activity patterns when generating control commands, which can be controlled by the operator and, by correcting errors in the training mode, can improve algorithms of the intelligent system (self-learning classification system), and second, to control the operator’s mental states recognized by the intellectual system. For example, during the rehabilitation of a patient with paresis after a stroke, such a system with feedback can determine those attempts of imaginary movement that were unsuccessful and, therefore, did not involve necessary brain areas, providing the patient with the most efficient training for the rehabilitation BCI.

The first neural interfaces mentioned in the scientific literature were developed in 1973–1977 by the research group of the University of California with the support of the National Science Foundation and the Directorate of Advanced Research Projects of the United States Department of Defense (DARPA) [22,23]. In these studies, the scientists analyzed the EEG structure during visual stimulation (so-called *visual evoked potentials*). Despite the fact that the evoked potentials were used to identify the characteristic features of the EEG by averaging a large number of signal segments (trials), the authors proposed a technique for classification of individual trials in real time. In their experiments, the researchers used five electrodes located in occipital and parietal areas. The EEG signals were recorded at a 250-Hz frequency and processed with a 1–70 Hz bandpass filter. Then, they used a special procedure to remove oculomotor and muscle artifacts and Wiener filtering to increase the signal-to-noise ratio. As a result, they found distinctive features of the EEG patterns associated with individual events, which were classified using a linear Bayesian decision rule.

Recently, significant progress has been achieved in neural interfaces which allow a cursor movement [24], partially synthesize speech [25] and control of simplest movements [26]. The possibilities of using neural interfaces for rehabilitation of disabled people, paralyzed people, people with brain damage, post-stroke patients with limb paresis, etc. were also demonstrated [4,9]. A great effort was underway to the development of neural interfaces for exoskeleton control [13,27]. Further development of this technology, along with revealing features related to simplest motor functions, requires the detection of more complex cognitive processes associated with fine motor skills, positioning, attention, etc. [28,29]. In this context, the development of interfaces which allow assessing and controlling psychophysical states of a person attract a great interest of various researchers.

The research in the field of BCIs is undoubtedly interdisciplinary. It involves several scientific areas, including physics, neuroscience, digital signal processing, computer science and computing. The success of the BCI technology has been achieved, first, due to a recent progress in recording brain activity, that allowed highlighting the most significant features of brain signals in an economic, compact and easy way, and second, due to a progress in intelligent processing of the brain activity in real time. The latter required both the development of effective and sensitive methods for classification and extraction of CNS state properties from multichannel noisy signals, and a more efficient technique for computer processing of big neurophysiological data using parallel computing methods [30], for example, embedded high-performance systems based on graphic NVIDIA Jetson processors, combining compactness with high computational capabilities [31].

## 2. Neural interfaces overview

The functionality of neural interfaces is based on the real-time detection of characteristic waveforms (patterns) of brain activity using neuroimaging methods, such as electroencephalography (EEG), electrocorticography (ECOG), magnetoencephalography (MEG) and functional magnetic resonance imaging (fMRI), and on the transformation of the obtained information into control commands for hardware (for example, exoskeleton, bioprostheses, wheelchair, neurointerface for attention control, etc.).

### 2.1. Classification of brain–computer interfaces

#### 2.1.1. Control command based classification

The central core of any HSC BCI is an intelligent system able to classify brain states in real time according to recorded brain activity due to either spontaneous physiological processes or an external stimulation. The revealed features of the brain states are then transformed by the BCI into control commands for external applications. According to a type of the control commands given by the BCI operator, neural interfaces can be classified as follows [32].

- **Active BCIs** use changes in the brain activity, directly and consciously controlled by the neurointerface operator, regardless of external events, for control commands.
- **Reactive BCIs** detects and classifies the brain response (for example, evoked potential) to external stimulation (visual, auditory, tactile, etc.) for control commands.
- **Passive BCIs** analyze the current brain activity of the user without any target monitoring to obtain information about the actual brain state, for example, attention, switching activity, emotional state, etc.

Typical examples of active BCIs are neural interfaces in which the imagination of various types of movements is used to form control commands (for example, motor imagery of right hand and right foot in the well-known BCI for printing text "Hex-o-Spell" [18]), that will be discussed in Section 2.4. The prominent examples of reactive BCIs are a neural interface (in particular, on-screen keyboard) based on the P300 potential [33] and the systems based on so-called *steady-state evoked potentials* (SSVEP), which are the brain response to periodic visual stimulation with a certain frequency [34–36] (for detailed description see Sections 2.4.1 and 4.1.2). The systems based on passive BCIs can be useful for creating monitoring systems that can detect the probability of errors, decrease the user's attention span or the operator's perceived loss of control over the system [37–39] (see Sections 4.1.2, 2.4.6, and 3). Passive BCIs can also be used for purely medical purposes of diagnosis and treatment of various neurological diseases, for example, to predict and suppress epileptic seizures by adding biological feedback [40,41] (see Sections 6 and 3).

While active and reactive BCIs are primarily of interest for disabled people with completely or almost completely closed consciousness due to an extremely slow generation and transmission of information (see details in Section 2.4), passive BCIs are aimed at assessing human conditions in real time and hence can widely be used in the entertainment industry, computer games, neuromarketing, as well as for monitoring certain emotional and functional states restored in human-machine systems with biological feedback (see Section 2.4.6).

#### 2.1.2. Input data processing modality based classification

Another type of the BCI classification is based on synchronization of the input data processing modality [28], i.e., a BCI can be classified either as *synchronous BCI* (SBCI) or *asynchronous BCI* (ABCi).

SBCIs analyze brain signals during only predefined time intervals, while any brain signal outside these time windows is ignored. Therefore, the operator can create commands during only specific periods of time determined by the SBCI system. On the contrary, ABCIs continuously monitor brain signals, no matter when the user acts. Therefore, ABCIs provide more natural human–machine interaction than SBCIs. However, ABCIs are more complex and computational demanding. Table 1 summarizes advantages and disadvantages of both SBCI and ABCI systems. Basically, SBCIs are reactive systems, although they can be passive, while active and passive BCIs are usually asynchronous ones.

**Table 1**

Main properties of synchronous and asynchronous BCIs.  
Source: Based on [28].

BCI type	Advantages	Disadvantages
SBCI	Simpler design and performance. The user can avoid artifacts caused by blinks and eye movements.	A typical human–machine interaction occurring in predetermined time intervals.
ABCI	No requirements for waiting external cues. More natural interaction mode.	More complicated design. More difficult continuous processing of brain activity.

### 2.1.3. Invasive and noninvasive brain–computer interfaces and brain–machine interfaces

In 2006 Lebedev and Nicolelis [3] suggested a classification of brain–machine interfaces (BMIs) based on the type of electrophysiological recordings depending on their invasivity.

- **Noninvasive BCIs** record brain activity from the head surface. This approach has proved useful for helping paralyzed or “locked in” patients to develop ways for communication with the external world or to evaluate and control mental states in healthy people. However, despite having the great advantage of not exposing the subject to the risks of brain surgery, noninvasive techniques provide communication channels of limited capacity.
- **Invasive BCIs** record brain activity intracranially using implanted electrodes. This approach provides much better quality of registered neural signals. The invasive BCI approach is based on EEG recordings from single brain cells (also known as single units) or multiple neurons (known as multi-units). However, these BCIs carry risks associated with a surgical procedure. Therefore, in humans this technology is only applied in the case of medical indications. At the same time, there are many examples of invasive BCI realizations with animals.

## 2.2. Neuroimaging methods for brain–computer interfaces

*Neuroimaging* is a new neurophysiological paradigm for studying brain activity. Neuroimaging in medicine is useful for detecting a damage of brain tissues, diagnosing skull fractures, brain injuries. Today, it is increasingly being used to diagnose behavioral and cognitive diseases (e.g., age-related neurodegenerative changes), metabolic disorders and small lesions (e.g., epileptic foci) [42]. Moreover, functional neuroimaging can be used for constructing a BCI enable to analyze brain dynamics,<sup>2</sup> blood flow rates inside vessels, and changes in metabolic activity causing by specific tasks solved by the central nervous system (CNS).

### 2.2.1. Electrocorticography

Electrocorticography (ECoG) or intracranial EEG (iEEG) is an invasive method of electrophysiological monitoring of the brain activity using electrodes implanted inside the brain. ECoG has high spatial resolution, wide bandwidth, high amplitude and small sensitivity to artifacts (e.g., electromyographic (EMG) signals) [43,44]. The ECoG signals are usually recorded using multi-electrode matrices implanted under the skull directly on the surface of the cerebral cortex, as illustrated in Fig. 2 [45]. The noninvasive recording sensors allow several patients to use the same interface without additional surgical procedures, that can be important for the development of public interfaces for widespread use. It should be noted that ECoG is mainly applied for medical purposes, for example, during neurosurgical operations or to control pathological brain activity. In particular, this technology is successfully used in systems for controlling epileptic activity, where, along with the recording electrodes, electrodes for transcranial stimulation are also implanted in cerebral cortex [46]. A high spatial resolution of ECoG allows efficient decoding of small brain signals, for example, related to fine motor skills [47].

In 2004 Leuthardt et al. [48] identified patterns of ECoG signals associated with various types of motor and speech activities for further use in the BCI. The authors achieved about 74%–100% accuracy in controlling a one-dimensional cursor movement on the monitor screen. The use of pre-recorded ECoG signals (i.e., off-line) allowed Chao and colleagues [49] to distinguish motion patterns corresponding to seven degrees of freedom of hand movement. Moreover, the ECoG signals associated with individual finger movements [50] and different types of natural grasps [51] were also decoded. By comparing invasive and noninvasive neuronal signals for BMIs, Waldert [52] concluded that invasive signals much better describe local brain processes in various cortical areas.

### 2.2.2. Electroencephalography

*Electroencephalography* (EEG) is one of the first proposed and mastered methods of neuroimaging. It consists in the recording of electrical brain activity using electrodes located on the head surface (so-called noninvasive or scalp EEG), or superimposed directly on the cortex (so-called invasive EEG or electrocorticogram). The both methods are widely used for clinical and fundamental research. However, due to its simplicity and noninvasivity, the noninvasive EEG is more popular and even allows intracellular neuronal recording [53].

<sup>2</sup> As distinct from functional neuroimaging, structural neuroimaging only enables to analyze the structure of brain tissues.



**Fig. 2.** Picture taken during neurosurgical operation, showing the left hemisphere with multi-electrode matrices superimposed on the brain surface. Source: Reprinted from [45].

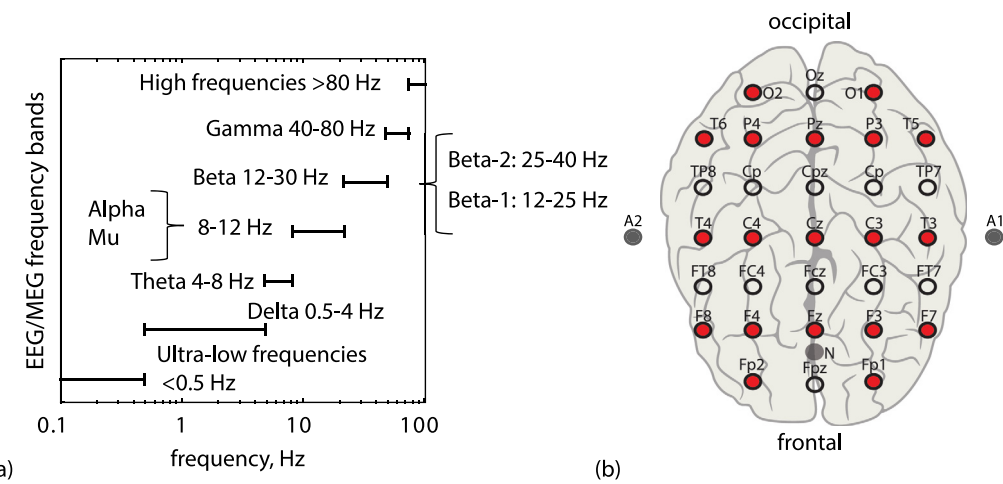


**Fig. 3.** (a) Traditional frequency ranges of EEG or MEG signals. Alpha waves dominate in occipital area, while mu waves in somatosensory cortex. Beta waves is sometimes divided into two subbands (beta-1 and beta-2) for more accurate frequency sampling. (b) Electrode positions according to “10-20” (red dots) and extended “10-10” (all dots) international schemes. A1 and A2 are reference electrode positions and N is the ground electrode position.

The important advantage of the intracortical EEG over the noninvasive EEG is a higher rate of information transfer, which is still very low. Therefore, the invasive EEG is widely used in medicine for diagnosis of various brain diseases, such as Alzheimer, epilepsy, sleep and attention disorders, as well as for monitoring the brain response during neurosurgical interventions. In addition, the invasive EEG is particularly appealing to patients, who exhibit a lack of reproducibility of neural network activity during natural movement control. Their performance can be increased using a BCI which allows tuning neural ensemble [54], i.e., the brain learns how to control the BCI (so-called closed-loop control). Since the invasive BCI affects individual neurons [55], it facilitates the use of already tuned neural activity [56], followed by a transition from externally assisted to full brain control. Looking ahead, we would like to note that local evoked potentials are more stable [57,58], and therefore it is more difficult to tune them by the feedback. Unlike spiking activity of individual neurons, the activity of an entire neural cluster remains coherent, so that any change requires a structural reconstruction of a large group of neurons during learning. Although the finding of necessary neural activity patterns is also possible using a noninvasive EEG [59], it is much more difficult and requires very sophisticated computational techniques.

The EEG data are usually analyzed using physico-mathematical methods. Among many approaches, the most popular ones are Fourier and wavelet transforms, which reveal significant changes in time-frequency and space-frequency brain dynamics in the process of solving cognitive tasks [60,61], motor [62] and perception activity [63,64]. The analysis of electrical and magnetic brain activity allows distinguishing certain frequency ranges, traditionally separated to  $\delta \in [0.5, 4]$  Hz,  $\theta \in [4, 8]$  Hz,  $\alpha \in [8, 12]$  Hz,  $\beta_1 \in [12, 25]$  Hz,  $\beta_2 \in [25, 40]$  Hz, and  $\gamma \in [40, 80]$  Hz (Fig. 3(a)). In this review, we will adhere to this terminology.

One of the most powerful methods widely used for the EEG analysis in active BCIs is *event-related synchronization/desynchronization* (ERS/ERD) [65]. It consists in a rapid increase/decrease in the EEG oscillation amplitude in particular

frequency ranges (see Section 4.1.3). For instance, motor execution is typically accompanied by both ERD and ERS which form characteristic time-frequency patterns. During the motor action, ERS of delta activity takes place, while ERD is observed in alpha/mu and beta rhythms [62,66].

Another important characteristic EEG feature used in BCIs is an *event-related potential* (ERP) (see Section 4.1.2), that is an *evoked potential* (EP) arisen as brain response to external stimulation. The use of ERPs is very promising for control systems in reactive BCIs. It should be noted that ERP is the brain response not only to external, but also to internal mental processes (e.g., real and imaginary movements, changes in gaze direction, etc.) [67–69]. Since EP on a single recording is almost indistinguishable in a background EEG, it can be revealed by the use of the accumulation method and synchronous averaging over a large number of short EEG segments recorded after stimulus presentation. At the same time, there are efficient BCIs which use EPs (mainly P300) based on the paradigm of presenting stimuli and further highlighting characteristic features associated with events in real time.

The P300 EP consists in a positive peak in the EEG, 300 ms after presentation of a rare visual, auditory or somatosensory stimulus. It was shown that the less likely the stimulus, the greater the P300 amplitude [70]. For real-time BCI operation the finding of ERPs, best representing the operator's intention, is required. Then, the ERP features should be classified using special algorithms to create the corresponding command (see the review paper of Mak et al. [71]). For example, a similar P300-based BCI was developed for the gaming industry and rehabilitation of disabled people [72,73].

In noninvasive EEGs, brain signals are recorded in a noninvasive way by electrodes located on the head surface. The highest quality signals can be obtained using cup electrodes mounted on a pre-treated skin surface using a conductive gel or paste [74]. In this case we can obtain the impedance values which vary within the 2–5 kΩ interval. Another, less common, but at the same time more promising method implies the use of dry electrodes [75]. Despite low signal quality, the advantage of using dry electrodes is the ease of their installation and the possibility of long-term EEG recording without adding gel.

Along with a type of electrodes used, an important characteristic of neuroninterfaces is the number of EEG channels. Obviously, a small number of electrodes simplify their installation and increase the processing speed. However, this can decrease the quality of recorded signals. Among various electrode mountings, the international “10–20” scheme is the most often used. It includes 19 EEG electrodes covered all areas of cerebral cortex and two reference electrodes (A1 and A2) [76] (red dots in Fig. 3(b)). For specific tasks, the electrode arrangement can be modified to increase spatial resolution in a particular brain area, for example, to analyze motor activity in the motor cortex. In this case, the EEG includes 31 channels distributed according to the “10–10” electrode scheme shown in Fig. 3(b) (all dots). This scheme includes all electrodes of the “10–20” scheme plus additional electrodes shown by white dots.

A big advantage of the BCI based on the recording electrical brain activity is a very fast transmission of information from the brain to an external device. Indeed, the main purpose of active and passive BCIs is to interpret the user's intentions via monitoring brain activity. Brain signals include numerous single events related to a particular cognitive or motor task. Although most of these events are difficult to interpret physiologically and their origin is unknown, electrical activity signals corresponding to these events can be decoded and interpreted by the HSC BCI to create corresponding commands for an external device or for the operator himself/herself. At the same time, different types of events are characterized by different information transfer rates estimated as a number of transmitted bits per event or, more generally, transmitted bits per time unit [77–79]. In particular, the modulation of brain signals in visual cortex after visual stimulus presentation allows implementing a 60–100 bits/min BCI [80,81], while sensorimotor rhythms synchronized with real and/or imaginary motor activity provide a 3–35 bits/min information transfer speed [82–84]. At the same time, the P300 potential in the simplest case yields a very low accuracy and command generation speed [85], since a large number of repetitions of stimulus presentation are required to highlight the EP. Nevertheless, the optimization of the algorithm for monitoring EPs in real time and a small number of averaged EEG segments allowed the information transmission rate of around 10–25 bits/min [85,86].

### 2.2.3. Cerebral cortical registration of neural activity

A high spatial resolution is achieved by an invasive neuroimaging technique such as *cerebral cortical registration* (CCR) which allows *single-unit recordings* (SUR) and *local field potential* (LFP) registration, i.e., electrophysiological responses of single neurons and the electric potential in the extracellular space around neurons. CCR requires implanted microelectrode arrays deep into the brain to record signals generated by individual neurons. This technology is progressing rapidly thanks to new efficient designs of microelectrode arrays with minimal aliasing.

First intracortical neuron recordings were performed in animals [87,88]. However, since 2004 CCR has been performing for persons without a limb and experiencing certain forms of paralysis, using neural interfaces based on a 100-electrode silicon recording matrix, to provide effective interaction between motor cortex and external devices in order to restore motor functions [89]. The successful neural control of a robotic arm (anthropomorphic manipulator) with the aim to manipulate individual objects was realized by a quadriplegic person [90,91]. A similar system was used for communication with paralyzed patients [92]. It is remarkable that this system demonstrated high performance for a long time [93].

It should be noted that, depending on the type of CCR, different quality and resolution of detected signals are achieved. SUR provides the best spatial resolution and temporal resolution above 300 Hz. At the same time, LFP of a group of neurons in the vicinity of an electrode is recorded with temporal resolution lower than 300 Hz. In terms of digital signal processing, LFP can be considered as an analog signal, while SUR measures individual spikes of a single neuron and can be correlated

in time with discrete events. The disadvantage of CCR is that the sensitivity of implanted electrodes is not constant and can vary in time, that requires periodic calibration of SUR and LFP signal recording systems [94].

In their recent paper [95], Elon Musk & Neuralink suggested and successfully tested a next generation of invasive CCR-based BCIs by introducing a novel integrated platform which enables a high-quality registration of thousands of channels. Their device contains arrays of flexible electrode threads with up to 3072 electrodes per array distributed across 96 threads. To overcome a surgical limitation, the authors built a neurosurgical robot inserting 6 threads per minute with a micrometer spatial precision. To increase the biocompatibility, they created a neurosurgical robot capable of implanting polymer probes much faster and safely than existing surgical approaches. The electrode array was packaged into a small implantable device that contained custom chips for low-power on-board amplification and digitization. The package with 3072 channels occupied less than  $(23 \times 18.5 \times 2)\text{ mm}^3$ . A single USB-C cable provided full-bandwidth data streaming from the device, recording all channels simultaneously. Using this platform in freely moving rats, the authors obtained a spiking yield of up to 85.5%.

#### 2.2.4. Magnetoencephalography

Another widely used neuroimaging technique is magnetoencephalography (MEG), that measures weak magnetic fields generated by neurocortical ionic currents [28]. This is a safe noninvasive method of brain imaging that provides important information about neuronal activity in the living human brain with high temporal (about 1 ms) and spatial (about 1–2 mm) resolution. While the EEG modality benefits from the simplicity of the measurement equipment, it suffers from a relatively low (around 2 cm) spatial resolution. At the same time, MEG requires more sophisticated instrumentation and measurement methods due to extremely low magnetic fields generated by the brain tissue. Currently, there are two MEG techniques, one is based on superconductivity under low (helium) temperatures and another one explores quantum mechanical properties of alkali atoms under optical pumping and operates under room temperatures.

[Fig. 4\(a\)](#) schematically illustrates a typical experimental setup of the MEG study. In the MEG machine, a subject sits on a comfortable chair, while his head is inside the MEG scanner. The magnetic field is detected with a magnetometer known as superconducting quantum interference device (SQUID) [96] placed close to the scalp. SQUID can detect tiny magnetic signals, much less than one-billionth the strength of the Earth's magnetic field, and then convert these signals into electric voltages. The SQUID array is mounted in a close-fitting helmet and is cooled with liquid helium. The SQUID array is used in combination with superconducting pickup coils acting like antennae. When a magnetic signal from the brain traverses the coil, it induces a current measured by the SQUID.

A MEG scanner, for example, the widely used Vectorview MEG system (Elekta AB, Stockholm, Sweden) [97–101], contains 306 sensors covering the entirety of the scalp (see [Fig. 4\(b\)](#)). These sensors include magnetometers which measure magnetic fields directly, and gradiometers which are pairs of magnetometers placed at a small distance from each other, measuring the difference in magnetic field between their two locations. This difference measure subtracts out large and distant sources of magnetic noise (such as Earth's magnetic field), while remaining sensitive to local sources of magnetic fields (such as those emanating from the brain). Due to their positioning, the magnetometers and gradiometers provide complementary information about the direction of magnetic fields.

The use of MEG has several advantages as compared to EEG. First, the MEG technology allows a very high temporal and spatial resolution, enable to record events with duration of the order of a millisecond, and to determine with high accuracy the position of sources of the magnetic field in the cerebral cortex [102]. Therefore, MEG signals are more reliable for diagnosing brain states and speeding up the time for the formation of commands in the HSC BCI as compared to the EEG-based BCI [103]. Second, MEG is a completely noninvasive technique for recording brain activity. Moreover, the MEG scanning procedure is very comfortable for patients because it does not require a long-time installation of electrodes, so it is widely used for evaluating and diagnosing nervous system disorders in children and infants. The high frequency resolution of the MEG neuroimaging allows the analysis of brain activity up to 250 Hz. Therefore, this technology can be considered as an effective base for creating a HSC BCI for rehabilitation systems in a clinical setting, for example, to restore motor functions after brain damage [104].

On the other hand, there exist significant disadvantages of this neuroimaging technology to be used in BCIs. First, as compared to EEG, this technology is very expensive and requires a highly qualified professional service. Second, a stationary MEG system needs a special shielded room to reduce the influence of the Earth's magnetic field and industrial electrical networks (noise), which are, respectively, nine and six orders of magnitude higher than the brain's magnetic field generated by neural currents. These restrictions do not allow creating a compact mobile BCI on its basis (see, for example, Refs. [105,106]).

The majority of BCIs are based on extracranial EEG recordings during motor imagery. The first MEG-based BCI system was proposed in 2005 [107]. After a short training, the participants of the experiment were able to write a short name on the screen using imaginary movements of either their tongue or left little finger. The choice of these two imaginations was motivated by the relatively great distance of the respective cortical areas on the motor cortex. The authors analyzed brain signals in the mu-band recorded from the motor cortex and found a 3-s delayed feedback using machine learning techniques for movement classification. Online feedback was presented to 4 subjects in a tongue experiment. The authors used a trained support vector machine (SVM) to spell the short name. The subject had to write the word "JOHN" by selecting letters from the right margin, as shown in [Fig. 5](#). Approximately every seven seconds, the subject imagines a corresponding movement of either their tongue or finger. At the start of the spelling experiment, half of the letters of the

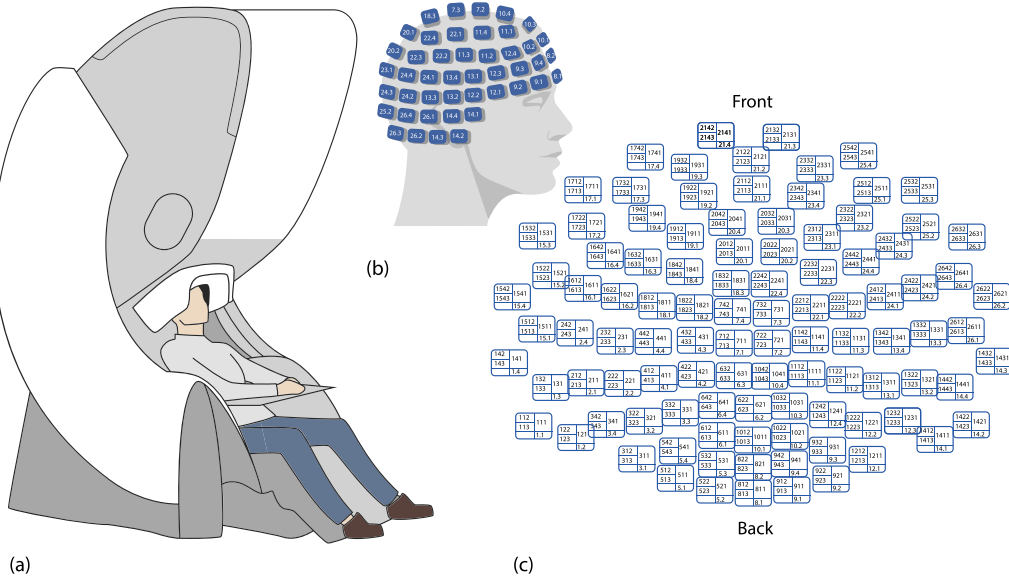


**Fig. 4.** (a) Schematic illustration of an experiment with a MEG machine. (b) Magnetic field sensors of the MEG machine cover the subject's head. (c) Vectorview of MEG channels of the Elekta AB system (Stockholm, Sweden) with 306 channels (102 magnetometers and 204 planar gradiometers).

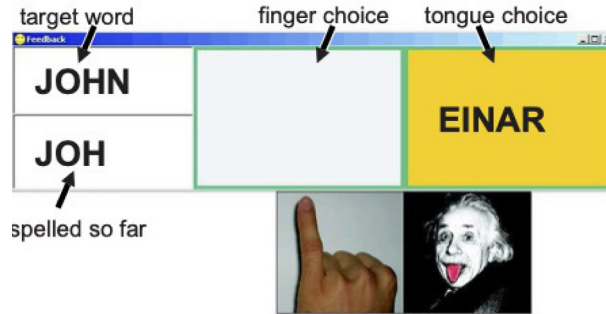


**Fig. 5.** Screenshot of the projection screen while subjects write the word “JOHN”. The lower left box contains the letters “JOH” spelled so far. The subject should pick the next letter from the right box by imagining a tongue movement. If the desired letter is not among the letters displayed in the right box, the subject imagines a finger movement, and an empty left margin is selected. In this case, the spelling editor switches to a sibling branch and a different set of letters appears. After several iterations, only one letter remains. If it is chosen by the subject, a letter is added to the already written word.

Source: Reprinted from [107].

alphabet are displayed. If the writing letter was among those displayed, the subject had to imagine a tongue movement. To let the experimenter know that the letter is not displayed, the subject imagined a finger movement. In the next step, the selected subset of the alphabet was again divided into two parts, one of which was displayed. In the last step of this process, the letter should have been confirmed and displayed on the left side of the screen. The procedure started again so that the next letter could be selected.

A further development of this BCI allowed researchers to shorten the feedback delay to almost real-time mu-rhythm control using the autoregressive spectral estimation method during imaginary movements of the limbs [103].

Rapid advances in atomic physics over the last decade have led to a new generation of MEG devices operating at room temperature, so-called *optically-pumped magnetometers* (OPMs), capable to achieve sensitivity similar to that of cryogenically cooled SQUID devices. The OPM sensors can be placed directly on the scalp surface giving, theoretically, a large increase in the magnitude of the measured signal. Further motivation to develop room-temperature alternatives to low-temperature SQUID magnetometers comes from the high helium costs, which complicate the operation of MEG systems, very promising for BCI applications [108]. The main advantage of OPMs is that they do not require cryogenic cooling, which decreases their price by 2–3 times as compared to the conventional SQUID-based MEG systems. Moreover, the OPMs can be placed within millimeters from the scalp, this almost doubles the signal-to-noise ratio (SNR) [109]. In addition, they are not as susceptible to muscle artifacts as EEG [110]. The location of OPMs in a field-nulling apparatus [111] decreases the influence of head movements in the ambient field. 3D-printed helmets

were used by various researchers [109,110,112–114]. Using median nerve stimulation, Boto and his colleagues [113] showed that the OPM can detect both evoked (phase-locked) and induced (non-phase-locked oscillatory) changes when placed over the sensory cortex, with signals approximately 4 times larger than the equivalent SQUID measurements.

All the above mentioned features show potential possibilities to develop a new generation of OPM-based BCIs, cheaper, more flexible and more sensitive than SQUID-based BCIs, which can serve for both motor and non-motor tasks. For example, Paek et al. [115] tested a real-time OPM-based BCI where participants were to control a cursor to reach two targets. The reported BCI system used alpha and beta-band power modulations associated with hand movements. They observed significant alpha and beta-band desynchronization due to the hand movements.

From June 2020 high-sensitive second generation (Gen-2) three-axis magnetometers are available from the QuSpin Company (Colorado). Meanwhile, researchers at the University of Nottingham have used the company's two-axis sensors to operate a whopping 50-channel array. QuSpin also produces a compact, high-sensitivity total-field magnetometer (QTFM) which can operate within the Earth's field and can resolve minute field changes for applications such as magnetic observatories and aboard small mobile platforms.

Despite the enormous progress, OPM-MEG is so far a developing technology that needs improvement. Due to their large size, the number of channels is relatively small (no more than 50) [110,113,116,117] and therefore cannot cover the entire head. In addition, OPMs can only be mounted in specific areas over the brain cortex. Although for many BCI applications only several sensors are required, their correct location over selected brain areas is very important. The miniaturization and universality of lightweight helmets would be an essential step toward further development of OPM wearable for BCI applications.

### 2.2.5. Functional magnetic resonance imaging

*Functional magnetic resonance imaging* (fMRI) uses magnetic resonance imaging (MRI) to record the neural activity in the brain by measuring changes in oxygenation and blood flow [118]. When a certain brain area is involved in a particular cognitive process, it consumes more oxygen, and the blood flow to this part increases to meet this demand. The fMRI is a very efficient method for mapping brain functions, where the activated brain areas are associated with different types of cognitive activity and mental tasks [119]. Although the temporal resolution of fMRI is relatively small (several frames per minute), the spatial resolution is very high. Therefore, the information obtained by this method can be useful for pre-tuning BCI algorithms, in particular, for selecting the most significant areas of the cerebral cortex [28,120]. Modern fMRI systems allow obtaining information about brain states in real time, that gave possibilities to create real-time clinical BCI systems [121,122]. However, the information transfer speed in the fMRI-based BCIs does not exceed 1.2 bits/min [123].

### 2.2.6. Functional near-infrared spectroscopy

Near-infrared radiation penetrates bones of the skull and adjacent tissues into frontal and occipital cortex to assess hemodynamic changes accompanying brain activation by assessing oxygenated and deoxygenated hemoglobin levels [124]. Therefore, *near-infrared spectroscopy* (NIRS) is a powerful tool of studying brain activity used more widely every year. Similar to fMRI, functional NIRS (fNIRS) is an indirect method for assessing the activity of the brain through its metabolism. However, fNIRS has important advantages over fMRI in terms of creating efficient BCIs. These are lower price, portability and higher temporal resolution. A key limitation of the NIRS application is related to the nature of the hemodynamic response, since vascular changes occur several seconds after the associated neural activity [28,125]. As a result, the information transfer rate in the fNIRS-based BCI is relatively small and does not exceed 4 bits/min [126]. Nevertheless, it can be increased in the future by increasing the sensitivity of the recorded equipment [127], as well as by detecting a fast optical response [128,129] and the so-called initial failure [130,131]. In addition, fNIRS is less sensitive to movement artifacts than other portable and mobile neuroimaging techniques. Nevertheless, it is fNIRS technology that can be considered as the only possible alternative to EEG for creating systems for recording brain activity in a mobile portable BCI in the nearest future [132].

The first step in the development of fNIRS-based BCIs is to get appropriate brain signals. The principal difference between EEG and NIRS is that the latter records signals of an optical nature. The two most common areas of the brain used by BCI are primary motor and prefrontal cortex [133]. While the signals corresponding to real and imaginary movements are recorded in the motor cortex, the signals associated with the mental score, landscape images, geometric images, logical tasks, etc., are detected from the prefrontal cortex. Although several different emitter-detector configurations are used in these two areas, the emitter-detector distance is usually maintained in a specific range, since it plays an important role in measuring fNIRS. For example, the increasing distance between the emitter and the detector corresponds to an increase in the image depth [134]. To measure signals of the hemodynamic response from the cortex areas, a distance of about 3 cm [135] was proposed.

A typical configuration of the emitter-detector on the head and the light paths traveled to reach two detectors are shown in Fig. 6. The appropriate number of emitter-detector pairs for an adequate neural activity isolation varies depending on the type of brain signals used. For the prefrontal cortex, 3 emitters and 8 detectors can be sufficient to adequately receive brain signals, allowing them to be decoded into commands for a BCI [136–141]. In the case of real or imaginary motor activity, 4 to 6 emitters and the same number of detectors are most often used, which cover the entire motor cortex [142,143].

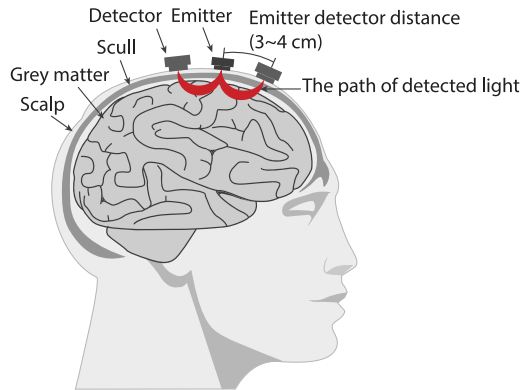


**Fig. 6.** NIRS scheme of emitter-detector pairs showing the light paths inside the brain.

**Table 2**  
Comparison of neuroimaging methods used in BCIs.

Method	Value	Measure	Resolution		Speed bits/min	Portability	Invasivity
			Hz	mm			
EEG	EP	Direct	~100	~10	3–100	Portable	NO
CCR	EP	Direct	(3–10) × 10 <sup>3</sup>	10–0.5	3–35	Portable	IN
ECoG	EP	Direct	~3 × 10 <sup>3</sup>	~1	3–35	Portable	IN
MEG	MF	Direct	(3–5) × 10 <sup>3</sup>	~5	>100	Stationary	NO
fMRI	MB	Indirect	~1	~1	0.6–1.2	Stationary	NO
NIRS	MB	Indirect	~1	~5	~4	Stationary	NO

EP — electric potential, MF — magnetic field, MB — metabolism, IN and NO — invasive and noninvasive techniques.

It is worth noting certain prospects for creating hybrid systems using fNIRS to improve the accuracy of command classification. Khan et al. [141] used the hybrid NIRS–EEG technique to extract and decode four different types of brain signals. The NIRS unit was located above the prefrontal area of the brain and the EEG above the left and right areas of the motor cortex. Four direction symbols (“forward”, “backward”, “left” and “right”) were presented to twelve subjects participated in the experiment. The control commands for moving back and forth were evaluated by performing arithmetic mental tasks related to changes in the oxyhemoglobin (HbO) concentration. The commands of the left and right directions were associated with real motor activity, namely, the movement of the right and left hands recorded with EEG. As a result, four different pilot signals were accurately evaluated using the fNIRS–EEG hybrid technology.

Table 2 compares the most important characteristics of different neuroimaging methods used in BCIs.

### 2.3. Functional models of neurointerfaces

When implementing a software and a hardware platform, one needs to determine its main blocks and their interaction for ease of upgrading the system and, if necessary, scaling such a platform. Since a wide range of tasks are trying to be solved using the BCI technology, there is no a unified scheme for constructing a HSC BCI, which would be universal for any application. As a consequence, there are several approaches to this problem. Nevertheless, we can determine general principles for constructing a BCI functional diagram for main classes of neurointerfaces mentioned in Section 2.1, according to the command generation by the BCI operator. The schemes presented below are fairly general and can be easily modified depending on specific requirements for each BCI application. Some structural elements can be combined into single blocks depending on the specific hardware and software implementation. Moreover, the presented functional diagrams are independent of the specific neuroimaging used, although while describing the diagrams we assume the use of EEG since it is the most often used neuroimaging method in modern BCIs.

#### 2.3.1. Active brain–computer interfaces

Fig. 7 schematically shows the functional diagram of an active BCI, in which a person (operator) controls a complex external device (for example, a wheelchair) through a series of functional components of the control system. The neurointerface user controls the device and sees the result of this control and/or the effort needed. The HSC BCI is often completed with a control display which shows the results of interpreting operator's mental commands in an understandable (semantic) format by the intellectual control system, both for monitoring the BCI operation and providing biological feedback.

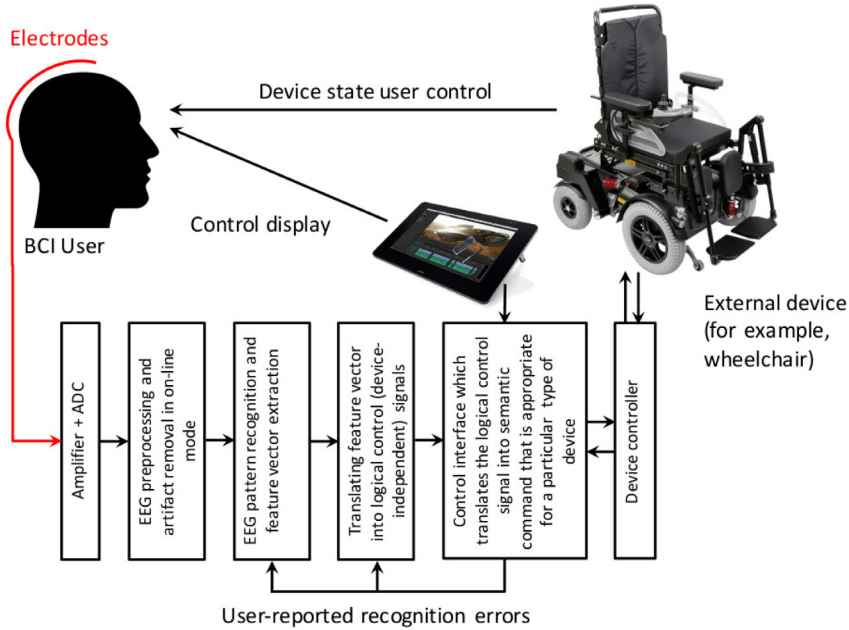


**Fig. 7.** Typical active BCI functional model for controlling an external device.

The BCI operator modifies in a certain way the state of brain activity, which is interpreted by the intellectual system as a control command for an external (controlled) device. An important aspect of the BCI is the ability of the operator to cause appropriate mental states in them, which can be uniquely and accurately classified by the BCI. This is commonly achieved by training the operator using biological feedback. In the mental states, such as those discussed later, active neural interfaces use motor imagery of various limbs to generate 2–4 relatively stable commands to control the external device [17,144,145].

As mentioned above, the multichannel recording of electrical brain activity is the most typical and frequently used method in BCIs. Often in practice, all full arrangements of 10–20 or 10–10 electrodes are not applied, but instead only a shortened scheme of several most informative channels are used, that cover only the region of the cerebral cortex of interest, for example, frontal and motor cortex in the case of motor imagery. This facilitates and accelerates the installation of EEG electrodes. Further, the recorded signals of electrical brain activity are amplified by a multichannel amplifier and digitized by an analog–digital converter with sampling frequencies between 250 and 2000 Hz.

As the next step, the processing of the recorded EEG signals is realized (see Section 3). The fundamental requirement for a good performance of neurointerfaces is to analyze and classify neurophysiological data in real time. It should be noted here that when recording EEG, the signal is exposed to various factors associated with eye movement, muscular activity, cardiac rhythms, etc., that lead to the appearance of recording artifacts which distort the EEG. When the amplitude of the artifacts significantly exceeds the amplitude of the useful signal, the data cannot be interpreted automatically. In clinical practice, usually the EEG fragments containing the artifact are removed from the analyzed signal, which can lead to a significant reduction in the duration of useful EEG segments. As a result, the useful records in healthy people can be reduced after artifact removals by about 10 times, and in people with pathologies and children even higher [146,147]. In real-time work, we cannot immolate data segments with artifacts, since at the time of artifact registration the operator can form a command for the BCI. Therefore, there is a need to develop methods for removing artifacts in real time, which would minimally distort the features of the recorded EEG that we are interested in. Often, as we will show below, this requires the recording of additional physiological signals.

It should also be noted that the real-time mode imposes stringent requirements on the power of the neural interface processor, which must be sufficient to perform a significant number of computational operations related to both the EEG processing and the classification of patterns to be allocated. At the same time, for portable neural interfaces, there is a need to reduce the BCI size. Given this requirement, it seems promising to use embedded high-performance computing systems, in particular, with the ability to implement computations on graphics processors (for example, NVIDIA Jetson [31,148]). In addition to hardware, as will be shown later, to optimize the processing of multichannel neurophysiological data, one needs an efficient use of optimization algorithms based on the features of the time–frequency and spatial–temporal structures of the studied neural activity.

The pattern recognition of the brain activity of interest is very important for optimization of the BCI control commands. In terms of the machine learning theory, the output of the HSC block is a feature vector determined by the peculiarity of

the registered pattern of brain activity. For example, if the operator controls brain activity in alpha (8–13 Hz) and beta (14–30 Hz) frequency bands, this block will form (at the signal sampling frequency) a feature vector containing the EEG powers in these specified ranges. The property converter translates the generated feature vector into a logical control signal, which is independent of any semantic knowledge about the device being controlled and its control methods. The control interface converts a logical signal into a semantic control signal, that is already defined by a specific managed device. The formation of the semantic command can be either instantaneous (i.e., the signal is formed directly from the current output logical signal of the transducer) or performed by integrating the output signal in time. For example, the binary state “braking/acceleration” of a wheelchair can be controlled by the BCI directly based on the instantaneous logical output, or the logical output can be monitored to form a semantic command on the base of temporal dynamics. In the latter case, one can avoid short-term errors in the interpretation of the operator’s mental states.

Basically, the semantic set of commands can be not only static, but also dynamic and even synchronized with the state of the controlled device. In this case, the dynamic set of commands can be formed directly in a menu, from which the operator can select a required action from a large number of commands. The advantage of this dynamic approach is that the operator can set a lot of semantic control commands with a limited set of logical commands. For example, two logical commands are enough to navigate in arbitrarily large and complicated hierarchical command menu. The result of forming a semantic command can be displayed on the computer monitor to visualize interpretation of the logical command in semantic. For example, the display may show a menu in which the “mental” navigation of the BCI operator occurs. Using the control display, it is also possible to use the biological feedback implementation during the operator’s training.

Finally, an external device or software is managed when a physical command is formed on the base of semantic commands. Generally, if an intelligent system of pattern recognition and formation of a feature vector and a logical signal is adaptive, then a registration error forms a feedback loop which can modify the adaptive control system (feedforward control scheme for BCI). On the other hand, certain elements of this general functional BCI scheme may be absent, for example, the neurointerface may not provide feedback to correct control system errors. In this case, the following simplified management chain can be used.

User Control → Logical Control → Semantic Control → Physical Control.

### 2.3.2. Reactive brain-computer interfaces

Recall that a reactive BCI for formation of control commands detects and classifies brain responses (e.g., caused by P300) to an external stimulation, usually visual, but sound, tactile or other stimuli can also be used. In this case, the functional scheme of the reactive BCI, inheriting many features of the active BCI, undergoes a significant change which provides the implementation of the stimulation system and the synchronous operation of other HSC BCI modules with presented stimuli.

[Fig. 8](#) illustrates a typical functional model of a reactive BCI. In this scheme, all elements, associated with the registration and pre-treatment of brain activity, persist, but subsequent functional units undergo changes. In this case, the control interface presents various stimuli to the BCI operator, whose brain response is interpreted by the pattern recognition system synchronized with the stimulus presentation system. Accordingly, control commands can be produced with certain periodicity related to the time interval of the stimulus effect on the person. In the case of visual effects, a screen can be used as a stimulant which may flash, or images or a set of symbols may appear. A typical system for dialing text on the base of P300 registration is described in Section [2.4.1](#).

The doubtless advantage of such a system is the absence of the necessity of continuous EEG monitoring and revealing characteristic patterns connected with a change in the person’s mental state of interest with respect to the background activity which can be very diverse. In this regard, reactive neurointerfaces are characterized by fewer errors and more reliable operation, although they also usually require the BCI operator training. Using this functional scheme it is possible to implement practically all functions of the active BCI described in the previous section. The control interface converts a logical signal into a semantic control signal at a certain frequency. However, the formation of a semantic command can, in this case, be based only on the value of the current output logical signal of the converter, taking into account the discreteness of the command generation as a response to a discrete stimulation effect. The alternative approach to reduce the error likelihood is to repeat the stimulus for choosing an alternative, however this approach tires the operator and reduces the information transmission speed. As in the case of active BCI, the semantic set of commands can be dynamic and formed depending on the pre-history. The example of typical implementation of such a system is shown in [Fig. 8](#), where the character selection is performed by successive selection of pre-ensue groups of characters. As in the case of the active BCI, the operator can inform the system about errors, so that the control system can be self-learning to correct algorithms of pattern recognition in the brain activity.

### 2.3.3. Passive brain-computer interfaces

Passive BCIs are designed to monitor the brain current activity without any purposeful control by the user. They provide important information about operator’s mental condition (for example, attention, activity type, emotional state, etc.), user’s intentions and situational interpretations. Although in both passive and active BCIs the user purposefully forms commands to control a connected external device or computer system, the automated passive BCI can be used to create a unidirectional communication channel “Brain → Control Interface” based solely on the interpretation of spontaneous

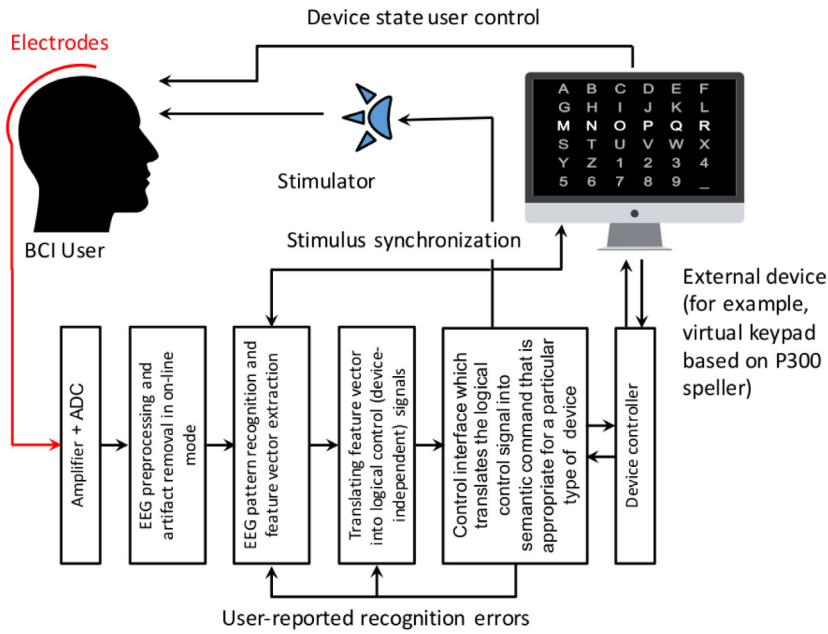


**Fig. 8.** Typical reactive BCI functional model for performing actions with virtual environment; dialing text using a virtual keyboard.

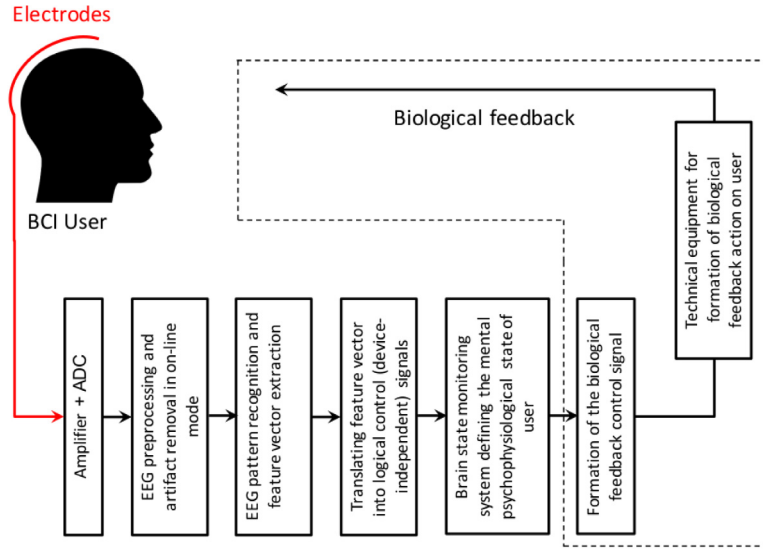


**Fig. 9.** Typical passive BCI functional model for monitoring and controlling operator's mental condition.

current brain activity of the user. This greatly simplifies the BCI functional model, but requires the creation of effective algorithms for the recognition and classification of different types of brain activity and its switching in real time.

As shown in Fig. 9, the BCI contains a system for monitoring the person's state, based on the revealed patterns of the brain activity of interest and, accordingly, on the formed feature vector which automatically interprets the mental state. The operation of this monitoring system can be strictly limited to the goals of improving the current human-machine interaction. Here, it is possible to programmatically exclude any ethically challenged approaches, such as detecting lies that also fall under control of cognitive states [149–151]. The registration and interpretation of the brain activity in the real-time automatic mode is similar to that in active BCIs.

The passive BCI can be implemented in two variants. In the first variant, the BCI monitors the operator's mental condition, fixes and uses it to set up the machine system. In the second variant, the BCI actively affects the user to maintain his/her mental state, for example, to sustain attention [152]. The functional unit of biological feedback of the passive BCI is bounded on the diagram in Fig. 9 by a dashed line. The BCI can affect the user by means of *biological feedback* or

*neurofeedback* [153,154] implemented in various ways, for example, by a visual stimulus in the form of a message on the monitor screen, sound signal, vibration, etc. [152,155]. On the other hand, the feedback can be used and affect directly the neural ensemble in the brain, bypassing standard channels of information transmission, for example, using the transcranial magnetic stimulation (TMS) [156] or transcranial electrical stimulation (tES) [157].

In this respect, visual or acoustic feedback seems inadequate for the active BCI based on motor imagery, that can explain a low performance of such BCI. The lack of the perceptual feedback depletes the information contained in the brain signals [158] and may disrupt the generation of the corresponding motor commands [159]. In this case, the intracortical microstimulation is more efficient to establish a direct input channel [160] with possible long-term stability of the neural signal generation [161]. This should eventually improve the performance of the neural interface with closed-loop feedback, as the feedback can directly affect the cortical area related to the problem being solved; this adequately closes the feedback loop.

The presented functional scheme of passive BCIs is characterized by a number of specific features which allow distinguishing them from reactive BCIs. The most important ones are as follows.

- Passive BCIs can use any number of passive detectors of different human states in parallel without any conflicts, that is almost impossible for active and reactive BCIs due to the limited ability of the user to consciously interact with several stimuli or consciously call several necessary mental states simultaneously.
- Passive BCIs can complement and/or easily be integrated into other human-machine interaction means. They can effectively operate both in presence and in absence of constant usual interaction between a person and a computer, i.e., be completely independent of the user.
- Since the use of passive BCIs (except the initial preparation of the system, attaching electrodes, etc.) does not require conscious user's efforts, the BCI determining the person's mental state with some accuracy can potentially be designed to take into account arbitrary levels of cost-effective solutions.

#### 2.4. Brain-computer interfaces applications

*BCI applications* can be described in terms of tools they use and goals they serve. Specifically, the word “BCI” refers to a HSC that registers, analyzes and transforms brain states into commands, while the word “application” denotes the environment in which the BCI commands are used. Therefore, the assessment procedures for BCI and its applications are very different.

The implementation of both active and reactive BCIs implies a new channel for communication of the operator with external devices and/or control them, without interference of peripheral nerves and muscles, instead of using keyboards, joysticks and more “exotic” equipment, such as eye trackers following a view direction, etc. Therefore, the majority of BCIs are designed for people with severe motor disorders. In the last years, significant progress has been achieved in decoding and interpreting brain activity recorded by EEG. Since EEG provides an acceptable signal quality with inexpensive, compact and easy-to-use hardware, it is widely used in most BCI applications. Thanks to the modern BCI technology, we expect that the quality of life of people with disabilities will be significantly improved. Moreover, the BCI is a potentially powerful tool for detecting hidden information in the user's brain that cannot be revealed by conventional communication channels.

The main target audience of patients with disabilities for the use of active and reactive BCIs can be divided into three groups.

- Group I includes patients with a complete loss of consciousness, i.e., patients who have lost all motor control functions due to the last stage of amyotrophic lateral sclerosis or a severe form of cerebral palsy.
- Group II includes patients with a partial loss of consciousness, i.e., almost paralyzed patients, but with residual motor control activity, for example, who can move eyes or blink, twitch lips, etc.
- Group III includes patients with remaining neuromuscular control functions, but suffering from other neural dysfunctions, such speech disorders, paresis, etc.

For the third group of patients, the use of BCI for communication tasks is inefficient, because alternative ways of human-machine interaction can provide a higher and more stable speed of information transmission. In particular, eye motion detection is faster, simpler and more accurate than detecting the modulation of brain potentials (e.g., desynchronization in a given frequency range). The speed of a set of ten words per minute can be obtained at unimpeded movement of eyes, with the help of the control technology of eye movement (eye tracker) [162]. In this regard, hybrid HSC BCIs are used to improve the performance and speed of information transmission. They are based on the combination of different types of BCIs or the combination of a BCI with other assist technologies, in particular, eye trackers, etc. [163].

It should be noted that the efficiency of the BCI application is closely related to the patient's condition. So, Kubler et al. [164] report on a strong correlation between the level of CNS physical disorders and BCI characteristics. The patients from group I practically cannot consciously manage BCI. Only patients of groups II and III are able to have a stable and conscious control of brain functions to produce a command for BCI. Fig. 10 shows the relationship between the required data transfer rate, the capabilities of the BCI operator and BCI applications available for these groups.

The BCI neurorehabilitation technology is very promising for restoration of lost motor and cognitive functions of post-stroke patients and with damaged spinal cord [165]. Such BCIs use biological feedback [166,167] for self-regulation of the brain activity by activating plasticity mechanisms underlying the neural network topology [168].

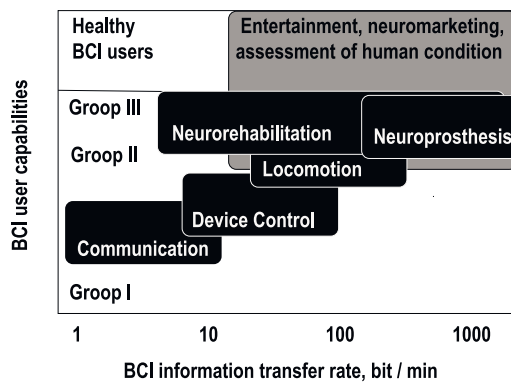


**Fig. 10.** Possible fields of neurointerface applications depending on the data transfer rate by BCI and capabilities/restrictions on the operator's health.

Another important, though less developed, application of neurointerfaces is to improve human cognitive abilities. Such a system known as a passive BCI implies the monitoring of human cognitive activity when the person solves a cognitive task followed by a noninvasive stimulation with the purpose of training his/her cognitive abilities [32]. Unlike active neurointerfaces designed for people with disabilities (e.g., paralyzed patients) to manage external devices by generating commands using characteristic patterns of neural activity [10], the main purpose of passive neurointerfaces is to improve cognitive abilities of healthy people in performing high load tasks [64,169] (top row in Fig. 10).

At present, passive BCIs are being increasingly used in neuromarketing and video games as a tool for obtaining additional information about the user's brain state (for example, emotions, fatigue, attention), that is difficult to estimate via common interfaces (see Section 7). At the same time, passive BCIs have important clinical applications for patients suffering from neurological disorders, such as schizophrenia or depression. In addition, the HSC BCI is sometimes used as an alternation to drug therapy, the way which allows suppression of epileptic seizures. Modern BCIs enable to detect pre-seizure early-warning signals in EEG and then apply an electrical stimulation to avoid or suppress the seizure [40,41,46] (see Section 6).

Currently, there are a large number of BCI applications, such as simplest word processors, adapted web browsers, mental management of wheelchairs or neuroprostheses, as well as gaming applications. However, most of the developed applications are intended solely for teaching or demonstration. Despite recent significant advances in the BCI technology, there are still many obstacles in using this technology to solve real problems [2]. The main drawbacks of the BCI technology are as follows.

1. The data transfer rate in the BCI is too low to maintain natural interaction between the technical system and its operator or other persons, even in the case of a trained operator and a well-tuned BCI (see Table 2).
2. When using a BCI, a very large percentage of incorrectly recognized commands are generated by the intelligent control system.
3. A HSC BCI cannot be used by a disabled patient alone, without assistance of classified personnel, because any BCI requires the installation of electrodes and recording equipment.
4. The operator often enables to turn out the BCI using specific brain activity as an input signal, but usually cannot turn it back on. In neuroscience, this problem is called "Midas touch" in analogy with the legend about King Midas whose touch transformed any object into gold, that did not allow him using his hands for everyday functions. Due to this problem, mental states arisen from natural brain dynamics cannot be distinguished from the states purposefully formed for interpretation as BCI commands.
5. The work with HSC BCI is a high cognitive load for the operator and can only be performed in calm laboratory conditions, but not in a real environment. Therefore, the most successful experiments on BCI applications were obtained in clinical conditions.
6. Any BCI differs from other, even similar, devices, in particular, in the way in which the neural interface performs certain functions, for example, forms a set of commands for a particular application. The ability a BCI to perform specific functions is one of its important evaluation characteristics.

Nevertheless, despite all these difficulties, the first steps toward a long-term use of the BCI at home conditions have already been made [170,171].

Consider now some BCI applications following the scheme shown in Fig. 10.

#### 2.4.1. Communication

One of the first BCI applications was the communication with patients suffering from severe neurological diseases (group II), that caused difficulties in their communication with other people. Until now, this HSC BCI application remains

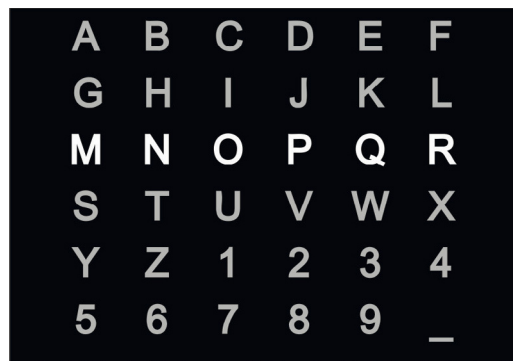


**Fig. 11.** Speller based on P300 potential recognition. The matrix of symbols displayed on the computer monitor serves as a virtual keyboard, where rows and columns of the characters blink on the screen leading to the P300 potential generation when coinciding with an expected symbol. Source: Based on [179].

most demanded, because communication is one of the basic needs for people. The application for communication purposes usually implies a virtual keyboard on the screen, where the user (BCI operator) selects a letter from the alphabet using a neural interface. The distinctive features of such a system are the BCI type (active or reactive) and a type of control signal.

At the beginning, the BCI for communication was based on the method of *common spatial pattern* (CSP) which allowed classifying multi-channel data related to hand movement imagery [172]. Later, extensions of CSP were proposed for other classification tasks [173]. The CSP method consists in the decomposition of a raw multi-channel EEG signal into subcomponents with maximum differences between populations. The goal of this method is to increase the classification efficiency by creating a spatial filter that converts the input multi-channel EEG signals into output data with selected properties of a certain class for the subsequent classification [20]. Sometimes, to improve the quality of spatial filtering, not time, but frequency or time-frequency representation of multichannel signals is used by means of spectral or wavelet signal conversion, called *common spatial-spectral pattern* (CSSP) method [174] and *wavelet common spatial pattern* (WCSP) [175,176], respectively. However, these methods require much more computational power when realizing the HSC BCI for processing multi-channel EEG in real time.

It has been shown that during intense workouts, fully paralyzed patients can reproduce positive and negative changes in the CSP to control the cursor movement in the vertical/horizontal direction [177]. Based on this type of the control signal, a device with an on-screen display, in which the cursor is used to select letters of the alphabet, was developed [25]. The tests involving two patients in the late stages of amyotrophic lateral sclerosis (ALS) showed that when writing text messages they reached a speed of about two characters per minute.

The second type of BCI for the communication task implies the approach proposed by Obermaier et al. [178], consisting in a choice of letters using the evaluation of EEG features during imaginations of hand or foot movements by the BCI operator. The system worked in such a way that the entire alphabet (in the original work it included 32 letters) was divided in half, depending on the type of motor imagery, then in half again and so on, until a particular character was selected on the virtual keyboard. The speed of writing messages, achieved by healthy users, ranged from 0.5 to 0.85 characters per minute. Although this speed is lower than in the first example, it can easily be increased by increasing the number of classes of allocated imaginary movements.

The BCI communication system based on the P300 evoked potential is more promising for disabled people. In particular, Silvoni et al. [180] demonstrated that such a BCI provides a relatively high classification accuracy for ALS patients in the early and middle stages of the disease. The advantage of this type of BCI is that the operator does not need long training, because the P300 evoked potential is generated spontaneously. Moreover, a recent success achieved by using the P300 evoked potential-based registration systems allowed their commercial applications (see, e.g., [181,182]).

Let us now illustrate the operation of such a system using the BCI principle from the widely cited paper of Farwell and Donchin [179]. In their communication system, 26 letters of the English alphabet along with several other service characters and commands are displayed on the screen in the  $6 \times 6$  matrix (Fig. 11) with randomly flashing rows and columns. The user's task is to focus on the screen and deeply concentrate attention on a symbol to be identified, while his/her EEG response is analyzed in real time. The specified character, controlled by the operator, triggers two P300 responses when the desired row or column containing the given character flashes, that allows the control system to identify it. The results of this work have shown that for healthy people, this technique provides an acceptable typing speed of about 2 characters per minute. At the same time, this approach is not free from systematic perception errors, the source of which is the occurrence of the P300 response due to the flashing rows or columns adjacent to the target symbol.

This problem was solved by using an “insular” virtual keyboard [183], based on the P300 potential response (see Fig. 12). The main idea of this approach is that the operator focuses on the flashing area with symbols instead of alternately flashing rows and columns. The selection of a required symbol is carried out in a two-level way. At the first level, the

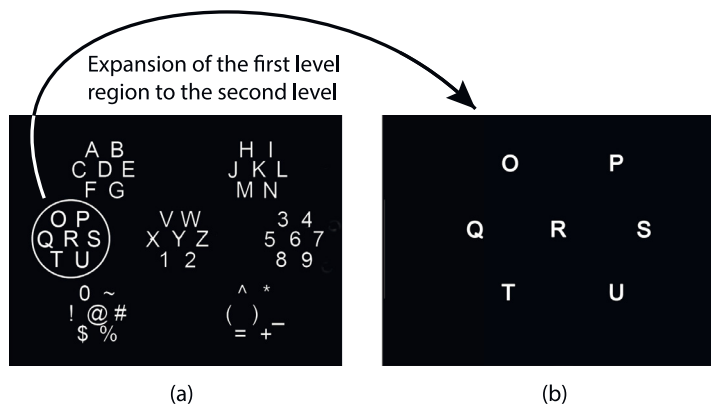


**Fig. 12.** Improved P300 speller based on the region paradigm. (a) The first level of identification, where each group contains up to 7 characters. (b) After recognition of one of the groups, the corresponding region is expanded to the second level.  
Source: Based on [183].

objects are divided into 7 groups (each containing 7 characters), which also blink randomly. The group containing the target symbol is determined by the diagnostics of the generated P300 potential. At the second level, the characters in the detected group are mixed, and the procedure of the first level is repeated, and so on, until the final choice is made.

Since the above BCI is based on the recording of events caused by visual stimuli, this technology is not appropriate for highly paralyzed patients with visual impairment or poor eye movement control. In this case, it is possible to implement audio stimulation, which makes P300-based communication systems suitable for this group of people [184–186]. An alternative method based on motor actions for communication with patients suffering from late-stage amyotrophic lateral sclerosis (ALS) was proposed by Vansteensel et al. [187]. The authors used a fully implanted BCI that consisted of subdural electrodes placed over the motor cortex and a transmitter placed subcutaneously in the left side of the thorax. By attempting to move the hand on the opposite side of the implanted electrodes, the patient accurately and independently controlled a computer typing program at the equivalent of two letters per minute.

It should be noted that a low communication rate is a key obstacle for BCI-based communication in humans. A significant advance in fast communications was achieved by Chen et al. [5], who developed a noninvasive BCI speller which allowed naturalistic high-speed communication with information transfer rates up to 5.32 bits per second. Based on extremely high consistency of frequency and phase observed between visual flickering signals and the elicited single-trial steady-state visual evoked potentials (see details in Section 4.1.2), they developed a synchronous modulation and demodulation paradigm to implement the BCI speller. Specifically, they proposed a new joint frequency-phase modulation method to tag 40 characters with 0.5-s long flickering signals and developed a user-specific target identification algorithm utilizing individual calibration data.

Considering the high efficiency of such neuroimaging method as fNIRS for classification of various mental states by registering hemodynamics in the prefrontal cortex (see Section 2.2.6), the effective fNIRS-BCI activated from the prefrontal area was created for binary communication [140,188]. The subjects had to perform a specific task, such as mental arithmetic or to imagine musics and answer mentally “yes” or “no” to the given questions. The average classification accuracy of the brain states in real time was achieved to be about 82% [140]. In another application, Sitaram et al. [142] proposed a virtual keyboard based on fNIRS-BCI which used motor imagery of the right and left hands to move a cursor on the screen to select letters.

Since Internet has become a very important part of everyday life over the past decade, we cannot fail to mention the important BCI communication application based on Internet browsers [189,190]. These BCIs, adapted for users with severe disabilities, use either CSP filters or evoked potentials. In the former BCIs, the browser interface arranges links in the decision tree in alphabetical order, so that the user can select or reject each element, making positive or negative changes in CSP [191,192]. In the latter BCIs, all parameters are represented as icons in the matrix of  $N \times N$  elements (usually  $N$  is between 6 and 8) [193,194].

In the modern world, social networking platforms are starting to be created on the basis of neurotechnologies using the registration of evoked events (P300 potential) associated with visual stimuli, for communication of patients with severe disabilities. The example is Neurochat [182], that is a communication system for networking people who do not have the ability to speak and move, people with severe neural diseases, such as cerebral palsy, ALS, stroke, multiple sclerosis, and neurotrauma (head injury, spinal injuries and others).

#### 2.4.2. Assistive technologies

One of the main goals of HSC BCI applications is to achieve maximum independence for patients with any motor impairment. Since people who suffer from severe motor disabilities often spend most of time in their homes, the BCI

applications aimed to control household appliances significantly improve the quality of life of such people. The assistive technologies based on neural interfaces reduce guardian's efforts and make the lives of relatives less burdensome.

In their pioneering paper, Cincotti et al. [195] proposed an integration framework of the BCI technology in the home environment. The BCI was tested on 14 patients with severe motor disabilities caused by progressive neurodegenerative diseases. The device provided environmental control through the interface designed to support the users with different levels of residual motor features. Depending on the severity of the motor disorder, the following facilities can be used to control appliances.

- A keyboard, mouse or joystick, using residual motor abilities of limbs.
- Head trackers and voice. Recognition microphones are available for people with weakened limbs, but with intact neck muscles and speech abilities.
- For people with complete disability, the system can be controlled by modulating sensorimotor rhythms recorded by the EEG-based BCI.

The BrainGate electrodes implanted in the primary motor cortex were used to control a cursor position on the screen. Initial tests of such an invasive BCI gave promising results when the patient could handle email applications or control household appliances, imagining limb movements even while talking [196]. At present, various methods of neurovisualisation and recognition of the corresponding EEG patterns are being considered for the application of BCI assistive technologies (see, for example, [197]).

Besides, other applications of BCI-based assistive technologies are also possible. For example, the authors of Ref. [198] suggested that BCIs can be a promising way to transfer instructions directly from the astronaut's mind to the control command of the equipment without physical motion or relying on the peripheral nervous and motor systems.

#### 2.4.3. Movements

The BCI applications which allow people with disabilities to control vehicles are definitely very important. Thanks to these applications, people suffering from paraplegia can independently manage a wheelchair, making them more autonomous and improving quality of life. An important condition for the use of such systems is their compactness, that can be ensured by using a EEG-based BCI. The disadvantage of this system is that EEG signals usually contain many artifacts, a high level of noise and strong variability. During long intervals between BCI commands, these artifacts lead to high uncertainty and false alarms. Therefore, the important tasks of the BCI technology are sufficiently high classification accuracy and the possibility of real-time control, in spite of extremely slow transfer rates of data provided by BCIs (see Table 2). In some cases, it is preferable using invasive methods for recording EEG signals, that allow achieving better spatial resolution and signal-to-noise ratio. For example, the experiments with monkeys [199] showed that the monkey could managed to move a cursor to any position on the screen, using signals recorded by the electrode matrix implanted into the motor cortex.

At the same time, noninvasive BCIs are more convenient for human's use, taking into account risks of the invasive intervention techniques. The first noninvasive EEG-based BCI for controlling a wheelchair was introduced only in 2005 [200]. In that study, the floor surrounding the wheelchair was divided into squares, between which the user decided to move, imagining movements of the left and right hands. As a result of the user's decision, the wheelchair moved from one square to another. The tests with six healthy subjects demonstrated the viability of the wheelchair control solely via the EEG signals. Later, the wheelchair control system was modified by including the automatic assessment of environmental conditions (in particular, obstacles) and the HSC allowing a high speed of information transfer based on the P300 potential and mu/beta rhythms [201–204].

#### 2.4.4. Neuroprosthetics

Spinal cord injury, as well as other neurological diseases, associated with a loss of sensory and motor functions, drastically reduce the quality of life of the patients. Even partial restoration of motor functions can improve their psychological state and social situation. The restoration of some motor functions, for example, the ability to take objects, gives paralyzed patients the possibility to use neuroprostheses controlled by functional electrical stimulation (FES) [205], which compensates the inability to implement motor functions, by causing artificial muscle contractions. Electric currents generate artificial action potentials by depolarizing intact peripheral motor nerves, which innervise the target muscle and cause its contraction [206]. In 1999, Lauer et al. [207] reported on the first EEG-based BCI enable to generate a control signal for FES.

Thanks to the combination of BCI and FES, in 2003 Pfretscheller and colleagues [208] developed a BCI which can help paralyzed patients, having traumatic injury of the spinal cord, to control their paralyzed limbs, so that the patient was able to take a cylindrical object (e.g., a glass with water). The control command in this BCI was generated from beta-wave EEG activity due to motor imagery, that was classified by the BCI, which output was then used to control the FES device to activate the limb. Furthermore, Ajiboye et al. [12] reported about a combined implanted FES and invasive BCI neuroprosthesis for restoring both reaching and grasping movements of people with chronic tetraplegia due to spinal cord injury. The participant was able to cortically control single-joint, and coordinate multi-joint arm movements for point-to-point target acquisitions (80%–100% accuracy), using firstly a virtual arm and secondly his own arm animated by FES.

Using the paralyzed arm, the participant voluntarily performed self-paced reaches to drink a mug of coffee, successfully completing 11 of 12 attempts within a single session.

The disadvantage of such a system is the fact that the use of FES presupposes the possibility of limb movements, impossible for patients with severe injuries. For this reason, in some cases, HSCs were developed to combine neuroprostheses and BCI without the use of FES. It was shown that a paralyzed patient whose residual muscular activity of upper limbs was confined to left biceps due to an injury to the upper spinal cord was able to effectively control the right-hand orthosis using changes in the dynamics of the EEG signal observed due to motor imagery of different movements [209]. The disadvantage of this method was the need for a prolonged training. Later, it was shown that it is also possible to classify motor imagery in non-trained subjects [62,145].

At present, we can undoubtedly state that the BCI is a very promising option for controlling neuroprostheses [210,211]. Here, the rehabilitation problem of patients with paresis after brain injury (e.g., after stroke) is of particular interest for BCIs which use imaginary movements of limbs to assist an exoskeleton [10,212–214]. Another promising way to control neuroprostheses is the use of electrical activity of muscles and electromyography (EMG) [215,216] for neurorehabilitation [217].

#### 2.4.5. Neurorehabilitation

HSC BCIs are widely used for the recovery of some lost motor and/or cognitive functions in people with stroke and damaged spinal cord [165,218,219]. The basic idea of neurorehabilitation is the ability of biological feedback implemented by the BCI to regulate brain activity. Among different neuroimaging methods, EEG is the most common neurocontrol technique, due to its high temporal resolution, simplicity, affordability and a relatively low price [167].

A significant success in neurorehabilitation using BCI was made for patients after stroke. Stroke is the main cause of disability in the US and Europe [220]. The usual consequences of stroke are hemiparesis and hemiplegia, that lead to a deficiency of movements of one side of the body, contralateral damaged hemisphere. The main clinical symptoms of these diseases are muscle weakness, abnormal muscular tone, incorrect posture adjustment, reduced mobility, lack of coordination and sensitivity. As a result of the stroke, about 50% of patients remain permanently in wheelchairs [221]. The spinal cord injury usually leads to the inability to walk independently and perform basic motor functions for self-sustaining daily needs. Thus, the main goal of the rehabilitation of post-stroke patients is to restore lost functions, return their independence and integrate them into the social life. Thanks to BCIs, people can control auxiliary devices (orthosis, exoskeleton), as well as restore motor functions by activating plastic mechanisms aimed at changing the brain neural network topology [168]. In the recent paper, Orlov et al. [222] reported on the use of the EEG-based BCI to restore the vestibular function needed to maintain equilibrium in the movement.

The disadvantage of using EEG with implemented biological feedback for neurorehabilitation is its low spatial resolution and, as a result, inaccurate localization of activity sources, as well as unavailability of subcortical areas. To overcome these problems, hemodynamic brain activity was measured using fMRI [223,224] and fNIRS [133]. For example, in 2012 Michara et al. [166] demonstrated the possibility of the fNIRS-based neurocontrol to deliberately regulate the user's hemodynamic reactions. Such neurocontrol strengthened hemodynamic correlates related to motor imagery. Later, the researchers from the same group implemented a similar neurocontrol for post-stroke patients [225]. The fNIRS-based neural feedback was also successfully used for long-term learning.

While repetitive neurocontrolled communication activates specific brain areas, false feedback causes diffuse patterns in a large brain area. The significant disadvantage of hemodynamics (fMRI and fNIRS) in neurocontrol is the latency in the brain response, that makes command generation much slower than when using EEG (see Section 2.2.6). However, in the case of fNIRS this drawback can be eliminated if instead of hemodynamics, a decrease in HbO and an increase in HbR are taken into account [131].

#### 2.4.6. Assessment of human conditions using passive brain-computer interfaces

Unlike active and reactive BCIs, the main users of passive BCIs are healthy people. The primary aim of passive BCIs is to increase cognitive abilities of the user while performing difficult cognitive tasks. In addition, passive BCIs are basic parts of neurosystems for monitoring, controlling and training psychophysiological states, such as attention, cognitive fatigue, and emotions. For example, passive BCIs can increase the operator's attention span [226,227]. Passive BCIs can also be used in medical practice for diagnostics and treatment of some neurological diseases, e.g., to predict and suppress epileptic seizures. Such systems include passive BCIs and biological feedback to deliver neural stimulation [41,228] (see Section 6).

The most common application of passive BCIs is neural activity monitoring to detect different mental states, e.g., attention and fatigue. According to recent neurophysiological studies [229], these mental states are associated with specific characteristic structures of evoked potentials (e.g., P300). At the same time, different mental states are characterized by similar neurophysiological activity, that complicates their detection in EEG. For example, 4–8 Hz fluctuations in the frontal cortex can be associated with both high cognitive load and fatigue [230]. Therefore, cognitive state monitoring by passive BCIs requires powerful methods of neurophysiological data analysis [231].

It is important to note that passive BCIs are already successfully used to monitor driver's cognitive status [232,233], workload [234], degree of attention [235] and fatigue [236]. Along with drivers, passive BCIs are used in aviation to monitor

psychophysiological conditions of pilots [237] and dispatchers [238]. The interesting direction of using passive BCIs is monitoring cognitive status of students or schoolchildren during a learning process [239].

Along with mental state monitoring, passive BCIs can be used to estimate emotional states. According to the recent review [240], emotional states can be detected by analyzing EEG signals, for example, based on the frontal EEG asymmetry and induced synchronization/desynchronization. The approaches based on the EEG analysis allow recognizing up to six emotions [241]. For instance, Jatupaiboon et al. [242] offered systems allowing real-time recognition of happy/unhappy emotions caused by pictures or music.

In the context of emotional state recognition, we divide passive BCIs into two classes, for patients and for healthy people. Passive BCIs for medical applications estimate emotional states using special scales [243,244] and enable diagnose several neural disorders, including depression [245,246], schizophrenia [247,248] and Parkinson disease [249]. Among non-medical applications, active BCIs are used in such areas as entertainment, gaming and emotional state monitoring [240]. The last application includes the study of the influence of various external stimuli and personal features on emotional states [250]. In the context of entertainment, the main purpose of passive BCIs is to detect and analyze the emotional response to the entertaining content (music and video) [251,252]. In the gaming industry, passive BCIs are aimed at real-time detecting the player's emotional state in order to automatically adapt the game conditions [253].

As mentioned above, passive BCIs, besides monitoring, can manage brain activity using biological feedback. Along with controlling epileptic activity, this technology is also important for healthy people in the context of training and enhancing their cognitive abilities [254].

### 3. EEG preprocessing methods for brain-computer interfaces

Not only electrical activity of a neural ensemble, but also various physiological processes occurring in the body have an inevitable impact on the resulting EEG signal. External interference cannot also be excluded from consideration. The sources of external electrical signal include an accumulated static charge, bad contacts of registering electrodes, environmental noise, etc. Noise in the EEG signal can significantly be reduced by ensuring good electrode contacts and shielding techniques for electrical equipment.

The EEG signal artifacts usually have physiological nature and caused by various non-stationary processes. In addition to brain activity occurring in the body during EEG registration, these processes include eye movement, cardiorhythm, activity of facial and cervical muscles, etc. Most of the EEG artifacts have a significant amplitude, exceeding in many cases the carrier electrical activity of the neuron ensemble. In addition, many artifacts lie in frequency ranges where patterns for classification commands occur. Indeed, ophthalmic, cardio and muscular activity artifacts are detected in the range of 0.5–15 Hz, which covers three important high-informative bands (delta, theta and alpha), often used in the analysis of EEG and MEG data. Therefore, artifacts and their strong variability considerably complicate the time-frequency analysis of EEG signals, that makes preliminary filtration of EEG signals very important for any BCI application.

In Fig. 13 we present experimental human EEG signals containing the most typical oculomotor artifacts (Fig. 13(a)), cardiorhythm (Fig. 13(b)), and muscle activity artifacts (Fig. 13(c)) [255]. These signals were recorded using the electroencephalograph "Encephalan-19/26" (Medic-MTD, Taganrog, Russia) having a standard electrode arrangement scheme (10–20 international system) [76] operating at a sampling rate of 250 Hz, certified for medical use in Russia, CIS countries, EU and UK. The EEG was filtered by highpass and lowpass filters of 0.016 Hz and 70 Hz, respectively, and a 49.5–50.5 Hz bandpass filter to eliminate electromagnetic interference caused by a power system network. In this experiment, the subjects performed standard physiological tests.

Methods for removing artifacts from EEG signals are based on various approaches for signal decomposition and transformation, for example, independent component analysis and its modifications [256–258], regression analysis [259], and empirical mode method [255,260]. All these methods have a fairly high accuracy of artifact selection and a small distortion of the EEG signal structure.

#### 3.1. Independent component analysis and its modifications

Many researchers have paid attention on the development of methods for removing ophthalmic artifacts, which significantly distort EEG signals in the frontal brain area, where, in the first approximation, neural activity signals and artifacts were considered as uncorrelated processes [261,262]. To suppress these artifacts, Bell and Sejnowski [263] proposed an approach based on the *independent component analysis* (ICA). Later, different modifications of this method were developed by other scientists [257,264,265]. The ICA method divides the EEG signal into statistically independent components so that the components responsible for artifacts can later be eliminated.

At the same time, the effective removal of eye-sight artifacts requires information about eye movements obtained by electrooculogram (EOG) and the combination of two procedures: (i) linear subtraction of the EOG signal from EEG using empirically selected weights depending on the distance of the EEG channel from the place of the EOG registration, followed by the selection of EEG fragments containing artifacts, and (ii) deleting manually EEG fragments containing the artifacts. However, these procedures are rarely used in everyday practice because of their high computational complexity, as well as a high risk of error determining the time of the artifact occurrence. In addition, there are great difficulties in adapting these methods to operate in real time [259]. Also, several researchers [146,266] noted that the ICA can lead to

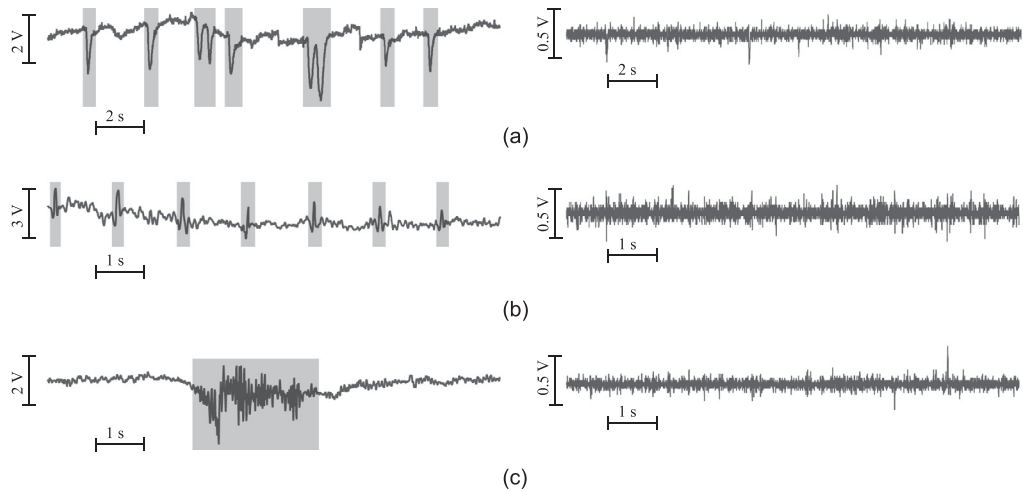


**Fig. 13.** (Left panel) Experimental EEG trials containing typical artifacts of three types: (a) oculomotor, (b) cardiorhythm, and (c) muscle activity with artifacts indicated by shaded frames. (Right panel) The same EEG trials with removal artifacts using the empirical mode method.  
Source: Based on data from [255].

the distortion of the actual neural activity power spectrum. Although this is not an obstacle to the BCI creation, this can change essential features of brain state properties.

The ICA method is based on three main assumptions.

- Experimental data is a collection of uncorrelated processes of neural activity and artifact sources.
- Superposition of potentials from different brain parts at the electrode location is linear, and the duration of the signal propagation from the source to the electrode is negligible.
- The number of sources does not exceed the number of electrodes.

The ICA assumes that  $K$  of simultaneously recorded EEG signals  $X(t) = \{x_1(t), \dots, x_K(t)\}^T$  is a linear combination of  $N$  ( $N \leq K$ ) initially unknown independent components (sources)  $S(t) = \{s_1(t), \dots, s_N(t)\}^T$ , including neural activity processes, and artifacts, i.e.,

$$X(t) = MS(t), \quad (1)$$

where  $M$  is a matrix of unknown elements defining a weight input of each source into the recorded EEG signal. In the ICA method,  $S(t)$  and  $M$  are defined directly from  $X(t)$  using the algorithms proposed by Amati et al. [267] and Lee et al. [268], which use neural networks that maximize the joint entropy and minimize mutual information on output components of a neural processor.

After the algorithm was applied, the temporal structure and spatial dynamics of the  $S(t)$  component were analyzed, and components which took into account artifacts were identified among them. These components were then zeroed out, and a new  $\hat{S}(t)$  matrix was formed with the removed artifact sources. For example, if the first component contains artifacts, then  $\hat{S}(t) = \{0, S_2(t), \dots, S_N(t)\}^T$ . At the final stage, the EEG signals “purified” by the ICA method were reconstructed as

$$\hat{X}(t) = M\hat{S}(t). \quad (2)$$

Bell et al. [263] proposed to zeroed the components which contain artifacts, forming a new matrix  $\hat{S}(t)$ . After deleting the artifacts sources with the help of ICA, the “pure” EEG signals were reconstructed.

This approach, however, raises a number of difficulties related to the fact that, while the EEG is processing, independent components including sources of artifacts are often associated with neural activity which can “penetrate” the component due to a limited maximum number of independent sources or other reasons [269]. The removal of such a component means the loss of a part of neural activity and, as a consequence, the distortion in the EEG representation [270].

In Fig. 14 we present the example of such a situation [258]. The signal from the frontal EEG contains two eye-trapping artifacts, i.e., the first independent component  $s_1(t)$  contains two artifacts. In accordance with *a priori* assumptions, this component may not include other artifacts, independent of eye movements. This component can be divided into high-amplitude artifact  $A(t)$  (Fig. 14(b)) and low-amplitude neural signal  $\eta(t)$  (Fig. 14(c)) as follows

$$s_1(t) = A(t) + \eta(t). \quad (3)$$

Within the standard method, the  $s_1(t)$  component is zeroed before the reconstruction of a purified EEG signal, while the part of neuronal activity is lost. The resulting signal is

$$\hat{x}_j(t) = r_j(t) - m_{j1}\eta(t), \quad (4)$$

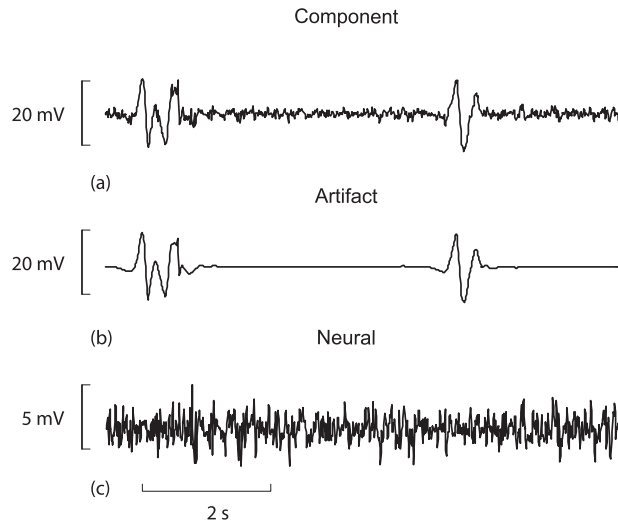


**Fig. 14.** Decomposition of the independent component into two components related to the artifact and neural activity (see Eq. (3)). (a) Independent component  $S_1(t)$  allocated by the ICA method demonstrating two eye blinking events (around 0.8 s and 5.5 s). (b) Two artifacts  $A(t)$  associated with blinking. (c) Neuronal activity  $\eta(t)$  with removal artifacts.

Source: Based on data from [258].

where  $r_j(t) = x_j(t) - m_{j1}A(t)$  is the signal with resolved artifact and  $m_{j1}$  is the corresponding weighting coefficient of matrix  $M$ .

If we could isolate the neuron component of the signal  $\eta(t)$  from  $s_1(t)$ , then it would be possible to reconstruct the filtered EEG record. Since the initial decomposition of the independent component  $s_1(t)$  into two components (Eq. (3)) is unknown, we can separate these components using the signals  $A(t)$  and  $n(t)$  properties. So, the artifact  $A(t)$  is characterized by a high power and can be localized in time and frequency, while the signal  $n(t)$  has a lower amplitude and a wider spectrum (see Fig. 14). These EEG signal features allow their separation in time–frequency representation using a wavelet transform, well suited to study complex processes with time-varying characteristics and widely used for time–frequency analysis of EEG data, especially for non-stationary signals which include a variety of oscillatory patterns with significantly different waveforms and frequencies [271].

*Continuous wavelet transform* (CWT) is a widely accepted method for the time–frequency analysis of multimodal nonstationary processes [271–276]. During the last decades, this method was effectively used for the analysis of experimental biological data providing essential information about complex dynamics of physiological systems. In the case of multi-channel EEG/MEG recordings, the wavelet spectrum is calculated for each channel  $X_n(t)$  in the frequency range  $\Delta f$  of interest [258,277]. In general, the complex-valued wavelet coefficients can be numerically found as [271]

$$W_n(f, t) = \int_{t-4/f}^{t+4/f} X_n(t) \psi_{f,\tau}^*(t) dt, \quad (5)$$

where  $n = 1, \dots, N$  is the EEG/MEG channel number ( $N$  being the total number of channels used for the analysis) and “ $*$ ” denotes the complex conjugation. The wavelet basis  $\psi_{f,\tau}(t)$  is constructed as

$$\psi_{f,\tau}(t) = \sqrt{f} \psi_0(f(t - \tau)), \quad (6)$$

where  $\psi_0(\eta)$  is the mother wavelet function, and  $f$  and  $\tau$  represent the frequency and translation parameter, respectively.

An important issue of wavelet analysis applications for data processing is the choice of the mother wavelet function, because the CWT properties are strongly dependent on the mother wavelet specific type. For example, the complex Morlet wavelet provides an optimal relationship between spectral and temporal resolutions and can be successfully used to analyze a fine time–frequency structure of complex non-stationary neurophysiological signals [258,278–282].

The complex mother Morlet wavelet [283] is defined as

$$\psi_0(\eta) = \pi^{1/4} e^{j\omega_0\eta} e^{-\eta^2/2}, \quad (7)$$

where  $\omega_0 = 2\pi$  is the central frequency of the Morlet mother wavelet.

Among other types of the mother wavelet function, we should mention the popular real wavelet called *Mexican hat* (MHAT)<sup>3</sup> mother wavelet, the analytical form of which is given as [284]

$$\psi_0(\eta) = (1 - \eta^2)^2 e^{-\eta^2/2}. \quad (8)$$

<sup>3</sup> This name arose from the sombrero-like shape of a 2D-image processing kernel.

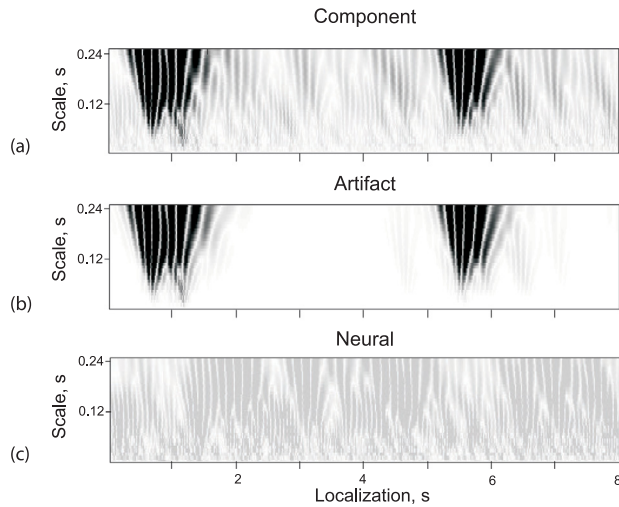


**Fig. 15.** CWT results using (a) mother MHAT wavelet independent components  $s_1(t)$  and their constituent parts related to (b) artifacts and (c) neural activity. The presented results correspond to the data shown in Fig. 14.

Source: Based on data from [258].

Although the wavelet spectra obtained by means of the MHAT wavelet have a low frequency resolution, they represent sharp peaks, because any EEG event with a sharp waveform produces intense amplitude bursts in the frequency range of interest. The disadvantage of real wavelets is the difficulty in the determination of main frequencies, since maxima/minima of the wavelet surface correspond to an increase/decrease in the EEG amplitude. The advantage of the real MHAT wavelet is its high time resolution that allows tracking a rapid increase in the wavelet spectrum power and the time when the examined rhythm appears in the EEG.

Next, we present the results of time-frequency analysis using the complex Morlet or real MHAT mother wavelets or their modifications.

Since the first independent component  $s_1(t)$  is the sum of the two terms of Eq. (3), its CWT, due to its linearity, also represents the sum:

$$W_s(a, b) = W_A(a, b) + W_n(a, b), \quad (9)$$

where  $W_A(a, b)$  and  $W_n(a, b)$  are wavelet conversion ratios of the signals  $A(t)$  and  $n(t)$ , respectively. As mentioned above, the artifact dynamics is characterized by relatively large coefficients and their localization in a specific time-frequency region, while neural dynamics reveals itself in a wider range of scales and has significantly less energy. This situation is illustrated in Fig. 15, where we plot the results of CWT with the mother MHAT wavelet defined by Eq. (8) of three signals shown in Fig. 14.

The wavelet spectral fragments, where large-amplitude dynamics dominates, clearly visible in Fig. 15, are associated with artifacts characterized by short times and relevant large-scale areas. At the contrary, neural dynamics is characterized by a more homogeneous distribution of the wavelet coefficients which are relatively small. In this regard, the procedure of the artifact removal can be carried out by the threshold filtration, when the wavelet coefficients, exceeding the threshold and therefore describing the artifacts, are zeroed, and then, the reverse wavelet transform is performed. Note that this procedure is much easier and faster for a discrete wavelet transform, though the CWT yields better results. The procedure of revealing neuronal activity is very similar to the noise filtration using wavelets [285]. However, our goal here is different, namely, we need to separate a useful small broadband signal from more energetic artifacts.

The proposed method of the artifact removal implies the following sequence of actions.

- Application of standard ICA to EEG data to obtain weight matrix  $M$  and temporal dynamics of independent components  $\{s_1(t), s_2(t), \dots, s_N(t)\}^T$ .
- Conducting a direct wavelet transform component  $s_i(t)$  to obtain coefficients  $W(a, b)_i$ .
- Empirical introduction of a threshold value  $W^*$  and zeroing coefficients which exceed the specified threshold level  $W(a, b) = 0$  if  $|W(a, b)| > W^*$ .
- Carrying out an inverse wavelet transform to obtain corrected components reflecting only neural dynamics  $\{n_i(t)\}$ .
- Receiving corrected EEG signal  $X^*(t) = M \cdot (n_1(t), \dots, n_N(t))^T$ .

The selection of an appropriate threshold value  $W^*$  is important within this algorithm. Debhath et al. [286] discussed of how to choose a suitable threshold and proposed an algorithm for automatic artifact identification. Their recommendations can effectively be applied in practice to adjust algorithms for best artifact removal.

We should also mention that the wavelet enhanced ICA (wICA) method [287] allows removing artifacts associated with eyes blinking and heartbeats. At the same time, wICA introduces significantly less distortion to neural activity signals in brain areas not affected by the artifacts. However, the wICA method is very difficult to apply for the analysis and real-time processing of a multi-channel EEG because of a very high computational cost required for forward and backward wavelet transforms.

### 3.2. Removing artifacts using Gram–Schmidt transformation

The efficient and easy technique for removing oculovigatory artifacts is based on the Gram–Schmidt transformation (GST) [288,289]. It is known that eye movements are accompanied by changes in the electrical potential because the eyeball has an electric distal moment due to the difference of potentials between the eye's retina and cornea [269,290–292]. The form of EEG ophthalmic artifacts depends on the eyeball motion type in the horizontal/vertical plane in the presence/absence of the rotational torque. According to this, the oculovigatory artifacts can be divided into several types [259,269]. EEG signals recorded in subjects with open eyes can be represented as a linear combination of signals of the brain electrical activity and disturbances caused by eye movements in the vertical and horizontal directions [291,293]. In this case, the removal of interference (eye-to-mouth artifacts) can be done by mathematical conversion of the EOG and EEG signals using the Gram–Schmidt orthographic method [294] which consists as follows.

Let  $x_i(t)$  be the EEG signal from an  $i$ th channel and  $c_v(t)$  and  $c_h(t)$  are the EOG signals containing information about vertical and horizontal eye movements, respectively. These signals are subjected to the orthogonality Gram–Schmidt procedure as

$$x'_i(t) = x_i(t) - c_v^0(t) \int_{t_1-T}^{t_1} c_v^0(t') x_i(t') dt', \quad (10)$$

$$\tilde{x}_i(t) = x'_i(t) - c_h^0(t) \int_{t_1-T}^{t_1} c_h^0(t') x'_i(t') dt', \quad (11)$$

where  $\tilde{x}_i(t)$  is the signal cleared from eye-testing artifacts,  $t \in [t_1 - T, t_1]$  ( $t_1$  and  $T$  being the currently logged time and the duration of the interval to convert, respectively). The signals  $c_v^0(t)$  and  $c_h^0(t)$  are normalized “support” EOG signals corresponding to vertical and horizontal eye movements, respectively, defined as [257,293]

$$c_v^0(t) = \frac{c_v(t)}{\|c_v(t)\|}, \quad c_h^0(t) = \frac{c_h(t)}{\|c_h(t)\|}, \quad (12)$$

$$\|c_{v,h}(t)\| = \sqrt{\int_{t_1-T}^{t_1} (c_{v,h}(t))^2 dt}. \quad (13)$$

**Fig. 16** shows the original EEG signals with artifacts (left-hand traces) and without them (right-hand traces) after removing procedure from different EEG channels. To remove eye-moving artifacts caused by horizontal/vertical eyeball movements and blinking, the Gram–Schmidt orthogonality procedure described in Eqs. (10)–(13) was applied in real time. The eye movement artifacts, as seen in the figure, are more pronounced in the frontal area.

The GST method provides a very high accuracy of the artifact selection efficiency and a small distortion of the EEG signal structure, both for processing of prerecorded signals and for real-time operation [295]. A remarkable feature of the GST is that the orthogonality procedure does not change the EEG signal shape. The efficient real-time artifact removal was experimentally achieved for  $T \in [1.5, 5]$  s [288,296].

### 3.3. Removing artifacts using empirical mode decomposition

The disadvantage of the above methods is the need for the joint analysis of EEG together with other physiological signals containing information about certain types of artifacts. Therefore, the use of these methods requires recording additional signals, that is not always convenient when creating HSC BCIs, because this leads to the increasing cost and design complication, as well as to the inconvenience for the system user. Therefore, the creation of efficient methods for artifact detection and removal, not distorting the EEG structure and at the same time not requiring additional physiological signals is the important task of modern neurophysiology. One of such methods is based on the signal decomposition by empirical models. Although this method does not require the registration of additional physiological signals, it involves additional presetting [255,255].

*Empirical mode decomposition* (EMD) is a part of the Hilbert–Huang transformation, one of the modern methods of time-frequency analysis of nonlinear non-stationary signals [297–299]. This method allows presenting the investigated signal in the form of a set of amplitude-modulated components with zero average, so-called *empirical modes*. The decomposition procedure of the investigated signal  $x(t)$  on empirical models implies the following algorithm.

- (i) Find all extrema (minima and maxima) of the signal  $x(t)$  under study.
- (ii) Interpolate the signal between minima and maxima and plot two matching envelopes,  $e_{\min}(t)$  and  $e_{\max}(t)$ .

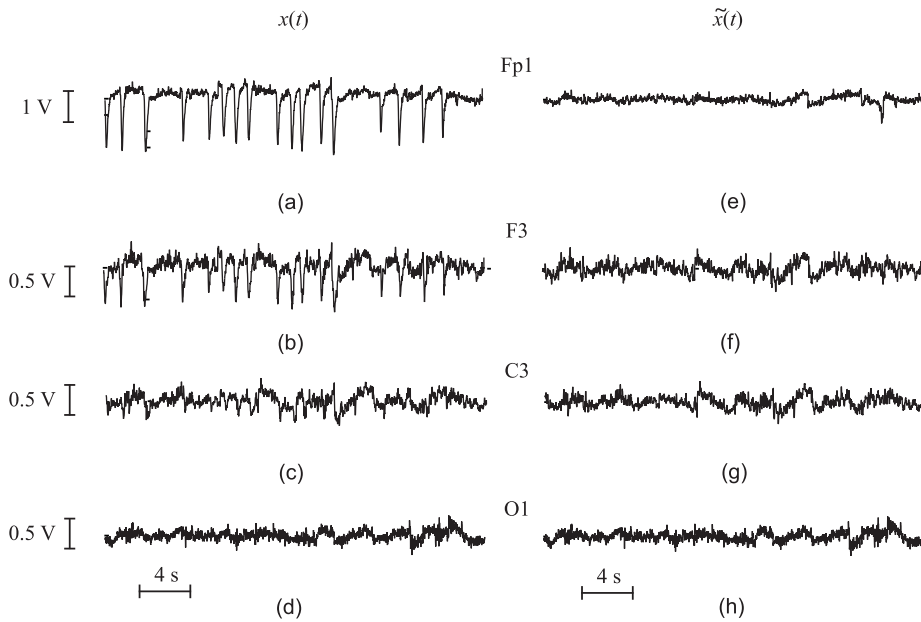


**Fig. 16.** Typical EEG fragments detected in (a,e) frontal area (Fp19), (b,f) motor cortex (F3), (c,g) parietal area (C3), and (d,h) occipital area (O1). (a–d) Original EEG records. (e–h) Real-time EEG signals with removed ocular artifacts.

- (iii) Calculate the low-frequency component of the signal (trend) as the average of the two envelopes,  $m(t) = [e_{\min}(t) + E_{\max}(t)]/2$ .
- (iv) Calculate the high-frequency component of the signal (empirical mode) as the difference between the initial signal and the trend,  $d(t) = x(t) - M(t)$ .
- (v) Repeat steps (i)–(iv) for the trend  $m(t)$  instead of the original signal  $x(t)$  to find the next empirical mode, etc.

From the viewpoint of the time–frequency analysis, EMD considerably differs from the majority of methods of signal analysis. The basic functions, on which decomposition is made, are not specified beforehand (as, for example, in Fourier or wavelet analysis), and defined in the course of decomposition from the investigated signal. The total number of empirical modes and the time–frequency characteristics of each individual mode depend directly on the signal being investigated. This property makes EMD a highly adaptive signal analysis tool. The first empirical mode in the decomposition has the highest frequency, which decreases as the ordinal number of empirical modes increases. Recent studies [260,300] show that in many cases different empirical modes correspond to different characteristic oscillator patterns in EEG signals, according to their frequency composition. Thus, the time–frequency analysis and highlighting specific oscillator patterns (including artifacts) can be reduced to the analysis of one or more empirical modes of the EEG signal.

The artifact selection algorithm includes the following four stages.

- Decomposition of the investigated EEG signal to the set of empirical modes.
- Finding empirical modes containing physiological artifacts.
- Removal of empirical modes containing physiological artifacts.
- Restore of the EEG signal from the remaining empirical modes.

In the case of real-time selection, the second stage is carried out at the preliminary stage of the method configuration.

An important step of the algorithm is a search for the decomposition of those empirical modes that contain artifacts. This procedure is performed with the help of the CWT [271]. For this purpose, on the source EEG signal and all empirical modes the same small segment containing a typical artifact is chosen. From clinical practice and EEG research, it is known that most of physiological artifacts have specific frequency and temporal characteristics, such as frequency range, main frequency, duration, wave form, etc. These properties together create a characteristic time–frequency pattern on the wavelet spectrum for each artifact type. For example, in the case of ophthalmic artifacts, on the wavelet spectrum there is a sharp increase in the wavelet energy in the frequency range of 0.5–5 Hz for about 300–500 ms. Therefore, for the EEG segment the wavelet spectrum is built, on which the time–frequency artifact pattern is determined (see Fig. 17(a)). It is believed that an empirical mode contains the desired type of artifacts, if its wavelet-spectrum has an image of this artifact (cf. Fig. 17(b–d)). This stage can easily be automated by comparing time–frequency characteristics (wavelet spectra) of the empirical mode. Further, all empirical modes, on which the presence of artifacts were discovered are removed from consideration (2nd and 3th modes in the considered example), after which the EEG signal is restored.

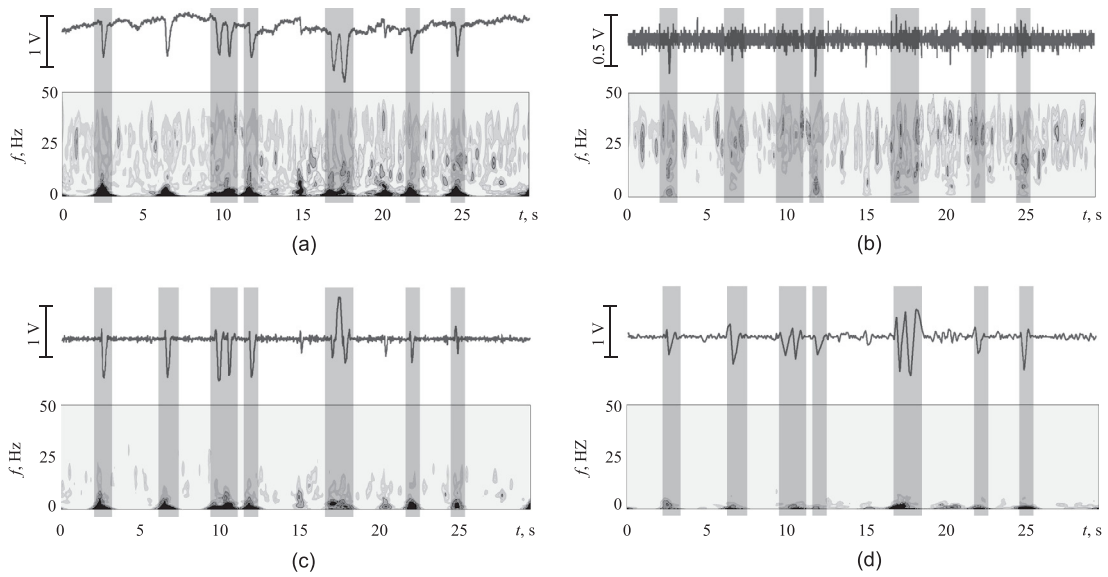


**Fig. 17.** The example of empirical mode decomposition. (a) The EEG signal with several eye-moving artifacts and (b,c) first three empirical modes for it. The signal time-frequency structure is illustrated by the wavelet spectrum with the mother Morlet-wavelet. Artifacts are marked with shaded frames.

For this, the remaining empirical modes which do not contain artifacts are summarized as

$$U(t) = \sum_{p=1}^{N, p \neq n_1, n_2, \dots} m_p(t), \quad (14)$$

where  $U(t)$  is the recovered EEG signal,  $m_p(t)$  is empirical modes,  $p$  is a current mode number,  $N$  is the total number of empirical modes,  $n_1, n_2, \dots$  are empirical mode numbers containing artifacts. The result of the proposed method is the recovered EEG signal with removed physiological artifacts.

The results of the EMD method are presented in the right-hand panels in Fig. 13, which show the EEG signals after filtration. One can see that for each case the artifacts are removed during the filtering process. It should also be noted that the low-frequency envelope of the EEG signal, which does not contain useful information, is also removed after the application of the EMD method. Thus, the EMD method can be used not only to remove different types of physiological artifacts in the EEG, but also for filtering some noise components.

The efficiency of the method can be quantitatively estimated as the signal spectrum distortion after filtration [255]:

$$\gamma = \frac{1}{E} \int_{\Delta f} \int_0^{\tau} |W(f, t) - W_{EM}(f, t)| dt df, \quad (15)$$

where  $W(f, t)$  is the amplitude of the wavelet spectrum of the EEG signal before filtration,  $W_{EM}(F, t)$  is the amplitude of the wavelet signal spectrum of the EEG after filtration by the EMD method, normalized to the averaged wavelet spectrum amplitude  $E$  of the original signal. During  $\tau = 600$  s EEG recording of the subject in a rest state, 95 eye-moving artifacts with the amplitude from 1 to 4 V were detected. The calculations yielded  $\gamma < 10^{-2}$  and hence, the distortion of the EEG signal caused by the EMD procedure and the artifact removal can be considered insignificant.

The undoubtedly advantage of the method is its ability to remove artifacts only using EEG signals without registering additional physiological artifacts. The last two methods are mainly used for real-time signal preprocessing. Fig. 18 shows the result of a special algorithm for removing real-time eye-moving artifacts, muscle artifacts caused by jaw movements, and cardiorhythms, using the GST and EMD methods, for all 19 EEG channels.

#### 4. Brain activity pattern recognition and classification in multichannel data

The main goal of BCIs is to recognize and translate brain activity into a command for a technical system without any peripheral muscular activity. To achieve this goal, different physical characteristics and methods can be used to identify EEG patterns of the brain activity. The performance of the pattern recognition depends on both personal features and classification algorithm employed. In this section, we focus on the selection and classification of the EEG patterns related to brain activity.

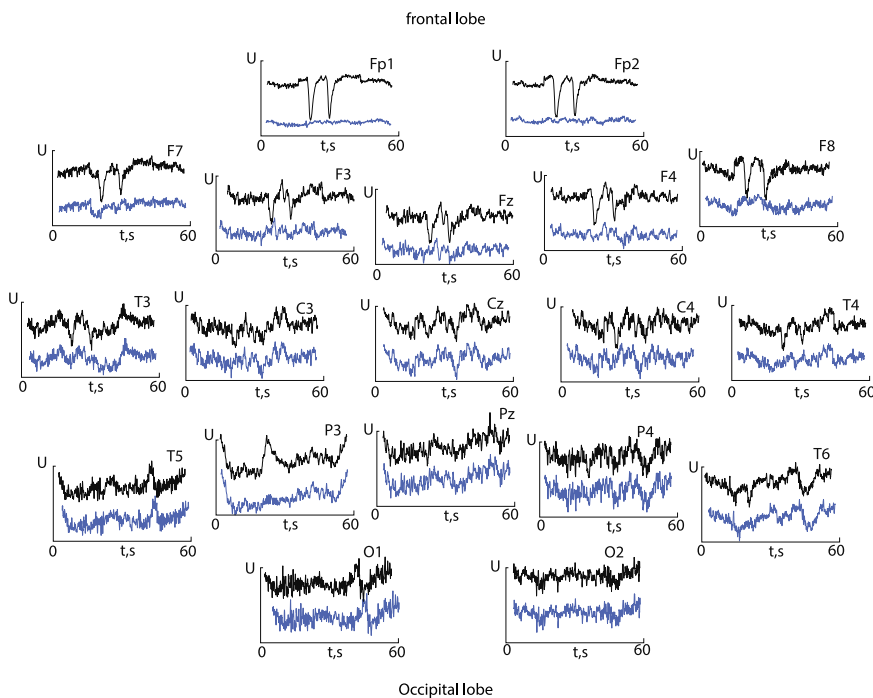


**Fig. 18.** Results of physiological artifact removal (eyes, jaw muscles and cardiorhythms) during a wake state with open eyes, obtained using a standard 10-20 EEG arrangement. 60-s EEG fragments are presented. The original (top red curves) and filtered (bottom blue ones) signals are shown for each of all 19 channels inside circles.

The brain contains a huge number of neurons connected by many synapses, thus forming a very complex network with a time-varied structure. Any mental task activates neural ensembles in different parts of the brain by generating electromagnetic fields at various frequencies. These fields produce spatial-temporal patterns in EEGs and MEGs. For example, the process of primary processing of visual information is known [64] to be performed by neurons in the occipital and parietal areas and results in increasing beta-wave activity. On the other hand, when a person is engaged in motor activity, the neurons of the sensorimotor area are involved [62] that results in decreasing beta activity referred to as *event-related desynchronization* (ERD) and increasing alpha-activity amplitude known as *event-related synchronization* (ERS) [301].

Obviously, the neural interaction processes occurring on a microscopic level due to peculiarities of separate neurons dynamics and the neural network structure, are reflected on the structure of macroscopic signals registered by different methods of neuroimaging (see Section 2.2). Macroscopic characteristics of neural interaction are revealed by means of EEG, which is the most common registration type of the brain activity used in BCIs. The main aim of the development of neurointerfaces is the detection of characteristic features (or patterns) of the EEG signals recorded from different brain areas followed by the analysis of their time-frequency-spatial structure [302] (see Section 4.2), which are further classified using different classifiers (see Section 4.2.1). It should be noted that the registered signals of the brain activity involve a number of simultaneous phenomena in the brain neuronal network related to cognitive tasks and physiological processes. Although most of them are still incomprehensible and their origins are unknown, some brain signals can be decoded by the BCI to interpret the subject's intention and utilized as possible control commands (see Section 4.1).

In this section, we describe the methods of automatic processing of electrical brain signals recorded in a noninvasive way. These methods can also be used for the analysis of brain signals of another nature, such as, for example, ECoG, MEG, fNIRS, fMRI, etc.

#### 4.1. Brain activity patterns for control commands

There are numerous studies on searching specific features of brain activity that can be transformed into control commands for BCI systems. An important requirement for the recorded brain signals is the possibility of their use by the operator for controlling neurophysiological processes underlying these signals. This can be achieved by a special training, for example, using biological feedback [303,304]. For example, specific EEG patterns related to imaginary movements of left/right limbs were found in the motor cortex [305], whereas mental intentions, mental score, imagination of music, etc. were recorded using fNIRS in the prefrontal cortex [133,306]. Some processes are very difficult to control. Among them,

**Table 3**

Comparative characteristics of neurophysiological brain signals used to control BCIs.

Signal type	Neurophysiological process	Number of commands	Training	Information transfer rate
SCP	Slow cortical potential shifts in brain electrical signals due to increasing/decreasing activity of individual cells.	Low (2–4)	Yes	4–10 bits/min
ERP	Brain signal modulation induced by an external or internal event.	High	No	3–35 bits/min
EEG	Synchronous firing neurons generate observed rhythmic oscillations.	Low (<5)	Yes	3–60 bits/min
FBC	Different types of high nervous activity accompanied by strong interaction between various brain regions lead to the formation of functional neural networks of different topologies and dynamics.	High	No	2–10 bits/min

we should note the processes related to the reaction of the central nervous system to a tactile stimulation [307,308], cognitive activity [309,310], and various brain pathologies [311,312].

Let us now consider the most popular characteristics of EEG control signals, such as slow cortical potentials (SCPs) (Section 4.1.1), event-related potentials (ERP) including visual evoked potentials (VEP), P300 evoked potentials, event-related synchronization/desynchronization (ERS/ ERD), error potentials (ErrP) (see Section 4.1.2), multiscale oscillatory EEG activity including sensomotor rhythms (Section 4.1.3), and functional brain connectivity (FBC) (Section 4.1.4). Table 3 summarizes common features of brain signals of different types.

#### 4.1.1. Slow cortical potential

*Slow cortical potential* (SCP) is a short event-related EEG shift lasted from 300 ms to several seconds. SCPs are associated with changes in cortical activity related to the local mobilization of excitation or inhibition in cortical neural populations, caused by inputs from the thalamus. SCPs belong to the part of the EEG signal spectra below 1 Hz [313]. A negative SCP indicates a growth of the sum of synchronized potentials, i.e., an increase in the neuronal activity, whereas a positive SCP with the reduction of synchronized potentials from dendrites, i.e., a decrease in the activity of individual neuronal cells. It is important that SCPs as control signals for BCI can be self-regulated by both healthy users and paralyzed patients. For example, the BCI operation using SCPs was successfully realized by ALS patients [314–316]. Typical accuracy rates achieved in the SCP classification are about 70%–80%, although the rates of information provided by the SCP-based BCI are relatively low due to slow changes in the brain signals associated with SCP. It should be noted, that the operation with the SCP-based BCIs requires a prolong continuous training of several months [177].

An individual's learning ability to voluntarily control SCPs using feedback has led Birbaumer with colleagues [313] to propose the use of SCPs for designing a BCI which they call a *thought translation device* (TTD). Later, Kübler et al. [314] trained 13 healthy subjects and 3 ALS patients with total motor paralysis during several months to control their SCPs by TTD. The training task was to hit a cursor on a top or bottom edge of the screen. The cursor's position was calculated from the Cz-linked mastoid signal  $x(t) = (Cz - A1 + Cz - A2)/2$ , to be proportional to the difference between the baseline EEG amplitude and the EEG amplitude recorded by the Cz electrode, both averaged over the last 500 ms.

Fig. 19(a) shows the average SCP waveforms generated by healthy subjects on cue after training. One can see the clear deviation from the baseline activity in the positive or negative direction. This difference from the baseline was used to proportionally move the cursor up/down or left/right. It should be noted that among 13 subjects under study, 4 were able to produce positive-going responses, 3 generated significant negative-going responses, and 3 were able to generate both. Figs. 19(b) and 19(c) demonstrate similar results for one of the ALS patients. As seen in these figures, the patient, after several months of training, was able to generate a negative-going SCP at Cz when required to hit the bottom target.

#### 4.1.2. Event-related potential

As was already mentioned in Section 2.2.2, *event-related potential* (ERP) is a time-locked response of the brain neuronal network induced by an external stimulus or an internal event, for instance, due to a sensory or mental event, or, on the contrary, due to the omission of a constantly occurring stimulus. While exogenous ERP components occur due to processing an external event, endogenous ERP components appear when an internal event is processed. The relationship between these components depends on the context in which the stimulus occurs [317]. The main ERP types can be classified as follows.

- Visual evoked potentials (VEPs).
- P300 evoked potential.
- Event-related synchronization/desynchronization (ERS/ERD).
- Error potential (ErrP).

We will now consider the events most frequently used in BCIs in more detail.

*Visual evoked potentials* (VEPs) are brain activity responses which occur in visual cortex after receiving a visual stimulus [318]. The VEP can be detected in EEG since its amplitude is very large when the stimulus is in the central visual field [319]. Therefore, the user can increase VEPs by focusing his/her gaze on the object, that requires coherent ocular motor control [320].

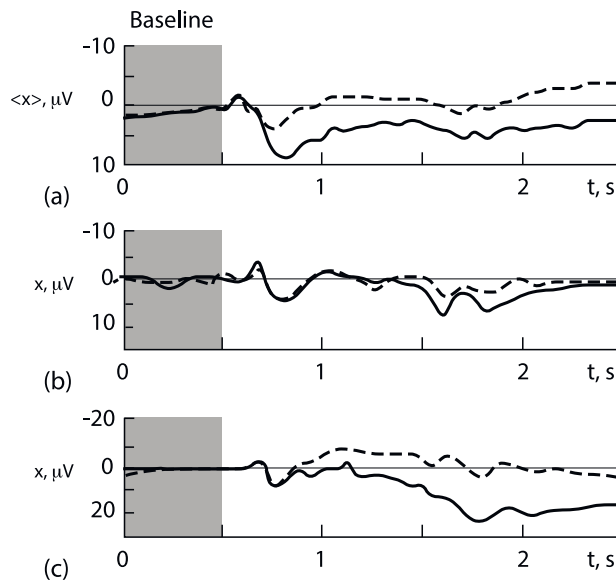


**Fig. 19.** Slow cortical potentials during a single training session (a) averaged over all 13 subjects ( $\langle x(t) \rangle_t$ ). (b,c) SCP for an ALS patient (b) at the beginning of training and (c) after several months training. Shaded areas correspond to baseline time intervals.  
Source: Based on data from [314].

In turn, VEPs can be classified according to the following criteria [28].

- Morphology of a visual stimulus which can be either a flash or graphic regular images, such as checkerboard lattice, gate, etc, or random images.
- Frequency of visual stimulation, i.e., transient VEPs (TVEPs) which occur for frequency of visual stimulation below 6 Hz and steady-state VEPs (SSVEPs) which are the reaction of the brain to a high-frequency stimulation [318,321].
- Field of visual stimulation, i.e., VEPs can be either the whole field, half field, or part field if the visual stimulus is only presented on a part of the screen.

TVEPs can be produced by any change in the visual field and vary with the stimulus presented [322]. In the case of flash stimulation, TVEPs represent a series of negative and positive peaks. The onset/offset patterns of TVEPs caused by letting a graphical pattern appear abruptly on a diffuse background have three main peaks: C1 (positive, 75 ms), C2 (negative, 125 ms), and C3 (positive, 150 ms). Pattern reversal TVEPs caused by reversing the phase of a pattern, i.e., a checkerboard lattice that changes the checks from black to white and from white to black, present one negative peak at 75 ms, one positive peak at 100 ms, and one negative peak at 135 ms [322].

SSVEPs can be elicited by the same visual stimulus with a frequency higher than 6 Hz. SSVEP shows the oscillations at the same frequency as the blinking frequency of the stimulus and their harmonics [323]. To illustrate this fact, Fig. 20 illustrates the example of the steady-state visual evoked field (SSVEF) evoked by 6.67-Hz and 8.57-Hz visual stimulation MEG signals in the occipital cortex, i.e., visual area, while the subject was observing an image with modulated brightness [324]. The Fourier spectra of SSVEF are shown for the stationary image (without flickering) (Fig. 20(a)) and with modulation frequencies  $f_1 = 6.67 \text{ Hz}$  (Fig. 20(b)) and  $f_2 = 8.57 \text{ Hz}$  (Fig. 20(c)). One can clearly see from Fig. 20(a) that in spectrum background noise is 1/f noise (or pink noise), typical in biological systems [325]. The broaden peaks in the alpha and delta regions are also seen around 10 Hz and 1 Hz, respectively. When the modulation is applied to the image, the brain responds at the flicker frequency ( $f_1$  or  $f_2$ ), as well as at its well-pronounced higher harmonics. It is noteworthy that the power of the second harmonic component is higher than the power of the first harmonic component.

In contrast to TVEP, frequency components of SSVEPs remain almost constant in amplitude and phase over long periods of time [326]. SSVEPs are less susceptible to distortions due to oculomotor artifacts [327] and myographic signals [328]. Therefore, due to similar sustainability, SSVEPs are most often used to create BCIs [329–331].

P300 evoked potential is a ERP component elicited in the process of decision making. P300 EPs represent positive peaks in the EEG due to infrequent auditory, visual, or somatosensory stimuli. P300 EPs are usually elicited using the oddball paradigm, in which low probability target items are mixed with high probability non-target items [332]. These endogenous P300 responses are observed about 300 ms after attending to an oddball stimulus. The P300 potentials are thought to reflect processes involved in stimulus evaluation and classification. Some studies have proven that the less probable the stimulus, the larger the amplitude of the response peak [70].

The most strong P300 EP is generally observed over the parietal lobe, although some components also originate in the temporal and frontal lobes. The exact neural mechanisms responsible for the P300 are not yet clear, but brain structures

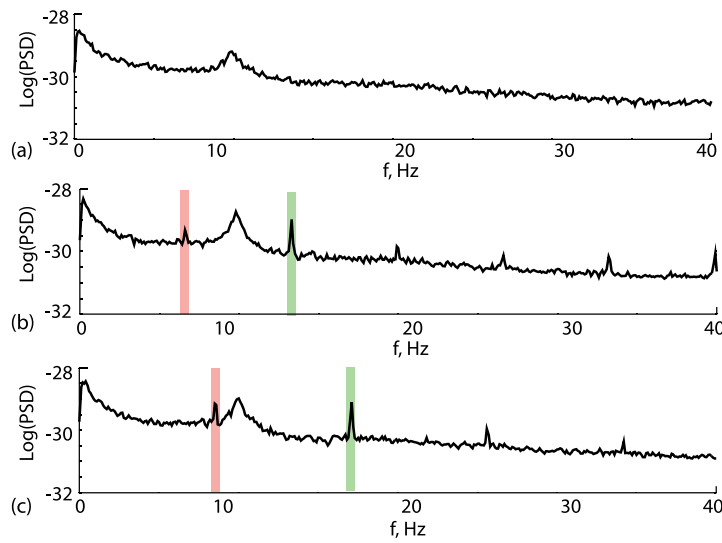


**Fig. 20.** Fourier spectra of SSVEF for the stationary image (a) and for the image under sinusoidal modulation at 6.67 Hz (b) and 8.57 Hz (c) obtained with the help of the magnetoencephalography. The vertical dotted and solid lines indicate tags at flicker frequencies and their second harmonics. Source: Based on the data from [324].

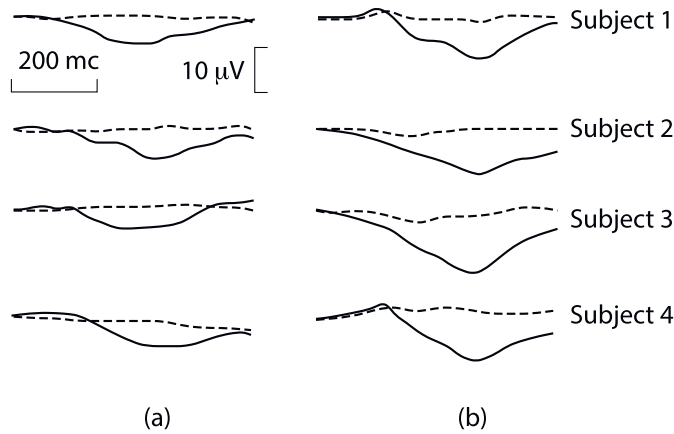


**Fig. 21.** Examples of P300 evoked potentials of four subjects. Each plot shows the average EEG response to flashes located on attended (solid) and unattended (dashed) areas, for inter-stimulus interval (ISI) (between flashes) of (a) 250 ms and (b) 500 ms. EEG was recorded by the Pz channel in the parietal cortex.

Source: Based on the data from [179].

such as the parietal cortex, cingulate gyrus, and temporoparietal cortex as well as limbic structures (hippocampus, amygdala) have been implicated as possible substrates. It is very important that the use of P300-based BCIs does not require training.

A typical application of a BCI based on visual P300 evoked potentials comprises a matrix of letters, numbers, or other symbols or commands (see, for example, Figs. 11 and 12). The row or column of characters blinks randomly. The BCI user should mark the column of interest and closely monitor the image on the screen. Since P300 EP is only generated when the selected column or row blinks (see Fig. 21), the P300-based BCI uses the evoked potential symbol or command. Due to a low signal-to-noise ratio on the EEG, the accurate determination of the target command by a single test (single EEG trial) is almost impossible. Therefore, one needs to repeat the procedure several times in order to improve the recognition quality by averaging the EEG response over a large number of trials. In the case of 15 repetitions for selecting one command, the information transfer rate should be approximately 1–2 commands per minute [179]. The P300-based BCI provides the very low information transmission rate because the classifier based on the average EEG response is too simple [85,86]. The transmission rate can be increased by using more complex algorithms and choosing the optimal visual representation of the matrix on the screen for more accurate detection of the P300 evoked potentials [333–335].

The information transfer rate in such systems can be increased by the use of error correcting codes [336,337]. However, optimizing the code solely according to the maximal minimum-Hamming-distance implies an increase in the target

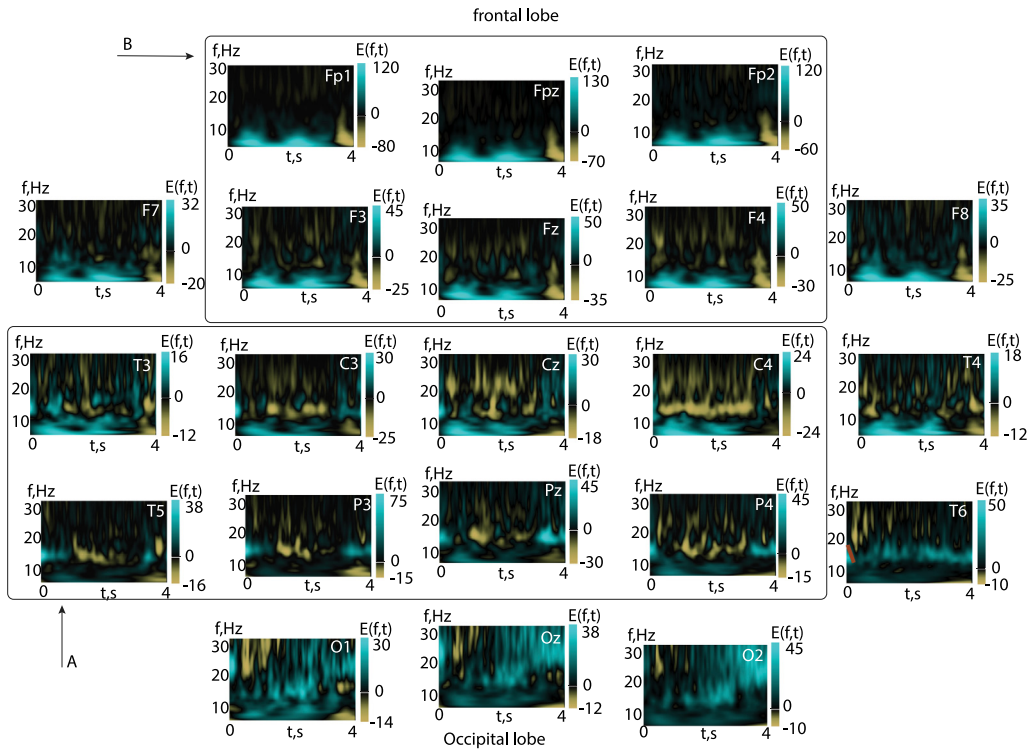


**Fig. 22.** Illustration of simultaneous ERD/ERS observation during motor execution (cp. with Fig. 24 illustrated the SMR for imaginary motion). Figure shows the time–frequency plots of changes in wavelet energy  $E(f, t)$  associated with real movement of the right arm with respect to the background EEG. Presented data was averaged over 100 trials and shown for each of 21 EEG channels. Red and blue colors indicate the time–frequency plane for which the energy value, respectively, increased and decreased during real movements. Color saturation shows the degree of changes..  
Source: Based on the data from [62].

frequency of the target stimuli which might violate physiological constraints leading to many errors in classification of individual ERPs, due to overlapping and refractory effects [333]. Some recent novel approaches have tried to reduce them, by superimposing the targets on a checkerboard [338] or using alternative stimulus type methods based on motion [333]. The high efficiency of the MEG-based BCI was demonstrated by analyzing the dynamics of the second harmonic in the stimulation frequency, which is more pronounced in the instantaneous MEG signal spectra [339].

Similarly the visual stimuli P300 EPs can be observed with audio and tactile stimuli, which can be used, for example, for people with visual impairment [184]. Compared to a visual-based BCI users' performance in auditory evoked potential-based BCI was sufficiently lower. Halder et al. [340] obtained the average information transfer rate of up to 2.46 bits/min and accuracies of 78.5% in 20 healthy participants using an auditory BCI. However, the issue of creating an audio BCI is less studied than the P300-based BCI with visual commands.

*Event-related desynchronization* (ERD) and *event-related synchronization* (ERS) are particular types of ERP characterized by a decrease/increase in synchronization of neurons caused by a decrease/increase in the power at a specific frequency band.

Fig. 22 represents the time–frequency diagrams calculated with the help of the continuous wavelet decomposition using the complex-valued Morlet wavelet (7). The diagrams illustrate changes in the energy  $E(f, t) = W^2(t, f)$ ,  $f \in (1, 30)$  Hz,  $t \in (0, 4)$  s associated with real movement with respect to the background EEG. The presented data were averaged over 100 EEG trials recorded from all 21 EEG channels of one subject. The time–frequency plots are labeled and located on the head-like layout, according to the position of the recording electrodes. Fig. 22 shows that electrical activity in the temporal lobe is characterized by a decrease in the wavelet energies at  $f \in [8, 12]$  Hz (mu-rhythm) and  $f \in [15, 30]$  Hz (beta-rhythm) together with an increase in the delta-wave ( $f \in [1, 4]$  Hz) amplitude. The former effect observed in mu- and beta-ranges is known as ERD, while the latter effect in delta-band is referred to as ERS. So, the motor execution is characterized by both ERD and ERS. The ERD was usually observed in mu and beta-bands [66], while the ERS effect in delta-band was less studied [341]. At the same time, according to Fig. 22, ERS in delta-activity takes place during motor execution together with ERD of mu- and beta-rhythms. The colored areas A and B in Fig. 22 indicate the brain segments where the event-related behavior was most pronounced. The ERD in mu-rhythm prevailed in temporal, central, and parietal lobes (area A), corresponding to the motor area [342]. It should be noted that this area is shifted from the center to the left side, which is connected with hemispheric asymmetry, associated with right arm movements [343]. The

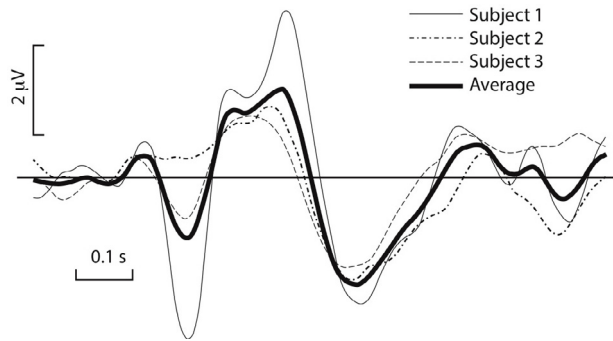


**Fig. 23.** Typical average ErrPs for three subjects, along with the average ErrP across subjects.  
Source: Based on data from [346].

accompanying ERS in the amplitude of the low-frequency delta-activity is more pronounced in the frontal lobe (shaded area **B**).

It should be emphasized that the time–frequency structure of the EEG signal is much more complicated. The features of the brain signal during motor execution are characterized by the transition and distribution of the energy between different frequency bands that significantly complicates the classification of the ERD/ERS-based commands in the BCI. Nevertheless, there is a possibility to recognize the real and imaginary movements by processing EEG-signals using more sophisticated mathematical techniques, such as detrended fluctuation and multiresolution analysis [344,345], however, they are not yet implemented in real time data processing.

Error potential (ErrP) is a slow cortical potential in the EEG signal corresponding the brain's reaction to an error. ErrP can be a potentially critical component of a BCI to detect whether the BCI has committed an error (misclassification of a command given by the user). ErrPs can be detected in single EEG trials and can potentially be used to improve the BCI accuracy. In the experiments of Butfield et al. [346], three operators controlled the robot's movement to the left or right direction in the room, by pressing the corresponding key on the hand interface. The experiment was conducted in such a way that in 20% of cases the system issued an incorrect command to simulate EEG noise and BCI errors. The ErrPs were typically observed in frontocentral regions along the midline. EEG signals from the Cz and Fz channels were used to recognize the reaction of the operator on the error. The experimental results of the ErrPs registration for all three subjects are presented in Fig. 23. The mixture-of-Gaussians classifier trained on the EEG data from a window of 50–650 ms after visual feedback from the user's action, detected the ErrP with a 79.9% average accuracy that opens the possibility to improve the overall accuracy of the BCI system.

#### 4.1.3. Multiscale brain activity

Oscillatory EEG activity is caused by the complex neural network. The synchronized neuron firing in different brain areas generates rhythmic brain waves. As was discussed above, the free-running EEG is characterized by a multiscale time–frequency oscillation structure in different frequency ranges. The electrical brain activity reflects the person's brain functions as well as his/her health status including

- sensorimotor rhythm (SMR),
- multiscale oscillatory EEG patterns associated with the person's psychophysiological state and cognitive abilities,
- EEG patterns (biomarkers or hallmarks) corresponding to different brain disorders.

SMR is an oscillatory idle rhythm of synchronous electromagnetic brain activity appeared as spindles in recordings EEG, MEG, and ECoG in the frequency range of 7–13 Hz [347]. SMR is one of the most interesting manifestations of the brain activity to be used for creating BCI control commands. The SMR amplitude in mu- and beta-frequency bands varies when cerebral activity is related to any motor task, as shown in Section 4.1.2 and Fig. 22, although real movement does not modulate the amplitude of sensorimotor rhythms without any overt motor output. Motor imagery results in similar modulation patterns of the motor rhythms without any overt motor output. Fig. 24 shows the time–frequency dependencies which illustrate the SMR dynamics of an untrained subject, associated with motor imagery with respect to the background EEG [62].

Motor imagery is also associated with significant changes in delta-activity, that can be observed in the frontal area (colored area **B** in Fig. 24). At the same time, the delta-energy decreases due to ERD. One can also see that mu-rhythm exhibits ERS, well pronounced in the most of brain areas, reaching a maximum value in the central and parietal lobes, and significantly decreases in temporal lobes (colored area **A** in Fig. 24). This SMR signature of motor imagery is caused by the lack of the subject training. One can expect that in trained subjects the time–frequency and spatial–temporal structures of EEG signals corresponding to motor imagery are very similar to those for real movements [66].

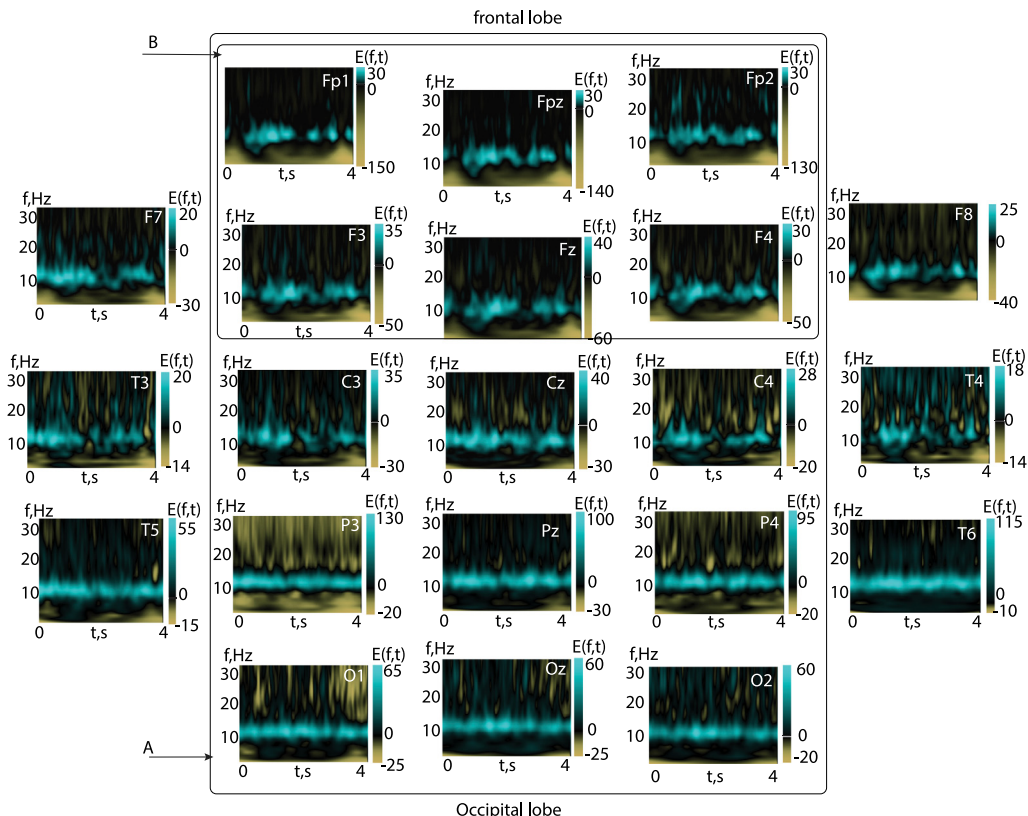


**Fig. 24.** Illustration of SMR during motor imagery (cp. with Fig. 22 for real motion). Time–frequency plots of changes in wavelet energy  $E(f, t)$  associated with imaginary movement of the right hand, with respect to the background EEG of the untrained subject. Presented data are averaged over 100 trials for each of 21 EEG channels. Red/blue colors indicate the time–frequency plane for which the energy value increases/decreases during imaginary movements. Color intensity shows the degree of changes.

Source: Based on the data from [62].

SMRs are often used to control BCIs, because the BCI operator can learn how to voluntarily generate the required ERD/ERS in the sensorimotor cortex by imaging the movement of a particular limb [348,349]. The BCIs based on SMRs can operate in either synchronous or asynchronous mode. As a consequence, SMRs have extensively been studied and used in the BCI research. Many well-known “classical” BCI systems, such as Wadsworth [82], Berlin [83], or Graz [350] BCI systems employ SRMs as control signals.

One of the important problems encountered in the development of SMR-based BCIs is the variability of neural activity associated with motor imagery among different subjects. This problem is well known in the context of developing active neurointerfaces for controlling bioprostheses and anthropomorphic manipulators [351–353]. Since the brain activity associated with motor imagery has a different structure in untrained subjects [62], characteristics of used biomarkers may vary from one to another experimental session. To stabilize the EEG patterns generated by the BCI operator, it is necessary either to use long-term training [66] or additional information about the signal nature [145]. For instance, in the above example, it is possible to divide subjects into two large groups, visual and kinesthetic, characterized by general regularities [354]. Having *a priori* information about which group the tested subject belongs to, allows better optimization of the BCI configuration in order to increase the classification efficiency [355].

Multiscale EEG oscillatory patterns associated with person’s psychophysiological states and cognitive abilities can be used to control passive BCIs [356]. The work in this direction is connected, basically, with evaluation and control of such psychophysiological factor as alertness [239,357] related to the retention of information about an object in short-term memory. According to the results of neurophysiological studies, people who need to maintain a prolonged attention during professional activities (operators of complex installations, air traffic controllers, pilots) often experience problems with maintaining a high level of attention over long time. It is known that enhancing attention is possible with the help of special medications, but a safer and more effective way is training with the use of passive BCIs. In addition, on the basis of similar BCIs, training systems can be developed for children with attention deficit disorder and hyperactivity [358], as well as neuroassistive systems that allow controlling attention while performing monotonous tasks for a prolonged period of time. Currently developed passive BCIs are able to estimate the degree of human attention in real time, based

on changes in time-frequency multiscale EEG structures, and provide the possibility to control attention with the help of biological feedback [64].

EEG patterns (biomarkers) related to different brain disorders are used in passive BCIs for monitoring and controlling pathological brain activity, especially in early stages, when symptoms are not yet well pronounced. As known, the EEG of a normal healthy brain will differ from that of a brain with disease or functioning abnormally. The analysis of EEG activity provides the possibility to study patients with brain dysfunctions, such as coma, memory disorder, tumors, brain death or even malfunctioning of certain body parts. A number of brain diseases are possible to diagnose, study and analyze by EEG. Among diseases which can be evaluated, we should mention brain aneurysm, Parkinson's disease, meningitis, epilepsy, encephalitis, brain tumor, stroke, autism, cerebral edema, schizophrenia, traumatic brain injury, Alzheimer's disease, attention deficit hyperactivity disorder, etc. In particular, there is a considerable interest in the creation of a HSC BCI for early prediction an epileptic seizure, based on early-warning EEG precursors [359–361] (see Section 6). The epileptic activity can be suppressed by electrical stimulation of the thalamo-cortical brain network to destruct epileptic discharges [40,41,362]. Such systems are of considerable interest due to the limited capacity of epilepsy drug therapy which has no effect on about 30% of patients suffering from epilepsy [363,364].

#### 4.1.4. Functional brain connectivity

In the previous sections, we considered relatively simple and somewhat rough mechanisms of the BCI command formation, based on the analysis of those or other "standard" EEG patterns. However, the emerging field of neurointerfaces promises to improve learning and memory for patients with cognitive impairment. Unfortunately, our understanding of neural mechanisms underlying these cognitive processes remains partly limited due to the strong individual variability in neural coding and circuit functions [365,366]. The development of cognitive BCI technology requires robust tools which would allow quantification of time-varying task-dependent brain states. Unfortunately, measuring local, regional, or global metrics of neural activity are not enough to provide an ideal control signal for a cognitive BCI, because critical regions involved in high-order cognitive functions, such as experiential learning, executive control, dynamic online cognitive performance, etc., are spatially distributed in the brain [367–369] and require coordinated activity [370–376]. Rather, the addition of quantitative measures of coordinated activity, so-called *functional brain connectivity* could improve the reliability and generalizability of the control signal [377–379]. The formation of control signals for cognitive BCIs should be based on mathematical complex network approaches, enable the analysis of the distributed dynamical neural system [380].

Actually, all types of the highest nervous activity are accompanied by a strong interaction between various brain regions [381]. The measurement of this interaction allows accessing the functional neural network corresponding to a specific brain state or activity which, in turn, can be used to reveal main principles underlying this activity [382]. Using modern techniques for recording brain activity, one can represent a functional brain structure as a graph, where separate nodes are brain areas whose temporal dynamics is described by a signal from a particular sensor and edges indicate the presence of a functional relation between the brain areas (nodes). Recent research shows that a cognitive load manifests as specific connectivity patterns of electrical brain activity in various frequency ranges [383–386]. In a weighted network, edges between nodes  $i$  and  $j$  can be characterized by a continuous value of weight  $w_{ij} = w_{ji}$ , which captures the strength of the connection between nodes  $i$  and  $j$ . Moreover, we can talk about directed links, if the  $i$ th node affects the  $j$ th node. In this case, the link's weights between the nodes obeys the following condition:  $w_{ij} \neq 0$  and  $w_{ji} = 0$ . The pattern of weights across edges connecting nodes is referred to as the network topology [381] described by the adjacency matrix  $W$  of size  $N \times N$ , where  $N$  is the number of nodes. In a non-directed network the connectivity matrix  $W$  is symmetric, while in a directed network it is asymmetric.

It is known that brain dynamically adjusts the structure of its functional neuronal network to enhance the efficiency of information processing under increasing cognitive demand [387,388]. This mechanism is described in the framework of the global workspace theory, which implies that the performance of increasing cognitive demanding tasks requires coherent activity of multiple distributed brain regions [389,390]. The mechanisms underlying the emergence of neural connections between remote brain regions are still unknown, and their search remains a widely debatable problem in neuroscience. There are several well-known theories which are about to explain how neural ensembles communicate in the brain. In particular, Fries [391] hypothesized that neuronal communication is subserved by neuronal coherence. According to his theory, activated neuron groups communicate during temporal windows when they are coherent. Furthermore, Gregoriou et al. [392] suggested that the mechanism of neuronal communication is implemented through high-frequency gamma-band oscillations. The authors showed that time-shifted coupling at gamma frequencies may optimize a post-synaptic impact of spikes from one area upon the other, and, by this, improve cross-area communication. Moreover, Lisman and Jensen [393] demonstrated that along with gamma frequencies, theta frequencies also play important role in neuronal communication. They found that gamma and theta oscillations occur in the same brain regions and interact with each other, coordinating communication between other brain areas. Finally, it was concluded that neuronal communication is simultaneously conducted at different frequency bands and requires coherence [394]. This requirement for efficient communication known as *communication through coherence* implies that a postsynaptic neural group, receiving input signals from several presynaptic groups, responds primarily to those group with which it is more coherent. In the absence of the coherence, the inputs arrive at random phases of the excitability cycle and therefore have a very low connectivity efficiency.

Therefore, *functional brain connectivity* (FBC) can be found through synchronization or, in more general case, coherence of oscillating neural sources [378,395–399]. This means that brain areas which display synchrony, i.e., a statistical relation between instantaneous phases of the signals in considering frequency bands [378,400,401], can be interpreted as being functionally connected [402,403]. To estimate the coherence in neural ensembles, different approaches which take into account nonstationarity and stochasticity of brain signals are used [404]. Among them, the most often used for the formation of BCI control commands are

- wavelet bicoherence [378,405,406];
- band-path filtration and phase synchronization [407–409],
- wavelet spectra product [41,361];
- wavelet-based similarity degree at macroscopic network level [302];
- time-scale synchronization [302];
- feed-forward artificial neuronal networks and recurrent neural networks [410,411].

More generally, FBC reflects pairwise statistical relationships that can display complex patterns indicating nontrivial network topologies. A statistical relationship between two neuronal signals can be estimated by numerous methods based on different mathematical and physical approaches, such as

- regression-based methods including the coherence function CF and nonlinear correlation coefficient  $h^2$  [381,407],
- Granger causality and related metrics [406],
- entropy and mutual information [412],
- recurrence plot [413,414].

Recently, multiscale connectivity was used as a very efficient approach for studying FBC. It is based on the fact that different layers of a recovered multiplex network correspond to different frequency ranges of EEG and MEG signals. Furthermore, the FBC features can be quantified using numerous statistics, commonly referred to as graph statistics, network measures, or connectomic metrics, such as different measures of centrality [415–417], assortativity properties [418], graph clustering coefficients [419], etc. The quantification of FBC network features can provide robust estimates of task-dependent interregional coordination, and its relation to multisensory processing, alertness, cognition, memory and learning [381,420–425].

Similar approaches based on FBC measurements can be used in passive BCIs to evaluate and train cognitive brain functions. In this case, the BCI operator has no task to learn how to develop the necessary mental states. The problems of precise determination of the brain states of interest comes out on top, as well as possible periodic retraining of the classifier in the case of brain evolution in the course of training with the help of biological feedback systems [426].

#### 4.2. Brain–computer interface as a system for real-time pattern recognition

The main aim of any BCI is to distinguish patterns of brain activity and translate them into certain commands of a machine system (computer). In fact, building an intelligent BCI system is reduced to the creation of an image recognition system in which the resulting vector signal (e.g., multichannel EEG) should be assigned to one of the predefined classes (brain activity types). An intelligent BCI control system is usually built in two parts: a feature extraction subsystem usually operated without training, and a pretrained classifier (Fig. 25(a)). An input image to be classified can be represented by a vector  $\mathbf{x}$  in an  $m$ -dimensional data space. The feature extraction is described as an  $F$  conversion which translates the vector  $\mathbf{x}$  into an intermediate  $n$ -dimensional feature vector  $\mathbf{y}$  ( $n < m$ ) (Fig. 25(b)). The  $F$  conversion is a data compression operation for reducing dimension, which simplifies the next step of the classification described as a  $G$  transformation that displays the feature vector  $\mathbf{y}$  in one of the classes in the  $k$ -dimensional solution space, where  $k$  is the number of allocated classes. The solution space is divided into separate areas, each of which is associated with a particular class.

So that the classifier could solve the problem of recognition of brain activity types, it must first be trained by feeding a sequence of  $h$  input images (EEG signals) along with corresponding classes (types of brain states), which these signals (images) belong to. After learning the sequence of  $h$  images, a new image, belonged to the same set of classes as many images used for training, enters the classifier. Thanks to the information selected from the training data, the classifier is able to classify new data into a particular class from  $k$  classes allocated in the solution space. The boundaries of the class regions in Fig. 25(b) are formed as a result of statistic training based on the variance, inherent in the data of individual classes.

It should be borne in mind, that the amount of data  $h$  required to represent different classes increases exponentially with a growth of dimension  $n$  of the feature vector [427,428]. If the training set  $h$  is small compared to the dimension  $n$ , then most likely the classifier will give bad classification accuracy. Some researchers [429,430] indicate that in order to obtain an acceptable classification accuracy, the size of the training set  $h$  must be between  $5nk$  and  $10nk$ . However, at work with BCI classifiers it is difficult to reach this accuracy, because usually the dimension  $n$  of the feature vector is so large as the size of the training sample, which can be accumulated due to subject's physiological peculiarities turn out to be small. This significant problem restricts the achievable accuracy in detecting brain state by various HSC BCIs.

Another barrier, which faces on the route of the creation of efficient BCIs, is the so-called *bias-variance tradeoff* problem [20]. From the mathematical point of view, the classification problem consists in finding a true class  $\hat{\mathbf{g}}$  of a feature vector  $\mathbf{y}$  using a mapping  $G$ . This mapping is learned from a training set with a number of samples  $h$ , while the optimal mapping  $\hat{G}$  generated the class is unknown. If we consider the *mean square error* (MSE), the classification errors

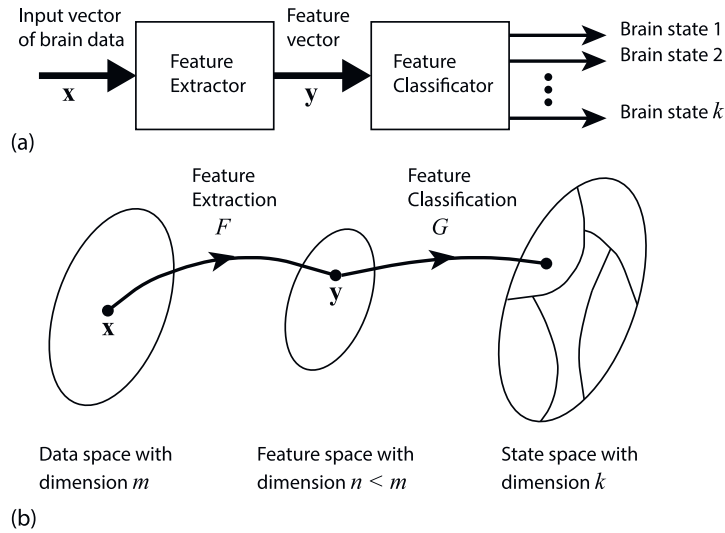


**Fig. 25.** Illustration of a BCI intelligent system for recognition and classification of brain activity patterns. (a) Structural scheme. (b) Transformation of a data space to feature and state spaces.

$\mu$  are decomposed in three terms [427,431] as

$$\begin{aligned} \mu &= E[(\hat{\mathbf{g}} - G(\mathbf{y}))^2] = E\left[\left(\hat{\mathbf{g}} - \hat{G}(\mathbf{y}) + \hat{G}(\mathbf{y}) - E[G(\mathbf{y})] + E[G(\mathbf{y})] - G(\mathbf{y})\right)^2\right] = \\ &= E\left[\left(\hat{\mathbf{g}} - \hat{G}(\mathbf{y})\right)^2\right] + E\left[\left(\hat{G}(\mathbf{y}) - E[G(\mathbf{y})]\right)^2\right] + E\left[\left(E[G(\mathbf{y})] - G(\mathbf{y})\right)^2\right] = \\ &= \xi^2 + \text{bias}(G(\mathbf{y}))^2 + \text{variance}(G(\mathbf{y}))^2, \end{aligned} \quad (16)$$

where  $E$  is the square root of the sum of squares of each vector component.

From Eq. (16), we can conclude that there are three terms which define the main possible sources of the classification error. They are

- noise  $\xi$  in the BCI system<sup>4</sup>;
- bias, reflected the divergence between estimated ( $G$ ) and best ( $\hat{G}$ ) mapping, that depends on the method chosen to construct the function  $G$ ;
- variance, depended on the training set  $h$  used.

To minimize the classification error  $\mu$ , both the bias and the variance should be small. However, there is a discrepancy between simultaneously reached minimum bias and variance. Stable classifiers, for which small variations in the training set does not affect considerably their performance (e.g., linear discriminant analyzer with low complexity or capacity [432]), have high bias and low variance, whereas unstable classifiers with small variations of the training set may lead to significant changes in their performances (e.g., an artificial neuronal network (ANN) such as a multilayer perceptron (MLP) having high complexity) and have low bias and high variance. This can explain why simple classifiers sometimes outperform more complex ones [433]. Here, the use of mathematical approaches, in particular, stabilization techniques [431] can significantly decrease the variance of unstable classifiers with high bias. In particular, we should mention regularization procedures based on careful controlling complexity of a classifier to prevent overtraining [428,434].

It should be noted that EEG signals are non-stationary in time for one user or among various users. Nevertheless, a high efficiency can be achieved using adaptive classifiers whose parameters are incrementally updated online. Such classifiers are developed to deal with non-stationary EEGs in order to track changes in the EEG properties over time [435–439]. The adaptive classifiers can also be used to deal with limited training data by online learning, thus requiring fewer offline training data [21]. Moreover, low variance can be a solution to cope with the variability problem in BCI systems.

#### 4.2.1. Features extraction and selection

BCIs can select characteristic features of the EEG signal related to a certain type of the brain activity, and highlight characteristic properties to be classified into a certain class corresponding to a particular type of activity. At the same time, the differences allow clear separating different types of brain activity. These features are differentiated in one way

<sup>4</sup> In the specific type of neurovisualization, we cannot affect this error.

or another in the analyzed signals which contain discriminatory information allowing to reliably distinguish different types of brain dynamics.

Among different physical properties of processes taken place in BCIs, the most frequently used are

- EEG signal amplitudes [440];
- amplitude and energy of an EEG signal in a particular frequency range [440];
- spectral power density [441];
- autoregressive and adaptive autoregressive coefficients [442,443];
- time–frequency feature measured using wavelet coefficients [444–446];
- spatial features, for example, the localization of EEG activity sources, inverse model-based features [447,448];
- graph statistics and network measures of functional brain connectivity (FBC) [377,449].

The choice of a suitable set of features is a challenging issue. The information of interest is hidden in highly complex multichannel nonstationary brain signals, which comprise a large number of simultaneous sources. A significant feature extracted from EEG data can be overlapped in time and space by multiple signals from different brain tasks. Let us now consider the most important features of electrical brain activity that should be taking into account while designing efficient BCIs [20].

- Brain signals are very noisy [450,451]. EEG signals obtained with the help of dry electrodes [452,453] have a poor signal-to-noise ratio.
- Brain signals contain outliers and artifact peculiarities due to the influence of other types of life activity (eye blinks, muscle activity, cardiorhythms, etc.).
- The signal vector is characterized by high dimensionality because several features are generally extracted from several channels and time segments before being concatenated into a single feature vector. The reducing dimension of a feature vector is one of the main problems in the BCI classification algorithm development.
- The signal vector can contain components corresponding to different frequency bands (theta, alpha, beta, etc.) due to a multiscale structure of EEG signals.
- Since brain activity permanently varies in time, space and frequency, the EEG patterns should be related to specific time, brain area and frequency.
- Features may rapidly vary in time and more especially over sessions since EEG signals are typically characterized by a nonstationary behavior. It should be noted that selected features of the operator can be rebuilt from one experimental session to another, for example, during the operator's training.
- We need to work with classifiers trained from a small amount of data, since training sets for the classification algorithm are usually relatively small due to high time consumption of the training process because of nonstationarity and constant restructuration of the EEG data.

#### 4.2.2. Nonstationary and multiscale features of brain activity

Many patterns of brain activity used for constructing BCI control commands are varied in time in different frequency ranges. This nonstationarity of the EEG signals should be taken into account at formation of a feature vector for subsequent classification and BCI commands. To stabilize the time–frequency dynamics within the patterns, the following basic approaches can be used.

- **Concatenation.** The features are extracted from different time epochs and concatenated into a single feature vector to be used for classification by a single classifier.
- **Combination.** The extraction and classification processes are divided on several steps corresponding to sequential time epochs, and then, the results of different classifiers are combined.
- **Dynamical classification.** The features extracted from sequential time epochs form a time-depended feature vector, which can be classified using a dynamical classifier.

Another important problem arisen from nonstationarity of brain activity is that statistical parameters of generated patterns change in time. In this case, the training of the classifier only on a predetermined training set of events is not effective, because the classifier does not have means of tracking statistical variations of the feature vector with which it deals. Therefore, in this situation it seems more convenient to constantly adapt the classifier to the input signal variation in real time. The training of the classifier never ceases during the BCI operation, while new patterns are received for processing and interpretation of the brain activity. Taking into account nonstationarity of the feature vector, the adaptive classifiers are of a special importance for rehabilitation problems, when in the course of the patient recovering with a BCI (e.g., while restoring motor activity after a stroke), the brain activity undergoes significant changes. This may occur due to formation of real and imaginary motor commands for post-stroke rehabilitation.

Similarly, many EEG processes flow not only in time, but also in different frequency ranges characterized by a complex multiscale structure. In this case, there is also a problem of accounting the multiscale structure at formation of a feature vector. Here, as in the previous case, it is possible to distinguish several approaches based on classification methods.

- Signal properties selected from different frequency ranges are merged into a single feature vector classified by a single classifier. This approach works well if there are no lags between processes in different scales.

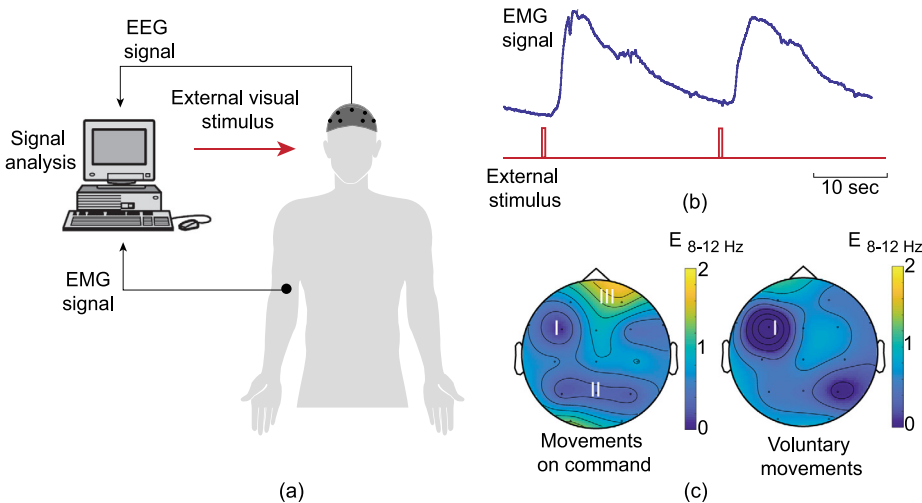


**Fig. 26.** (a) Experimental scheme on human motor activity with simultaneous EEG and EMG recordings. (b) Myographic signals which allow precisely identifying the beginning of the hand movement. (c) Space-temporal distribution of wavelet energy in the alpha range associated with movements initiated by visual stimulation and voluntary movements determined by the participant.

- In the case when we need to take into account the time ratio (lag) between the occurrence of various events in different scales, it is more efficient to use a dynamical classifier.
- It is also possible to select a feature vector for each scale and a combination of classifiers which operate simultaneously in different frequency ranges.

Nevertheless, if we take into account a multiscale structure of EEG signals, then we complicate the classification process, increasing the dimension and/or number of feature vectors.

#### 4.3. Time-frequency and spatial-temporal feature extraction

The formation of brain activity patterns which can be used to develop control commands for HSC BCIs, reflects complex neurophysiological processes in the neural ensemble of the cortical brain network. From the viewpoint of physics and nonlinear dynamics, these processes are associated with the formation of coherent states in a spatially distributed network of coupled oscillators. As an example of such dynamics, we consider motor activity already discussed above. The scheme of the conducted experiment is present in Fig. 26(a). The experiment consisted of two sessions. In the first session, the subject moved his/her right hand on the visual command (external stimulus), and in the second session, he/she moved the hand voluntary at random time without external stimulation. The movement was monitored by the miography from the humeral muscles, and simultaneously a multichannel EEG was recorded according to the 10–10 scheme (see Fig. 3(b)). Fig. 26(b) shows a typical myogram for the first session, which allows to determine the beginning of the movement by a sharp increase in the signal amplitude. This is very important for the second session, where the beginning of the movement was arbitrarily chosen by the subjects themselves. In the left panel of Fig. 26(c) we show the wavelet spectral energy of the brain activity in the alpha/mu-range (8–12 Hz).

In the first case, brain dynamics represents a complex spatial structure in the alpha/mu-range. In area I of the motor cortex, one can see the pattern of sensomotor rhythm due to ERD in the alpha/mu-range. It should be noted that since the movement was carried out by the right hand, the area I with ERD was observed in the left hemisphere of the brain. In area II in the parietal area, ERD also takes place in the range of 8–12 Hz associated with perception of visual stimulus. Finally, in area III in the frontal cortex, there is ERS in the alpha-range associated with increasing subject's attention on the experimental task performance when the stimulus was presented. Thus, in one short period of time during the motor task performance, several activity patterns are formed in one frequency range, and the spatial selectivity of activity features is needed for their subsequent classification. In the case of voluntary movement, the situation is more simple, as shown in the right panel of Fig. 26(c), where only the well-selected pattern of motor activity is observed in the alpha-range (area I). Therefore, we can conclude that at the stage of the feature vector formation, time-frequency and spatial-temporal properties of the brain activity pattern should be accounted for, because at the task performance, the BCI operator is often involuntarily distracted by solving other problems.

Let us dwell on some mathematical and physical methods which allow us to take into account a similar spatial-temporal separation of the distinguished features of brain activity signals.

#### 4.3.1. Common spatial pattern

Common spatial pattern (CSP) is a feature extraction method that projects multichannel signals into a subspace where differences between classes are highlighted and similarities are minimized. CSP aims to make the subsequent classification much more efficient by developing a spatial filter that converts input data into output data with optimal variance for subsequent discrimination. CSP finds spatial filters so that the variance of the filtered data from one class is maximized, while the variance of the filtered data from another class is minimized. Thus, the resulting feature vectors increase the distinction between the two classes. CSP has become a popular filtering method for synchronous EEG-based BCI, when control is done by estimating the oscillation power in a frequency band. Since the dispersion of EEG signals filtered at this frequency band corresponds to the power in this band, CSP essentially maximizes the legibility of, for example, ERD/ERS effects [83,454].

In the SCP method, the input data consist of a set of  $K$  EEG/MEG trials  $X_j^c$  ( $j = 1, \dots, K$ ), each of which belongs to one of two classes  $c = 1, 2$ . Each  $X_j$  is an  $N \times T$  matrix, where  $N$  and  $T$  are the numbers of EEG/MEG channels and time samples for each channel in the trial, respectively. Preliminary signals  $X_j$  are normalized and lead to a zero average. The goal of the SCP method is to find  $M$  spatial filters defined by an  $F$  matrix of the  $N \times M$  size, each column of which represents spatial filter coefficients by linearly transforming the input signal leading to the formation of new feature vector

$$\mathbf{x}_{\text{CSP}}(t) = F^T \mathbf{x}(t), \quad (17)$$

where  $\mathbf{x}(t)$  is the vector of the length  $N$  of the input signal at the moment of time  $t$ , composed of the signal values in all channels. To find the filter matrix  $F$ , one needs to calculate the conditionally covariance matrix for each class, as follows

$$R^c = \frac{1}{K} \sum_j X_j^c (X_j^c)^T, \quad (18)$$

where the matrix  $F$  is defined from

$$F^T R^1 F = \Lambda^1, \quad F^T R^2 F = \Lambda^2. \quad (19)$$

Here,  $\Lambda^i$  is the diagonal matrix,  $\Lambda^1 + \Lambda^2 = I$  is the identity matrix, and  $R^1$  can be found by solving the generalized eigenvalue problem:

$$R^1 \mathbf{f} = \lambda R^2 \mathbf{f}. \quad (20)$$

Generalized eigenvectors  $\mathbf{f} = \mathbf{f}_j$ , which satisfy Eq. (20), form columns of the  $F$  matrix and represent the CSP spatial filters, while generalized eigenvalues  $\lambda_j^1 = \mathbf{f}_j^T R^1 \mathbf{f}_j$  and  $\lambda_j^2 = \mathbf{f}_j^T R^2 \mathbf{f}_j$  form diagonal elements of  $\Lambda^{1,2}$ . Since  $\lambda_j^1 + \lambda_j^2 = 1$  means that the output of the  $\mathbf{w}_j$  filter creates high/low variance for input signals in class 1 and low/high variance for signals in class 2, such spatial filtering can significantly improve the recognition ability. As a rule, a small number of eigenvectors (usually no more than 4–6) are used as CSP filters in BCI applications. A more detailed overview of the CSP method can be found in Ref. [83].

We should also note that CSP improves the accuracy of synchronous BCIs, where signals are only analyzed during certain predefined periods of time. However, the use of CSP in asynchronous BCIs is not very efficient, mainly due to nonstationary properties of EEG/MEG signals [176]. In addition, spatial resolution and a choice of channels also affect the CSP efficiency. Specifically, the recording of a particular type of brain activity requires the adequate choice of electrode locations on the scalp. For these reasons, several approaches have been proposed to improve the original CSP method performance. Among them, we will highlight the methods of wavelet common spatial pattern (WCSP) [176], common spatio-spectral pattern (CSSP) [174], and common sparse spectral spatial pattern (CSSSP) [455].

#### 4.3.2. Wavelet-based skeleton method

CWT-based skeleton is an effective diagnostic tool that takes into account nonstationarity of the time–frequency structure of EEG/MEG signals during brain activity of interest [152,456,457]. This method is based on the estimation of the number of skeletons in the wavelet spectrum falling into particular frequency ranges.

Let the one-dimensional signal  $x_i(t)$  recorded by a channel  $i$  of a multidimensional signal  $\{X(t)\}_{i=1}^N$  of  $N$ -channel EEG or MEG during time  $t \in [T_s, T_s + \Delta t]$  be a linear superposition written as

$$x_i(t) = \sum_{n=0}^{\infty} \alpha_i^n y_i^n(t) + \xi_i(t) + \eta_i(t), \quad (21)$$

where  $\alpha_i^j$  is the amplitude,  $y_i^n(t)$  is the signal component at frequency  $f_{y^n}$  varied over a certain time interval  $t_f^n$ ,  $t_f^n \leq \Delta t$  for all  $j$ , and  $\xi_i(t)$  and  $\eta_i(t)$  are regular interference (artifacts) and noise, respectively. The signal components arranged in a decreasing order of amplitude are

$$\alpha_i^0 \geq \alpha_i^1 \geq \dots \geq \alpha_i^j \geq \dots \geq \alpha_i^{n_p} \dots \geq \alpha_i^{\infty}.$$

If we suppose that the number of components of  $y_i^j(t)$ , significant for processing and analyzing a task, are finite and take the value  $n_p$ , then the remaining terms of the sum  $\sum_{j=n_p}^{\infty} \alpha_i^j y_i^j(t)$  can be attributed to regular interference  $\xi_i(t)$  and not be taken into account in further analysis. In this case,

$$x_i(t) = \sum_{n=1}^{n_p} \alpha_i^n y_i^n(t) + \tilde{\xi}_i(t), \quad (22)$$

where

$$\tilde{\xi}_i(t) = \sum_{j=n_p}^{\infty} \alpha_i^j y_i^j(t) + \xi_i(t) + \eta_i(t)$$

is the recorded regular interference (artifacts) and EEG/MEG noise.

Obviously, the time intervals, where the amplitude of the  $y_i^j(t)$  signal component does not significantly change, can vary within 0.1–1 s. For such nonstationary short segments of time series, CWP allows a simultaneous analysis of the experimental signal  $x_i(t)$  in both frequency and time domains, resistant to sudden frequency changes [271,379,458].

Since the wavelet spectra carry redundant information for pattern identification, a *skeleton* method is often used [64, 457,459–462]. The essence of this method is to simplify the analysis of an entire surface of the signal sweep by studying, at each time moment, only those frequencies which account for the maximum CWP amplitude. Then, for each time  $t_0$  one needs to search for maxima in the wavelet spectrum:

$$E^n(f_{max}^n, t_0) = \max_{f_b - \delta/2 < f < f_b + \delta/2} W(f, t_0), \quad (23)$$

where  $f_{max}^n$  is the  $n$ th CWP skeleton lying within the analyzed frequency range with width  $\delta$  and central frequency  $f_b$ . It should be noted that the skeleton  $f_{max}^n$  can vary in time  $t_0$ , i.e., the skeleton is not constant and may eventually leave the frequency range under study.

From the physical point of view, the skeleton  $f_{max}^n$ , which is the global maximum of the surface  $W_i(f, t_0)$ , will be a frequency component of the signal spectrum, which accounts for the maximum fraction of the oscillation energy. Formally, it is possible to consider any number of skeletons for  $t_0$ . However, when analyzing experimental signals, the number of skeletons are determined by both the signal nature (the number of significant frequency components) and recording features, for example, the time–frequency sampling.

Applying CWT to both the left and right sides of Eq. (22), we can represent the signal in the time–frequency domain as

$$W_i(f, t) = \sum_{n=1}^{n_p} E_i^n(f_{max,i}^n(t), t) + W_{\tilde{\xi}_i}(f, t), \quad (24)$$

where  $W_i(f, t)$  is the wavelet spectrum of the signal  $x_i(t)$ ,  $E_i^n$  and  $f_{max,i}^n$  are the amplitude and frequency of the  $n$ th skeleton, describing the dynamics of the component  $y_i^n(t)$ ,  $W_{\tilde{\xi}_i}(f, t)$  is the wavelet spectrum of regular interference and noise. So, for each channel  $x_i(t)$  at each moment of time a discrete set of skeletons  $f_{max,i}^1, f_{max,i}^2, \dots, f_{max,i}^{n_p}$  is ordered by their amplitudes as

$$E_i^1 > E_i^2 > \dots > E_i^{n_p}. \quad (25)$$

Further studies of the processes using the signal  $x_i(t)$  are possible based on the analysis of skeletons and their amplitudes  $E_i^n(t)$  ( $n = 1, \dots, n_p$ ). For example, to real-time study the brain processes associated with conscious relaxation of a person with open eyes, one needs to analyze first and second skeletons which hit the alpha-range.

To extract the feature vector for each moment  $t$ , the pattern amplitude  $A_i$  is estimated in the frequency range of  $f_b \pm \delta/2$  as

$$A_i^{f_b \pm \delta/2}(t) = \sum_{n=1}^{n_p} \begin{cases} 1/n_p, & \text{if } (f_b - \delta/2 < f_{max,i}^1(t) < f_b + \delta/2) \cap \dots \\ & \cap (f_b - \delta/2 < f_{max,i}^n(t) < f_b + \delta/2) \cap \dots \\ & \cap (f_b - \delta/2 < f_{max,i}^{n_p}(t) < f_b + \delta/2) \\ 0, & \text{if } (f_{max,i}^1(t) \leq f_b - \delta/2) \cup (f_{max,i}^1(t) \geq f_b + \delta/2) \cup \dots \\ & \cup (f_{max,i}^n(t) \leq f_b - \delta/2) \cup (f_{max,i}^n(t) \geq f_b + \delta/2) \cup \dots \\ & \cup (f_{max,i}^{n_p}(t) \leq f_b - \delta/2) \cup (f_{max,i}^{n_p}(t) \geq f_b + \delta/2). \end{cases} \quad (26)$$

The expression (26) is convenient for automatic formation of a feature vector in real time, that is not only a qualitative criterion in presence or in absence of oscillatory activity in the selected frequency range, but also a quantitative characteristic of the intensity of this oscillatory activity. As noted above, in practice it is not necessary to consider the entire set of skeletons  $n_p$ , but only dynamics of  $n'_p \in (3, 7) < n_p$  first skeletons.

Although Eq. (26) is obtained for an  $i$ th channel, this approach can easily be generalized to an arbitrary number of EEG/MEG channels. Let us introduce an integral parameter of the intensity of the activity pattern by summing intensities of the patterns diagnosed in specific frequency ranges in a certain spatial region, characterized by a set of components  $i = 1, \dots, M$ :

$$A^{f_b \pm \delta/2}(t) = \frac{1}{M} \sum_{i=1}^M A_i^{f_b \pm \delta/2}(t). \quad (27)$$

This value allows integrating spatial and frequency dynamics of brain activity which the researcher knew *a priori*, e.g., from preliminary pilot experiments.

To illustrate this approach, we present the method of real-time evaluation of attention to a visual stimulus, for example, the Necker cube. The ambiguous image can be interpreted as a left-oriented or right-oriented cube. The BCI operator's task is to classify the cube orientation [288,463,464]. The aim of the BCI is to adjust the level of attention according to the person's mental state. When the level of attention decreases, the BCI activates biological feedback in the form of an audible signal to alarm the operator about a loss of his/her attention [152] (see Section 7.1).

The algorithm flowchart is schematically illustrated in Fig. 27. It includes the following six steps.

- EEG acquisition.** EEG signals are recorded by five electrodes ( $O_1, O_2, P_3, P_4, P_z$ ) with a 250-Hz sampling rate, typical for visual perception tasks [64]. The typical recording set is shown in Fig. 27(a). The starting time of the  $i$ th image presentation is shown by the vertical dashed line in the right panel.
- Time-frequency analysis.** The CWT with mother Morlet wavelet is performed [258]. The wavelet spectrum  $W_n(f, t)$  is calculated for every EEG channel  $X_n(t)$  in the  $f \in [1, 30]$  Hz range.
- Extracting spectral components.** In order to describe changes in time-frequency structure of EEG signals, induced by presented visual stimuli, skeleton dynamics of the wavelet spectrum is analyzed. For each channel, up to five skeletons ( $f_{\max}^1, \dots, f_{\max}^5$ ) are considered, which are characterized by maximal values of the wavelet amplitude  $E^1 > E^2 > \dots > E^5$ . Having calculated the wavelet spectrum and extracted the skeletons for next moments of time, the temporal evolution of the values of ( $f_{\max}^1, \dots, f_{\max}^5$ ) is found. Since visual attention is associated with the interplay between alpha (8–12 Hz) and beta (15–30 Hz) waves in occipital and parietal areas, we consider the skeletons belonging to these particular frequency bands. Fig. 27(c) shows typical time-dependent skeletons belonging to alpha- and beta-frequency bands during the transition from the background EEG ( $\Delta t_l$ ) to the perception of visual stimuli ( $\Delta t_H$ ). The red and blue colors indicate the belonging of the spectral components to alpha- and beta-bands, respectively.
- Quantification of perceptual process.** In order to quantify the efficiency of the stimulus processing by the observer, the brain dynamics is compared in 1-s intervals immediately before and after the onset of stimulus presentation. For this purpose, the values  $A_i^{1,2}, B_i^{1,2}$  are calculated using Eq. (27) during the presentation of an  $i$ th stimulus. These values statistically describe the location of maximal spectral components using EEG data taken from all occipital and parietal channels before and after the onset of image presentation, as follows:

$$A_i^{1,2} = \sum_{n=1}^N \int_{t \in \Delta t_{1,2}^i} \left[ \sum_{k=1}^K \xi_k^n(t') dt' \right], \quad \xi^n(t) = \begin{cases} 1/k, & \text{if } f_k^n \in \Delta f_\alpha, \\ 0, & \text{if } f_k^n \notin \Delta f_\alpha. \end{cases} \quad (28)$$

$$B_i^{1,2} = \sum_{n=1}^N \int_{t \in \Delta t_{1,2}^i} \left[ \sum_{k=1}^K \xi_k^n(t') dt' \right], \quad \xi^n(t) = \begin{cases} 1/k, & \text{if } f_k^n \in \Delta f_\beta, \\ 0, & \text{if } f_k^n \notin \Delta f_\beta. \end{cases} \quad (29)$$

Here,  $N = 5$  is the number of EEG channels used,  $f_k^n$  is the location of  $k$ th maximal spectral component, belonging to  $n$ th channel,  $K = 5$  is the number of analyzed spectral components, and  $\Delta t_{1,2}^i$  indicate 1-s time intervals preceding and following the  $i$ th image presentation (see Fig. 27(c)). The histogram in Fig. 27(d) shows typical  $A$  and  $B$  values calculated for each image presentation.

- Assessment of subject's attention.** Visual attention is known [64,378] to be associated with activation of an “attentional center” in the parietal cortex, which operates at 15–30 Hz frequencies [465]. This means that an increase in visual attention activates beta-waves in the parietal area. In addition, visual stimuli processing strengthens connectivity between occipital and parietal areas in alpha- and beta-bands [466,467], that in turn causes a growth of beta-activity in the occipital cortex. Finally, many studies evidence that visual information processing along with an increase in beta-activity simultaneously inhibits alpha-activity. According to our recent studies [378], an increase in visual attention causes a percept-related increase in beta-activity with an accompanying decrease in alpha-activity.

Taking into account the above observation, the subject's attention during visual stimulus processing can be quantified as

$$I(t_i) = \frac{(\bar{A}_i^1 - \bar{A}_i^2) + (\bar{B}_i^2 - \bar{B}_i^1)}{2}, \quad (30)$$

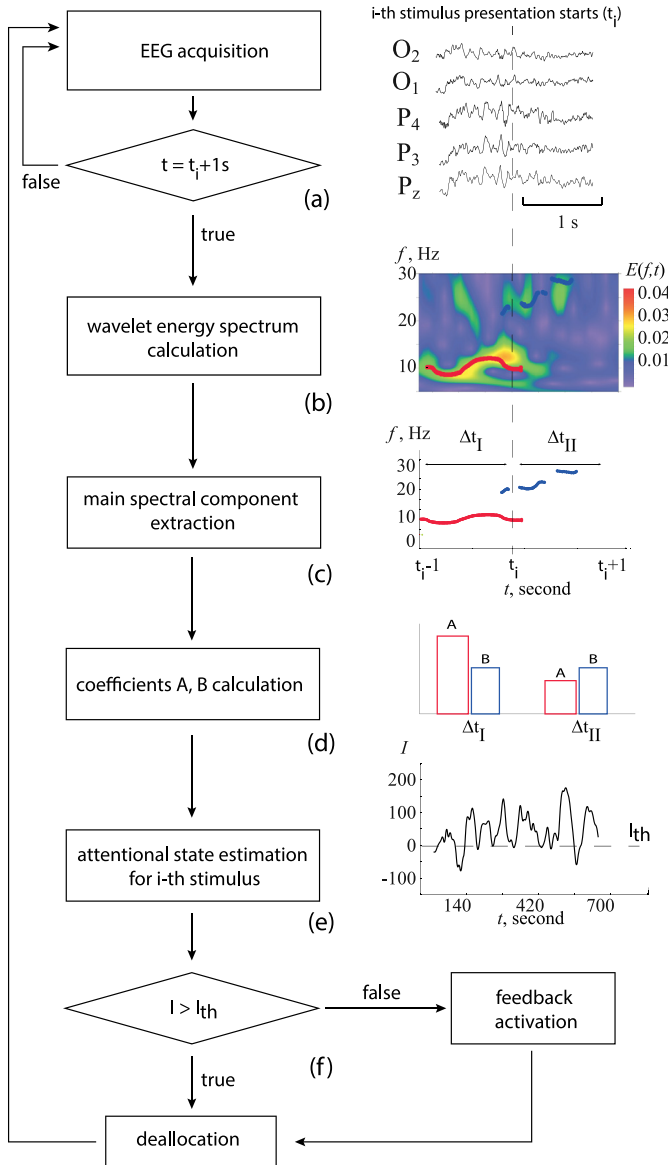


**Fig. 27.** Algorithm flowchart of the skeleton method for feature extraction. (a) EEG acquisition and a typical set of EEG recordings from 5 channels ( $t_i$  is the starting time of  $i$ th presentation). (b) Wavelet energy spectrum calculation and a typical fragment of wavelet energy distribution during perception of  $i$ th stimulus. (c) Extracting spectral components and typical evolution of main spectral components during transition from background EEG ( $\Delta t_I$ ) to perception of visual stimulus ( $\Delta t_{II}$ ). Red and blue colors indicate alpha (red) and beta (blue) frequency bands, respectively. (d) Histogram showing the values of  $A$  and  $B$  calculated by Eqs. (28) and (29) in time intervals  $\Delta t_I$  and  $\Delta t_{II}$ . (e) Temporal evolution of the value  $I$  which quantifies the degree of visual attention during an experimental session. The threshold value  $I_{th} = 0$  is shown by the horizontal dashed line. (f) Logical condition for feedback control activation. Reprinted from [152].

where  $\bar{A}_i^{1,2}$  and  $\bar{B}_i^{1,2}$  define the values of  $A_i^{1,2}$  and  $B_i^{1,2}$  averaged over six preceding events ( $i-6, \dots, i$ ). Such averaging is performed in accordance with [64], where the authors demonstrated that when stimuli are processed in a short time, the subject sometimes exhibits a low level of attention  $I$  during a single event, even while demonstrating overall high attention during the whole session.

One can see that  $I(t_i)$  reaches a maximal positive value, if the values in both brackets in Eq. (30) are high and positive. It corresponds to a state of high attention when  $\bar{A}_i^1 > \bar{A}_i^2$  and  $\bar{B}_i^2 > \bar{B}_i^1$ , i.e., alpha-activity decreases and beta-activity increases. On the contrary,  $I(i)$  reaches a minimal negative value when  $\bar{A}_i^1 < \bar{A}_i^2$  and  $\bar{B}_i^2 < \bar{B}_i^1$ . Finally,  $I(i)$  is zero when changes in alpha- and beta-activity are insignificant.

Fig. 27(e) shows a typical distribution of attention  $I$  during the experiment.

**6. Biological feedback activation.** The value of attention  $I$  is calculated after each visual stimulus is processed by the subject and compared to the threshold value  $I_{\text{th}}$  (see Fig. 27(f)). The value of  $I_{\text{th}}$  is set to zero and the feedback is organized as a short audio tone after the stimulus is processed, each time when  $I \leq I_{\text{th}}$ . The subject is previously instructed to associate this sound message with a low attention state.

#### 4.3.3. Wavelet-based coherence measure

The described above method for extracting signal features effectively works only in the case when a detected pattern has a clearly defined frequency and localization in space. Otherwise, this method cannot be applied due to large amplitudes  $W_{\xi}(f, t)$  in Eq. (24). Therefore, methods which take into account microscopic dynamics of the neural ensemble are required [302]. Spatially distributed EEG patterns of brain activity indicate the presence of coherent dynamics in different areas of the neural network. For implementation of state detection algorithms in real time, one needs to effectively isolate such coherent dynamics from the background of highly noisy neurophysiological (EEG, ECoG or MEG) data.

As an example, let us consider the ECoG set of WAG/Rij rats with genetic predisposition to absence epilepsy [468] before the formation of an epileptic discharge, shown in Fig. 28(a). The task of the neurointerface (see Section 6) is to register the rat brain activity and isolate EEG markers of seizure precursors to predict the seizure formation and then suppress it by electrical brain stimulation. In this case, the epileptic spike-wave discharge (SWD) develops due to the hypersynchronous activity of the thalamo-cortical network and has low-frequency delta and high-frequency theta/alpha precursors [469].

The analysis of signals taken from the Crtx4 and Crtx5 layers of the somatosensory cortex and the postero/lateral nucleus of the thalamus (PO), shown in Fig. 28(b)), does not allow distinguishing characteristic patterns. This situation is illustrated in Fig. 28(c) with the wavelet spectra obtained using a mother Morlet wavelet for each of the analyzed channels. It is clearly seen that at the beginning of the SWD, it is not possible to visually identify any characteristic activity, although peaks in the delta and theta/alpha ranges are traced. In this case, the fundamental condition for the effective allocation of features of the previous dynamics is a simultaneous analysis of multichannel recordings.

Recently, van Luijtelaar et al. [361] proposed using coherence  $\Pi(s, t)$  of multichannel EEG in BCIs. This value was defined as a product of spectra obtained for all set of EEG recordings at every time moment as

$$\Pi(s, t) = \prod_{i=1}^M W_i(s, t), \quad (31)$$

where  $i$  is a number of the analyzed EEG/ECoG/MEG channel. In the considered case, two subgranal cortical signals were recorded from the somatosensory cortex and thalamic PO.

The EEG/ECoG/MEG channels are represented by subscript  $i$ . Two subgranal cortical signals from the thalamic PO are also possible. Fig. 28(d) shows the corresponding result of the value calculated by Eq. (31). Unlike individual wavelet spectra, this measure clearly indicates the presence of coherent dynamics preceding the beginning of a peak-wave discharge, which can be used as a feature for a further automatic search of the precursor.

At the same time, it is not convenient to work directly with the wavelet surface in real time. Therefore, the following method for reducing the feature vector dimension was proposed [41].  $K$  characteristic frequency ranges were considered and the spectral energy of the timescales  $\Delta s_j$  was calculated as

$$G_{\Delta s_j} = \frac{1}{\Delta s_j} \int_{s \in \Delta s_j} \frac{1}{\tau} \int_{t_0=t-\tau}^t \Pi(s, t_0) ds dt_0, \quad j = 1, \dots, K, \quad (32)$$

where the integration was performed both over the range of timescales and time interval  $\tau = 500\text{ ms}$  chosen experimentally considering the minimal duration of the precursor.

In the simplest case, the criterion for detecting the pattern under study can be the threshold criterion:

$$G_{\Delta s_j} > G_{\text{th}}^j, \quad j = 1, \dots, K. \quad (33)$$

For prediction of epileptic activity, as the first step of the selection of the precursor's features, the value of  $G_{\Delta s_j}$  defined by Eq. (32) is considered in the 5–10 Hz range. It was found that this value increases at the seizure onset. The corresponding threshold value  $G_{\text{th}}^j$  was determined for an individual rat according to the preliminary analysis of the wavelet energy in the preictal state and in different types of background activity. As a result, the possibility to set the threshold energy which exceeded the energy of wakefulness states, but at the same time remained less than the preictal state energy, was found and precursors were detected via the condition Eq. (33). Unfortunately, such criterion caused a large amount of false alarms during the sleep due to an increase in the EEG signal power.

In order to reduce the number of false alarms caused by any other patterns of synchronized neuronal activity, the additional “sleep criterion” was introduced [41]. This criterion included the simultaneous consideration of three timescale ranges corresponding to common patterns of synchronous neuron activity: the range of sleep spindles (7–20 Hz), the range of theta/alpha precursors (5–10 Hz) and the range of low-frequency delta precursors (3–5 Hz). For all these ranges the mean wavelet energy Eq. (32) was calculated by averaging energies over the range of the timescales in the time interval  $\tau = 500\text{ ms}$ .

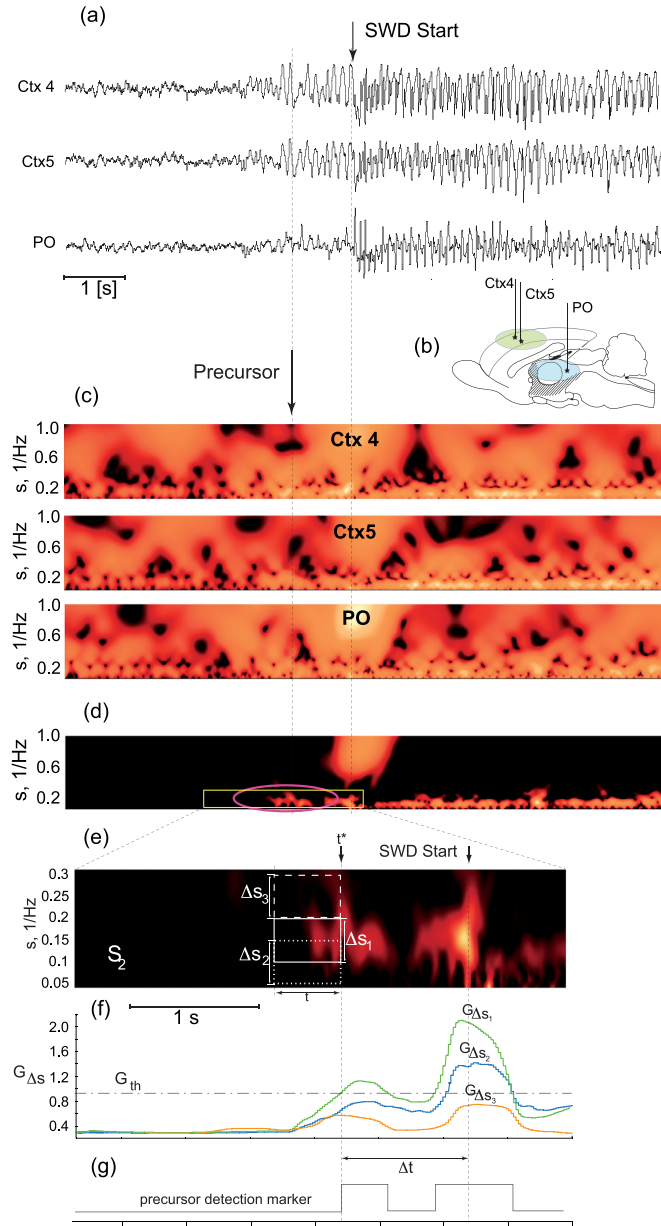


**Fig. 28.** (a) Set of EEG recordings taken from subgranular layers 4 (Ctx4) and 5 (Ctx5) of the somatosensory cortex and postero/lateral nucleus of the thalamus (PO). (c) Wavelet transform energy of the EEG signals (shown above) distributed over the range of time-scales  $s = 1/f$ . (d) Resulting product surface  $\Pi$  defined by Eq. (31). The circle shows the oscillatory pattern occurred prior the SWD onset and considered as its precursor. (e) Details of the rectangle area in panel (d) illustrating inter- and preictal  $\Pi(s, t)$ . The rectangular windows in panel (e) represent different time scales (frequency bands)  $\Delta s_j$ , for which the value of  $G_{\Delta s_j}$  is averaged. (f)  $G_{\Delta s_j}$  as a product of three values at every moment of time, averaged over time interval  $\tau$ .  $G_{th}$  is the threshold energy used for prediction. (g) Precursor detection marker defined by Eq. (34). Based on the data from [41].

The rectangular windows in Fig. 28(e) of lengths  $\Delta s_1$ ,  $\Delta s_2$ , and  $\Delta s_3$  marked by dotted, solid and dashed lines, respectively, indicate the regions on the  $(s, t)$  plane, over which  $G_{\Delta s_j}$  are calculated at time  $t^*$ . In online EEG data processing, the current time  $t$  is at the right-hand side of the rectangle, so that the algorithm stores 0.5-s prehistory for averaging. One can see from Fig. 28(f) that the mean energy  $G_{\Delta s_j}$  obtained during the precursor activity significantly exceeds the energy of the background activity. So, using the threshold value  $G_{th}$  one can automatically detect the precursor using the following three conditions:

$$G_{\Delta s_2} > G_{th}, \quad G_{\Delta s_2} > G_{\Delta s_1}, \quad G_{\Delta s_3} > G_{\Delta s_2}. \quad (34)$$

The second and third conditions were used to distinguish the precursor events from sleep spindles and low-frequency delta activity. Similar to the seizure, these types of activities are also induced by synchronous neuronal dynamics, but

have higher (up to 20 Hz) and lower (up to 5 Hz) frequencies, respectively. Using these criteria, the intelligent BCI system forms a binary control command in the presence of the seizure precursor shown in Fig. 28(g) (“1” is the epileptic discharge precursor and “0” is the background activity).

#### 4.4. Pattern recognition and classification approaches

The recorded signals of the brain activity intended for real-time diagnostics of the patterns of interest, are a complex set of rhythms and noises. Their frequency composition varies in time, sometimes very fast, so that the characteristic duration of desired patterns can be of several hundred milliseconds. Since the pattern amplitude is often smaller than the amplitude of the background activity, to highlight the activity of interest one needs either to average a significant amount of data or to search “thin” features of the pattern structure with the aim of creating a classification algorithm, which would allow revealing these features with a high degree of accuracy. Synchronous BCIs can be useful for this task because they allow accurate classification of the observed activity into one of the classes without a need for time detection (see Section 2.1). Instead, in asynchronous BCIs, besides the classification problem, there is also the problem of finding the moment of time when the mental command was “worked out” by the operator. This task, of course, requires not only the formal application of physico-mathematical analysis and machine learning for digital signal processing, but also a deep understanding of physiological processes, in order to reduce complexity of the analyzed data, in particular, the dimension of the data vector, basing on the structure of a neurophysiological brain response to cognitive or motor tasks [145].

Highlighting the approaches that can bring success in the allocation and classification of brain activity signals, we should note, first, semiempirical methods based on the time-frequency-spatial analysis of brain activity, which include the selection and classification of brain activity in different frequency bands and distinct brain areas (e.g., the secretion of sensomotor rhythms), as well as the analysis of functional brain connectivity while performing various cognitive and motor tasks or revealing different types of pathological activity. All accumulated tools of statistical physics, nonlinear dynamics, theories of synchronization and complex networks are actively used for the analysis of brain signals in real time, that is very important for applications in intelligent control systems, such as BCIs. Disadvantages of such approaches are usually high computational costs of these methods, which, nevertheless, with the development of parallel computing technologies and optimization of computational algorithms, ceases to be an obstacle for real-time implementation, even for relatively low-performance computing systems [31,470].

Recent advances in mathematics and computer science open wide possibilities on the use of various methods of machine learning for the development of intelligent systems which translate neural activity into appropriate control commands for BCIs. In general, machine learning methods can be divided into two classes, supervised and unsupervised learning. In supervised learning, we train the classifier using a training data set that consists of a set of inputs and corresponding outputs. The purpose of the training is the approximation of the classifier function on the basis of the training set, which at classification of new data belonging to the same class, correctly classifies them. If the output must be classified to a particular class (typically for BCI systems based on EEG, MEG, fNIRS, etc.), the problem is referred to as a *classification problem*, otherwise the problem is called a *regression problem*. The latter is often used in BCIs which control position and velocity of prosthetic devices, exoskeletons or robots. The choice between classification and regression, when designing a BCI, depends on the types of both the brain signal being recorded and the device being controlled [471].

The source data is usually a set of large-dimensional vectors, and the purpose of training is to build a statistical model which allows clustering the source data into classes. Therefore, learning without a teacher involves finding hidden statistical patterns in a big data array.

Very often both approaches, time-frequency-spatial and one on the basis of machine learning are utilized together in the same BCI to increase its efficiency. One of such approaches is based on the allocation of the vector of time-frequency properties of the input data using the wavelet analysis, followed by its classification using ANN [258,271,472].

Numerous reviews are devoted to machine learning methods in intelligent control systems of BCI (see, for example, [20, 21,433,471,473,474]), so we will not dwell on these issues in detail, giving a brief introduction to the main methods used in BCI classifiers. We start our consideration with the methods that solve the classification problem, and then proceed to the methods that implement the solution of the regression problem.

##### 4.4.1. Linear discriminant analysis

*Linear discriminant analysis* (LDA) is a simple mathematical technique widely used in HSC BCIs for classification. The main advantage of LDA is its low computational cost [475]. LDA usually classifies patterns into two classes (so-called binary classification), although it is also possible to extend this method to multiple classes [476].

For a two-class classification problem, LDA assumes that two classes are linearly separable [476], and the class of a feature vector  $\mathbf{x}$  depends on which side of the hyperplane

$$\omega_0 + \omega^T \mathbf{x} = 0 \quad (35)$$

it is, as shown in Fig. 29. Here,  $\omega$  is a weight vector and  $\omega_0$  is a threshold. LDA assumes normal distribution of the input data, with equal covariance matrix for both classes. The separating hyperplane is obtained by seeking a projection which maximizes the distance between means of the two classes, and minimizes the inter-class variance. In the case of an  $N$ -class problem ( $N > 2$ ), several hyperplanes are used [477].

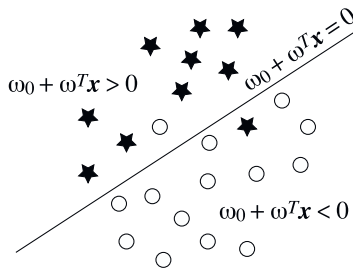


**Fig. 29.** Graphical illustration of the method of linear discriminant analysis (LDA). The hyperplane separates two classes shown by circles and stars.

The LDA technique is very suitable for online BCI systems and generally gives good results. However, LDA can result in a completely erroneous classification in the presence of outliers or strong noise.

There are various modifications of this algorithm, in particular, a regularized LDA [20] which introduces a regularization parameter  $C$  that can allow or penalize classification errors on the training set. The resulting classifier can accommodate outliers and obtain better generalization capabilities. Since outliers are common in EEG data, this regularized version of LDA may give better results for BCIs than its non-regularized version [478,479].

#### 4.4.2. Bayesian classification

Let us briefly consider two Bayesian classifiers used for BCIs, namely, (i) Bayes quadratic classifier and (ii) hidden Markov model (HMM), which produce nonlinear decision boundaries and provide more efficient rejection of uncertain data points under classification than discriminating classifiers.

The Bayesian classification aims at assigning to a feature vector the class it belongs to with highest probability. The Bayes rule is used to compute the so-called a posteriori probability that the feature vector has of belonging to a given class [480]. The Bayes quadratic classifier consists in assuming a different normal distribution of data that leads to quadratic decision boundaries. This classification approach was successfully applied in BCI intelligent systems for classification of motor imagery [481] and mental tasks [482].

HMM is a popular dynamical classifier in the field of pattern recognition [483]. HMM is a kind of probabilistic automaton of feature vectors, where each automaton state can shape the observation probability of a given feature. The main advantage of HMM for the BCI development is its perfect suitability for classification of time series. Since EEG is widely used to drive BCIs, HMM is often applied to classify temporal sequences of BCI features [484,485] and even raw EEG data [486].

#### 4.4.3. Cluster analysis

The above discussed methods provided a binary classification. However, there is often the problem of multi-class classification or cluster analysis. The simplest technique allowing such classification is *nearest neighbor* (NN) classification, based on the assumption that an input can be simply assigned to the class of its nearest neighbor [487]. The main problem with the simplest NN classification is its strong sensitivity to noise and outliers. This effect is illustrated in Fig. 30, where 2D-data are present as sets of points belonging to two classes: white circles (first class) and black stars (second one). The red square is a new data point to be classified. The simplest NN technique classifies this point as belonging to the second class because it is closer to the black star (innermost dashed circle) (Fig. 30(a)).

The NN technique can be improved by using  $k$ -nearest neighbors ( $k$ -NN). The main idea of this technique is as follows. An input vector is assigned to the class which is most common among  $k$  nearest neighbors, where  $k$  is a positive integer. Fig. 30(b) illustrates how  $k$ -NN can overcome the problem of outliers and make classification more robust. Thus, in the case of  $k = 3$ , the  $k$ -NN classifier correctly classifies the red square point as belonging to the first class (white circles) because the majority of the NNs are from the first class (for  $k = 3$  there are two white circles versus one black star).

For BCIs, the  $k$ -NN technique is usually applied using a metric distance. With a sufficiently high value of  $k$  and large enough training samples,  $k$ -NN can approximate any function which enables it to produce nonlinear decision boundaries. The  $k$ -NN algorithm is known to be very sensitive to the amount of data needed to properly describe different classes [427], that make them fail in neurointerfaces [479,488,489]. However, when used in BCI systems with low-dimensional feature vectors,  $k$ -NN may prove to be more efficient, for example, for classification of motor imagery EEG data [490,491].

Another clusterization technique used in asynchronous BCIs [492] for a multi-class feature analysis [488] is the Mahalanobis distance classification algorithm [493]. This method assumes a Gaussian distribution for each prototype of the class. Then, a feature vector is assigned to the class that corresponds to the nearest prototype, according to the Mahalanobis distance which is a measure of the distance between a data point and the distribution [493].

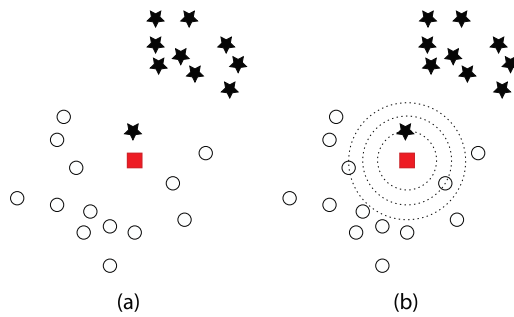


**Fig. 30.** k-NN illustration: classification of 2D-data by the nearest-neighbor technique.

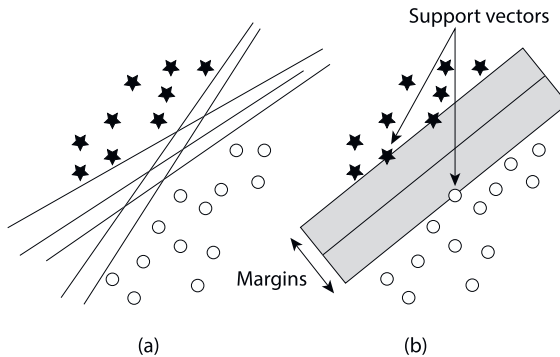


**Fig. 31.** Support vector machine (SVM) illustration. The method finds a separating hyperplane with the maximum “margin” (the line at the center of the shaded rectangle), which provides the best generalization performance.

#### 4.4.4. Support vector machine

Support vector machine (SVM) is a classifier that finds a separating hyperplane or a set of hyperplanes for which the margin between the samples of the two classes is maximized. Fig. 31 illustrates the main idea of the SVM approach. The circles and stars in Fig. 31(a) depict data points from two different classes, which are separated by different hyperplanes. There are an infinite number of such hyperplanes. Which of them is “optimal” for generalizing new data? Vapnik [494] showed that among the hyperplanes, the best generalization is achieved by selecting a hyperplane with the largest separation (“margin”) between two separable classes (Fig. 31(b)). The points from the training data which define this maximum margin are called *support vectors*.

SVM was applied to detect physiological patterns for EEG and EMG-based brain-machine systems [495]. It was also successfully used in a large number of synchronous BCIs [86,476,478]. This classifier is regarded as a linear classifier, since it uses one or several hyperplanes. Nevertheless, there is a possibility to develop SVM with a nonlinear decision boundary by means of a kernel function  $K(\mathbf{x}, \mathbf{x}')$ . The nonlinear SVM allows a more flexible decision boundary in the data space, that increases classification accuracy [496].

The kernel, often used in BCIs, is a *radial basis function* (RBF) represented as vectors in an input space and defined as

$$K(\mathbf{x}, \mathbf{x}') = \exp\left(-\frac{\|\mathbf{x} - \mathbf{x}'\|^2}{2\sigma^2}\right), \quad (36)$$

The SVM-RBF was applied in BCIs to classify P300 EPs [440,497] and motor imagery [498,499] using either EEG or EEG-fNIRS data.

SVM is widely used in BCIs because it is robust to the course of dimensionality, meaning that a large training set is not required for good results, even with very high-dimensional feature vectors [488]. These advantages come at the expense of processing speed.

#### 4.4.5. Combinations of classification techniques

In the majority of BCI applications, the classification of brain activity data sets is achieved using a single classifier. However, the combination of the outputs of several classifiers can provide better classification results. The outputs may even be disagree with each other on some training data set. Ensemble methods for classification produce an overall classifier with better generalization performance than any of the individual classifiers. Let us briefly consider the main classifier combination strategies used in BCI applications [20,471].

One of the simplest ensemble learning methods is *bagging*, that includes the following steps.

- Generate  $s$  new training data sets by sampling initial training data set.
- Train  $s$  classifiers (for example, ANN), one for each newly created data set.
- Classify a new feature vector by means of  $s$  classifiers to a class which receives a maximum number of “votes” (i.e., a class chosen by the majority of classifiers).

Perhaps the most popular bagging technique today is the method known as *random forests* (RF) [500]. RF is comprised of a collection of decision-tree classifiers which are simple types of a classifier that takes the form of a tree [501]. Each node in the tree represents a test of one of the input variables; depending on the outcome of the test, one of the tree sub-branches is taken. In this way, one follows a path all the way down to a leaf, which predicts an output class for the tree. In the case of RF, a feature vector is first run through each of the trees in the forest. Each tree predicts an output class, i.e., the tree “votes” for a particular class. The forest chooses a class which receives a maximum number of votes from all trees in the forest.

During the training, each tree in the RF is obtained in the following manner.

- According to bagging, an individual training set is obtained by sampling the original training data set  $h$  times, where  $h$  is the size of the training data set.
- The individual data set is used to grow a decision tree. Starting from the root node, at each subsequent node, a subset of  $m$  features is randomly selected. A test of these  $m$  features, that provides the best classification of the sample into two separate classes, is then used as the test for the node.

The RF classification technique was used in BCIs together with filter bank common spatial pattern feature extraction for EEG-based motor imagery classification [502] and P300-based spelling neurointerface [503].

A more sophisticated ensemble technique is *boosting*, which combines several classifiers in cascade, where each next classifier focuses on errors committed by previous classifiers. In this method, feature vectors for which the current set of classifiers predict incorrectly, are given higher weights than for feature vectors correctly predicted. This allows finding a new classifier that works better with a training data set for which the current set of classifiers works poorly. The final output of the ensemble classifier is based on a weighted sum of the outputs of all classifiers. Boosting differs from bagging where each new classifier is selected based on the performance of previous classifiers, whereas in bagging, the resampling of the training set at any given stage does not depend on the performance of earlier classifiers. To develop BCI intelligent systems, the boosting approach was applied with ANNs [504,505] and the ordinary least square method [506]. This technique together with common spatial patterns was recently applied for classification of spatial-spectral EEG-based data of post-stroke patients for their rehabilitation training [507].

The main advantage of the combination of classification techniques is the variance reduction (see Section 4.2) and hence a decrease in the classification error [427].

#### 4.4.6. Linear regression

In the introduction of Section 4.4, we have shown that the classification involves mapping inputs to a finite number of classes or a continuous output, i.e., a real-valued scalar or a vector. This is the case of a *linear regression* (LR) which consists in the learning of a function that maps arbitrary input vectors to appropriate outputs based on a given training set of  $h$  example input-output pairs of vectors  $(\mathbf{y}_m, \mathbf{g}_m)$ , where  $m = 1, \dots, h$ .

LR assumes that the mapping function generating the data is linear, i.e., the output vector  $\mathbf{g}$  is a linear function of the input vector  $\mathbf{y}$ . Let us consider a simplest case, when the input  $\mathbf{y}$  is the  $n$ -dimensional vector (e.g., EEG potentials of  $n$  channels) and the output  $g$  is a scalar value. The output is then given by the linear function

$$g = \sum_{i=1}^n \mathbf{w}_i \mathbf{y}_i = \mathbf{w}^T \mathbf{y}, \quad (37)$$

where  $\mathbf{w}$  is a weight vector determined from the training data. The linear least squares regression finds a weight vector that minimizes the sum of squared output errors over all training examples

$$E(\mathbf{w}) = \sum_m (d_m - g)^2 = \|\mathbf{d} - \mathbf{Y}\mathbf{w}\|^2, \quad (38)$$

where  $\mathbf{d}$  is a vector of training outputs,  $\mathbf{Y}$  is an input matrix whose rows are input vectors  $\mathbf{y}$  from the training set, and  $\|\cdot\|$  is the square root of the sum of squares of each vector component. Minimizing the error by taking the derivative  $dE(\mathbf{w})/d\mathbf{w}$  and setting the result to zero, we can obtain the weight vector

$$\mathbf{w} = (\mathbf{U}^T \mathbf{U})^{-1} \mathbf{U}^T \mathbf{d}, \quad (39)$$

where  $(\mathbf{U}^T \mathbf{U})^{-1} \mathbf{U}^T$  is a pseudoinverse transformation. This technique is called the *Moore-Penrose pseudoinverse method* [508].

LR is often used in invasive BCIs due to the fast and easy computational procedure. At the same time, LR is too simple for noninvasive EEG-based BCIs where the mapping from brain signals to control commands is typically nonlinear.

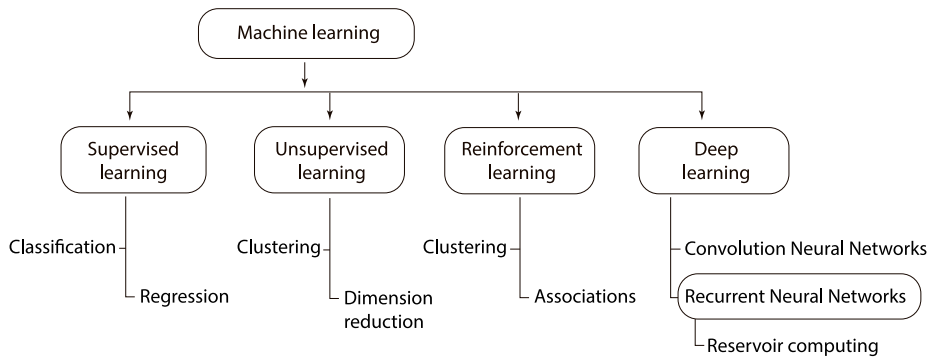


**Fig. 32.** Classification of modern machine learning approaches.

#### 4.5. Machine learning and reservoir computing

The modern and promising approaches to analyzing neurophysiological signals are machine learning (ML) and reservoir computing (RC). These methods imply data analysis without prior knowledge of the data origin, i.e., the model-free data. In other words, the underlying mathematical model (or dynamical system) that generates time series is unknown. At the same time, ML and RC can build this model based on sample data, known as “training data”. Thus, these methods, being trained on a reasonable and representative amount of training data, enable performing different tasks (classification, detection, prediction) on the newly acquired data.

The ML approach to data analysis meets the fundamental requirements for the BCI. On one hand, the brain activity patterns (biomarkers) that can be found in ECoG/EEG/MEG and fNIRS signals do not give a clear understanding of the underlying physiological mechanisms. Despite the large number of mathematical models aimed at explaining collective neuronal activity, precise mathematical equations describing the emergence of a particular biomarker do not yet exist. On the other hand, brain activity varies between different subjects (BCI's operators) and even between different experimental sessions in the same operator. Thus, if such a model would exist, its results seem to vary significantly under external and internal factors. Finally, ML demands low computational costs. Although the training procedure is quite demanding, the trained ML performs data analysis very fast, even on mobile computers or modern cell phones [509].

The analysis of neurophysiological signals in BCI can successfully be performed by machine learning techniques. Despite a long history associated with this research, the performance of ML methods in BCI is still not up to par. Since ML suggests solving tasks without an interpretable rule, the improvement and optimization of these methods lack an appropriate control. To improve our understanding of ML, one needs special approaches of nonlinear physics and dynamical system theory. First, ML can predict the evolution of a dynamical variable in the phase space, reconstruct an attractor, or infer features of the underlying mathematical model. In this context, the ML application to a study of dynamical systems enables validating ML outcomes via other numerical and analytical tools of nonlinear analysis.

Second, ML itself represents a dynamical system exhibiting steady states and demonstrating a variety of nonlinear phenomena. For instance, the training facilitates the convergence of the system to a steady state. The robustness of this steady state to input data deviations plays a crucial role in the ML ability to analyze the data.

Finally, the ML ability to approximate the functional relationship between input and output variables contributes to dynamical system analysis. It is related to generalized synchronization (GS) manifested by the functional relationship between the drive  $\mathbf{x}(t)$  and response  $\mathbf{y}(t)$  states of the coupled dynamical systems [510]:

$$\mathbf{y}(t) = \mathbf{F}(\mathbf{x}(t)) \quad (40)$$

or in the case of mutually coupled systems [511]:

$$\mathbf{F}(\mathbf{x}(t), \mathbf{y}(t)) = 0. \quad (41)$$

Along with the dynamical systems, this ML-based approach is very promising for neurophysiological data analysis [411] focused on the FBC-based BCI problem (see Section 4.1.4).

In the following section, we will briefly review the ML techniques concentrating on their physical principles and applications in the field of BCI.

##### 4.5.1. Basics strategies of machine learning application

Machine learning approaches are traditionally divided into three broad categories, depending on the nature of input data and learning strategy (see Fig. 32)

– *Supervised learning* represents a strategy where the ML is initially fed the training data (the example inputs and their desired outputs). Thus, the ML learns a general rule that maps inputs to outputs.

– *Unsupervised learning* suggests that no input–output associations are given to the learning algorithm, leaving it on its own to find structure in the input.

– *Reinforcement learning* implies that ML interacts with a dynamic environment in which it must fulfill a specific goal (such as driving a vehicle). As ML navigates through its problem space, it receives feedback similar to the reward it is trying to maximize.

According to the review [512], conventional ML techniques have a limited ability to process natural data in its raw form. Therefore, they require a feature extraction to transform the raw data into a suitable internal representation or feature vector beforehand.

*Representation learning* overcomes this limitation allowing ML to be fed raw data and to automatically discover the representations needed for detection or classification.

*Deep learning* is a type of representation learning involving computational models that are composed of multiple processing layers to learn representations of data with multiple levels of abstraction [512]. Starting with the raw input, each layer transforms its representation of the input data to the next, higher layer. As a result, higher layers of representation amplify aspects of the input that are important for discrimination and suppress irrelevant variations.

#### 4.5.2. Deep learning

Deep learning (DL) is a form of ML that enables computers to learn and understand the environment in terms of a hierarchy of concepts. It provides two main advantages. First, the DL model gathers knowledge from experience; therefore, there is no need for an operator to specify the data to learn. Second, the hierarchy of concepts allows learning complicated concepts by building them out of simpler ones [513,514]. Due to its ability to extract functions from raw data, DL has shown great promise in the interpretation of EEG signals [515].

**Deep feed-forward networks.** A feed-forward (FF) neural network is an artificial neural network (ANN) wherein connections between the nodes do not form a cycle. In this network, the information moves in only one direction from input nodes to output nodes through hidden layers. Deep FF ANNs known as multilayer perceptrons (MLPs) were introduced by Rumelhart and McClelland [516,517] in 1986. Fig. 33 illustrates the MLP scheme that consists of  $l$  hidden layers. A layer with  $l = 0$  is the input layer that receives EEG signals from  $n$ -channels and translates them to the next layer. The  $i$ th element of the  $l$ th layer transforms the input signal according to the following equation [518]

$$u_i^l(t) = F^l \left( \sum_{p=1}^{H^{l-1}} \omega_{pi}^l u_p^{l-1}(t) - \theta_i^l \right), \quad (42)$$

where  $H^l$  is the number of neurons in the  $l$ th layer,  $u_i^l(t)$  is the output signal of the  $i$ th neuron belonging to the  $l$ th layer ( $u_i^0(t)$  being signals from analyzed EEG channels,  $\mathbf{W}^l = \{\omega_{pi}^l\}$  is a weight matrix of the  $l$ th layer of dimension  $(H^{l-1} \times H^l)$ ,  $\omega_{pi}^l$  ( $p = 1, \dots, H^{l-1}$ ,  $i = 1, \dots, H^l$ ) are synaptic weights of input signals for the  $i$ th neuron in the  $l$ th layer,  $\Theta^l = \{\theta_i^l\}$  is a threshold vector for neurons in the  $l$ th layer, and  $F^l(\eta)$  is a nonlinear activation function for neurons in hidden and output layers  $l$ . Among many activation functions [519], the logistic function (or sigmoidal function) is the most frequently used one, defined as

$$F^l(\eta) = \frac{1}{1 + \exp(-\beta\eta)}. \quad (43)$$

The sigmoid is the smoother version of the threshold function, which squashes the input to be between “0” and “1”, while the parameter  $\beta$  controls the function slope. The differentiability of the logistic function is important when we derive a backpropagation learning rule [513]. The unknown matrix  $\mathbf{W}^l$  and vector  $\Theta^l$  can be obtained during the learning process by minimizing the classification error. MLP without hidden layers is a simple perceptron, equivalent to LDA (see Section 4.4.1) and sometimes used for BCI applications [520,521].

The MLP is a very flexible classifier that can classify any number of classes and solve many problems. In the field of BCIs, the MLPs were applied to classify up to five different mental commands [522,523] for both synchronous [524] and asynchronous BCIs [441]. Although MLP is a powerful and universal tool, it often suffers from overfitting training data, especially when dealing with noisy and nonstationary data, such as EEG [525,526]. In their recent work, Assi et al. [527] used MLP to predict epileptic seizures. They extracted features from the bispectrum, including normalized bispectral entropy, normalized bispectral squared entropy, and mean magnitude. They used them as inputs to a 5-layer multilayer perceptron classifier and achieved accuracies of 78%. Recently, the MLP and SVM-based techniques were applied for recognition and classification of EEG patterns associated with motor imagery [145]. The combination of MLP with evolutionary algorithms allowed the selection of the most informative EEG features to optimize the network hyperparameters [528]. However, MLP still requires operator supervision to achieve better performance.

For automatic identification of ambiguous stimulus interpretation from the EEG data, we used the network properties of brain neuronal activity [529]. Having analyzed functional neural interactions, we specified the brain area in which neural network architecture exhibits differences for different classes of EEG trials. This allowed us to optimize the FF MLP and develop a strategy for the training set selection to maximize the classification accuracy, being 85% when all EEG channels were used. The revealed localization of the percept-related features provided about 95% accuracy when the number of EEG channels was reduced up to 90%.

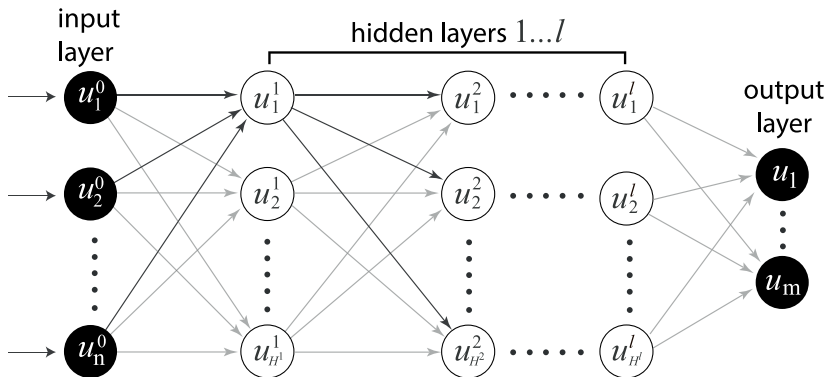


**Fig. 33.** (a) Multilayer perceptron architecture with  $l$  hidden layers.  $n$  and  $m$  are the numbers of input and output nodes and  $H^i$  defines the number of nodes in the  $i$ th layer.

**Convolutional neural network (CNN).** A convolutional neural network consists of an input and an output layer, as well as multiple hidden layers (Fig. 34). Each hidden layer includes a convolution layer and a pooling layer. These layers alternate forming a set of features to be fed to a MLP.

Let us consider the input of CNN as  $N$  matrices  $w_0 \times h_0$ . To define a convolution layer, one has to define hyperparameters: convolution kernel size ( $n_1 \times n_2$ ) and the number of channels ( $M$ ). Researchers determine the number of channels according to the task's requirements. If one takes many channels, the recognition quality will increase, but the computational complexity will also increase. In Fig. 34 we demonstrate a general case with  $M$  channels, but in most cases  $M = 2$  is enough. Introducing  $M$  channels means that each map of the previous layer is associated with  $M = 2$  maps of the convolution layer. Thus, for  $N$  input matrices one has  $MN$  matrices in the first convolution layer. The number of matrices increases from one layer to another, but their size decreases. Thus, in the  $i$ th layer the matrix size is equal to  $(w_i \times h_i)$ , where

$$w_i = w_{i-1} - n_1 + 1, \quad (44)$$

$$h_i = h_{i-1} - n_2 + 1. \quad (45)$$

Here,  $(n_1 \times n_2)$  is a size of convolution kernel. The kernel size usually varies in the range from  $3 \times 3$  to  $7 \times 7$ . If the size is too small, the CNN cannot distinguish any features. On the other hand, if the size is too large, then the computational cost increases. Finally, kernel size is usually chosen so that the number of maps in the convolutional layer are even. It prevents losing information when decreasing the dimension in the pooling layer, described below. The kernel represents a system of shared weights or synapses, which is the main feature of CNN. In MLP, there are many connections between neurons, which dramatically slows down the computational process. In CNN, the shared weights reduce the number of links enabling finding the same feature throughout the entire matrix (or image).

Initially, the matrices of the convolutional layer contain zeros. The values of the weights of the kernels are set randomly in the range  $[-0.5, 0.5]$ . The kernel slides over the matrix and performs the convolution operation:

$$[\mathbf{F} * \mathbf{G}](w, h) = \sum_{k=1}^{n_1} \sum_{l=1}^{n_2} \mathbf{F}(w - k, h - l) * \mathbf{G}(k, l), \quad (46)$$

where  $\mathbf{F}$  is a matrix and  $\mathbf{G}$  is a convolution kernel.

Each matrix in the convolution layer undergoes further processing in the pooling layer. As a result, the pooling layer also returns maps, but their number coincides with the number of ones in the convolutional layer (here, it is  $M \times N$ ). The pooling layer reduces the dimensions of the maps of the previous convolutional layer.

Suppose the previous convolution operation has already identified some features. In that case, such a detailed image is no longer needed, and the pooling layer compresses it to a less detailed one. Moreover, filtering out unnecessary information helps to prevent overfitting.

Compression is implemented by using a pooling kernel. It is a  $l \times l$  matrix that reduces the previous maps of the convolutional layer in  $l$  times. The entire feature map of the convolutional layer is divided into cells of nonoverlapping  $l \times l$  elements from which the maximum value is selected. This algorithm is known as *MaxPooling*. Usually, the pooling kernel has a  $2 \times 2$  size allowing the dimension reduction in half.

Thus, the number of matrices grows from one convolutional layer to another as  $\sim N^k$ , where  $k$  is a layer number. Simultaneously, the matrix dimensions diminish due to convolution and pooling. Finally, after several convolutional and pooling layers, CNN forms a vector of features and feeds it to fully connected layers. Neurons in a fully connected layer have connections to all activations in the previous layer, as seen in regular (non-convolutional) ANNs.

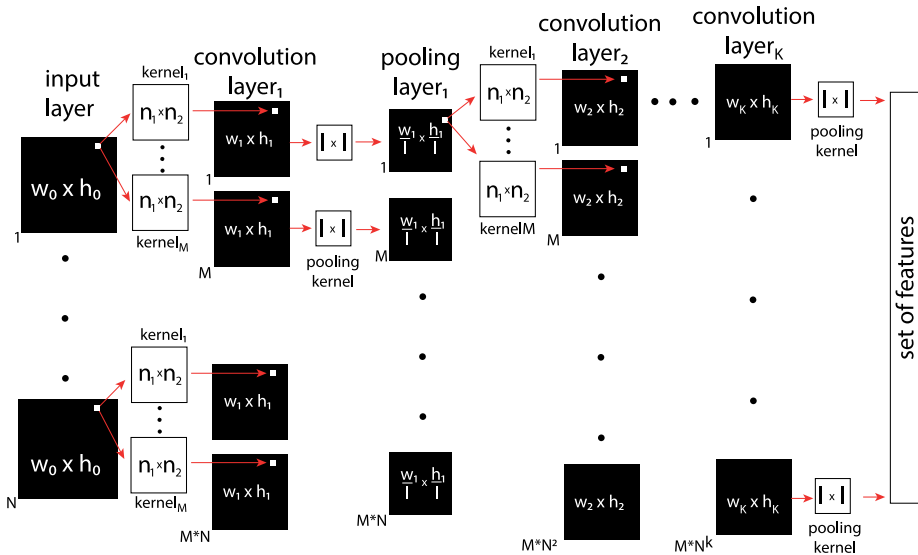


**Fig. 34.** Schematic representation of CNN composed of  $k$  convolution layers alternating with the pooling layers. CNN's input is the set of  $N$  matrices  $w_0 \times h_0$ . Each input matrix is processed with  $M$  kernels whose dimensions are  $n_1 \times n_2$ . They transform each input matrix in the set of  $M$  matrices with lower dimensions ( $w_1 \times h_1$ ). The obtained matrices pass through the pooling layer, and their dimensions reduce as  $(w_1/l \times h_1/l)$ , where  $l \times l$  are the kernel's dimensions. When passing through  $k$  layers, input matrices are transformed into the vector of features.

Moving from one layer to another, CNN first extracts local, low-level features and then increasingly more global and high-level features. They learn to detect increasingly complex visual elements (e.g., edges, simple shapes, complete objects) from raw images.

Over the past years, CNNs have become highly successful in computer vision and speech recognition [512]. There is also increasing interest in using CNN for EEG analysis in research and application areas, including BCI studies (see [530] for review).

CNNs used in computer vision and speech recognition to perform automatic feature extraction and classification, were successfully applied to EEG-based BCIs, however, to a single BCI paradigm only. Thus, it remains unclear how these architectures generalize to other paradigms. In their recent work, Lawhern et al. [531] studied whether a single CNN architecture can accurately classify EEG signals from different BCI paradigms while simultaneously being as compact as possible. As a result, they introduced EEGNet, a compact CNN for EEG-based BCIs. They showed that neurophysiologically interpretable features could be extracted from the EEGNet model. This is important as CNNs, despite their robust and automatic feature extraction, often produce hard to interpret features. For neuroscience practitioners, the ability to derive insights into CNN-derived neurophysiological phenomena may just be as important as achieving good classification performance, depending on the intended application.

The main restriction of using CNN is that the number of samples in most neuroimaging datasets is limited, making such data less adequate for training large-scale networks with many parameters. Nevertheless, many researchers inform on the successful use of CNN to classify fMRI and EEG data with moderate dataset sizes. For instance, Gao et al. [532] applied an EEG-based spatio-temporal CNN to monitor driver fatigue. They achieved a 97% classification accuracy in the classification of alert and fatigue states using 2800 EEG samples of eight subjects under within-subject splitting. In the same group [533], a simple CNN structure was proposed for EEG-based classification. Using a coincidence filtering-based approach the authors achieved up to 98% accuracy in the emotion recognition and fatigue driving detection task. Due to its generality, the proposed CNN design may be useful for broad applications in health monitoring areas.

According to Schirrmeister et al. [534], several critical methodological questions on EEG analysis with CNNs remain. First, the authors note that CNNs have both advantages and disadvantages when compared with other ML techniques. The main advantage is that CNN can learn raw data features without any prior feature selection. The disadvantages are a risk of false predictions with high confidence, many hyperparameters, and difficulty in data interpretation. They also point out that EEG signals differ from inputs usually used for CNN, for example, an image. Unlike a two-dimensional static image, EEG is a dynamic time series obtained from the three-dimensional scalp surface. Also, the EEG has a comparatively low signal-to-noise ratio. Thus, random fluctuations often affect the EEG more strongly than task-relevant sources. Finally, they concluded that these properties could make the learning process using EEG signals more difficult than using images. Thus, the existing CNN architectures from the field of computer vision must be adapted for EEG input, and the resulting decoding accuracy must be rigorously evaluated in comparison with more traditional methods of feature extraction.

**Recurrent neural network (RNN).** RNN is an ANN class in which connections between nodes form a directed graph along in time sequence. This allows the RNN to exhibit dynamic behavior over time. RNNs include finite impulse response

(FIR) and infinite impulse response (IIR) networks. The FIR network is a directed acyclic graph that can be unrolled and replaced with a strictly feedforward neural network. In contrast, the IIR network is a directed cyclic graph that cannot be unrolled.

The FF network model (such as MLP) described above forms a complex mapping from the first layer input to the output of the last layer. It is, nevertheless, a static mapping, i.e., there are no internal dynamics. The FIR linear filter can replace each static synaptic weight in MLP. By FIR, we mean that for an input excitation of the finite duration, the filter output will also be of the finite duration. The most basic FIR filter can be modeled with a tapped delay line, as illustrated in Fig. 35(a). For this filter, the output  $y(k)$  corresponds to a weighted sum of the past delayed values of the input:

$$y(k) = \sum_{n=0}^T w(n)x(k-n) \quad (47)$$

From a biological perspective, the synaptic filter may reflect the processes of axonal transport, synaptic modulation, and charge dissipation in the cell membrane. Thus, the weight of the link between  $i$ th and  $j$ th neurons in layer  $l$  is specified by vector  $\mathbf{w}_{ij}^l = [w_{ij}^l(0), w_{ij}^l(1), \dots, w_{ij}^l(T)]^T$ . The vector  $\mathbf{x}_i^l(k) = [x_i^l(k), x_i^l(k-1), \dots, x_i^l(k-T)]^T$  denotes delayed states along the synaptic filter. The output  $x_j^{l+1}(k)$  of a neuron in the  $i$ th layer at time  $k$  is now a sigmoid function of the sum of all filter outputs which feed the neuron:

$$x_j^{l+1}(k) = F\left(\sum_i \mathbf{w}_{ij}^l \mathbf{x}_i^l(k)\right). \quad (48)$$

This equation is similar to one of the static MLP model Eq. (43) with the difference that the scalars and multiplications are replaced by vectors and vector products, respectively.

The IIR filter output is written in the form

$$y(k) = \sum_{n=0}^T a(n)x(k-n) + \sum_{m=1}^M b(m)y(k-m), \quad (49)$$

where the second term means that some of previous output samples of the filter are used to calculate the current output sample. The schematic illustration of the IIR is present in Fig. 35(b).

Both the FIR and IIR networks can have additional stored states, and the storage can be under direct control by the neural network. Such controlled states are referred to as a gated state or gated memory and are part of long short-term memory networks (LSTMs) and gated recurrent units.

The central idea behind the LSTM architecture is a memory cell, which can maintain its state over time, and nonlinear gating units, which regulate the information flow into and out of the cell [535]. The first LSTM was designed by Hochreiter and Schmidhuber [536]. They proposed that RNNs can use their feedback connections to store representations of recent input events in the form of activations (short-term memory). Simultaneously, they noted that learning RNN to store information over extended time intervals via recurrent back propagation may fail due to insufficient decaying error back flow.

When an ANN is trained using the gradient-based learning methods and back propagation, each of the neural network's weights receives an update proportional to the partial derivative of the error function for the current weight in each iteration. In some cases a so-called *vanishing gradient problem* occurs when the gradient is vanishingly small, effectively preventing the weight from changing its value. In the worst case, this may stop further ANN training.

This issue causes the memory content to be influenced by the perturbation of irrelevant inputs (input weight conflict) and outputs (output weight conflict). To address this issue, Hochreiter and Schmidhuber [536] proposed a memory cell, including the input and output gates. Fig. 36 illustrates the LSTM memory cell. At its core, it has a recurrently self-connected linear unit called *constant error carousel* (CEC), whose activation is called the cell state. The CECs solve the vanishing error problem: in the absence of new input or error signals to the cell, the CEC local error back flow remains constant, neither growing nor decaying. The CEC is protected from forward flowing activation and backward flowing error by the input and output gates. When gates are closed (activation around zero), irrelevant inputs and noise do not enter the cell, and the cell state does not perturb the remainder of the network. The cell state ( $S_c$ ) is updated based on its current state and three sources of input:  $net_c$  is the input to the cell itself, while  $net_{in}$  and  $net_{out}$  are the inputs to the input and output gates.

Later, Gers, Schmidhuber and Cummins [537] showed that LSTM fails to learn in order to process continuous time series that are not a priori segmented into training subsequences with clearly defined ends. The problem is that a continuous input stream may cause the cells' internal values to grow without bound, even if the nature of the problem suggests they should be reset occasionally. To overcome this limitation, the authors proposed using forget gates that learn to reset memory blocks once their contents are out of date and useless. Mathematically, they replaced standard LSTM constant CEC weight 1.0 by the multiplicative forget gate activation  $y^\phi$  calculated like the other gates activations and squashed using a logistic sigmoid. Initially, the LSTM gates weights were negative for input and output gates and positive for forget gates. Therefore, when training begins, the forget gate activation is almost 1.0, and the entire cell behaves like a standard LSTM cell. It does not explicitly forget anything until it has learned to forget.

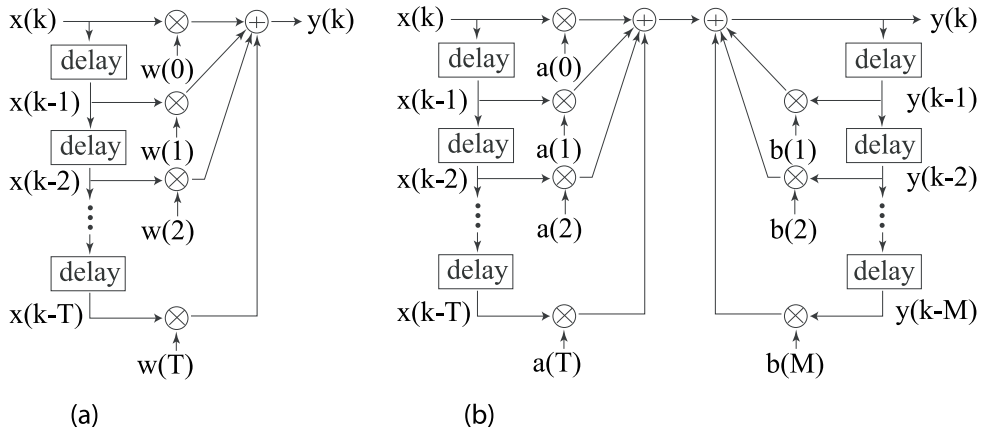


**Fig. 35.** Schematic illustration of (a) finite impulse response (FIR) and (b) infinite impulse response (IIR) models.

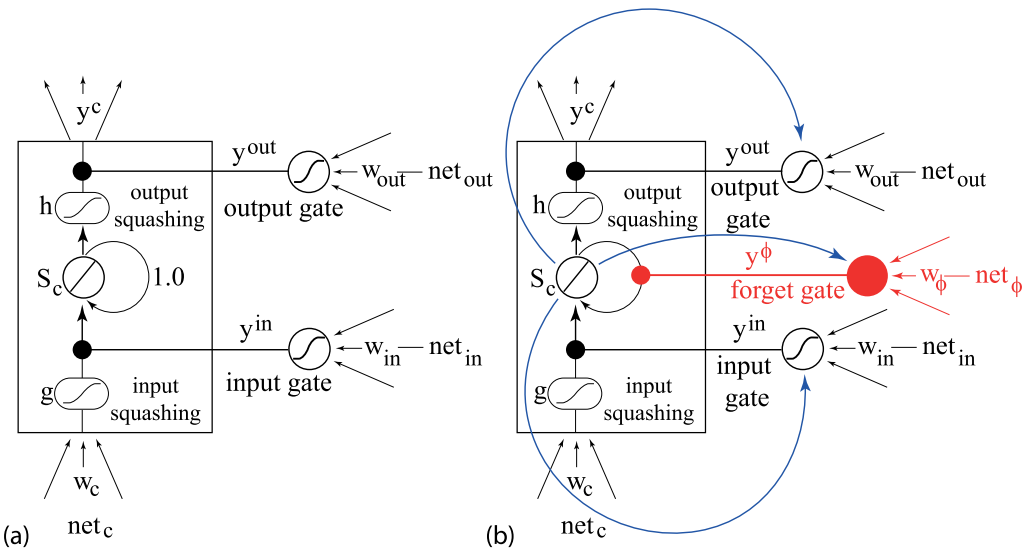


**Fig. 36.** (a) The LSTM cell has a linear unit with a recurrent self-connection. Input and output gates regulate read and write access to the cell whose state is denoted by  $S_c$ . The function  $g$  squashes the cell input;  $h$  squashes the cell output. (b) The LSTM cell with a forget gate unit (red dot) and the peephole connections (blue curves) allowing the cell to control the gates.

In the next work, Gers and Schmidhuber [538] argued that the cell needs to control the gates to learn precise timings. To do so, they added the peephole connections (blue curves in Fig. 36(b)). Afterward, Cho et al. [539] proposed a simplified LSTM architecture called *gated recurrent unit*. They used neither peephole connections nor output activation functions and coupled the input and the forget gate into an update gate. Finally, their output gate (called *reset gate*) only blocks reconnections to the block input.

Over the past few years, many different modifications of RNN were proposed to solve tasks in various fields [540] including BCI applications where the RNN plays an important role [541,542]. Recent studies highlight advantages of RNN in a p300 BCI [543]. The LSTM-based EEG analysis algorithms are used in the motor imagery BCI [544,545] and allow decoding the trajectory of the arm movement from MEG signals [546].

**Reservoir computing (RC)** is originally an RNN-based framework and is therefore suitable for temporal/sequential information processing. In RC, input data are transformed into spatiotemporal patterns in a high-dimensional space by an RNN in the reservoir. Then, a pattern analysis from the spatiotemporal patterns is performed in the readout. The specific RC feature is that input weights ( $w^{in}$ ) and weights of recurrent connections within the reservoir ( $w$ ) are not trained, while only the readout weights ( $w^{out}$ ) are trained with a simple learning algorithm such as linear regression. This simple and fast training process makes it possible to drastically reduce the computational cost of learning as compared with standard RNNs, which is the major RC advantage [547]. The physical principles of the reservoirs and their ability to solve the tasks of sequence learning and temporal pattern discrimination are described below in this review. In the field of BCIs, the RC, especially echo state networks, are used for brain activity detection and classification [548,549].

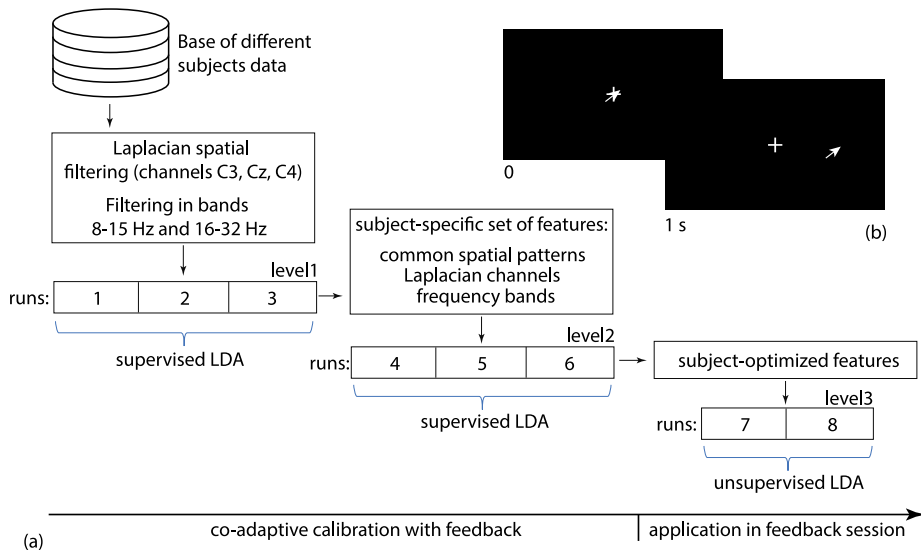


**Fig. 37.** The example of the co-adaptive learning. Level 1: A database is used to calculate an initial subject-independent classifier in Laplacian channels C3, Cz, and C4. For three runs, the linear discriminant analysis (LDA) is adapted. Level 2: The collected data of the first three runs are used to select a subject-dependent frequency band and calculate CSP and Laplacian channels. Then, three more runs are performed, where the Laplacian channels are reselected after every trial and the classifier retrained. Level 3: Data are used to recalculate CSP and perform the last two runs, with an unsupervised adaptation of the classifier that allows tracking the features drift and estimate an unbiased BCI performance.

Source: Redrawn from [552].

#### 4.5.3. From supervised to unsupervised strategies in BCI research

As mentioned above, supervised learning requires ML training with some “training data”. This means that subjects undergo a calibration session beforehand. During calibration, they perform a series of predefined tasks to collect example data, for which their intentions are known. ML methods then use this labeled data to learn subject-specific brain signal characteristics and predict the user’s intention on new data. In the field of BCI studies, these predictions can enable the user to control applications and physical devices by translating brain activity into control commands.

In a classic ML approach to BCIs, the participants undertake a calibration measurement without any feedback to acquire data to train the BCI system. After the training, they can control the BCI and improve their performance through feedback.

According to Shenoy et al. [436], the main difficulty in the ML-based BCIs is the transition from offline calibration to online feedback. A common assumption in supervised learning is that the input points in the training set follow the same probability distribution as the input points that will be given in the future test phase. At the same time, this assumption is usually not satisfied [550]. For some subjects this problem is successfully addressed in a supervised fashion, i.e., by using the first trials from the feedback session. An alternative approach is using an adaptive learning strategy [551] that combines supervised and unsupervised strategies.

As an example, we consider a co-adaptive principle, proposed by Vidaurre et al. [552] and schematically illustrated in Fig. 37(a). In their experiment 80 volunteers used the motor imagery BCI to control a 1D cursor on the screen. At the first stage, all participants performed the task without any feedback to collect a data-base. Then, they performed eight feedback runs, each of them consisting of 100 trials (50 trials of each class, left or right direction). After each run, there was a short break (1–5 min) for the BCI users to relax. The structure of the experiment is illustrated in Fig. 37(b). At the beginning (time is zero), the cue was provided in the form of a small arrow over a cross placed in the middle of the screen; 1-s interval later, the cross started to move in order to provide feedback. Its speed was determined by the classifier output.

Adaptation of ML was performed during a feedback session in three incremental levels.

In level 1, a subject-independent classifier was computed from a database of all users and used as a starting point for BCI calibration during the feedback session. The input variables at level 1 included three Laplacian channels C3, Cz, C4, where the signals were filtered in fixed, subject-independent frequency bands 8–15 Hz and 16–32 Hz. A linear discriminant classifier was adapted in a supervised manner after every trial.

In level 2, three more runs are recorded using a more complex and subject-specific set of features, CSP, and subject-selected Laplacian channels to provide feedback. Here, the linear discriminant analysis (LDA) classifier is retrained in a supervised way after each trial.

In level 3, the last two runs use subject-optimized features, and the LDA is adapted in an unsupervised manner to track the features possible drift during the feedback. These last two runs serve as well to estimate the performance of the participant in a feedback application because no class information is used.

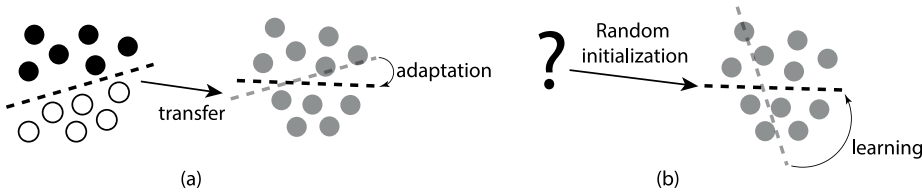


**Fig. 38.** (a) Unsupervised adaptation and (b) unsupervised learning. Black and white circles indicate labeled training data from two classes. Gray circles depict unlabeled data. Dashed lines indicate classification models. The general goal is to find a model which separates the two classes as good as possible. Label information is necessary only in the adaptation scenario. For transferring the classification model, only a slight adaptation may be needed while the unsupervised learning algorithm has to learn the model from a random initialization.

Using this approach, without any offline calibration, six users, including one novice, obtained good performance after 3–6 min of adaptation. More important, this novel guided learning also allows participants with BCI illiteracy to gain significant control with the BCI in less than 60 min. In addition, one volunteer without sensorimotor idle rhythm peak at the beginning of the BCI experiment developed it during the course of the session and used voluntary modulation of its amplitude to control the feedback application.

Generally, the calibration is challenging in BCI due to a low signal-to-noise ratio and a large subject-to-subject variability [553]. To reduce the calibration phase, different strategies were proposed (see [554] for review).

In the recent review paper, Hübner and colleagues [554] distinguish two main strategies. The first strategy is referred to as *unsupervised adaptation*. It takes a pre-trained classifier and updates it with unlabeled new data from the current session. Unsupervised adaptation relies on the assumption that the relevant training data is available or recorded to pre-train a classifier. However, it might not work for subjects with a limited attention span or atypical brain patterns, e.g., stroke survivors.

To overcome this limitation, the second strategy, *unsupervised learning*, was proposed for BCIs. This strategy enables learning individual brain characteristics from scratch without requiring any labeled data. Fig. 38 illustrates the difference between the two strategies. The authors summarized that unsupervised adaptation crucially relies on a pre-trained classifier, but unsupervised learning can also rely on a good initialization of the model parameters. At the same time, even if the model is initialized poorly, unsupervised learning methods have a high chance of learning a good classifier, which is not the case for unsupervised adaptation methods.

As BCIs transit from laboratory settings into daily living activities, an important goal is to minimize the reliance of neural decoding algorithms on the calibration or to enable calibration with a minimal burden on the user. The latter may provide stable control for extended periods despite the fluctuations in the decoder's neural input space [56,555] but represents a significant challenge for static neural decoding algorithms that assume stationary input/output relationships.

For BCIs which use chronically implanted microelectrode arrays, these fluctuations include the loss or addition of neurons to the electrode recordings, failure of the electrodes themselves, and changes in neuron activity that affect properties of input firing patterns over time [556]. Moreover, in some cases (paralysis or limb amputation), there is no explicit user-generated kinematic output available to train a decoder properly. Some studies utilize unique training paradigms (e.g., desired target information or imagined movements) to calibrate the BCI [557,558]. Others initialize the decoder using baseline neural activity, ipsilateral arm movements, and then refine it through adaptation [559].

As discussed above, the unsupervised adaptation allows updating the ML model without labeled training data. However, in most cases, BCIs require supervised adaptation (see [556] for review).

Rather than using supervised adaptation, a new class of neural decoders can be used. These decoders are based on so-called *reinforcement learning* (RL) [560], that is an interactive learning method which allows the decoder to obtain a reward by learning to interact with the environment. The RL implies that adaptation is built into the algorithm itself and relies on the feedback signal [561]. Similarly to the supervised adaptation, the RL decoders can adapt their parameters to respond to user's performance. Unlike supervised adaptation, the RL does not rely on known (or inferred) outputs (such as kinematics) as the desired response for training or updating the decoder.

In this regard, we have to mention the paper of Pohlmeier and colleagues [560] who provides a large list of references to earlier works in the field of the RL application to BCI. In their work, the authors proposed an *actor-critic* RL architecture that allows the encoder to adapt neural reorganizations and maintain its performance over long periods. Moreover, the user is not required to produce specific kinetic or kinematic activities to calibrate the BCI.

The actor-critic systems include the actor and critic modules (see Fig. 39). The actor interacts with the environment via generated actions based on a specific input state (here neural states). The critic provides feedback regarding the success of the actions in terms of some measure of performance. This feedback is utilized by the actor to refine the mapping of its state into action. The actor was a fully connected 3-layer feed-forward neural network that used a Hebbian update structure. The actor input was a vector (length  $n$ ) of the spike counts for each of the  $n$  motor cortex neural signals during a 2-s window following each trial's go cue. The actor weights were initialized randomly and updated using the critic feedback. The feedback was +1 if the previous action were successful and -1 otherwise. The authors used an "ideal"

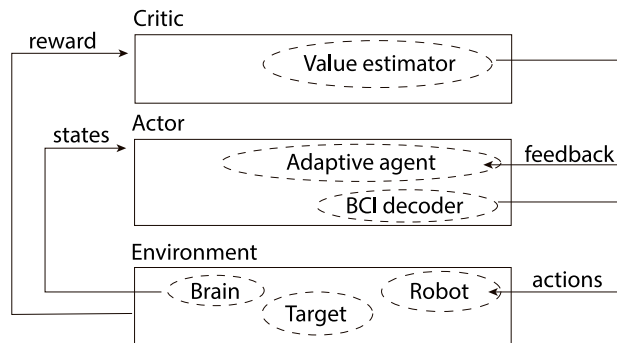


**Fig. 39.** The defined architecture characteristic is the interaction between the actor and critic modules. The actor interacts with the environment by selecting actions given input states (here, the BCI decoder). The critic is responsible for producing reward feedback that reflects the actions impact on the environment, and which is used by the actor to improve its input to action mapping capability (here the adaptive agent).

Source: Redrawn from [560].

critic that always provided accurate feedback. However, they noted that the RL architecture did not intrinsically assume perfect feedback.

In the experiment, two monkeys used the described RL architecture to control a robotic arm during a two-target reaching task. The randomly initialized decoder quickly learned to control the robot from brain states using only binary feedback regarding whether previously chosen robot actions were good or bad. As a result, the decoder demonstrated good accuracy throughout sessions spanning multiple weeks. Furthermore, it quickly adapted to dramatic perturbations to the neural inputs, including a series of tests where the neuron input space was deliberately halved or doubled.

Notably, the reward was provided depending on the success evaluated on the behavioral level. The next step toward the RL-based BCIs was to give feedback based on the features of neuronal activity. However, this possibility relied on the existence of a reward-like signal in the brain neural network (e.g., in the sensorimotor cortex).

In the experiment of Marsh and coworkers [562], neurons in the primary motor cortex of nonhuman primates were modulated by reward expectation during reaching movements. Moreover, a similar modulation was presented even while the animals passively viewed cursor motions predictive of either reward or non-reward. The authors proposed that the RL could then use this reward information toward an autonomous BCI. These BCIs would use neural signals to decode movement intention and extract reward expectation information as feedback to update the decoding algorithm.

Later, the next step in this direction has been made. Prins, Sanchez, and Prasad [563] extracted feedback from a biologically realistic source, using both the quantity and the quality of the feedback to maximize the decoder performance in the actor-critic RL manner. To deal with complexity and nonstationarity of biological reward signals, they introduced a confidence metric to estimate the degree of feedback accuracy. This confidence was added to the actor weight update equation. If the confidence was high, the decoder used this feedback to update its parameters. However, if the confidence was low, the decoder ignored the feedback and did not update its parameters. The distinguished feature of this work is that the authors used neural network models to generate synthetic data for motor imagery (Izhikevich model) and reward signals (Humphries model) to validate proposed controller architecture. As a result, they demonstrated that using such a threshold could be applied to any decoder with a feedback signal that is less than perfect. It allowed to avoid erroneous feedback and increase the system stability.

More recently, Wirth with colleagues [564] investigated the feasibility of single-trial EEG classification between different errors. They used a linear classifier with a small feature set. First, they reported neurophysiological distinctions between the ErrPs related to each error type. They then achieved statistically significant single-trial classification rates for most participants with a mean overall 65% accuracy. This study appears to be the next step toward more efficient learning in BCI, and thus more autonomous human-machine interaction.

#### 4.5.4. Machine learning for physics

One of the ML applications, in particular, reservoir computing (RC), in modern nonlinear physics is the modeling and prediction of the behavior of chaotic systems. Because of its high ability to analyze chaotic signals [565], RC is very relevant for studying and predicting nonstationary brain activity signals. The speed of the BCI command formation could be increased if one would predict the brain activity.

From the physical point of view, a reservoir computer, originally known as an echo state network [566] or a liquid state machine [567] (see [568] for review) is a high-dimensional nonautonomous dynamical system that is driven by an input signal to be analyzed. The reservoir computer transforms the input time-varying signal into another time-varying signal (the output signal), acting as a nonlinear filter. The reservoir computer is usually created by connecting a set of nonlinear nodes in a network so that the entire dynamical system has a stable fixed point. Training the RC engine comes about by forming a linear combination of many signals from the dynamical system to fit a training signal. Following Lu

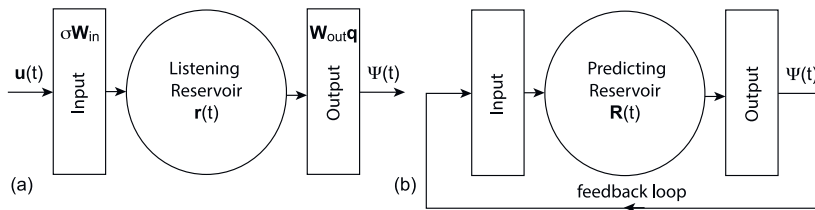


**Fig. 40.** (a) Listening and training reservoir phases. (b) Predicting phase.

et al. [569], the reservoir computer in the training mode is driven by one of time-varying variables. To be more specific, for a 3D chaotic dynamical system, this can be a variable  $x_1(t)$  which drives the reservoir computer which produces a signal associated with a time-dependent variable  $x_3(t)$ . In the computational mode, the same reservoir computer is then driven by the  $x_1(t)$  signal of the same system but with other initial conditions. Using the previously fitted coefficients to make a linear combination of the signals from the reservoir computer, the  $x_3(t)$  variable corresponding to the particular driven  $x_1(t)$  signal is reproduced.

There are a lot of papers on modeling low- and high-dimensional chaotic systems by using RC [569–578]. Most of them are devoted to the prediction of chaotic time series [566,573,578,579] and estimation of the parameters of dynamical systems, as well as the calculation of Lyapunov exponents [569–571,580]. For example, Lu et al. [571] considered the problem of predicting a future behavior of an unknown dynamical system from a short time series. The main idea was as follows. The authors considered a signal  $u(t)$  which is a measurement function  $\mathbf{h}$  of the finite-dimensional system state  $\mathbf{s}(t)$ :  $u(t) = \mathbf{h}(\mathbf{s}(t))$ , where  $\mathbf{h}$  and  $\mathbf{s}$  are unknown. To predict future values of  $u(t)$  three steps were suggested: (i) listening, (ii) training, and (iii) predicting.

(i) The listening consists of using the training time series as an input to the reservoir (see Fig. 40(a), which can be considered as the discrete time deterministic process

$$\mathbf{r}(t + \Delta t) = \mathbf{f}(\mathbf{r}(t), u(t)), \quad (50)$$

where  $\mathbf{r}(t)$  is the reservoir state and  $\Delta t$  is a discrete time increment. It should be emphasized that in practice, the function  $\mathbf{f}$  should be known, and only reservoir outputs are used for further training and prediction.

(ii) The training consists of determining a post-processing function  $\Psi$  that, when applied to the reservoir output  $\mathbf{r}(t + \Delta t)$ , estimates the next input  $u(t + \Delta t)$ . The training implies finding such a function  $\Psi$  that

$$\Psi(\mathbf{r}(t)) \approx u(t). \quad (51)$$

To find  $\Psi$ , a fitting procedure, for example, linear regression, is applied to the training time series  $\{u(t)\}$  of measurements and the corresponding time series  $\{\mathbf{r}(t)\}$  determined from Eq. (50).

(iii) The predicting proceeds by modifying the reservoir computer to run autonomously with a feedback loop (see Fig. 40(b), replacing its input  $u(t)$  with its post-processed output Eq. (51) from the previous time increment

$$\mathbf{R}(t + \Delta t) = \mathbf{f}(\mathbf{R}(t), \Psi(\mathbf{R}(t))). \quad (52)$$

After initialization from the listening reservoir phase with  $\mathbf{R}(t_0)$  iterating the predicting reservoir Eq. (52) forms a time series  $\{\Psi(\mathbf{R}(t_0 + \Delta t)), \Psi(\mathbf{R}(t_0 + 2\Delta t)), \dots\}$  of predictions for future measurements  $\{u(t_0 + \Delta t), u(t_0 + 2\Delta t), \dots\}$ .

This approach can only be successfully used for short forecasting of chaotic time series. If the predicted dynamical system has a chaotic attractor, then, as in the case of any imperfect model, the prediction error  $\|\Psi(\mathbf{R}(t)) - u(t)\|$  cannot remain small for a long enough time due to the instability of the system and the presence of one (or more in the case of hyperchaotic systems) positive Lyapunov exponents. At the same time, in some cases the long-term time series  $\{\Psi(\mathbf{R}(t_0 + \Delta t)), \Psi(\mathbf{R}(t_0 + 2\Delta t)), \dots\}$  demonstrate a behavior similar to the measurements from a typical trajectory on the original attractor, i.e., the predicting procedure Eq. (52) approximately reproduces the ergodic properties of the dynamical system which generated the measurements. In this sense, we can talk about attractor reconstruction, which allows one to recover various properties of the attractor of the original system, including the estimation of the Lyapunov exponents spectrum.

RC is closely related to the notion of generalize synchronization (GS) [510,581], which in a drive-response configuration requires that the response state be asymptotically a function of the drive state. In our case, there is a continuous function  $\varphi$  such that  $\mathbf{r}(t) - \varphi(\mathbf{s}(t)) \rightarrow 0$  as  $t \rightarrow \infty$ . For both the short-term prediction and the reconstruction of the attractor properties, the four following conditions are sufficient [571].

1. Dynamical system Eq. (50) demonstrates GS with a time-varying process  $\mathbf{s}(t)$ , so that  $\mathbf{r}(t) - \varphi(\mathbf{s}(t)) \approx 0$  for a continuous function  $\varphi$ , within the time interval covered by the training time series.
2. The function  $\varphi$  carries enough information about its input to recover  $u(t) = \mathbf{h}(\mathbf{s}(t))$  from  $\varphi(\mathbf{s}(t))$ .
3. Training is successful from the viewpoint of GS, so that  $\Psi(\varphi(\mathbf{s}(t))) - \mathbf{h}(\mathbf{s}(t)) \approx 0$ .

#### 4. The attractor approached by the listening reservoir Eq. (50) is also stable for the predicting reservoir Eq. (52).

We can suggest that the measurements  $\{\mathbf{u}(t)\}$  for  $t \geq t_0$  are available, so that we can evolve both the training reservoir Eq. (50) and the predicting reservoir Eq. (52), and compare their outputs. Let the outputs of both reservoirs coincide exactly  $\mathbf{R}(t) = \mathbf{r}(t)$  and  $\Psi(\mathbf{R}(t)) = \mathbf{u}(t)$  for  $t \geq t_0$ . This means that  $\mathbf{u}(t_0) = \Psi(\mathbf{R}(t_0)) = \Psi(\varphi(\mathbf{s}(t_0))) = \mathbf{h}(\mathbf{s}(t_0)) = \mathbf{u}(t_0)$ . Then,  $\mathbf{R}(t_0 + \Delta t) = \mathbf{f}(\mathbf{R}(t_0))$ ,  $\Psi(\mathbf{R}(t_0)) = \mathbf{f}(\mathbf{r}(t_0))$ ,  $\mathbf{u}(t_0) = \mathbf{r}(t_0 + \Delta t)$ , and  $\mathbf{r}(t_0 + \Delta t) = \varphi(\mathbf{s}(t_0 + \Delta t))$  due to GS. Similarly, it has the same equalities for other time moments  $t_0 + 2\Delta t$ ,  $t_0 + 3\Delta t$ , ... . This agreement between the trajectories shows that reservoir dynamics observed through  $\Psi$  is equivalent to the dynamics of the analyzed system observed through  $\mathbf{h}$ . However, this is an idealized situation of an exact reconstruction of the attractor of the analyzed measured system. Usually, we have only approximation of the measured attractor, and as a consequence the actual predicting reservoir Eq. (52) is still initialized near an invariant set. Obviously, the better the approximation, the more accurate the predictions will be, at least in the short term. If the dynamical system that generates the measurements  $\{\mathbf{u}(t)\}$  is chaotic, the prediction error  $\|\mathbf{u}(t) - \Psi(\mathbf{R}(t))\|$  will grow exponentially with time. At the same time, it remains possible that  $\Psi(\mathbf{R}(t))$  will maintain a reconstructed attractor of the measured system  $\mathbf{u}(t)$  in the long term [570,571]. In the latter case, it is possible to estimate the parameters of the measured attractor along the reservoir trajectories. For example, we can calculate Lyapunov exponents if we have a sufficiently long time series  $\{\mathbf{u}(t)\}$ . For this purpose we use the time series  $\{\mathbf{u}(t)\}$  to generate a trajectory  $\{\mathbf{r}(t)\}$  of the listening reservoir Eq. (50), which will approach the reconstructed attractor under the conditions for GS. Then, along this trajectory which is an approximate trajectory of the predicting reservoir, we compute Lyapunov exponents using the Jacobian matrix of the predicting reservoir Eq. (52).

Let us consider the numerical examples of the RC-based predictions for the chaotic Lorenz system

$$\dot{x} = 10(y - x), \quad \dot{y} = 28x - y - zx, \quad \dot{z} = xy - 8z/3, \quad (53)$$

where the measurement function  $\mathbf{h}$  is the identity, so that  $\mathbf{u}(t) = \mathbf{s}(t) = \{x(t), y(t), z(t)\}^T$ . To describe the reservoir Eq. (50) the ANN is used in the following continuous-time form [571]

$$\dot{\mathbf{r}}(t) = -\gamma (\mathbf{r}(t) - \tanh(\mathbf{M}\mathbf{r}(t) - \sigma \mathbf{W}_{in}\mathbf{u}(t))). \quad (54)$$

Here, the reservoir dimension is  $N = 2000$ ,  $\gamma = 10$ ,  $\mathbf{M}$  is the adjacency matrix representing reservoir network connections,  $\mathbf{W}_{in}$  is the mapping from the three-dimensional input state  $\mathbf{u}$  space to the  $N$ -dimensional reservoir state space in the considered numerical results,  $\mathbf{W}_{in}$  is fixed and the scalar input strength  $\sigma$  is only varied. The post-processing function is given in the form  $\Psi(\mathbf{r}) = \mathbf{W}_{out}\mathbf{q}(\mathbf{r})$ , where  $\mathbf{q}(\mathbf{r})$  is the  $2N$ -dimensional vector consisting of the  $N$  coordinates of reservoir state  $\mathbf{r}$  followed by their squares, and  $\mathbf{W}_{out}$  is the mapping from reservoir state space to the 3D output state space.

During the training procedure the post-processed output signal  $\Psi(\mathbf{r}(t + \Delta t))$  based on the input up to time  $t$  estimates the subsequent input value  $\mathbf{u}(t + \Delta t)$ . The  $N \times N$  adjacency matrix  $\mathbf{M}$  is randomly chosen with sparse Erdos–Renyi connectivity and a spectral radius of 0.9 that corresponds to common practice in RC. The  $N \times 3$  matrix  $\mathbf{W}_{in}$  is chosen randomly so that each row has one non-zero element, chosen uniformly distributed in the  $[-1, 1]$  interval. For training, the  $3 \times 2N$  matrix  $\mathbf{W}_{out}$  is limited to have only  $3N$  non-zero elements, namely, the first  $N$  elements of its first two rows, and the first  $N/2$  and last  $N/2$  elements of its third row. Thus, the  $x$  and  $y$  coordinates of the Lorenz state are fitted with linear functions of  $\mathbf{r}$ , and the  $z$  coordinate with a linear combination of the first  $N/2$  coordinates of  $\mathbf{r}$  and the squares of the second  $N/2$  coordinates. As a consequence, the error function

$$\delta = \sum_{k=1}^{3000} \|\mathbf{W}_{out}\mathbf{q}(\mathbf{r}(k\Delta t)) - \mathbf{u}(k\Delta t)\|^2 + 10^{-6} \|\mathbf{W}_{out}\|^2 \quad (55)$$

is minimized to select  $\mathbf{W}_{out}$ . The last term in Eq. (55) introduces an ordinary linear least-squares regression in order to discourage overfitting.

To switch to the prediction mode, the external input in a feedback loop can be replaced by the post-processed output, as shown in Fig. 40(b). In this case the reservoir evolves according to

$$\dot{\mathbf{R}}(t) = \gamma (-\mathbf{R}(t) + \tanh(\mathbf{M}\mathbf{R}(t) + \sigma \mathbf{W}_{in}\mathbf{W}_{out}\mathbf{q}(\mathbf{R}(t)))), \quad (56)$$

where the predicted value of  $\mathbf{u}(t)$  is  $\Psi(\mathbf{R}(t)) = \mathbf{W}_{out}\mathbf{q}(\mathbf{R}(t))$ .

Figs. 41(a) and (b) show the results of the RC prediction of the chaotic Lorenz system Eq. (53) trajectory  $z(t)$ , using two different input strengths  $\sigma$ . Both calculations predict a short-term future similarly well. For larger values of the prediction time  $t$ , the first prediction approaches a periodic orbit, whereas the second prediction continues with a Lorenz-like reconstructed attractor. Based on these calculations, there is an attracting invariant set for the predicting reservoir. However, between  $\sigma = 0.012$  and  $\sigma = 0.014$  there is a bifurcation that causes this invariant set either to become unstable or to be destroyed entirely.

Fig. 41(c) shows how three largest Lyapunov exponents of the predicting reservoir Eq. (52) depends on the input strength  $\sigma$ . Two exponents are approximately independent of  $\sigma$ , while the dependent exponent, so-called the transverse Lyapunov exponent, determines stability of the reconstructed attractor stability according to the GS theory [581,582]. This varied exponent passes through zero at the bifurcation point  $\sigma \approx 0.013$ . To compare the stability using the transverse Lyapunov exponent, Lu et al. [571] used a direct method for estimating the accuracy of the attractor reconstruction in the

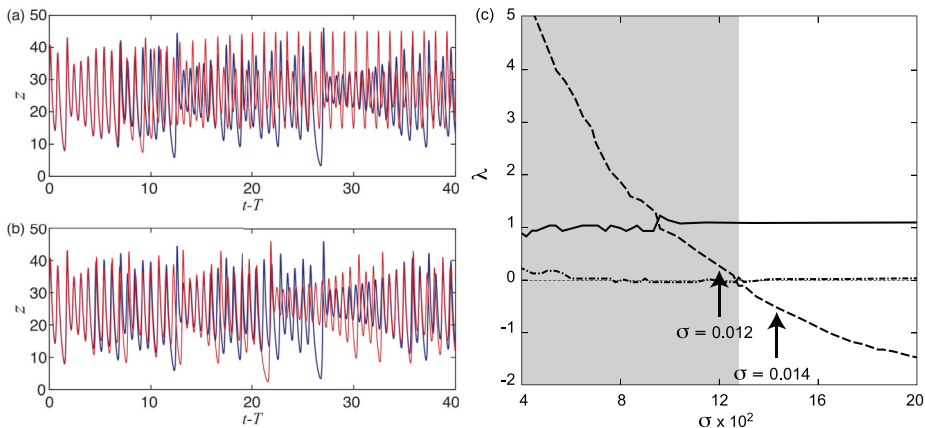


**Fig. 41.** Reservoir-based prediction (red) and measurement (blue) of a chaotic Lorenz system Eq. (53) trajectory  $z(t)$ , using different input strengths  $\sigma = 0.012$  (a) and  $0.014$  (b). The predictions remain well correlated with the actual trajectory for first 10 time units. After divergence of trajectories, the calculation with  $\sigma = 0.012$  approaches a periodic orbit, whereas the second calculation appears to continue with a trajectory similar to that of the Lorenz system trajectory. (c) Three largest Lyapunov exponents of the reservoir Eq. (52) versus the input strength  $\sigma$  for the same reservoir as in panels (a) and (b). The gray area corresponds to the parameter  $\sigma$  at which the attractor reconstruction fails.

Source: Based on the data from [571].

form of calculating the vector field discrepancy  $\Delta$  between the vector fields implied by the predicting reservoir and the vector field of the Lorenz system Eq. (53). If  $\Delta$  does not exceed a threshold value 20, which is small compared to the typical magnitude of the Lorenz vector field, the attractor can be considered to be approximately reproduced. In Fig. 41(c) the gray area shows the region of  $\sigma$  for which we detect an escape from successful reconstruction. These values are the same as those for which the computed transverse Lyapunov exponent is positive.

Similar approaches to the reconstruction of attractors and the prediction of the behavior of dynamical systems were developed by various scientists. For example, Griffith et al. [574] reported that the Bayesian optimization of RC hyperparameters gives the possibility to create high-performance reservoirs quickly for forecasting a chaotic Lorenz attractor. They found reservoirs with very low internal connectivity that perform just as well as their higher-connectivity counterparts. Moreover, Weng et al. [583] demonstrated that a well-trained reservoir computer can synchronize with its learned chaotic systems by linking them with a common signal. They also found that the necessary condition for achieving synchronization is negative sub-Lyapunov exponents. Pathak et al. [573] proposed a general method combining a knowledge-based model and a machine learning technique to build a hybrid forecasting scheme. It is well-known that a model-based approach to forecasting chaotic dynamical systems utilizes knowledge of the mechanistic processes governing the dynamics to build an approximate mathematical model of the system. In contrast, machine learning techniques have demonstrated promising results for forecasting chaotic systems purely from past time series measurements of system state variables (training data), without prior knowledge of the system dynamics. Such data-driven methods regardless the derived knowledge of the system, may be computationally intensive and may require an unreasonably large amount of data. Pathak et al. [573] demonstrated the efficiency of this technique for prediction of the behavior of chaotic systems that hybridizes the data-driven RC and knowledge-based prediction. They proved their method with two numerical examples, namely, the low-dimensional Lorenz system and the spatio-temporal chaotic Kuramoto–Sivashinsky equation (KSE).

Another approach to increase the efficiency of the RC-based forecasting, namely, the prediction time extension, is the incorporation of time-dependent but sparse data inputs into reservoir computing. Recently, Fan et al. [578] demonstrated that such rare “updates” of the actual state practically enable an arbitrarily long prediction horizon for a variety of chaotic systems, including spatio-temporal chaos.

A large number of papers are devoted to the study of RC-based prediction schemes for the dynamics of high-dimensional systems demonstrating spatio-temporal chaos. Typically, the research object is a high-dimensional chaotic system described by partial differential equations (PDE), such as, for example, the KSE or complex Ginzburg–Landau equation [572,575,578]. In this regard, Pathak et al. [572] proposed a parallelized scheme consisting of a large set of reservoirs of a moderate size, each of which predicts a local region of the spatiotemporal chaotic system. They tested their efficient computational scheme on the KSE and good forecasting of PDE dynamics. Jiang and Lai [575] considered the effect of reservoir network spectral radius and a structure on model-free prediction of large spatio-temporal chaotic systems. They have shown that there is the emergence of an interval in the spectral radius of the neural network in which the prediction error is minimized. In addition, Zimmermann et al. [576] combined the concepts of RC and local states and derived an efficient method for cross-predicting dynamical variables of the Barkley and Bueno–Orovio–Cherry–Fenton models describing two chaotic excitable media related to cardiology. The obtained results suggest that RC offers an effective potential means for model-free prediction of large spatio-temporal chaotic systems.

At the same time, it is also possible to use RC for input data classification. Let us go back to the already considered example of the Lorenz system. The selected fit matrix  $\mathbf{W}_{out}$  can be used as a feature vector to identify individual signal driven reservoir [565]. For each class of signals, a driving signal and a training signal are chosen. For example, one signal may drive the reservoir with  $x(t)$  signal of the Lorenz system and train on  $z(t)$  signal of the same system. The fixed reservoir network and the mapping  $\mathbf{W}_{out}[\text{Lorenz}_1]$  found by training form a classifier for the Lorenz system. One may then form a classifier for another system, say the Rössler system, by driving the same network with  $x(t)$  signal and training on  $z(t)$  signal of this new system, and new mapping  $\mathbf{W}_{out}[\text{Rossler}_1]$  is found. It should be noted that the reservoir network never changes. If the Lorenz system with the same parameters is started with different initial conditions, the same reservoir network may be driven with the new Lorenz  $x(t)$  signal and trained on the new Lorenz  $z(t)$  signal to obtain a new mapping  $\mathbf{W}_{out}[\text{Lorenz}_2]$ . The new signal may be classified by computing the measure  $d_{ij} = \|\mathbf{W}_{out}[i] - \mathbf{W}_{out}[j]\|$ , where  $i$  indicates Lorenz<sub>2</sub>, and  $j$  Lorenz<sub>1</sub> or Rossler<sub>1</sub>. The smaller value of  $d_{ij}$  will be found when taking the difference between the two mappings for the Lorenz system. Carroll [565] has shown that the RC-based classifier was able to detect one out of the 19 different Sprott systems. An RC advantage for this problem is that no embedding is necessary. The RC-based classifier is also robust to moderate amounts of added noise.

The RC-based classification is possible even when, instead of the usual spatially extended dynamical system, purely time-delayed dynamical systems are used as a way to simulate dynamical complexity traditionally provided by a network of artificial neurons [584]. The time-delayed dynamical systems are characterized by the infinite-dimensional dynamics, which was shown to be able to act as complex dynamical reservoirs, efficiently replacing the traditional neural-network architectures [585–587]. The RC, based on this architecture, allows the implementation of the technology-friendly hardware solutions using available high-performance signal processing tools and devices designed for modern telecommunications. In addition, photonic implementations can realize information processing rates at the picosecond or even femtosecond time scales available in standard optical telecommunications. Later, Larger and colleagues [588] considered an electro-optic phase-delayed dynamics built with telecom bandwidth devices and providing ultrafast information processing while implementing RC concepts with dedicated hardware. Developed by them a novel electro-optic phase architecture provides an improvement by a factor of “three”, reaching a million words per second when tested on a standard speech-recognition database. Another way to physically implement the RC is the field programmable gate arrays described by Haynes et al. [589]. It should be noted, that as reservoir computing is a universal computational concept, many other complex intelligence-related problems can, in principle, be addressed by time-delayed system approach, such as real-time information extraction from high bit-rate optical data flow or the prediction of a high-dimensional deterministic time series.

Another challenging problem is the analysis of connectivity structures in the big multivariate data. In neuroscience predicting the functional brain network using multichannel EEG/MEG signals uncovers mechanisms of neuronal interaction during various physiological or cognitive processes and can be applied to the detection of FBC patterns to use in BCI (see in detail Section 4.1.4). ANN is known to be a biologically inspired computational system, whose main purpose is to fit unknown and usually complex relationship between input and output data [513]. Since functional connectivity in coupled systems implies the existence of functional dependence between them, ANN seems to be an essential tool in this context. Ibáñez-Soria et al. [410] applied echo state networks for the detection of functional interrelations in terms of GS.

In our recent paper [411] we used such ML technique known as feed-forward (FF) ANN to formulate a method for detecting functional dependence (GS regime) in unidirectionally Eq. (40) and bidirectionally Eq. (41) coupled systems without additional information about them (model-free approach). Based on the approximation theorem, MLP with nonlinear activators in hidden layers is able to approximate any arbitrary given function [590,591]. FFMLP may also approximate any function mapping from any finite dimensional discrete space to another [513]. This property of FFMLP is especially useful for the approximation of the functional relation  $\mathbf{F}$  in Eq. (40) considering only an experimental data set of  $\mathbf{x}(t_i)$  and  $\mathbf{y}(t_i)$ , where  $t_i = i\Delta t$  is the discrete time moments and  $\Delta t$  is the sample rate.

Fig. 42 illustrates the proposed FFMLP method for data-driven functional connectivity detection. Considering two coupled processes, whose dynamics is represented by multivariate signals  $\mathbf{x}(t)$  and  $\mathbf{y}(t)$ , functional connectivity implies  $\mathbf{y}(t) = \mathbf{F}[\mathbf{x}(t)]$ . Since from a mathematical point of view ANN defines a function  $f : \mathbf{x} \rightarrow \mathbf{y}$ , one may use ANN to build a model of the unknown relation  $\mathbf{F}(\bullet)$  and predict the  $\mathbf{y}$  state based on the  $\mathbf{x}$  state. Thus, if a true functional relation  $\mathbf{y}(t) = \mathbf{F}[\mathbf{x}(t)]$  exists, ANN is able to approximate it and give a precise prediction  $\mathbf{y}'(t)$  of the  $\mathbf{y}(t)$  state on the basis of  $\mathbf{x}(t)$ . On the contrary, if functional dependence is not established, ANN fails to learn it and therefore is not able to predict the  $\mathbf{y}$ -state accurately enough. Summarizing the above, the criterion for functional connectivity inference is the equality of predicted and actual values of  $\mathbf{y}$  processes:  $\mathbf{y}'(t) = \mathbf{y}(t)$ . To quantify the degree of functional dependence we use a metric called  $R^2$ -score, which evaluates “goodness of fit” of the original data measured from a response system  $\mathbf{y}(t)$  and its ANN prediction  $\mathbf{y}'(t)$ , defined as

$$R^2 = 1 - \frac{\sum_{d=1}^D \sum_{i=1}^N (y_d(t_i) - y'_d(t_i))^2}{\sum_{d=1}^D \sum_{i=1}^N (y_d(t_i) - \bar{y}_d)^2}, \quad (57)$$

where  $D$  is the number of dimensions,  $N$  is the length of the data set, overbar denotes mean value,  $y_d(t)$  and  $y'_d(t)$  are the  $d$ th component of response system vector state  $\mathbf{y}(t)$  and its prediction via ANN, respectively.  $R^2$  ranges from 0 to 1 and quantifies the fraction of data being well predicted by the ANN model. As  $R^2 = 0.5$  indicates that only a half of data

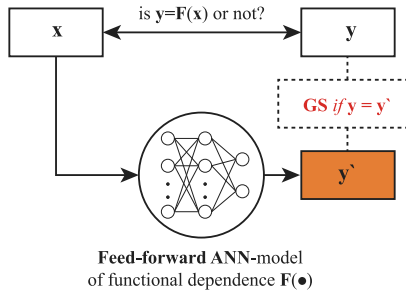


**Fig. 42.** Inference of functional connectivity using proposed FFANN-based approach. Dependence of  $y$  on  $x$  is detected if ANN-model of functional relation  $F(\bullet)$  provides accurate prediction  $\hat{y}'(t)$  of  $y(t)$ -state by the  $x(t)$ -state. Reprinted from [411].

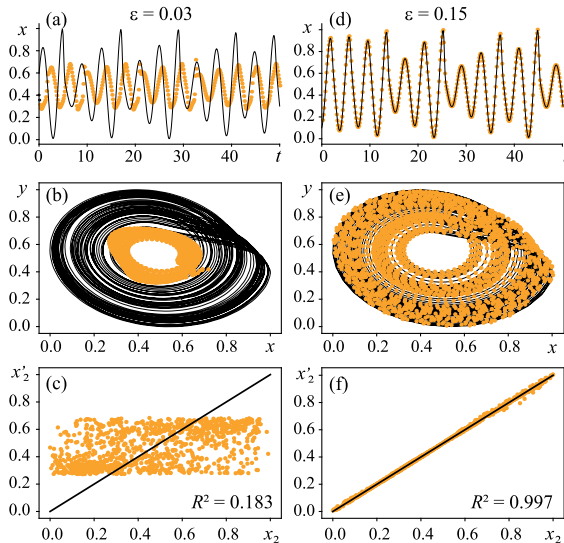


**Fig. 43.** Inference of functional dependence in mutually coupled Rössler oscillators below ( $\varepsilon = 0.03$ , left column) and above ( $\varepsilon = 0.15$ , right column) GS threshold  $\varepsilon_{GS} \approx 0.12$  [511]. (a,d) Test sample of the second Rössler oscillator time series  $x_2$  (black curve) and its prediction  $x'_2$  via ANN (orange points). (b,e) Phase portraits of the second oscillator on the plane  $(x_2, y)$  (black) and its prediction by ANN ( $x'_2, y'_2$ ) (orange points). (c,f) Regression analysis of  $x_2$  variable prediction by ANN model. Reprinted from [411].

is fitted by the model (almost random prediction), this value is further considered as a threshold value for functional dependence inference.

Let us consider the numerical test of the FF MLP-based technique to detect functional dependence in a pair of coupled chaotic Rössler oscillators, which is one of the classical models for the GS study [510,592,593]:

$$\dot{x}_{1,2} = -\omega_{1,2}y_{1,2} - z_{1,2} + \varepsilon(x_{2,1} - x_{1,2}), \quad \dot{y}_{1,2} = \omega_{1,2}x_{1,2} + 0.15y_{1,2}, \quad \dot{z}_{1,2} = 0.2 + z_{1,2}(x_{1,2} - 10), \quad (58)$$

where  $\omega_1 = 0.99$  and  $\omega_2 = 0.95$  by the analogy with [511]. Fig. 43 illustrates the recognition of functional dependence between mutually coupled Rössler oscillators. ANN accurately detects the absence of functional interdependence below the GS threshold  $\varepsilon_{GS} \approx 0.12$  (left column in Fig. 43) and its presence above the GS threshold (right column in Fig. 43) with  $R^2 = 0.183$  and  $R^2 = 0.997$ , respectively.

This approach was also applied to experimental neurophysiological data to identify functional connections between brain regions during an epileptic discharge initiation [411] that can be important for the development of BCIs for seizures prevention and mitigation [361,594,595]. We analyzed a multichannel set of ECoG recordings taken from Wistar Albino Glaxo from Rijswijk (WAG/Rij) rats, a genetic animal model giving rise to spontaneous absence seizures [596]. In Fig. 44(a) we present typical ECoG signals recorded in cortical layer ctx6 and thalamic nucleus ANT before and during SWD onset. According to the described approach, to infer functional dependence between ctx6 and ANT we try to predict the brain state in ANT area based on one in the ctx6 area using the FF ANN. We have considered the emergence of functional dependence between ctx6 and ANT in a floating 1-s window, inside which we have calculated the  $R^2$ -score (Fig. 44(b)). The SWD onset is accompanied by an increase of  $R^2$ -score over the threshold value of 0.5 and, therefore, the establishment of a functional relationship between ctx6 and ANT. Figs. 44(c,d) illustrates the possibility to predict ANT signal from the ctx6 signal in a 1-s interval during the background activity and the beginning of SWD, respectively. It is clearly seen

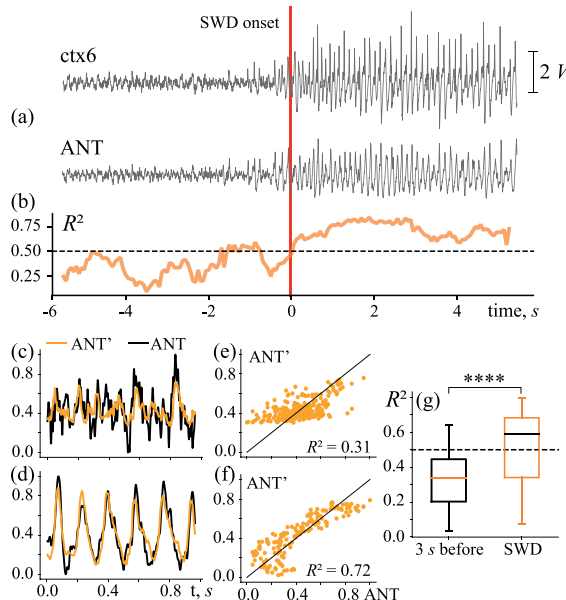


**Fig. 44.** (a) Typical ECoG signals recorded in cortical layer ctx6 and thalamic nucleus ANT of epileptic rat's brain. (b)  $R^2$ -score computed in a floating 1-s window. Illustrations of ANT signal predictability 3 s before (c) and during SWD onset (d). Plots (e) and (f) present results of regression analysis for (c) and (d). (g) Comparison of  $R^2$ -scores computed 3 s before and during SWD onset over 20 seizure trials collected over 5 rats ( $p < 0.0001$  via Wilcoxon signed-rank test for related samples). Dashed line in (b) and (e) defines  $R^2$  threshold level of 0.5. Reprinted from [411].

from regression analysis in Fig. 44(e,f) that the background activity is characterized by low prediction accuracy, while the pathological epileptic activity is characterized by a high  $R^2$ -score value. This trend is observed for all analyzed rats. Fig. 44(g) shows the comparison of  $R^2$ -score averaged over 40 trials of background and epileptic activity, collected from 6 different rats. There is a significant difference between two samples of  $R^2$ -scores, confirmed by the Wilcoxon signed-rank test for related samples ( $p < 0.0001$ ). Besides, one can see, that median value of  $R^2$ -score during seizure onset exceeds the threshold value of 0.5.

The problem of reconstructing nonlinear dynamical systems from measured data is central to many scientific disciplines, including physics, biology, and BCI development. A complex dynamical system (such as the human brain) exhibits a wide variety of dynamics. It is of great interest to detect, classify, predict, and control the dynamics using acquired data (EEG, MEG, fNIRS, fMRI, etc.). In turn, prediction and control require an accurate reconstruction of the original system.

To address these issues, compressive sensing (CS) methods were developed. They enable to reconstruct sparse signals using only limited data and has a broad range of BCI applications. The physical principles of CS were described in the recent review of Wang, Lai, and Grebogi [597]. The basic principle of CS is that the system dynamics is determined by smooth enough functions approximated by finite series expansions. The CS task is to estimate coefficients in the series representation of the vector field governing the system dynamics. In general, the series contain high order terms and the total number of coefficients can be large. This is a challenging problem, because if the most coefficients are zero (or negligible), the vector constituting all coefficients will be sparse, that is typical for real systems. Thus, for realistic nonlinear dynamical networks, the vectors to be reconstructed are typically sparse, and the problem of sparse vector estimation can then be solved by the paradigm of compressive sensing that reconstructs a sparse signal from limited observations.

Nowadays, scientists often use CS-based methods to analyze EEG signals [598,599] and translate them to the control commands for BCIs. In their study, Ma et al. [600] combined CS with deep learning to improve the motion-onset visual evoked potential (mVEP) BCI performance. Recently, CS was used with the RBF ANN for an automatic sleep-stage classification system [601]. The CS-based approach was also applied to detect epileptic seizures [602].

#### 4.5.5. Optimization techniques for machine learning

Optimization is a finding of a set of inputs to an objective function that results in maximum or minimum function evaluation. It is a challenging problem that underlies many machine learning algorithms, from fitting logistic regression models to training ANNs. There are two broad classes of optimization algorithms, classical and stochastic. Classical algorithms use derivatives, while stochastic algorithms do not. Classical algorithms include the first- and the second-order optimization methods, depending on the derivative they utilize. First-order optimization algorithms assume the use of the first derivative (gradient) to choose where to move in the search space. They are usually referred to as a gradient descent [603]. Second-order optimization algorithms assume the use of the second derivative (Hessian) to choose the direction. These algorithms are only appropriate for those objective functions where the Hessian matrix can be calculated or approximated [604].

Stochastic algorithms use randomness in the search procedure for objective functions for which derivatives cannot be calculated. Stochastic optimization algorithms include simulated annealing, evolution strategy [605] and cross-entropy methods [606]. Among the stochastic algorithms, one can highlight population optimization. This class of techniques maintains a population of candidate solutions to sample, explore, and hone in on an optimum. Population optimization algorithms enable solving more challenging objective problems with noisy function evaluations and many global optima. Examples of population optimization algorithms are genetic algorithms and particle swarm optimization.

A genetic algorithm (GA) is a search algorithm that imitates natural selection mechanics, and natural genetics [607]. In GA, a population of candidate solutions is evolved toward better solutions. Each candidate solution has a set of properties that can be mutated and altered. The evolution usually starts from a population of randomly generated candidate solutions called a generation. In each generation, every candidate solution fitness is evaluated. The fitness is usually the value of the objective function in the optimization problem. The more fit candidate solutions are stochastically selected from the current population, and their genomes are modified (recombined and possibly randomly mutated) to form a new generation. The new generation of candidate solutions is then used in the next iteration of the algorithm. Commonly, the algorithm terminates when either a maximum number of generations has been produced, or a satisfactory fitness level has been reached for the population [608]. In BCI, GA is often used to determine optimal features [609,610].

Particle swarm optimization (PSO) is a population-based optimization technique inspired by bird flocks and schooling fish's motion. It starts from the initialization of a population of random solutions. Then, the search for the optimal solution implies their updating [611]. Unlike GA, PSO has no evolution operators, such as crossover and mutation. In PSO, the potential solutions, called particles, move in the problem space by following the current optimum particles. PSO is computationally more efficient in terms of both speed and memory requirements. The undeniable drawback of PSO is that it is less accurate and hence less practical than GA. Therefore, many researchers use a combined PSO–GA algorithm for optimization [612]. Similarly to GA, PSO is used for channel and feature selection in BCI systems [613,614].

Finally, in their original versions, nature-inspired search algorithms, such as evolutionary algorithms and those based on the swarm intelligence, the lack of a mechanism which deals with numerical optimization problem constraints. Nowadays, however, there exists a considerable amount of research devoted to the development of techniques for handling constraints within a nature-inspired algorithm [615].

As a rule, the optimization requires many iterations to locate the global optimum. In turn, each iteration involves high-fidelity, time-consuming simulations to evaluate the current design objective function. Consequently, the whole optimization process could easily take up to days or even weeks if the objective function is complex. Since the simulations slow down the optimization process, the possible solution is to replace expensive simulations with a pre-trained statistical model to accurately approximate the objective function, given the same design parameters. This is the basic idea of the surrogate optimization strategy [616]. A surrogate model is a statistical model that can accurately approximate a function output given the inputs. In general, a single evaluation of the surrogate model is much faster than a single evaluation of the original expensive computer simulation. As a result, performing hundreds and thousands of output evaluations given various combinations of design parameters would no longer be a problem. This feature enables exploring the “landscape” of the objective function, therefore significantly accelerating the optimization speed.

Another approach for the derivative-free global optimization is Bayesian optimization [617]. Recently it has become trendy for tuning hyperparameters in machine learning algorithms, including deep neural networks [618]. This approach is best suited for optimization over continuous domains and tolerates stochastic noise in function evaluations. It builds a surrogate for the objective and quantifies the uncertainty in that surrogate using a Bayesian machine learning technique, Gaussian process regression, and then uses an acquisition function defined from this surrogate to decide where to sample. According to Gelbart and colleagues [619], Bayesian optimization can successfully address the constrained problems in the optimization.

Bayesian optimization provides improvements of the ML algorithms of EEG signals analysis. According to the recent work of Ke et al. [620], the ML performance often becomes unstable because conventional end-to-end models (e.g., a deep neural network), largely remain static. At the same time, brain states are highly dynamic and exhibit significant individuality. To address this issue, the authors used the Bayesian optimization algorithm to quickly optimize the deep neural network for EEG classification, that allowed them to achieve up to 99% classification performance.

In their paper, Lorenz et al. [621] describe another advantage of Bayesian optimization for the brain signals analysis. The authors highlight that cognitive neuroscientists are often interested in broad research questions yet use overly narrow experimental designs by considering only a small subset of possible experimental conditions. It limits the generalizability and reproducibility of many research findings. They proposed an alternative approach, namely, *neuroadaptive Bayesian optimization*, as a powerful strategy to efficiently explore more experimental conditions than are currently possible with standard methodology.

Finally, Bayesian optimization enables developing subject-specific BCIs. Since human brain characteristics are not the same for different subjects, BCIs should be customized for each person. Thus, a number of parameters, including the EEG frequency bands, channels, and time intervals of interest, should be pre-determined based on each subject's brain characteristics. In their work, Bashashati et al. [622] demonstrated the efficiency of Bayesian optimization in tuning these hyper-parameters. In the recent work, Shahtalebi et al. [623] used Bayesian optimization to construct optimized subject-specific spectral filters, resulting in significantly discriminant features, which is a crucial requirement for any EEG-based BCI system.

## 5. Brain–computer interfaces for controlling exoskeletons and robots

Traditionally, one of the main areas of BCI applications is the control of external devices, for example, anthropomorphic manipulators, robots and exoskeletons, using neural activity generated by motor imagery [624]. In this context, the use of the BCI is aimed at improving the quality of life of people with impaired motor functions due to neurodegenerative diseases or a loss of limbs. In particular, a large number of papers are devoted to the development of BCIs for rehabilitation after a stroke [625] and spinal cord injury [626], controlling bioprostheses after limb amputation [353] and paralysis [11].

Control commands generated on the base of motor-related patterns of neuronal activity are actively used to move a two-dimensional cursor the screen [24], a wheelchair [627] and more complex devices in three dimensions, for example, anthropomorphic prostheses and exoskeletons [628]. In this context, neural activity patterns associated with movements of upper and lower limbs [629,630] are used to control such devices.

The developed neural interfaces to control motor activity can be divided into two large groups: invasive and noninvasive BCIs (see Section 2.1.3). In the former devices, the registration of brain activity is carried out using electrode matrices implanted in various areas of the cerebral cortex. Such matrices provide a high spatial resolution and allow recording the interaction processes in the framework of localized neural brain assemblies (up to 500 neurons). Primarily, the research in this direction was carried out on primates, however, several scientists used invasive interfaces in humans with electrodes implanted in the brain to monitor the course of neurological diseases (most often epilepsy [631]). Significant progress has been made in the field of invasive interfaces, in particular, those which allow controlling complex movements of anthropomorphic manipulators [632]. These devices are based on the EEG patterns associated with lower limb movements [633], commands for controlling a wheelchair [634] and simultaneous movement of two phantom hands [635].

Noninvasive interfaces are based on recording electrical brain activity from the head surface. Since these interfaces record the averaged activity of large groups of neurons, the data contain a number of artifacts. It should be pointed out that first neurointerfaces used noninvasive methods. For example, according to Wolpaw et al. [636], noninvasive interfaces can control the cursor movement by detecting slow cortical potentials, mu/beta-rhythms modulation or P300 EP. Currently, the development of noninvasive interfaces allows solving a wide range of tasks. By analogy with invasive interfaces, noninvasive BCIs are used to control anthropomorphic manipulators [628,637], wheelchairs [627], and exoskeletons [638].

Many publications on both invasive and noninvasive interfaces indicate that these two solutions have some advantages for specific applications. For example, the main advantage of invasive BCIs is a high quality of recorded signals. At the contrary, noninvasive BCIs do not allow a high-quality feature detection and require averaging across several channels and trials. Therefore, the techniques for generating control commands for noninvasive BCIs are relatively slow. On the other hand, the main disadvantages of invasive BCIs are that the electrode implantation into the brain and long training sessions to achieve a required efficiency of the algorithm, i.e., they are very subject-dependent.

Summarizing the above, it should be noted that the further development of invasive BCIs will involve human subjects [639]. In the field of noninvasive BCIs, the systems for untrained subjects are of great interest, since they allow minimal preparatory procedures. At the same time, the issue of optimizing BCI control algorithms is also being actively studied in order to reduce the number of recording sensors and make more convenient and compact headsets [640].

At present, a new problem arises. It is associated with the need to control a robotic prosthesis of touch sensations. Yet, brain-controlled prosthetic limbs were not endowed with this critical sense. In their recent study, Flescher et al. [641] microelectrode arrays were implanted into the primary somatosensory cortex of a patient with a spinal cord injury and, by cortex stimulation through the microelectrodes, produced touch sensations that were perceived as coming from his own paralyzed hand. These sensations often resembled pressure, they could be measured in intensity, and they remained stable for several months. The authors suggest that this approach can be used to convey information about the location of the contact and the pressure required for a prosthetic hand to interact with objects. Such an interface can be considered as the first step for introducing information directly into the brain: “computer → brain”.

### 5.1. Invasive brain–computer interfaces for controlling limb movements

The first records of brain activity obtained using activity signals of individual neurons were obtained using invasive technology in primates in 1966 [642] and in humans in 1967 [643]. According to the 2002 survey [644], a significant progress was made in developing methods for invasive registration of cortical neuron activity, which initiated the development of invasive neurointerfaces.

#### 5.1.1. Upper limb control

In particular, in 2002 an invasive interface was developed, allowing primates to control the movement of a cursor without preliminary training. In particular, Serruya and colleagues [645] recorded the activity of a small group of neurons (7–30) located in the region of M1 cortex, which, as was previously shown, to be most closely associated with the generation of motor commands [646]. The experiments were performed with three Macaca mulatta monkeys. At the first stage, the monkeys controlled the cursor movement with a joystick. They tried to follow moving objects on the screen, which appeared and disappeared at random times and moved along pseudo-random paths. Then, a linear filter method was applied to restore the arm movement trajectory using the recorded neural activity. At the next stage, the

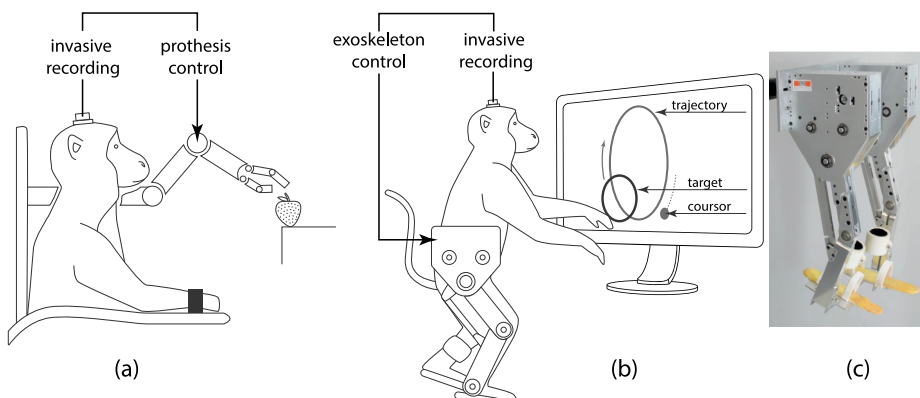


**Fig. 45.** The use of invasive BCIs for controlling (a) an anthropomorphic prosthetic arm during a self-feeding task [632] and (b,c) a lower limb exoskeleton [647]. The upper limb manipulator had five degrees of freedom: three on the shoulder, one on the elbow and one on the hand. This provided flexion/extension, shoulder abduction/adduction, internal/external rotation of the shoulder and flexion/extension of the elbow. The artificial hand consisted of a motorized grip that realized the associated movement of two “fingers”, providing proportional control of the distance between them.

cursor movement was only controlled by deciphering patterns of neural activity. In this case, first 60 s the cursor was continuously moved and the neural activity was registered for the initial calibration of the algorithm. The monkey needed to hover over the targets appearing in different places on the screen. Within 2 min the algorithm went through further tuning. In the final experiment, the monkey needed to hover over the appearing targets using both manual control (in some trials) and neural activity signals (in remaining trials). The task was considered completed if the goal was achieved in less than 20 s. It was shown that the effectiveness of achieving the goal was similar in the case of manual control and using neural activity.

Later, in 2008 an invasive interface was implemented, allowing the monkey to control an anthropomorphic manipulator [632] (Fig. 45). The control task included not only controlling the manipulator movement in 3D space, but also controlling the gripping force. Two monkeys were implanted with intracortical microelectrode arrays in their primary motor cortices. In the experiment, the signals from 15–25 cortical units were recorded and used to control a robotic arm.

According to Tillery et al. [648], neural activity forms characteristic EEG patterns depending on the food location in front of the monkey. On the base of these patterns, the speed of the end point of the manipulator was calculated. The clenching and unclenching of the hand, as well as the movement of the manipulator end point to the mouth, were activated by the corresponding patterns of neural activity.

At the first stage, the monkeys learned to control the manipulator with a joystick. In this case, the joystick controlled the movement of a point on the screen, whose position corresponded to the final position of the hand. The joystick was equipped with a button that allowed the monkey to adjust the gripping force. Then, the manipulator was controlled in a virtual environment using commands generated on the base of cortical neuron activity patterns. In this case, assisting effects were used. The entire workout took about two weeks, after which the monkeys could control the manipulator in 3D space and carry out the capture using cortical activity. The performances of these operations reached 98%. The population vector algorithm [649] was used to decipher the patterns of cortical activity.

The final experiment lasted for two days with two *Macaca mulatta* monkeys. The monkeys' arms were restrained to prevent them from grabbing the food directly by their hands. The restraints did not prevent them from making small wrist and hand movements. The first monkey performed the continuous self-feeding task during two days with a combined success rate of 61% (67 successes out of 101 attempted trials on the first day, and 115 out of 197 on the second day). The performance of the second monkey was 78% (1064 trials over 13 days).

During the experiment, the following interesting features were identified. After gripping the food and pulling it off the presentation device, the monkey gradually opened the gripper on the way back to the mouth and the gripper was typically fully open before it reached the mouth. On the contrary, in an earlier training session, the monkey kept the gripper closed all the way back to the mouth. Thus, over the course of training, the monkey learned that keeping the gripper closed was unnecessary. The time taken for one iteration was 3–5 s, that significantly exceeded the time required to complete this task using hands (1–2 s). The difference was due to visual feedback, which was used to adjust the motion of the manipulator.

In 2013 a BCI was developed, allowing monkeys to control both hands simultaneously (bimanual movements) using cortical activity patterns [635]. According to [650,651], during the coordination of bimanual movements in areas of motor cortex (supplementary motor area (SMA), primary motor cortex (M1)), a generation of special patterns of neuronal activity was observed, that were not a combination of patterns responsible for motor activity of the left and right hands separately.

The studies were conducted with two monkeys. Eight 96-channel multielectrode microwire arrays (768 channels in total) were implanted into bilateral SMA, M1, primary somatosensory cortex (S1), dorsal premotor (PMd), and posterior

parietal cortex (PPC) of monkey 1. Due to the system limitations, 386 channels were simultaneously registered. At the same time, PMd channels were excluded from consideration, since they did not contain useful information. For monkey 2, 48 electrodes were implanted in each of eight arm and leg areas (M1 and S1) in both hemispheres. During the experiments, signals from all 384 channels were recorded, however, only arm M1/S1 channels were used for both online and offline predictions. The electrodes recorded activity of up to 500 units. At that time, this was the largest indicator achieved in nonhuman primates. In addition, it was shown that a greater number of units can be successfully registered up to 48 months after surgery.

In the experiment, the monkeys were supposed to control the movement of two avatar arms displayed on the monitor screen. Each trial began with the appearance of two square goals on the screen. Their positions were the same in all trials, and they served as starting positions for the avatar's hands. The monkey needed to place the avatar's hands for these purposes and hold these positions for a time chosen randomly from a uniform distribution (from 400 to 1000 ms). Then, two squares were replaced with two round targets. Their locations were chosen from 16 possible configurations. The monkey had to place both avatar's hands on two circles and hold the targets simultaneously for at least 100 ms in order to receive the award (fruit juice).

At the initial stage, the monkeys controlled the avatar's hands using a joystick and then using brain signals to move the hand. After 15 days of training, the monkeys were able to perform bimanual operations without involving hand movements. Thus, as a result of training, the monkeys could control the avatar's hands using a joystick with a more than 97% accuracy. The control using brain signals, not excluding hand movement, was carried out with accuracy of more than 70%, including more than 90% correct trials for each arm individually. In the final sessions of managing the avatar's hands (without moving own hands), the performance accuracy for the left and right arms was not the same (monkey 1: left, 98.5%; right, 94.4%; monkey 2: left, 96.4%; right, 77.7%; averaged over the last three BCIs without arms sessions). Besides, the authors discovered plastic changes in firing patterns of cortical ensembles. These changes were particularly revealed in the functional reorganization of cortical representation of the avatar during a passive observation task, that was measured at the beginning of each session of brain control without arms. The decoding accuracy of passively observed avatar kinematics was clearly enhanced as the training progressed. Furthermore, the authors observed a gradual reduction in firing rate correlations among cortical neurons as the animals were training in the brain control without arm tasks. During earlier sessions, correlations between neurons were 1.7 to 2.2 times greater than during passive observation periods tested on the same day. Over the next few days, however, these cortical correlations decreased until they reached the same level as for passive observation. During this reduction, the correlations between neurons from the same hemisphere and the same cortical area remained higher than the correlations between neurons from different hemispheres or areas.

### 5.1.2. Lower limb control

Along with the management of upper limbs, invasive interfaces were designed to control the movement of lower limbs. One of the first attempts in this direction was made by Fitzsimmons and colleagues [652], who identified the relationship between kinematic walking parameters of the monkey and the activity of neural brain ensembles. They also suggested possible approaches to manage artificial drivers which reproduced walking patterns. The researchers used rhesus macaques, who were trained to walk on two legs on a custom modified treadmill. The training period took about one month. During the experiment, the activity of cortical neurons was recorded in the areas of primary motor (M1) and somatosensory (S1) cortices. Invasive electrodes made it possible to successfully register and sort the activity of 200–300 single units. Along with the brain activity during the experiment, a set of kinematic characteristics were recorded to characterize the walking. Movements of the right legs of the monkeys were tracked using a wireless video-based tracking system. The 3D coordinates of fluorescent markers applied to the hip, knee and ankle were tracked using two cameras at a 30-Hz frame rate, that allowed registration of such parameters as joint angles (hip and knee), foot contact with the treadmill, walking speed, step frequency and step length.

All leg kinematic parameters were also reconstructed from neuronal ensemble activity using a linear decoding algorithm referred to as a Wiener filter, which represented each decoded parameter as a weighted sum of neuronal rates measured before the time of decoding [54]. The prediction of leg kinematics was performed using multiple Wiener filters applied to the entire population activity of the recorded neurons or subpopulations recorded in separate cortical areas. Thus, the activity of simultaneously recorded cortical neural ensembles allowed simultaneous extraction of a variety of motor parameters: position of hip, knee and ankle, hip and knee angles, foot contact, direction of walking, and periods of standing still.

At the first stage, the efficiency of predicting kinematic parameters using cortical activity signals was evaluated. For these purposes, different indicators, such as signal-to-noise ratio (SNR), signal-to-error ratio (SER), and neuron dropping were calculated. Analyzing the obtained values, the authors showed that the prediction accuracy depended on the number of neurons in the population. Simultaneous prediction of four parameters was achieved with 75% accuracy using 30 neurons. For 95% accuracy, they needed to record the activity of 110 neurons. As the number of simultaneously predicted parameters increased, the required number of neurons were also increased. For example, for simultaneous prediction of 12 kinematic characteristics of walking with 75% accuracy, 40–50 neurons were sufficient, while for 95% accuracy, 140 neurons were required.

As a result, the authors achieved the highest accuracy in recognizing X and Y ankle coordinates and knee angles; SNR was in the range of 3.8–6.0 dB and SER in the range of 0.79–0.87. However, a Z coordinate (lateral movement) was

not predicted because of small lateral movements during walking sessions. The X and Y coordinates of the knee and the hip were extracted with average SNR in the range of  $(-0.7, 4.3)$  dB and average SER around 0.42–0.79. The average SNR and R for the hip angle ranged from 0.9–3.0 and 0.58–0.73, respectively. Meanwhile, the extraction accuracy for the foot contact state (swing or stance) ranged in 1.2–3.1 for SNR and 0.58–0.61 for SER, whereas the average SNR and SER for slowly modulated parameters were in the range of  $(-2.0, 1.4)$  and  $(0.24, 0.42)$  for walking speed,  $(-1.8, 0.9)$  and  $(0.48, 0.57)$  for step frequency and  $(-1.5, 1.9)$  and  $(0.30, 0.40)$  for step length. The low average accuracy in predicting the walking speed reflected the fact that in many experiments the treadmill speed was constant for long periods of time and thus had a very low variance.

At the second stage, the prediction of kinematic characteristics of walking in real time was carried out in 22 daily recording sessions. In each session, the first 5 min of walking were used to obtain training data, which were sent to a buffer in order to calculate a set of linear models for leg kinematic parameters. These models were then used to generate real-time predictions from neural spike data alone. As a result, the real-time predictions were not statistically different from offline predictions.

Capogrosso et al. [653] interfaced leg motor cortex activity with epidural electrical stimulation (EES) protocols to establish a brain–spinal interface that alleviated gait deficits after a spinal cord injury in nonhuman primates. It is well-known, that spinal cord injury disrupts the communication between the brain and the spinal circuits that orchestrate movement. To bypass the lesion, BCIs have directly linked cortical activity to electrical stimulation of muscles, which have restored grasping abilities after hand paralysis [654,655]. Restoration of leg muscle activity control for walking is also complex task due to necessity of realization of the complex sequence of individual muscle activation patterns underlying natural and adaptive locomotor movements [656,657]. Previously, EES of lumbar segments restored adaptive locomotion in paralyzed rats [658].

Recent studies showed that EES is also capable of activating lumbar spinal circuits in people with paraplegia. However, volitional locomotion requires the brain to control the activity of spinal circuits. In this context BCIs provide the tools to link the intended motor states to EES protocols to reestablish voluntary control of locomotion after injury. In the discussed study, rhesus monkeys were implanted with a microelectrode array into the leg area of the left motor cortex to record spiking activity from neuronal ensembles. Electromyographic signals were monitored using bipolar electrodes implanted into antagonist muscles spanning each joint of the right leg. To deliver EES, the technologies previously developed in rats [658] were adapted to the characteristics of spinal segments and vertebrae measured in three monkeys. These spinal implants were inserted into the epidural space over lumbar segments, and connected to an implantable pulse generator commonly used for deep brain stimulation therapy. The authors designed and implemented wireless control systems that linked online neural decoding of extension and flexion motor states with stimulation protocols promoting these movements. These systems allowed the monkeys to behave freely without any restrictions or constraining tethered electronics.

First, the natural spatiotemporal pattern of motoneuron activation underlying locomotion was identified and reproduced this pattern after injury. The muscle activity recorded during locomotion was projected onto motoneuron locations to visualize the spatiotemporal maps of motoneuron activation. These maps showed that locomotion involves the successive activation of well-defined hotspots located in specific regions of the spinal cord that were reproducible across monkeys. The most intense hotspots emerged in the caudal and rostral compartments of lumbar segments around the transitions between stance and swing phases which were labeled as extension and flexion hotspots, respectively.

Second, motor cortical recordings were exploited to decode the temporal structure of hotspots activation. The spiking activity recorded from the left motor cortex displayed cyclic modulations that were phase-locked with right leg movements. The developed classifier was able to calculate the probability of foot strike and foot off events from this modulation to anticipate the activation of extensor and flexor hotspots associated with right leg movements. Evaluations in two intact monkeys showed that the decoder accurately predicted these gait events in real-time over extended periods of locomotion, including when initiating and terminating gait, and during rest.

Third, without prior training of the monkeys, brain-controlled stimulation of the extension and flexion hotspots immediately modulated kinematic and muscle activity parameters related to the extension and flexion of the leg ipsilateral to stimulation. Finally, the BCI ability was tested to alleviate locomotor deficits after a lesion of the corticospinal tract extending in the right dorsolateral column of mid-thoracic segments in two monkeys. This lesion initially led to a paralysis of the leg ipsilateral to the lesion, followed by an extensive yet incomplete recovery. During the first week after lesion and without training of the monkeys, the BCI restored weight-bearing locomotion on a treadmill and overground, improving both the quantity and quality of steps performed by the impaired leg. Improvement of decoding performance during the following week suggested that this decrease was primarily due to the reorganization of cortical dynamics. This recovery coincided with improvement in the quantity and quality of steps, indicating that the monkeys had spontaneously regained some degree of neural control over the impaired leg. At this stage, the BCI alleviated many of the remaining gait deficits. Tuning EES frequency maximized the quantity and quality of steps, whereas the same stimulation protocols applied continuously failed to facilitate locomotion or were markedly less efficient than brain-controlled stimulation. The recovery of coordinated, weight-bearing locomotion in a primate model of spinal cord injury emphasizes the therapeutic potential of the BCI for such clinical applications.

The first exoskeleton of lower limbs was proposed in 2017 by Vouga et al. [647] (Fig. 45(c)) and tested with the monkey, who controlled the cursor movement on the screen. The cursor should follow the target which moved along a closed circular path of a 250-mm diameter at a revolution frequency from 0.1 to 0.16 Hz (Fig. 45(b)).

Monkey was implanted bilaterally with six movable volumetric 3D multielectrode implants including a total of 576 microwires [659]. They were located in arm and leg representation areas of both primary motor and primary somatosensory cortices. The signals from 128 electrodes were recorded simultaneously. The horizontal and vertical cursor positions were used as setpoints for the exoskeleton end-effector (ankle) and so a stoppage of the cursor would incur a stoppage of the exoskeleton. Joint angular positions were deduced using the inverse kinematic model of the leg and sent to the position controller. To perform a walking motion, at least two degrees of freedom are required: hip and knee. Since brain control occurs in two dimensions and for the sake of simplicity and safety, no other active degrees of freedom were added. The exoskeleton moved the monkey's legs, while monkey was trained to keep the muscles relaxed during the experiment.

The BCI performance was assessed via the time, the cursor spent in the target in increments of 0.6 s, and compared to the time spent in the control target. In the best sessions, the accuracy over 90% was reached, both with and without the exoskeleton. In sessions during which the monkey was well-trained, the task accuracy was between 80% and 95%.

Thus, the invasive registration of cerebral cortex neuronal activity provides good enough accuracy in decoding many markers associated with the movement of upper and lower limbs. Currently, this research area continues to grow rapidly. In particular, in their recent paper Ma et al. [633] proposed a system for decoding neural activity patterns in the monkey performing stand/squat movements. Else, Rajangam and colleagues [634] proposed a BCI allowing the monkey to control the movement of a wheelchair. The use of invasive BCIs allowed not only predicting trajectories of the monkey's hands, but also revealing mechanisms of neural activity responsible for movement planning [660].

## 5.2. Noninvasive brain-computer interfaces for controlling limb movements

As was shown above, invasive BCIs allow extracting information needed to control external devices, such as bioprostheses and exoskeletons. At the same time, there BCIs are mainly developed for primates and tested under laboratory conditions. A further development of this technology, including the transition to experiments with a human subject, requires overcoming complexities and clinical risks consisting in long-time functioning of implanted electrodes without brain issues infection.

Although extensive research is aimed at adapting invasive technology for humans [187,661], noninvasive interfaces are actively developing, allowing a person to control the movement of external devices using electrical brain signals (EEG) and hemodynamic responses (fNIRS).

### 5.2.1. Upper limb control

The first noninvasive control of a 2D cursor movement was implemented in 2014 by Wolpaw et al. [24], who recorded the subject's EEG using 64 noninvasive electrodes, referenced to the right ear, 0.1–60 Hz bandpass filtered and digitized at 160 Hz.

At the beginning of each trial, the target appeared in one of eight places on the screen periphery in a random order. One second later, the cursor appeared in the middle of the screen and began to move in two dimensions. The direction of the cursor movement was controlled using the EEG signals. As soon as the cursor reached the goal within 10 s, the test was considered successful and the subject received a reward. There were 1-s pauses between the tests. A daily series of the experiments for each subject included eight 3-min sessions separated by 1-min breaks. Each measurement of the cursor movement was controlled by a linear equation, in which the independent variable was a weighted combination of the EEG signal amplitudes in mu (8–12 Hz) and beta (18–26 Hz) rhythms recorded in the sensory-motor cortex in the right and left hemispheres (in the vicinity of electrodes C3, C4).

To determine the cursor displacement in vertical ( $M_V$ ) and horizontal ( $M_H$ ) directions, the right-side ( $R_V$  and  $R_H$ ) and left-side ( $L_V$  and  $L_H$ ) amplitudes were each multiplied by corresponding weights ( $w_{RV}$ ,  $w_{RH}$  and  $w_{LV}$ ,  $w_{LH}$ ) according to the following linear equations

$$M_V = a_V (w_{RV}R_V + w_{LV}L_V + b_V), \quad M_H = a_H (w_{RH}R_H + w_{LH}L_H + b_H), \quad (59)$$

where  $a_V$ ,  $a_H$  and  $b_V$ ,  $b_H$  are gains and intercepts essential if the user is to move the cursor to the target consistently [662]. The least mean-square (LMS) algorithm was used to adjust the weights to minimize the difference between the actual and target locations predicted by Eq. (59).

As a result, the users successfully completed 70% to 92% of the tests. The average task execution time ranged from 1.9–3.9 s. To be sure that the subjects did not use limb muscle contractions to control sensorimotor rhythms, EMG activity of the forearm muscles was recorded during the experiment. For the examined muscle groups, the correlations between the EMG amplitude and the vertical and horizontal movement components were very low. Moreover, the vertical and horizontal control did not appear to interfere with each other, i.e., the subjects controlled movements in both dimensions simultaneously. The results of this research were compared with similar results obtained using invasive interfaces. The authors showed that the performance of the proposed noninvasive BCI (movement time, movement precision, and hit rate) was comparable to invasive BCIs.

In 2016, a noninvasive interface was proposed for controlling a robotic arm manipulator [628]. The developed noninvasive BCI enabled a highly accurate control of 3D movements. The task was to select and seize an item (Reach and Grasp Task). The experimental design allowed increasing task complexity in the course of the experiment. The experiment

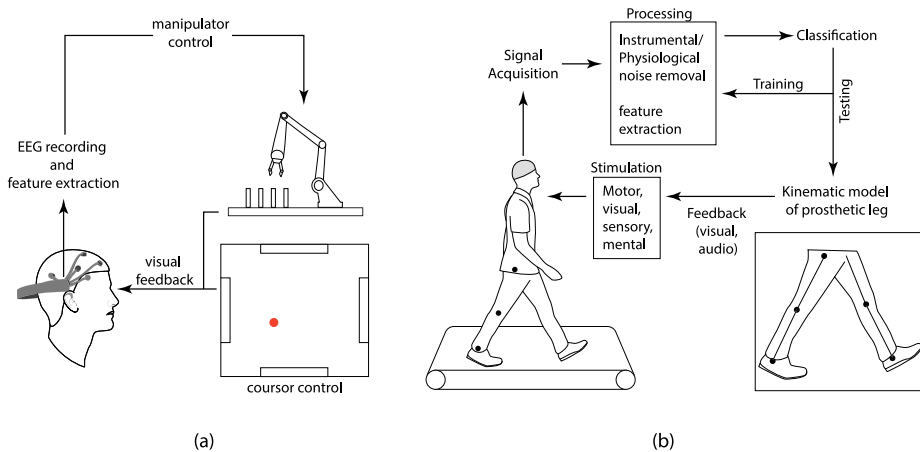


**Fig. 46.** Noninvasive interfaces for controlling (a) the anthropomorphic manipulator [637] and (b) exoskeleton [638], based on motor imagery.

included two stages. First, the subject had to direct the manipulator (in a 2D plane) to the area above the target and fix the target position. If the subject chose the right object, he/she had to point the manipulator down in the third dimension in order to grab the object.

Every subject participated in a series of experiments consisting of 8–15 sessions. Each session included 10–12 trials lasting 5–10 min. The experiment included five stages with different complexity: virtual cursor only, four-target grasp, five-target grasp, random-target grasp and shelf-target grasp. The subjects were instructed to represent movements of the left, right, both hands or the relaxation of both hands to control movements of the manipulator to the left side, right side, up, and down. Due to motor imagery, the SMR amplitude was modulated at the mu-frequency (10–14 Hz) and energy changes were evaluated using the 16-th order autoregressive (AR) model:

$$y_t = \sum_i w_{t-i} y_{t-i} + \epsilon, \quad (60)$$

where  $y_t$  is the estimated energy at time  $t$ ,  $w_i$  is the weight coefficient, and  $\epsilon$  is the estimation error. A 400-ms window was used to calculate the amplitude in real time. The weight coefficients were estimated by the least-squares criteria.

At the first stage, the subjects were trained, based on the control of one-dimensional movement (left-right) of the cursor on the screen. As a result of the training, the accuracy of the one-dimensional control reached 97%. At the second stage, the subjects were trained to move the cursor on a two-dimensional plane (left-right or up-down). In this case, 85% accuracy was reached. Finally, the subjects were able to move randomly-located objects in the limited three-dimensional space.

The average accuracy for a four-target grasp task was  $77.8 \pm 18.1\%$  in the first session and  $82.8 \pm 16.3\%$  in the second session, resulting in average of  $80.3 \pm 17.0\%$  for the two sessions. The average accuracy across the participants for the four-target grasp task sessions in the absence of the virtual cursor was  $90.1 \pm 7.7\%$ , whereas in its presence was  $89.9 \pm 8.9\%$ . The average accuracy across all participants for the five-target grasp task was  $74.5 \pm 17.3\%$  in the first session and  $84.9 \pm 6.6\%$  in the third session and resulted in average of  $77.9 \pm 14.7\%$  across the three sessions. The average accuracy of six participants for the five-target grasp task in the absence of the virtual cursor across sessions was  $79.0 \pm 8.3\%$ , whereas in its presence the accuracy was  $85.1 \pm 8.0\%$ . For all subjects, it took on average  $5.5 \pm 0.84$  s and  $5.0 \pm 0.6$  s to complete individual steps (trials) required to complete the reach-and-grasp sequence in the four-target and five-target grasp tasks, respectively.

Another approach to noninvasive manipulator control was proposed in 2018 by Kilmarx et al. [637] (Fig. 46(a)). The authors used the imagined body kinematics (IBK) technique to reduce the preliminary training time [663]. The IBK paradigm is based on natural imagined movements of the subject's dominant hand [664]. In contrast to the SMR of right/left hand motor imagery which required a long training time (from weeks to months), the IBK method demonstrated reasonable performance after only several minutes of training.

During the experiment, signals from 14 EEG channels were recorded using the Emotiv EPOC headset. For pattern recognition, the low-frequency signal component (0.16–1 Hz) was used, which contained information on the imagined body kinematics [665]. A multiple regression algorithm was developed to estimate instantaneous output velocities at time  $t$  in horizontal ( $u(t)$ ) and vertical ( $v(t)$ ) directions, as follows

$$u(t) = a_{0x} + \sum_{n=1}^N \sum_{k=1}^K b_{nky} e_n(t-k), \quad v(t) = a_{0y} + \sum_{n=1}^N \sum_{k=1}^K b_{nky} e_n(t-k), \quad (61)$$

where  $e_n(t-k)$  is the measured voltage for  $n$ th EEG channel at time  $(t-k)$  ( $k$  being a lag time),  $N = 14$  is the total number of EEG channels,  $K = 13$  is the total lag number, and  $a$  and  $b$  are the parameters which were calculated and optimized in order to obtain a minimum error between predicted and real velocities.

Two experiments were conducted. The first experiment implied controlling the cursor position and included three phases. The first phase was a learning one. At this stage, the subject was instructed to follow the cursor movement on the screen and at the same time imagine how his/her dominant hand followed the cursor. The phase two was a calibration one. A multiple regression model was trained to decode the cursor velocity as a function of the low-frequency power component. During the third phase, the subject controlled the cursor movement, while pointing it at one of four targets. In the second experiment, the subject controlled the manipulator. Since the computer did not offer one of the four goals, the subject could independently choose any of them. The subject was given a maximum trial time of 15 s to select a target corresponding to the desired action. Then, the manipulator joint movements associated with this action were adjusted to reach the target in 7 s.

In order to assess the algorithm accuracy, the Goodness-of-Fit (GoF) metric was used. As a result, during the training phase, the subjects demonstrated high accuracy of decoding speeds: 91.85% for horizontal and 67.47% for vertical directions. While during the test phase, the target accuracy was 77%, the manipulator control allowed 70% accuracy. The execution of one task took about one minute. The subject controlled the manipulator movements by following the cursor on the monitor. In addition, the participant could receive visual feedback by observing the manipulator movement. The authors note that the high accuracy of the manipulator control was achieved after a relatively short training time. The subjects demonstrated good accuracy on the cursor control after 10-min training.

Along with EEG, noninvasive hemodynamic response using fNIRS [666] was used to decipher patterns of brain activity associated with upper limb movements. Nasser and Hong [143] showed that hemodynamic response associated with motor imagery of right and left wrists, had clear features (the mean value and the slope of changes in the oxygen-containing hemoglobin concentration) to be used for controlling HSC BCIs. As a result, the average classification accuracies were 73.35% and 83.0% when these features were taken into account during 10-s intervals. Moreover, when the duration of the analyzed time windows was limited to 2–7 s, the average classification accuracies were improved to 77.56% and 87.28%, respectively. This means that fNIRS can be used for real-time BCI control. In addition, according to the paper of Piper et al. [667], fNIRS is a promising method for studying low-frequency brain patterns when performing tasks related to whole body movements.

### 5.2.2. Lower limb control

Currently, the development of noninvasive BCIs for controlling lower limb movements is an important challenge of modern physics and cognitive neuroscience. These interfaces are often used for post-stroke rehabilitation. In particular, Garcia et al. [668] proposed a BCI for stroke patients with walking disorders using a robot-assisted training protocol. The authors used a logistic regression classifier [483] to reveal EEG activity patterns associated with walking. Both conditionally healthy volunteers and stroke patients participated in this study. The exoskeleton "The Lokomat Pro" (Hocoma AG, Volketswil, Switzerland) was used in the experiment, where the subjects performed two types of tasks, active and passive walking, while the body weight support (BWS) and the guidance force (GF) were used as control parameters.

For passive walking, GF and BWS were set to 80% and 75%, respectively, meaning that the exoskeleton took upon itself 80% of the patient's force and 75% of the body weight. Whereas, for active walking, GF and BWS were set to 30% and 5%, respectively. The participants were asked to perform as small effort as possible during their passive walking to allow the robot to move their legs.

As a result, for healthy subjects, the average classification accuracy for active walking was  $94.0 \pm 5.4\%$ , whereas for passive walking it was  $93.1 \pm 7.9\%$ , as compared to the baseline. A classification performance of  $83.4 \pm 7.4\%$  was achieved when the active walking was compared to the passive walking. For stroke patients, the classification accuracy was 85%–97%, as compared to the baseline using the information from the beta band (20–30 Hz).

A similar classification accuracy of EEG-based walking-intention patterns in stroke patients was obtained by Sburlea et al. [669], who analyzed features from ten channels (F3, Fz, F4, FC1, FC2, C3, Cz, C4, CP1, CP2) located over precentral, central, postcentral motor and sensorimotor cortex. The extracted EEG features were the signal amplitudes in the 0.1–1 Hz frequency band and the logarithmic power in the 8–13 Hz frequency band. The sparse LDA [670] was used for classification. As a result, more than 80% classification accuracy was reached. Moreover, a connection was found between the classification accuracy and the subject's motivation level during the rehabilitation course.

As in the case of upper limbs, fNIRS were also used to detect the motor-related activity associated with lower limb movements. An increase in the level of oxygen-containing hemoglobin ( $O_2Hb$ ) in the bilateral supplementary motor area (SMA), primary motor (M1) and somatosensory (S1) cortical regions occurred when the subject was walking on a treadmill with a speed of 1 km/h [671]. An increase in the walking speed up to 4 km/h was accompanied by a hemodynamic reaction in the bilateral primary sensorimotor areas (SM1) [672]. During the transition to the run, there was additional oxygenation changes in the premotor cortex (PMC) and especially in the prefrontal cortex (PFC). The intention of walking was observed to induce changes in the SMA hemodynamic response immediately before walking [673] and when performing more complex movements, such as backward walking [674].

According to the Perrey's survey [675], the fNIRS-based prediction of the post-stroke recovery of movements is still difficult. Therefore, this research direction is under active development. In their work, Rea et al. [676] analyzed the fNIRS data during the preparation for hip movements in seven post-stroke patients. Using LDA, they showed the possibility to classify activity patterns in the PMC and/or posterior parietal cortex (PPC), corresponding to paretic and nonparetic movement preparation trials in most of the tested patients.

When PPC channels were used, the average performance of LDA reached  $67.77 \pm 11.35\%$  accuracy ( $72.27 \pm 10.94\%$  for paretic and  $63.27 \pm 17.51\%$  for nonparetic) in classification of hip movement preparation trials. However, the use of PMC channels resulted in classification accuracy of  $50.40 \pm 9.45\%$  ( $46.77 \pm 11.24\%$  for paretic and  $54.03 \pm 14.66\%$  for nonparetic). Finally, the use of combined PPC and PMC channels provided classification accuracy of  $62.28 \pm 15.51\%$  ( $60.64 \pm 20.46\%$  for paretic and  $63.92 \pm 11.50\%$  for nonparetic).

In the recent paper, Khan et al. [638] introduced a fNIRS-based BCI for managing prosthetic legs and rehabilitation of patients with movement disorders (Fig. 46(b)). fNIRS signals were used to initiate and stop a gait cycle, while a nonlinear proportional derivative computed torque controller with gravity compensation was used to control torques of hip and knee joints for position error minimization. The experiment involved healthy subjects and included walking sessions of 10-s durations alternating with 20-s rest sessions. During the experiment, the brain activity was recorded using 9 optodes located in the motor cortex (M1) of the left hemisphere. The signal sampling rate was 1.81 Hz. The conversed Beer-Lambert law [677] was used to convert recorded optical density signals into oxyhemoglobin and deoxyhemoglobin concentration changes.

Thereafter, for the removal of motion artifacts and physiological noises, six different filters (Kalman, Wiener, Gaussian, hemodynamic response filter, bandpass, and finite impulse response) were applied. Then, six different features were extracted from oxygenated hemoglobin signals, and their different combinations were used for classification. Classification performances of five different classifiers (k-NN, quadratic discriminant analysis, LDA, naïve bayes, and SVM) were evaluated.

At the first stage, the authors analyzed the obtained classification accuracy using various classifiers and various filters. As a result, the highest classification accuracy of 65%–86% was obtained using the SVM as a classifier and a hemodynamic response filter.

Finally, the authors adapted the developed algorithm for real-time calculations and showed the possibility of using it in the BCI to control a prosthesis. To develop a kinematic model of the prosthetic leg, two degrees of freedom were used: one for the hip joint and another for the knee. Using kinematic parameters, a dynamic model was developed to describe the prosthesis movement.

Recently, we identified biomarkers of hemodynamical response of the motor cortex on the motor execution obtained by fNIRS, and used them for designing a sensing method for classification of the type of movements [678]. The real and imaginary motor actions by left and right hands are reliably recognized using eight sources and eight fNIRS detectors, followed by data processing of spatial brain activity with the simple online decision tree-based classifier. The statistical analysis shows that the selectivity and specificity of the classifier are sufficiently high and reach 85%–100%. The accuracy of the classifier for motor execution is higher than for motor imagery. The number of incorrectly detected and uncertain events is about 5%–20%.

### 5.2.3. Brain-computer interfaces for untrained subjects

The above results evidence a significant progress in both invasive and noninvasive interfaces. In particular, invasive interfaces allow restoring arm and leg movement trajectories on the base of kinematic parameters of neural activity during walking. On the other hand, the noninvasive BCI technology allows controlling not only a cursor position on the screen, but also an anthropomorphic manipulator using motor imagery, as well as detecting moments of preparation and implementation of lower limb movements. Although the invasive technology allows detecting very small motor activity, its implementation in humans requires surgical intervention to implant electrodes into the brain. Moreover, signal processing techniques used to detect EEG patterns must specially be adapted to operate with ECoG [47].

One of the directions for the development of noninvasive interfaces is the creation of algorithms for detecting motor-related patterns of brain activity in untrained users. This is of particular importance for disable people, for whom the training process is difficult or impossible. In this context, Blankertz et al. [679] showed that untrained users were able to manage a BCI based on motor imagery after a 20-min calibration session. During the calibration session, the subjects performed motor imagery tasks guided by visual stimuli, and the EEG patterns associated to such brain activity were found. The recorded single trials were then used to train the classifier by machine learning techniques applied online in feedback sessions to produce a feedback signal for unlabeled continuous brain activity. In the calibration session, visual stimuli indicated which of the following three motor commands the subject should perform: (L) left hand, (R) right hand, or (F) right foot movement. After the calibration sessions, the experimenter screened the data to adjust specific subject's parameters for the data processing methods.

Then, the subjects participated in the feedback sessions, where they needed to control a one-dimensional movement of a cursor on the screen. For this aim, two classes of movements were used (for example, left and right hands), which were classified using LDA. The CSP algorithm was applied to identify features of the EEG signal structure.

Along with the simple cursor control, the users performed a “basket game” task, which consisted in controlling the horizontal position of a ball that was moving downward at a constant speed. Below there were three targets, one of which was highlighted in color, and the ball had to hit it. The experiment involved ten subjects, nine of which were able to control the object position with good accuracy. The obtained results evidenced the possibility of managing the BCI by untrained users. When studying inter-subject variability in generation of motor commands, the authors found specific EEG features in the time-frequency structure in mu- and beta-ranges. However, the boundaries of these ranges were different for different subjects. The differences were also observed in the spatial localization of the observed patterns.

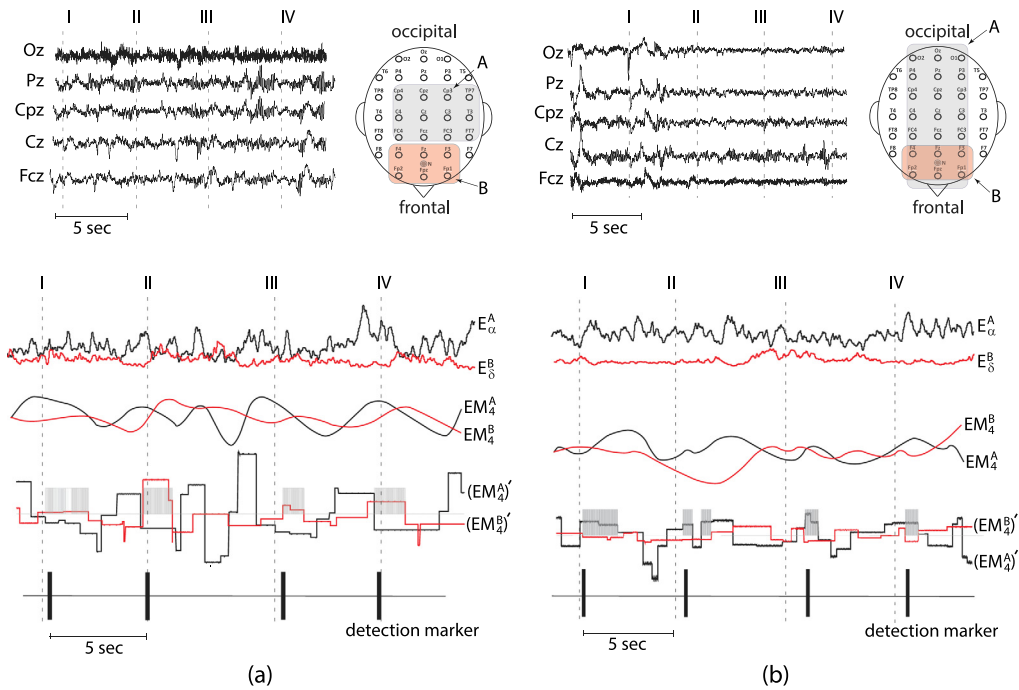


**Fig. 47.** Detection of time moments corresponding to (a) real and (b) imaginary hand movements in EEG of an untrained subject. (Upper row) Recorded signals and considered spatial regions (A and B), over which the averaging is performed. (Lower row)  $E_\alpha^A$  and  $E_\delta^B$  are EEG energies in alpha/mu and delta ranges, respectively, calculated in areas A and B.  $EM_4^A$  and  $EM_4^B$  are fourth-order empirical modes characterizing changes in the energy of EEG signals over time.  $(EM_4^A)'$  and  $(EM_4^B)'$  are derivatives of empirical modes obtained over time. The shadow areas show time intervals when all event detection conditions are simultaneously fulfilled. Based on the data from [62].

In our recent paper [62], we analyzed the time–frequency and space–time structures of EEG signals in a group of untrained subjects in exercises and imaginations of movements in the absence of feedback. We have found that, unlike real movements characterized by an ERD mu-rhythm in the motor cortex, motor imagery in the majority of subjects was accompanied by ERS of the mu/alpha rhythm in the parietal and central areas. This is due to the fact that untrained subjects can demonstrate various scenarios of motor imagery, for example, visual (VI) and kinesthetic (KI) imagination types [680]. While VI consists in self-visualization of a moving limb, KI implies the feeling of the muscle movement, that requires a special training [681]. At the same time, real and imaginary movements have common features associated with ERD and ERS of the low-frequency (1–5 Hz) rhythm.

The identified patterns allowed us to develop an algorithm for detecting time moments corresponding to real and imaginary movements by untrained subjects. The main stages of the proposed algorithm are presented in Figs. 47(a) and 47(b), respectively. In these figures, the times I–IV indicate the moments of a command presentation at the beginning of every action. The spatial regions A and B correspond to the regions of the cerebral cortex, where special features in the time–frequency structure associated with motor activity were found. One can see that for real movements, these features imply changes in the mu-rhythm in the left hemisphere of the central and prefrontal areas, whereas for motor imagery, larger brain areas are activated. The time–frequency analysis of the EEG signals was performed in the 1–15 Hz range using Morlet wavelet-based CWT. At the same time, the wavelet energy was calculated in the alpha/mu (8–15 Hz) and delta (1–5 Hz) ranges. The obtained values were averaged over the EEG channels entering the regions A and B. As a result, the coefficients ( $E_\alpha^A$ ) and ( $E_\delta^B$ ) were calculated. To identify the low-frequency trend in changing these values over time, empirical fourth-order modes ( $EM_4^A$ ) and ( $EM_4^B$ ) and their time derivatives ( $(EM_4^A)'$ ) and ( $(EM_4^B)'$ ) were considered. In the case of motor imagery, we observed a decrease in the mu-energy in region A and an increase in the delta-energy in region B.

The efficiency of this algorithm was tested on a group of twelve untrained healthy subjects, where  $92.9 \pm 7.8\%$  real movement events were detected with a  $5.5 \pm 4.24\%$  false alarm rate, whereas  $81.6 \pm 6.2\%$  motor imagery events were found with a  $9.1 \pm 6.2\%$  false alarm rate. The motor executions were recognized in average not later than  $0.5 \pm 0.2$  s after they had actually been started. The imaginary movements were sometime recognized  $1.9 \pm 1.1$  s after they started, that likely was caused by a lack of training.

Another important issue related to the further development of BCIs is the optimization problem, namely, a search for ways to reduce the number of registered channels. From a practical point of view, the development of compact BCIs based on a convenient and quickly installed headset, requires a small number of EEG channels which would allow obtaining necessary information about neural activity [682,683]. In addition, the optimization is needed in the context

of improving efficiency of the brain state classification. Irrelevant EEG channels are known may add extra noise and redundant information which can reduce the accuracy of signal processing [683]. Traditional methods of dimensionality reduction include the principal component analysis (PCA) and LDA, where the original features are mathematically projected onto a lower dimensional space. However, such methods are nongeneric and require the input data optimization for every subject due to strong inter-subject variability [684] and a lack of association of ongoing optimization with physiological processes in the brain.

A large number of EEG channels is not good for a fast working BCI because the information processing will require a long time that impedes its operation in real time. Therefore, the reduction of the number of channels is one of the important problems for the BCI development. Recently, we demonstrated that the number of EEG channels can significantly be reduced [145] using certain characteristics of time-frequency and spatial-temporal EEG structures. For this purpose, we recorded EEG signals using 31 channels when the subject imagined movements of lower limbs. The use of the SVM method allowed us to reach a  $76 \pm 12\%$  accuracy in the motor imagery classification by comparing different ANN structures. Then, this method was applied to select a set of channels belonging to occipital, parietal, frontal, temporal and central regions of the cerebral cortex, based on specific characteristics of the brain structure. In addition, particular cases were considered where channels located only in the left or right hemispheres were used for classification.

Although the highest (76%) classification accuracy was achieved when all channels were taken into account, the consideration of only channels from frontal and temporal areas provided a 75% accuracy, while from frontal and prefrontal areas 74% accuracy. In the last case, the channel set contained as many as 8 channels only. This result indicates that the channels located in the frontal and prefrontal areas are more significant for motor imagery classification. The additional time-frequency analysis revealed spectral components allowing higher classification accuracy. It was shown that high-pass filtering spectral components ( $>5$  Hz) improved classification accuracy up to 90% using only 8 electrodes located in the frontal cortex.

## 6. Prediction and prevention of epileptic seizures

Among many applications of BCIs for controlling pathological processes of brain neural activity, one of the most vivid examples is the monitoring and control of epileptic activity. Epilepsy is a neurological disease characterized by spontaneous seizures. At the moment, around 50 million people in the world suffer from different types of epilepsy. Epileptic seizures are associated with formation of patterns of rhythmic brain activity, involving neural populations located in different brain areas.

One of the most common ways to prevent epilepsy is the use of medical drugs. These medications affect through a variety of mechanisms, often acting to suppress ion channels. Despite the fact that the development of antiepileptic drugs began more than 20 years ago, so far one third of patients are not amenable to this type of treatment. For these patients, it seems effective to use methods based on the destruction of pathological neural activity by stimulating the corresponding brain areas. At the moment, there are several methods which allow effective suppression of epileptic seizures using electric [685], magnetic [686] and optogenetic stimulations [687].

### 6.1. Open-loop interfaces for brain stimulation

The external influence on a neural ensemble can automatically be activated according to a predetermined protocol. This action is the characteristic feature of the open-loop control using an antiepileptic device. This means that there is no direct feedback between the brain state and the stimulation protocol. One of the most prominent representatives of such systems is a *vagus nerve stimulator* (VNS) (Fig. 48(a)) developed by Cyberonics, Inc. (Houston, TX, USA) and approved by the US FDA in 1997 for adjunctive therapy in pharmacoresistant epilepsy. The VNS performed periodic electrical stimulation of the left vagus nerve in a repetitive “duty cycle” (“on” for 30 s and then “off” for 5 min). The stimulation parameters were programmed by a physician to specify stimulation voltage, on-time, pulse-width, on-off cycle duration, and the stereotyped response when the device was triggered manually. Despite the relative simplicity of the design, these devices were found to be quite effective for some patients. The VNS reduced the number of seizures by an average of 30%–40%, though 10% or fewer patients were rendered seizure-free [688]. One of the first “open-loop” antiepileptic devices for deep brain stimulation was a stimulator of the anterior nucleus of the thalamus in epilepsy (SANTE) (Fig. 48(b)), manufactured by Medtronic, Inc. (Minneapolis, MN, USA) for treatment of partial-onset epilepsy by stimulating the anterior nucleus (AN) of the thalamus [689].

### 6.2. Closed-loop devices for seizure detection and suppression

It is obvious that for more effective control of epileptic activity, the stimulation should be performed in accordance with peculiarities of the current state of the neural network. In other words, one needs to use the BCI which realizes the feedback between the brain and external stimulation. Such feedback is implemented in the BCI operating on the principle of closed-loop control, where the neural network monitoring is carried out using electrical brain signals. One of the first such “closed-loop” systems brought to the stage of clinical trials, was the responsive neurostimulator (RNS) designed by Neuropace Inc. (CA, USA) (Fig. 48(c)). It contained implanted electrodes for recording the intracranial EEG served as an

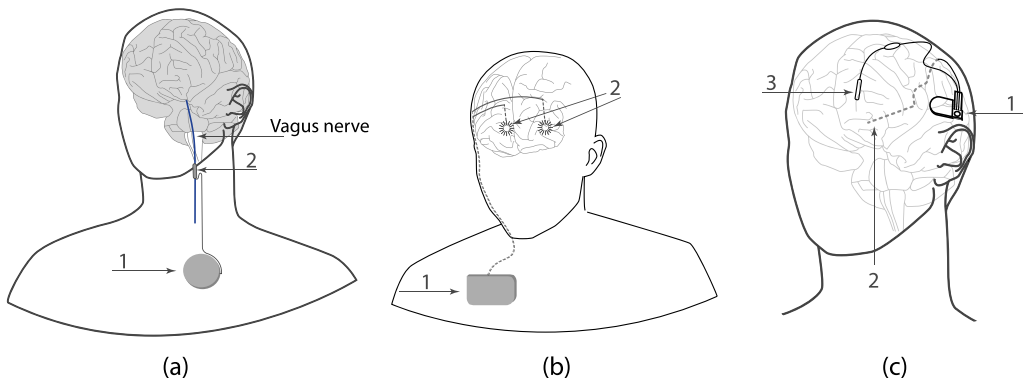


**Fig. 48.** Schematic illustration of neurointerface prototypes to suppress epileptic seizures using electrical stimulation. (a) Vagus nerve stimulator: 1 – an implantable pulse generator, 2 – a stimulation lead. (b) Stimulator of the anterior nucleus of the thalamus in epilepsy: 1 – an implantable pulse generator, 2 – intracranial electrodes placed in the anterior thalamic nuclei bilaterally. (c) Responsive neurostimulator: 1 – implanted deep electrodes for recording EEG signals, 2 – an implantable device for processing EEG signals from electrodes 1, 3 – strip electrodes receiving an electrical stimulation signal generated by the device 2 to stop seizures.

input for the algorithm which determined when a seizure has started. The triggered focal electrical stimulation was sent to a specific brain area to interrupt the seizure [690].

In addition to the above-mentioned devices, other BCIs were created to realize “closed-loop” and “open-loop” control of epileptic activity. According to the review of Stacey and Litt [14], the further development of antiepileptic brain stimulated devices should be aimed at a search for biomarkers of neural activity, allowing to predict the occurrence of epileptic seizures, as well as for the most effective stimulation parameters for destruction of pathological activity with the least impact on the normal brain functioning.

Today, there exist efficient algorithms that allow detecting the occurrence of epileptic seizures with a high degree of sensitivity and selectivity. For example, Ovchinnikov et al. [445] proposed an algorithm that allows detecting seizures of absence epilepsy in rats within 1 s with 100% sensitivity and about 96.6% accuracy. The efficiency of their algorithm was tested on 5–6 h records as well as on 24 h. The registration of electrical brain activity was carried out using only three invasive electrodes. One active electrode wire was positioned epidurally on the frontal cortex of the right hemisphere (A/P: +2; M/L: -3.5), the second epidural electrode on the occipital cortex (A/P: -6; M/L: -4), and the third electrode wire (ground electrode) on the top of the cerebellum (all coordinates were determined according to the stereotactic atlas of Paxinos and Watson (1998)). Then, the obtained records were processed using Moret wavelet-based CWT, and the energy in the high-frequency range was calculated.

It is known, that high frequencies (30–80 Hz) appear in the ECoG during spike-wave discharges (SWDs) [281]. The wavelet power for this frequency range at each moment in time will show a drastic increase in power in that specific band at the very beginning of a SWD and a rapid decrease of the power at its end. The obtained energy was compared to the threshold value for detecting the moment of time characterizing the occurrence of the seizure.

An efficient system which combines the detection and prevention of epileptic seizures in rats was suggested by Berenyi et al. [691]. To detect pathological activity, the authors used local field potentials (LFPs) and multiple-unit activity (MUA) recorded by chronically implanted tripolar electrodes placed in deep and superficial layers of the frontal and parietal cortical areas. They applied transcranial electrical stimulation (tES) between left and right temporal electrodes placed directly on the skull. Alternatively, tES was applied between the bitemporal electrodes and a frontal midline electrode. The authors used the algorithm to detect spikes of a SWD and applied the stimulation only during the spike generation. As a result, the tES modulated the spike amplitude of the SWD, without any influence on the animal's behavior, neither induced arousal effects when applied during sleep, nor affected overt its behavior during waking, as demonstrated by the lack of tES-induced head movements. Finally, the group analysis of closed-loop tES stimulation showed that the mean duration of the SWD episodes was significantly shorter in all nine experimental rats. In addition, the time spent in the SWD episodes in a given session was significantly reduced in seven rats. Overall, the feedback tES stimulation led to a >60% decrease of both the duration of the SWD episodes and the fraction of session time spent in the SWD across the animals. Thus, the tES activated when an epileptic seizure was detected, prevented its development.

Nowadays, there are efficient algorithms which allow detecting seizures with high accuracy. In the next section, we will describe some of them.

### 6.3. Seizure prediction and prevention

The development of antiepileptic interfaces allow seizure prediction and prevention by activating a stimulation before the seizure starts. However, the seizure prediction is a very difficult task for types of epilepsy characterized by spontaneous

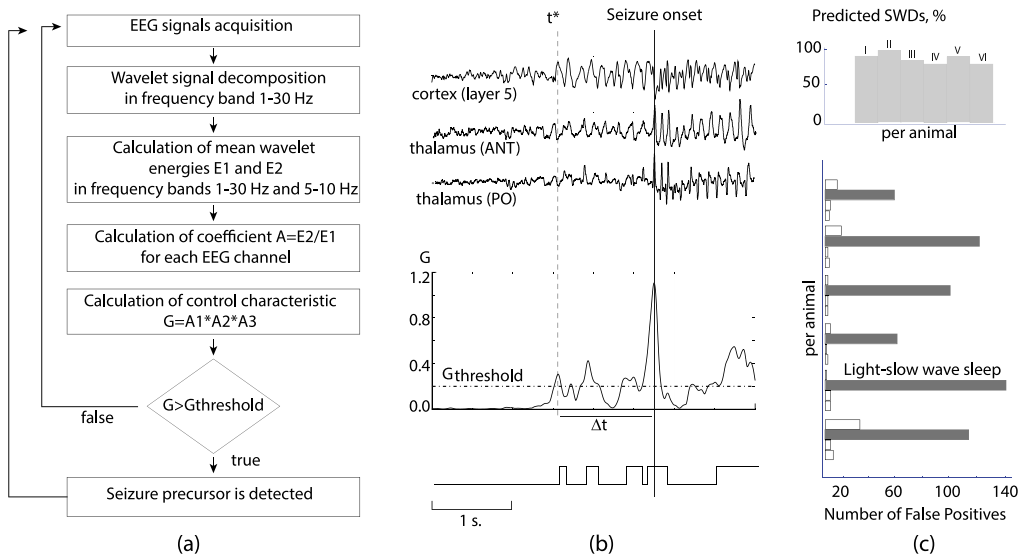


**Fig. 49.** (a) Algorithm for detecting predecessors of absence seizures. (b) Results of the algorithm implementation: (upper panel) recorded EEG signals, (middle panel) computed control characteristic  $G(t)$ , and (lower panel) the output of the telegraph signal. (c) Results of the statistical analysis: (upper panel) the percentage of predicted discharges and (lower panel) the average number of false detection for different animal activity types calculated for five 50-s intervals.

penetration, for instance, absence epilepsy without cramps which mainly occurs in children with normal development. This type of epilepsy was investigated using animal models, such as genetically modified rats WAG/Rij and GAERS, which have a genetic predisposition to the epilepsy development. In spite of the existence of a large number of methods that allow detecting absence seizures, e.g., using a time-frequency analysis and artificial intelligence [261], only a few approaches were proposed to predict the onset of these seizures. Although absence seizures occur suddenly [692–694], neurophysiological brain activity exhibits changes in energetic properties before the seizure starts [695]. The time-frequency analysis allowed distinguishing characteristic EEG patterns, predecessors of the seizures, in delta- and theta-frequency ranges in cortex and thalamus [469]. This results made possible to develop and implement a special algorithm for predicting absence seizures by analyzing time-frequency structure of a multichannel EEG signal.

In 2016 van Luijelaar et al. [261] proposed an interface for predicting epileptic seizures. The results are illustrated in Fig. 49. The developed algorithm (Fig. 49(a)) was based on the analysis of three EEGs recorded in layer 5 of the somatosensory cortex, posterior thalamic nucleus and anterior thalamic nucleus. The received signals were analyzed using CWT with the modified Morlet mother wavelet to increase temporal resolution of the transform, and the wavelet energy was calculated in the theta-range according to [469]. To identify common patterns in cortex and thalamus, the product of the obtained values of wavelet energy was considered. If the obtained value exceeded the set threshold, the system detected the seizure predecessor (Fig. 49(b)). The efficiency of this interface was demonstrated on the rats WAG/Rij with a genetic predisposition to absence epilepsy [41,696]. The neurointerface was tested on six animals during 6-h experimental sessions. The results of the statistical analysis presented in Fig. 49(c) show that the interface allowed predicting  $87.8 \pm 7.08\%$  of seizures  $0.8 \pm 0.16$  s before they started. However, along with the high performance of the prediction algorithm, a large number of false detections also occurred, especially in a sleep mode. Therefore, for efficient implementation of the developed algorithm, an additional criterion aimed at reducing the number of false detection should be applied together with the electrical brain stimulation.

Along with theta-waves (5–10 Hz), low-frequency (3–5 Hz) and high-frequency (7–20 Hz) brain activities were also considered for detecting EEG patterns known as *sleep spindles*, typical in a sleep mode [41]. As a result, epileptic seizure precursors were detected not only when the theta energy exceeded a predetermined threshold, but also when the energy at other frequencies exceeded the corresponding thresholds (see Section 4.3.3). With these additional conditions, the number of false positives was reduced by  $83 \pm 3.3\%$ , that allowed successful algorithm implementation in the BCI for predicting and suppressing epileptic seizures (Fig. 50).

At the first stage, in order to assess the sensitivity and selectivity of the algorithm, the BCI was used without feedback. Although epileptic seizures were predicted, the electrical stimulation was not applied. As a result, the algorithm marked received neurophysiological signals in real time, as shown in the upper trace of Fig. 50(b). The average number of predicted seizures was about 45%, and in three of six animals this value exceeded 50% (the second diagram in Fig. 50(c)).

During the second stage, the ability of the algorithm to prevent epileptic seizures was studied. For this purpose, electrical stimulation was delivered to the cerebral cortex at the moment of the predicted SWD. This allowed reducing the duration of epileptic activity by  $72 \pm 10\%$  in average for the group of animals, and for some animals up to 98%–100%.

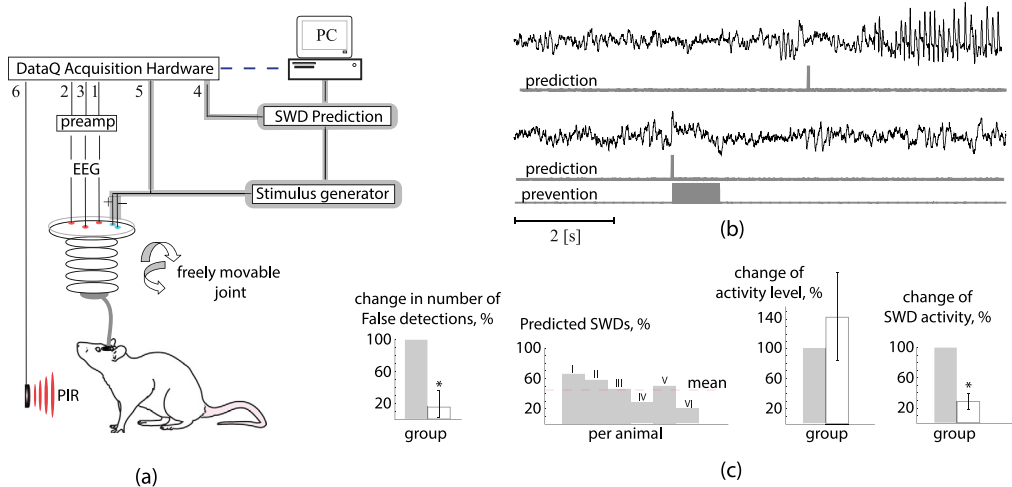


**Fig. 50.** Brain-computer interface for prediction and suppression of epileptic seizures. 1–6 are channels of the data acquisition hardware, where 1–3 are inputs from three EEG channels, 4 is used for a prediction marker, 5 for stimulation and 6 for a signal from a passive infrared registration (PIR) system for movement detection. (b) Prediction (upper trace) and prevention (lower trace) of the absence seizure SWD by delivering a 1-s stimulation pulse train.

Source: Reprinted from [41].

Thus, the developed BCI has a high efficiency in reducing not only the duration of epileptic seizures, but also their number. At the same time, a further use of the BCI to control epileptic activity in humans is limited due to a large number of false detection. Despite the fact that additional stimulation did not cause changes in animal activity, the safety of using BCIs for people requires additional efforts to increase the prediction selectivity and reduce the number of false detections.

#### 6.4. Current state and further direction

According to the Freestone's et al. survey [697] published in 2017, among a large number of systems for prediction of epileptic seizures, none of the systems can be used in clinical practice to suppress seizures. The main limitation of the existing systems is a small amount of data to validate the efficiency of prediction algorithms. In addition, a large number of modern algorithms based on machine learning methods do not take into account neurophysiological mechanisms of the epileptic activity formation.

Actually, the problem of seizure prediction is not a simple classification problem of the brain activity in interictal and preictal states because different types of epileptic seizures are characterized by different biomarkers of the preictal state [698]. Nowadays, modern hardware with implemented complex algorithms for processing neurophysiological data using mobile chips [473,699,700] enables forecasting seizures at their early stages. Moreover, the development of advanced machine learning methods [701] may further improve the accuracy in the brain state characterization in order to develop efficient BCIs for clinical use [702].

To date, only one BCI is known to predict the occurrence of epileptic seizures, brought to clinical trials [702,703]. However, this BCI does not imply electrical brain stimulation, but only warns the patient about the likelihood of a seizure. This BCI consists of intracranial implanted electrodes connected with a subcutaneous telemetric block implanted in a chest cell. This unit transmits the EEG data wirelessly to a special handheld device. The device implements the computational process of EEG data processing in real time using an individual algorithm. As a result, the system displays warning signals to the person about possible seizures. The device reports high, medium, or low seizure risks.

In order to verify the effectiveness of this BCI, two-stage studies were conducted. At the first stage, the device was implanted into the brain, and the signals of the brain activity were recorded for a long time, until a sufficient amount of data was accumulated to train the algorithm. As a result, a sufficiently large number of seizures were registered in nine patients, enough for training and verification of the prediction algorithm. During the second stage, the developed algorithm was launched in real time for four months. For three patients, the prediction accuracy (in the percentage of correctly predicted attacks) was 86%, 100%, and 100%. The percentage of time during which these three subjects were warned about the high probability of the seizure was 27%, 31%, and 3%, respectively. For the remaining six patients, the prediction sensitivity ranged from 54% to 71%, and the warning time of the high probability of a forthcoming seizure was between 15% and 41%.

The results of the study, on one hand, show the possibility of predicting epileptic seizures in humans using the BCI. On the other hand, there are a number of issues that require further research. In particular, it is still unclear how the patient environment affects variability of prediction accuracy.

According to a recent review of Kuhlmann et al. [704], the development of efficient systems for predicting epileptic seizures remains a challenging task of modern neuroscience. To approach this problem, new methods based on machine learning, artificial intelligence, and big data analysis [702,705,706] have been developed. To improve the efficiency of existing algorithms, one needs to collect a database of neurophysiological records containing a sufficiently large number of seizures for the statistical analysis of the efficiency of developed algorithms. Taking into account the significant progress in the development of devices for high-precision recording of brain activity, targeted stimulation of neural ensembles (for example, using optogenetic stimulation) and small-sized computational circuits, we can assert that in the nearest future the BCI will be widely used in clinic practice for prediction and suppression of epileptic seizures.

## 7. Brain-computer interfaces for evaluation and control of cognitive states

One of the most promising BCI applications is the continuous monitoring of brain activity with the aim of evaluating different aspects of cognitive states, such as alertness, drowsiness, fatigue, mental workload, emotions, different mental states and others. The knowledge of mental conditions can be useful for detection of attention failure when the person performs a cognitive task which requires sustained attention, for example, during an educational process [707,708]. Another applications of such interfaces are the monitoring of operator's work in a complex equipment, air traffic controllers, astronauts, etc. [198,237,356,709].

### 7.1. Monitoring of cognitive states: alertness and drowsiness

Alertness is known as a state of active attention by high sensory awareness, such as being watchful and prompt to meet danger or emergency, or being quick to perceive and act. Drowsiness is a state of strong desire for sleep. It can be dangerous when performing tasks that require sustained attention, such as driving a vehicle, piloting an aircraft, monitoring air traffic, etc.

It is known for more than 50 years, that in tasks requiring sustained attention, people cannot maintain alertness at a certain constant level [710]. It is also known, that changes in the alertness degree reflect features of brain activity signals. The first attempt to detect these hallmarks in real time was made in 1994 by the researchers from the Naval Health Research Center (USA) [711], who demonstrated a system for monitoring human alertness (Fig. 51). Their algorithm was based on EEG spectral properties and ANN and contained the following steps.

1. Simultaneous data collection and stimulation. EEG recordings were performed in parallel with two workstations. Workstation 1 implemented auditory stimulus synthesis and data recording, while workstation 2 performed real-time spectral and ANN analysis and produced auditory feedback. Visual stimuli were presented via a custom software.
2. Data preprocessing and artifact rejection. EEG signals were preprocessed using coefficients read from a file created by the ANN training software.
3. Real-time spectral estimation. The moving-averaged EEG spectral power was calculated using a 512-point fast Fourier transform (FFT).
4. Off-line ANN training. At the first step, optimum EEG frequencies were selected for each subject. Then, a two-layer perceptron was trained to use spectral power estimates at these frequencies to optimally predict a subject's local error rate in a current time window. Finally, networks were trained using a standard backpropagation method.
5. Real-time ANN implementation. During experimental sessions, the weights from the previously trained ANN for each subject were read into a real-time feedforward neural network module that estimated a local error rate from the smoothed real-time spectral energy every 1.64 s.
6. Auditory feedback. During feedback sessions, whenever the estimated error rate exceeded a predefined threshold, the system synthesized a 1-s burst of square-wave sound and translated the signal into the subject's headphones.

The proposed system was tested with six subjects, which were instructed to press one of two response buttons (auditory or visual) whenever they detected an auditory or visual stimulus. Each subject participated in five sessions, each lasted for 28 min. The first three sessions were ANN training sessions. The rest two sessions were feedback sessions in which ANN was applied to spontaneous EEG to estimate changes of alertness and activate feedback.

The authors demonstrated the possibility of ANN to determine a subject's score based on EEG signals. The score was measured as a percentage of missed stimuli during a moving time window of a 95-s length. A high percentage of missed stimuli (low score) was associated with low alertness, whereas a low percentage of missed stimuli (high score) was related to high alertness. Having considered the subjects scores, the authors have shown that the percentage of correct responses to the stimuli varied from 99% to 46% during a session. At the beginning of the experiment, the subjects usually demonstrated high performance, which then decreased after 10 min. The decreased alertness could be caused by mental fatigue. To control the subject's alertness, the authors implemented a feedback in the form of an auditory signal as soon as the subject's error rate exceeded a 40% threshold. The auditory feedback signal helped the subject to decrease the error rate, i.e., to increase attention.

After the pioneering work of Makeig et al. [711], who used a simplest ANN structure (a two-layer perceptron), more sophisticated ANNs were applied to recognize alertness and drowsiness from EEG signals. The main problem was to detect

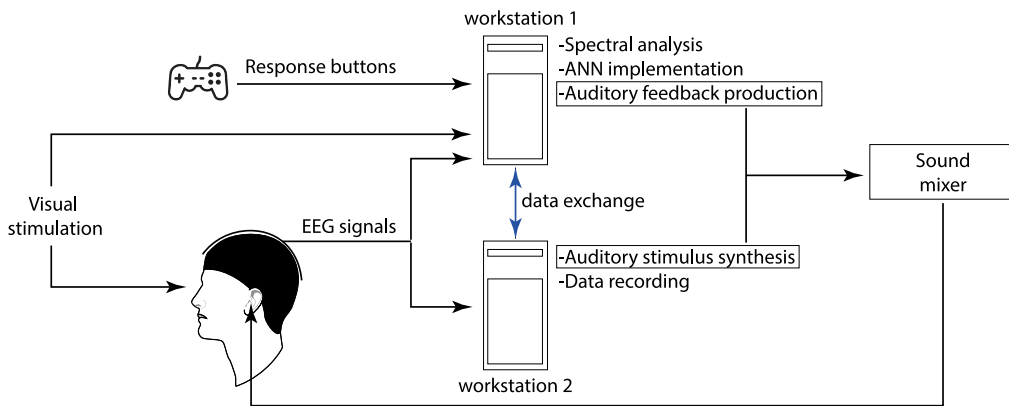


**Fig. 51.** Schematic illustration of the first system for alertness monitoring/management described in [711].

these states with short (1-s length) EEG trials. Vuckovic et al. [712] defined alert states as the alpha rhythm suppression in the occipital cortex. In the next years, scientists applied different approaches to detect brain activity patterns related to alertness and drowsiness state in real time and developed systems for alertness control in real environment.

For classification of states of alertness, Vuckovic et al. [712] used three different ANNs.

- The first ANN was a linear network trained by the Widrow–Hoff rule [713]. This network consisted of 14 neurons and trained with 100000 epochs. The error goal was  $SSE = 0.1$ . There were two alternative stopping rules applied during the ANN training: the number of training epochs and the error goal. An output neuron released “1” for alertness and “0” for drowsiness.
- The second ANN was a feed-forward network trained with the Levenberg–Marquardt (LM) learning rule [714]. This ANN operated with 8 neurons in the hidden layer and was trained with 75 epochs. The error goal was also  $SSE = 0.1$ .
- The third ANN consisted of two layers and used learning vector quantization (LVQ). The first layer was competitive and trained to classify data into one of subclasses. The second, linear layer transformed the subclasses into output target classes. The output neuron assigned to a winning competitive neuron obtained value “1”, while the other output neurons obtained “0”. Depending on which neuron had “1”, the EEG trial was classified as either drowsiness or alertness. This ANN had 12 neurons in the competitive layer and 2 neurons in the output layer, and was trained with 10000 epochs. The stopping rule was the number of training epochs.

All three ANNs were trained and tested on EEG recordings of three subjects. The authors reported 100% accuracy in alertness/drowsiness detection for second and third ANNs, while the first (linear) ANN demonstrated 75% accuracy. The ANNs obeyed the LM and LVQ rules were trained using the data of three subjects in order to test classification properties on the mixed data from several subjects. As a result, the LM ANN classified the drowsiness reasonably well ( $83.2 \pm 18.3\%$ ), but detected the alertness poorly ( $36.3 \pm 32.1\%$ ). The LVQ network performance was much better. It classified the drowsiness with  $97.6 \pm 4.3\%$  and the alertness with  $84.8 \pm 13.1\%$ .

Apart from ANNs, fNIRS is also a very promising tool for the development of noninvasive BCIs for revealing cognitive states [715–717]. Recently, Khan et al. [718] used fNIRS in a passive BCI for drowsiness detection during a driving task. In order to induce a drowsy state, the subjects were deprived of almost 10 h of sleep. After that, they stayed awake during night and the experiment was conducted in the morning. The subjects were asked to drive a car for one hour using a driving simulator keeping a speed of 40–60 km/h. The drowsy state was detected via the driving performance accessed with a driving simulator, as well as by analyzing eye movement and blinking. The fNIRS signals were acquired with a 1.81-Hz sampling rate using 7 sources and 16 detectors located on the prefrontal cortex (PFC) and left- and right dorsolateral prefrontal cortex (DPFC) according to the international 10–20 system. Gaussian filtering was used to remove the respiratory, heartbeat and other motion artifacts. Finally, the Beer–Lambert law [719] was used to convert the raw intensity values to the oxygenated and deoxygenated hemoglobin concentration changes ( $\Delta\text{HbO}$  and  $\Delta\text{HbR}$ ). At the first step, the authors estimated the data size appropriate for extracting the features of drowsiness and alert state. Three different time windows were used (5 s, 10 s and 15 s) and for each window 8 features were considered. The mean  $\Delta\text{HbO}$  and  $\Delta\text{HbR}$  were estimated as

$$M_k = \frac{1}{N} \sum_{j=1}^{\text{window}_k} X_j, \quad (62)$$

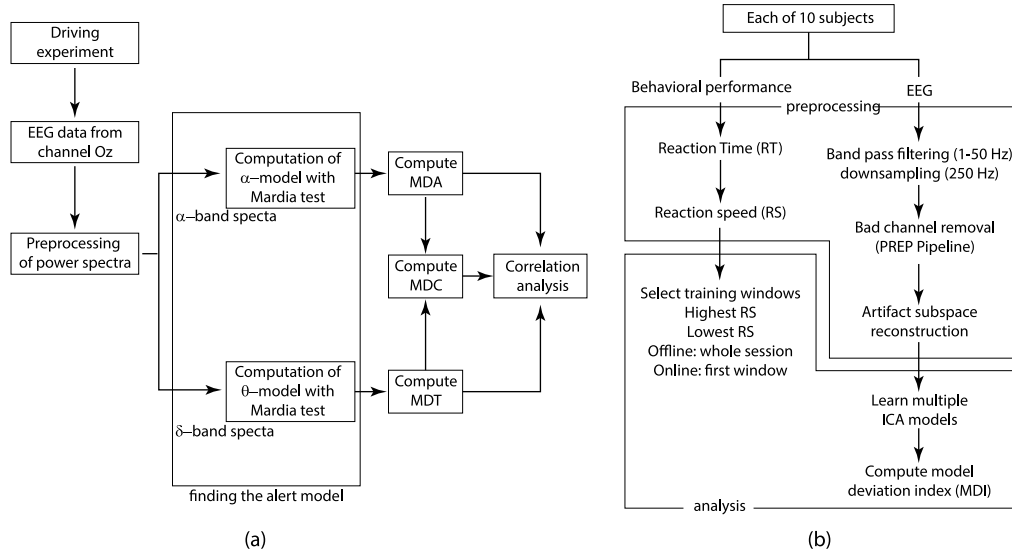


**Fig. 52.** Pipelines of algorithms for alertness/drowsiness assessment using (a) EEG power spectra in particular bands [720] and (b) EEG source reconstruction algorithm [722].

where  $k$  was the analyzed time window,  $X_j$  corresponded to the values of  $\Delta\text{HbO}$  or  $\Delta\text{HbR}$  belonging to this window. The skewness was computed as

$$\text{skew}_k = \frac{E(X - M_k)^3}{\sigma^3}, \quad (63)$$

where  $\sigma$  was the standard deviation of  $X$  in a single time window, and  $E$  was the expected value of  $X$ . In addition, kurtosis was computed as

$$\text{kurt}_k = \frac{E(X - M_k)^4}{\sigma^4}, \quad (64)$$

The signal slope (SS) was calculated using the polyfit function in MATLAB (Math Works, USA). The number of peaks (NoP) was gauged by counting the total number of local maxima of the averaged  $\Delta\text{HbO}$  signals. The sum of peaks (SoP) was computed by taking the sum of the maxima values. The frequency of peaks ( $f$ ) was determined by dividing NoP by the window size. All features calculated for each window were normalized and rescaled between 0 and 1. Then, these normalized feature values were used by the two-class classifier for training and testing data by means of LDA to find an optimal separation between drowsy and alert states.

As a result, the authors achieved the best classification performance using mean  $\Delta\text{HbO}$ , signal peak, and SoP as features. They obtained average accuracies of 83.1%, 83.4% and 84.9% in the 5-, 10- and 15-s time windows, respectively, in the right DPFC. The use of the SVM approach allowed increasing accuracy to 84.4%, 85.7% and 87.3%, however, the computational time also increased from 0.05, 0.03 and 0.02 s to 0.9, 0.6 and 0.4 s, respectively.

Before 2017, the majority of the methods for alertness evaluation were based on the spectral analysis of signals from individual EEG channels and the selection of discriminative features and machine-learning approaches. Sometimes, the interpretation of the results caused difficulties when the algorithms trained on one subject were applied to other subjects. To solve this problem, Pal et al. [720] proposed an unsupervised subject- and session-independent approach for detection of drowsy states in EEG recordings during the driving. Assuming that during the first few minutes of the driving, the driver is in a state of alertness, the authors defined this state from the EEG signals recorded in the first few minutes of the experiment. In order to estimate the driving performance, they measured a deviation of the center of the vehicle from the center of the cruising lane [721]. Having analyzed the time-frequency structure of the obtained EEG, they found that the spectral power of alpha- and theta-waves linearly correlated with driving performance.

The proposed algorithm for detecting drowsy states contained the following steps (Fig. 52(a)).

1. The EEG signal recorded from the occipital Oz channel was downsampled to 250 Hz and preprocessed using a 50-Hz lowpass filter.
2. The EEG power spectrum was calculated using FFT and smoothed with the help of a component-wise median filter.
3. The alertness model was derived using a multivariate distribution. Every two seconds the EEG power spectrum was calculated in the theta- and alpha-bands. As a result, a set of  $n = 30$  vector data  $x_1, \dots, x_{30}$  were generated every minute. The model was represented by a multivariate normal distribution  $N(\mu, \Sigma^2)$  ( $\mu$  and  $\Sigma$  being the mean

vector and variance–covariance matrix) using maximum likelihood estimates. Then, the Mardia's test was applied to validate the model and check whether or not the energy of the alpha- and theta-waves obeys a multivariate normal distribution.

4. The alertness model was used to assess the subject's cognitive state by finding the difference between the EEG power spectra during the current state and during the state represented by the alertness model. The deviation of the present state from the model was calculated using the Mahalanobis distance  $D$  [723], which was referred to as MDA for the alpha-band model and MDT for the theta-band model. Finally, a linear combination of MDA and MDT was used to compute a combined deviation (CMD) as

$$\text{CMD} = a \times \text{MDA} + (1 - a) \times \text{MDT}, \quad 0 \leq a \leq 1. \quad (65)$$

5. Correlation between alertness level  $d$  and calculated MDA, MDT and MDC values was estimated as

$$\text{Corr}_{d,D^*} = \frac{\sum(d - \bar{d})(D^* - \bar{D}^*)}{\sqrt{\sum(d - \bar{d})^2} \sqrt{(D^* - \bar{D}^*)^2}}, \quad (66)$$

where \* denotes MDA, MDT or CMD.

The efficiency of the derived alertness model based on a single subject's data was relatively high. The obtained correlation coefficients for MDA and MDT were 0.58 and 0.78, respectively. The combination CMD yielded the correlation coefficient of 0.78.

Recently, Hsu and Jung [722] proposed a EEG source reconstruction algorithm to estimate the degree of alertness. They hypothesized that neural activity underlying degree of alertness, can be modeled as a composition of statistically independent sources using ICA (see Section 3.1). The authors used different ICA models to detect states of alertness and drowsiness in EEG signals recorded in subjects performing a sustained-attention task with a driving simulator.

The schematic illustration of the algorithm evaluation is shown in Fig. 52(b). It includes two blocks, one for data preprocessing and another for data analysis. In the preprocessing block, the recorded EEG signals are filtered and downsampled. Flat and poorly correlated channels are removed and interpolated using the early stage preprocessing based on the Matlab package PREP-pipeline [724]. Along with EEG preprocessing, this block evaluates the behavioral performance, i.e., the reaction time (RT). High and low RTs are associated with states of drowsiness and alertness, respectively.

The algorithm was implemented in both offline and online modes. For the offline mode, the whole data from a 90-min session was split into 90-s blocks. Five alertness and five drowsiness ICA models were trained each with five 90-s windows with lowest and highest RTs, respectively. For the online mode, the ICA model was trained using first 90-s segments at the beginning of each session. The efficiency of the proposed algorithms was evaluated using a model deviation index (MDI).

Hsu and Jung [722] also demonstrated that the ICA models trained with only 90-s EEG segments were able to reach converged solutions and find dipolar components. The authors identified comparable ocular and neurophysiological independent component clusters in all of the four models. Having compared the ICA performance for the whole data, they obtained the following results.

- Alertness ICA models can model the data segments with low RTs (state of alertness) and yield small MDI values, but they fail to fit the data with high RTs (drowsiness) and thus yield large MDI values.
- Drowsiness BCI models well characterize source compositions and dynamics of the data with high RTs (drowsiness), leading to smaller MDI values.
- These BCI models can track the dynamics of the reaction speed with significantly positive correlation coefficients.
- Offline BCI models had the smallest correlation coefficient between the MDI and the reaction speed.
- Online BCI models were evaluated in a similar way with alertness BCI and provided possibility to track the dynamics of the reaction speed.

Having analyzed the obtained results, the authors concluded that the offline models attempted to learn the stationary sources over the entire session. At the same time, the EEG source composition was nonstationary because the subjects' levels of alertness fluctuated. They provided strong evidence for the hypothesis that the brain activity under different levels of alertness can be characterized by distinct compositions and activations of independent sources. Furthermore, this enabled online tracking of the level of alertness by using a BCI trained on a prerecorded alertness (or drowsiness) EEG.

While the approaches for evaluating a state of alertness were usually tested with a driving task, their potential applications are not limited to this. In 2017, Ko et al. [725] proposed a system for monitoring sustained attention in real classroom settings. Sustained attention is known to be a process that maintains persistent efforts over prolong time. In this context, performing attention-related tasks in real life involves the need to ignore a variety of irrelevant distractions. Obviously, human's ability to maintain sustained attention is related to the brain capability to acquire and process sensory information in a fast and efficient manner. This is very important in the educational process, where students must maintain a high level of attention during classes.

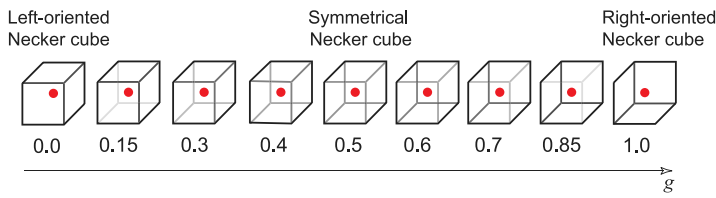


**Fig. 53.** Examples of Necker cubes with different values of control parameter  $g$ . The left-hand image with  $g = 0$  corresponds to the fully left-oriented Necker cube, while the right-hand image with  $g = 1$  to the fully right-oriented Necker cube. Each subject was instructed to fix his/her sight at the central red dot.

To implement attention monitoring in a realistic way, the experiments were carried out during regular lectures held at the National Chiao Tung University (Taiwan). The researchers analyzed visual attention of students using a specially designed test for visual target recognition. During the lectures, visual stimuli appeared on the screen with random time intervals, but no more often than one stimulus per minute. There were four types of stimuli (triangle, square, circle and star), one in a single trial. Each participant had a smartphone with an application that displayed all possible choices in the form of buttons with pictures and kept the smartphone unlocked during the whole experimental session. The subjects were instructed to press the corresponding button as fast as possible, ones they saw the image on the screen. A response time was defined as time interval between the stimulus appearance on the screen and the moment when the student presses the button. A larger response time meant a lower level of alertness and therefore a higher level of drowsiness.

The EEG signals were segmented into trials associated with the events of the visual target appearance. All trials were classified into four equal groups, separated by three thresholds: Q1, Q2 and Q3. The first 25% of all trials with  $RTs < Q1$  were classified into group I with highest level of visual alertness, while another 25% of the trials with  $RTs > Q3$  formed group IV representing the worst performance. The resting 50% of the trials formed groups II and III.

The recorded EEG signals were processed using FFT. Spectral energy was calculated for 30 frequency bins from 1 to 30 Hz with a 1-Hz step covering delta (1–3 Hz), theta (4–7 Hz), alpha (8–14 Hz), and beta (15–30 Hz) frequency bands.

As a result, the authors reported the following stimulus-related changes in the time-frequency and spatio-temporal EEG structures.

- The delta-band power decreases in the frontal cortex when response time increases. In the occipital region, the delta power fluctuates, dropping down in the second quarter of trials, but then starts to increase as the response time increases.
- The theta-band power monotonically decreases in the frontal and left temporal regions. An increase in the theta-power is observed in the occipital region comparing groups IV and I.
- The alpha-band power fluctuates in the frontal and temporal regions. The mean alpha-band power remains unchanged as the response time increases moderately, and decreases when the RTs are long.
- As the response time increases, the mean baseline power in the beta band decreases significantly in the last quarter of trials over the occipital and temporal brain regions as compared to the first quarter of trials.

Since the spectral power changed in the occipital area, the authors proposed measuring response time using changes in the power ratio  $\rho = \beta/\theta$ . As a result, they observed that when the current response time exceeded 1.3 times the mean alert state response time, the  $\rho$  monotonically decreased from 0.75 to 0.66.

Thus, human alertness can be estimated in real time during the task accomplishing. In this context, the most effective way to assess an attention state is to use visual stimuli and analyze the stimulus-related response of the neuronal brain network in attention-related brain areas. In the recent work [64], we proposed a similar experimental paradigm to monitor human's alertness in real time during accomplishing a prolonged task of visual stimuli classification. In order to focus the subject's attention on the stimuli, the authors explored the Necker cube. This popular ambiguous stimulus was used in many psychological experiments.

The Necker cube is a flat bistable image which looks like a cube with transparent faces and visible ribs (Fig. 53). The observer without perception abnormalities sees this image as a 3D-object due to the specific position of the cube's ribs. Bistability in perception consists in the interpretation of this 3D-object as to be either left- or right-oriented depending on the contrast of the inner ribs. The contrast of three middle lines centered in the left middle corner was used as a control parameter  $g$ . The values  $g = 1$  and  $g = 0$  correspond, respectively, to 0 (black) and 255 (white) pixels' luminance of the middle lines. Therefore, a contrast parameter was defined as  $g = y/255$ , where  $y$  is the brightness level of the middle lines using the 8-bit grayscale palette.

During the experimental session, the Necker cubes with different values of the control parameter were presented to the subject for short time intervals, each lasting between 1.0 and 1.5 s. In order to draw away the subject's attention and make the perception of the next stimulus independent of the previous one, different abstract pictures were demonstrated for about 5.0–5.5 s between subsequent demonstrations of the Necker cube images. The subjects were instructed to press either the left or right key depending on the first impression of the cube orientation at each presentation.

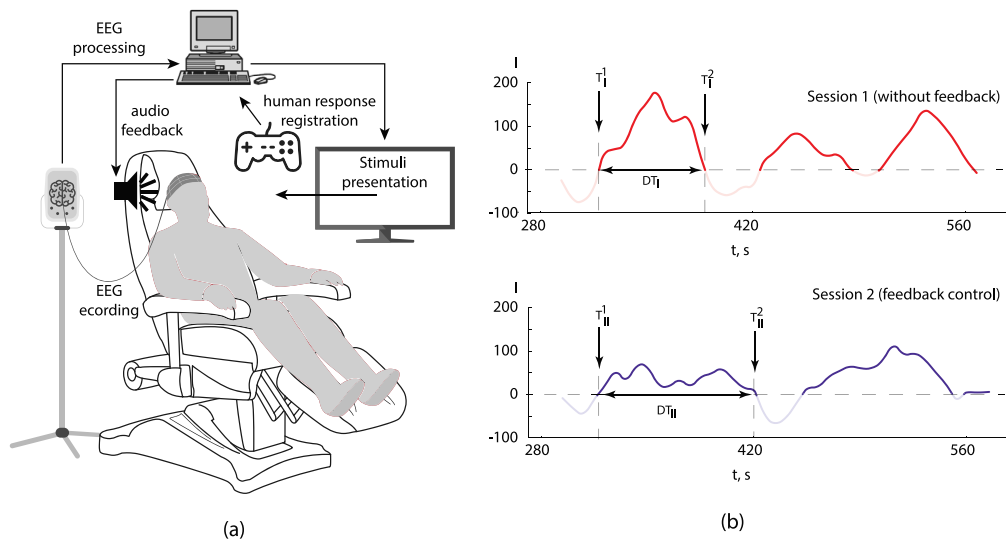


**Fig. 54.** (a) Brain–computer interface for monitoring and control human's alertness in real time during accomplishing a prolonged task of visual stimuli classification [64]. (b) Typical dependences of alertness degree on time estimated for a session without feedback (upper panel) and with feedback (lower panel).

Source: Reprinted from [152].

The EEGs were recorded by five electrodes (O1, O2, P3, P4, Pz) located in the occipital and parietal areas in accordance with the standard position of the 10–20 international system. The obtained data were analyzed in alpha- and beta-frequency bands in real time using a 2-s floating window. Similar to [725], the EEG signals were segmented into 2-s trials associated with every stimulus presentation. Namely, the moment of the stimulus presentation was in the middle of the trial. The authors analyzed stimulus-induced changes in alpha and beta-energies using the approach described above in Section 4.3.2. The characteristic feature of the state of alertness was a decrease in alpha-energy with a simultaneous increase in beta-energy during the stimulus presentation.

At the first stage, the authors analyzed the effect of motivation. For this purpose, they considered two groups of 10 participants in each. Group 1 consisted of financially motivated subjects, while group 2 was formed by non-motivated subjects. The members of group 1 had a concrete task, namely, they were asked to identify all Necker cubes as correctly as possible. The members of group 2 participated in experimental sessions daily at random hours. Having compared the mean values of the degree of alertness, the authors found that additional motivation in the first group increased alertness.

At the second stage, the effect of task complexity on the alertness was considered. The participants took part in two sessions. The design of these sessions was practically the same, but the contrast parameter  $g$  of the Necker cubes was different. In one session only cubes with low ambiguity ( $g = 0.15$  and  $g = 0.85$ ) were presented, whereas in another session only cubes with high ambiguity ( $g = 0.4, 0.5, 0.6$ ) were shown. An increase in subject's alertness was observed during the second session.

Finally, the authors demonstrated the possibility to estimate human alertness in real time via a BCI (Fig. 54(a)). The experiment lasted 12 min and was divided into three sessions (4 min each). During the first session, stimuli were presented to each subject seated in comfortable conditions in the absence of any additional tasks. The second session included the external influence on the subject in the form of an additional cognitive task. Namely, during the cube presentation the subject was asked to perform a recursive arithmetic operation. Specifically, he/she needed to subsequently subtract different numbers from a given large number. During the third session the additional task was excluded. As a result, a significant decrease in alertness was observed during the second session, whereas alertness rapidly increases in the third session.

Having considered the evolution of alertness, the authors found that the alertness degree fluctuates in time. Time intervals of high alertness ( $I > 0$ ) alternate with intervals of low alertness ( $I < 0$ ) with an average period of  $T = 150$  s (Fig. 54(b), upper panel). In order to control the degree of alertness, the authors implemented biological feedback [152]. As soon as the subject fell asleep, an audio alarm awoke him/her, that resulted in increasing attention. Having compared the experimental results with and without feedback control, the authors concluded that the feedback enlarged intervals of high alertness, but does not affect the mean degree of alertness during the session. Typical dependencies of the alertness degree on time are shown in Fig. 54(b) for sessions without feedback (upper panel) and with feedback (lower panel). One can see that while the duration of the intervals with  $I > 0$  increases in the presence of feedback, the mean value of  $I$  is lower than without feedback. According to this, the authors concluded that the brain cognitive resource is limited, and therefore, to maintain high performance for a prolong time, the brain, from time to time, needs to switch to a "safe-mode" regime of low-energy activity.



**Fig. 55.** (a) Driver's workload evaluation (reprinted from [742]). (b) Pilot's workload evaluation (reprinted from [743]). (c) Air traffic controller's workload evaluation. Reprinted from [744].

## 7.2. Workload and mental fatigue detection

**Workload** is an important characteristic of the human mental state, closely related to the subject's performance in solving cognitive tasks. Workload was defined by Kantowitz and Caper in 1988 [726] as an intervening variable, similar to attention, that modulates the tuning between demands of the environment and the capacity of the organism. This definition implies that unsatisfactory operator performance will occur whenever there is a mismatch between environmental demands and operator capabilities, i.e., if workload is too high or too low [727].

**Mental fatigue** is the brain inability to complete a mental task that requires a high level of sustained attention in the absence of discernible cognitive failure [728]. The effect of mental fatigue in terms of behavioral performances was observed in healthy subjects when they accomplished fatigue-inducing mental tasks [729]. In particular, fatigue causes accuracy and speed decline in time [730–732].

According to Gore et al. [733], mental fatigue and mental workload have to be evaluated during prolonged resource-demanded tasks involving risks of life, e.g., in drivers, pilots, flight operators, etc. For this purpose, measuring these cognitive states using brain activity signals via BCIs are considered as a very promising solution.

Increasing EEG power of theta-waves in prefrontal, frontal and parietal cortex as known to indicate cognitive performance degradation due to a sustained mental work [734,735]. In addition, the EEG spectral power in alpha-band decreases in fronto-central and parietal areas during complex and cognitive demanding tasks [736]. According to this neurophysiological background, Borghini and colleagues [737] proposed the use EEG activity to access mental workload during car driving. They performed five experiments with a driving simulator where the subjects drove a virtual car under different conditions. For each experiment, workload was measured in terms of physiological and behavioral performances. The experimenters also recorded heart rate and eye blink rate. Based on the works of Lal and Craig [738,739], they suggested that an increase in the heart rate is associated with growing mental workload, while the eye blink rate is inversely correlated with mental workload. In addition, they used behavioral estimates, such as questionnaire, RT, driving errors and errors occurring during the additional task accomplishing.

In order to estimate the workload index via EEG signals, they used 61 EEG signals recorded with a 200-Hz sampling frequency. The signals were filtered with 40-Hz low-pass and 1-Hz high-pass filters. Finally, they used the ICA to remove artifacts. Cortical EEG activity was modeled by solving the EEG linear inverse problem with distributed sources [740,741]. The workload index was estimated as a ratio between the theta-band power spectrum obtained from frontal EEG channels (F3, Fz and F4) and the alpha-band power from parietal channels (P3, Pz and P4) for the left side (F3/P3), central line (Fz/Pz) and the right side (F4/P4) of the brain. Having analyzed the correlation between the workload index and other workload estimates, the authors demonstrated that higher index was associated with higher task difficulty (estimated via a questionnaire), higher HR, RT and the number of errors. Although the obtained results evidenced the reliability of the workload assessment based on the EEG signals, no real-time estimations were made; the results were obtained offline using prerecorded EEGs.

Recently, a significant advance in the development of real-time BCIs was achieved by Babiloni and colleagues [742], who introduced a system enable to estimate driver's workload in real time with a 8-s resolution. In order to estimate workload, the authors used 12 EEG channels (FPz, AF3, AF4, F3, Fz, F4, P3, P7, Pz, P4, P8, and POz) located according to the international 10–20 system (Fig. 55(a)). The data were collected with a 256-Hz sampling frequency. The EEG signals were digitally bandpass filtered within 1–30 Hz and the eye-blink artifacts were removed. The FPz channel was used for eye movement detection. The EEG recordings from the rest 11 channels were segmented in 2-s epochs with a moving 0.125-s shifting. The power spectral density was then calculated using FFT in theta- and alpha-frequency bands. Finally, the workload was estimated in real time using the automatic stop step-wise linear discriminant analysis (asSWLDA) classifier proposed by Arico et al. [744].

The efficiency of the workload estimation was analyzed by calculating the following measures.

- *Subject eye fixation* (SEF) estimated with a eye-movement recorder. This parameter was shown to correlate with driver's workload [745].
- *Area under curve* (AUC). AUC is a widely used measure to test performance of a binary classifier. Classification performance is considered to be good when  $AUC > 0.7$  [746].
- *Workload index* (WI) provided by the classifier and averaged over different experiments performed with each subject.

The classifier was trained to classify driver's workload into two classes: "easy" (low workload) and "hard" (high workload). Having compared SEF for these classes, the authors found that during "easy" conditions the external environment caught  $12 \pm 10.7\%$  of the drivers' fixations (versus  $5 \pm 5.5\%$  fixations during "hard" conditions). The AUC analysis revealed a mean AUC value of  $0.755 \pm 0.11$ , which corresponded to classification accuracy of 75%. Having in mind that 75% classification accuracy was achieved with a 8-s time resolution, they concluded that the proposed system was suitable for online workload estimation. This result is important for the development of an adaptive automation (AA) system enable to adjust the proper level of automation and assistance depending on the current task difficulty and the driver's workload.

Recently, different approaches were used to increase the accuracy of driver's workload and fatigue detection. For example, the researchers from the Jiangxi University of Technology (China) [747] reported on an EEG-based system for driver's fatigue detection by analyzing the effects of multiple entropy fusion and calculating four entropies as features. To train classifiers, a fatigue state was estimated via the Chalder Fatigue Scale and Li's Subjective Fatigue Scale [748,749]. The authors used the following entropy measures: spectral entropy [750], approximate entropy [751], sample entropy [752], fuzzy entropy [753]. These measures were used to find fatigue features with the help of four different machine learning approaches: support vector machine [754], back propagation neural network [755], random forest [756] and k-NN [754]. Having applied the optimal combination of these techniques, the authors managed to achieve 98% accuracy in mental fatigue detection.

Along with the driving tasks, the assessment of fatigue was performed for pilot BCIs (pBCIs), both in a simulator and real flights. Recently, the scientists from the University of Toulouse and the Sapienza University of Rome [743] developed a fNIRS-EEG-based pBCI to monitor pilot's cognitive fatigue. The pilots were asked to perform four identical traffic patterns. The two first patterns were associated with low cognitive fatigue, whereas the two last traffic patterns with high cognitive fatigue. In order to implement a behavioral measure of cognitive fatigue, the pilots were subjected to a secondary auditory task during flight. This task was to respond to target auditory stimuli. 600 stimuli were presented during a single session, 25% were targets and 75% non-targets. The error rate (the number of missed targets) was considered as a measure of cognitive fatigue. The EEG signals were recorded with a 500-Hz sampling frequency using 23 dry electrodes located in accordance with a 10–20 EEG layout. The fNIRS data were recorded at 8.93 Hz using 7 sources and 8 detectors which resulted in 12 channels. EEG and fNIRS data were synchronized.

A fatigue state was estimated via EEG signals as the ratio  $\zeta = E_\beta / (E_\alpha + E_\theta)$ , where the spectral power of each frequency band was computed by estimating a one-sided Welch's power spectral density of the EEG signal. The value of  $\zeta$  was computed independently for each channel, resulting in as many features as EEG channels. The fNIRS data were used to estimate coherence. The wavelet bicoherence was calculated for 66 channel couples. According to the study of Cui et al. [757], the resulting coherence was averaged over the frequency band of 0.0781–0.3125 Hz. Finally, 66 averaged coherence measures were used as features by the classifier for the pBCI implementation.

Experimental sessions characterized by low and high cognitive fatigue were considered as class 1 and class 2. For each class, EEG and fNIRS recordings were divided into non-overlapping trials with 1-min length. These trials then were classified with LDA. At the first stage, the pilot's responses to the secondary tasks were analyzed. It was shown that in the second part (class 2) of the experiment the performance was lower than in the first part (class 1) (mean error = 6.6 for class 1, mean error = 18 for class 2). More specifically, the errors were higher in the real flight condition (mean error = 10 for class 1, mean error = 26.54 for class 2) than in the simulator condition (mean error = 3.25 for class 1, mean error = 9.5 for class 2).

Having analyzed the pBCI efficiency during the simulated flight, the authors reported 86.7% accuracy when using the EEG features, 81.5% when using the fNIRS features and 87.2% when combining the EEG and fNIRS features. In the real flight condition, the accuracies were 86.4% (EEG), 83.2% (fNIRS) 87.6% (EEG and fNIRS).

Finally, the pBCI was used to access mental workload of Air Traffic Controllers in a realistic environment. Aricó and colleagues [744] developed an approach enabled workload evaluation in real time. They implemented feedback control to keep workload demand within an appropriate level. As mentioned above, cognitive performance decreases when the workload becomes too small (under-load condition) or too high (over-load condition). Therefore, it is important to control the workload level in order to achieve optimal performance during task accomplishing. The proposed pBCI was able to adjust a task workload in accordance with operator's current cognitive state. In the experiment, the subjects were asked to manage a functional interface that simulated a realistic air traffic management (ATM) scenario. The task complexity was modulated by a number of aircrafts, clearances and trajectories of other interfering flights.

There were two levels of complexity implemented in the ATM: easy condition (low complexity) and hard condition (high complexity). The participants took part in two experimental sessions. During the first session (session 1), the task complexity was triggered by the EEG-based workload level, whereas during the second session (session 2) the workload level was calculated, but not used for triggering task complexity. After the experiment, the participants were requested

**Table 4**

Classification of emotion-recognition papers published in 2006–2016 according to BCI applications.  
Source: Based on the data from [760].

Non-medical applications 73%	Monitoring 43.6%		Entertainment 11.5%	
	Assistance 4.6%	Other 10.1%		
Method development 27.5%		Marketing 1.8%		
Medical applications 27%		Education 0.9%		
Assessment 32.8%		Monitoring 29.9%	Assistance 19.4%	Other 6%
			Diagnosis 11.9%	

to pass the questionnaire to evaluate their subjective workload estimate. The workload was also estimated based on the recorded information about reaction times and a number of airplanes.

The EEG signals were recorded using 9 wet electrodes (Fpz, Fz, F3, F4, AF3, AF4, Pz, P3, P4) with a 256-Hz sampling frequency. Then, the signals were band-pass filtered in the range of 1–30 Hz using a 5th order Butterworth filter. Similarly to Dehais et al. [743], the Fpz channel was used to remove eye-blink artifacts. Other artifacts were rejected with the help of the EEGLAB toolbox [758]. The EEG signals were segmented into 2-s epochs. For each epoch, the power spectral density (PSD) was calculated in frontal theta- and parietal alpha-bands related to mental workload. Finally, the authors used the classification algorithm based on the asSWLDA [759] to identify the most relevant features associated with different experimental conditions, i.e., “easy” and “hard”. The reported accuracy in classification of “easy” and “hard” intervals was  $75 \pm 10\%$ .

Having analyzed behavioral performance during session 1 and session 2, the authors demonstrated that operator’s performance was higher during session 1 than during session 2. The analysis of the workload level estimated via the EEG signals (WEEG) revealed a significant increase in the WEEG distribution between “easy” and “hard” intervals for session 2, while for session 1 no significant differences were observed between the corresponding WEEG values. Thus, the proposed pBCI was able to (i) classify workload levels related to “easy” and “hard” task conditions and (ii) trigger the task complexity when the workload was high to prevent overload situations.

These results have demonstrated advantages of the passive BCI in the workload level reduction by the operator during the ATM task execution and in the improvement of the task performance.

### 7.3. Emotions recognition

The development of EEG-based emotion recognition systems has recently become a new trend in the BCI research [760] because of their prospective applications in communication, education, entertainment, and medicine. Having reviewed the papers published in 2006–2016, Abeer Al-Nafjan and colleagues [760] reported that in 73% of articles BCIs devoted to emotion recognition were used for non-medical purposes, and in only 27% for medical ones (see Table 4).

Among many papers devoted to medical applications, in 32.8% the authors used EEG-based emotion recognition systems for assessment and in 29.9% for monitoring brain states in patients suffering from neurological diseases, such as schizophrenia, autism, depression and others, whose emotions are often hidden. Amongst few publications related to non-medical applications, in 43% of the papers, emotion recognition systems were used for monitoring brain states associated with different emotions of healthy subjects. The authors of these articles investigated how different stimuli induced specific emotional reactions. They also compared emotional responses of men, women and adolescents.

In 11.5% of the papers, emotion recognition systems were used for entertainment, where relationships between multimedia data (music/video) and human emotions were studied. For instance, Liu and colleagues [761] implemented an EEG-based system for recognizing emotions induced by film clips in real time.

At the first step, the authors constructed a standardized database of film clips. A group of experts selected 111 film excerpts that lasted from 1 to 3 min and contained a single target emotion, including four negative emotions (sadness, anger, fear, and disgust), eight positive emotions (joy, romance, warmth, well-being, love, mutual affection, amusement, and contentment), and a neutral state.

At the second step, 462 participants were divided into groups of 7–10 subjects. Each group was instructed to view and rate film excerpts. For this purpose, the participants completed questionnaires after viewing each film clip. The questionnaire results were analyzed with the R-type cluster analysis with an agglomeration approach to detect emotional clusters. Finally, a set of eight emotional categories were built: three positive emotional categories (joy, amusement, and tenderness), four negative emotional categories (anger, sadness, fear, and disgust), and the neutral state.

At the third step, they recorded EEG signals from 14 channels with a 128-Hz sampling rate. Then, these signals were filtered with a 1–45-Hz bandpass filter. EOG artifacts were removed with the help of ICA (see Section 3.1). To perform emotion recognition, the time-frequency EEG structure was considered. The spectral power was estimated in five frequency bands: delta (1–4 Hz), theta (4–8 Hz), alpha (8–12 Hz), beta (13–30 Hz), and gamma (31–45 Hz). In addition,

differences between the spectral powers were calculated for 7 symmetrical pairs of electrodes belonging to the right and left hemispheres in 5 frequency bands. As a result, a total number of 105 EEG features were used. The extracted features were processed using LDA. Finally, the selected features were used as inputs for a support vector machine (SVM) for classification.

The classification algorithm was implemented in real time and the following accuracies were obtained:

- 92.26% in recognition of high-arousal and valenced emotions from neutrality;
- 86.63% in recognition of positive from negative emotions;
- 86.43% in classification of three positive emotions (joy, amusement, tenderness);
- 65.09% in classification of four negative emotions (anger, disgust, fear, sadness).

In another interesting paper, Chanel and colleagues [762] presented the application of the EEG-based emotion recognition system in the game industry. In particular, the authors proposed a BCI to maintain player's engagement by adapting game difficulty according to his/her emotions assessed from EEG signals. Their system was tested during Tetris game sensors. The difficulty level was implemented via the frequency at which a new block appeared. For example, in the simplest level 1 a new block appeared every 0.54 s, whereas in the highest level 25 a new block appeared every 0.03 s.

At the first step of the experiment, each participant played Tetris several times to determine the game level where he/she reported engagement according to the player's skill level. At the second step, each participant was subjected to three experimental conditions: medium condition (game difficulty was adjusted to the player's skill level), easy condition (game difficulty was 8 levels lower than the player's skill level), and hard condition (game difficulty was 8 levels higher than the player's skill level). During the experimental session, the participants were equipped with several sensors to measure their peripheral physiological activity, e.g., skin resistance, blood volume pulse, chest cavity expansion, and a temperature. EEG signals were recorded by 19 electrodes arranged according to the 10-20 scheme at a 256-Hz sampling rate. After the experimental session, the participants were subjected to the questionnaire for estimating their emotions and the level of involvement in the game.

Then, the EEG signals were filtered with a 4–45 Hz bandpass filter and processed with a Laplacian filter [763] in order to render the signals independent of the reference electrode position and reduce artifact contamination. The EEG signal features were represented by the energy in frequency bands related to emotional processes [764], namely, in theta (4–8 Hz), alpha (8–12 Hz) and beta (15–30 Hz) ranges, recorded by each  $i$ th electrode. Along with the common features associated with individual channels, additional EEG features were calculated as

$$\text{EEG}_W = \log \frac{\sum_{i=1}^{N_e} \beta_i}{\sum_{i=1}^{N_e} (\theta_i + \alpha_i)}. \quad (67)$$

In total, the authors considered a set of 58 EEG features. Additional 18 features were associated with peripheral signals (for details see [762]). The acquired data were statistically analyzed based on the questionnaire, EEG recordings and peripheral signals. The results of the questionnaire evidenced that the participants felt lower pleasure, amusement, interest and motivation for both the easy and hard conditions than for the medium condition. Moreover, increasing the game difficulty led to higher excitation and pressure. This result demonstrated that an adequate level of difficulty is necessary to engage gamers so that they feel motivated and pleased to play.

The analysis of peripheral features demonstrated an increase in the electrodermal activity when progressing from an easy to a medium difficulty level, that indicated the increasing arousal level. In summary, an increase in the arousal level was observed when the game difficulty was increased, that was in a good agreement with the results obtained from the analysis of questionnaires.

Having considered the EEG features, the authors observed significant differences in the  $\text{EEG}_W$  feature among the three conditions. At the same time, the authors concluded that the  $\text{EEG}_W$  feature was more related to the workload than to the engagement, since the participants involved more executive functions in the hard condition than in the medium one, even if they were less engaged.

Finally, in order to classify the data in the three different conditions, the authors used LDA (in particular, quadratic discriminant analysis (QDA)) and SVM with RBF kernel. Three feature-selection algorithms were applied: ANOVA, fast correlation-based filter (FCBF) [765], and sequential forward floating selection algorithm [766]. The classification accuracy of the EEG and peripheral signals to recover the three states elicited by the gaming conditions were analyzed for different classifiers, feature-selection methods, and duration on which the features were computed. Without feature selection, the best classifiers demonstrated an accuracy around 55% for peripheral features and 48% for EEG features. The FCBF exhibited the best accuracy on the peripheral feature (59%), while the ANOVA selection showed 56% accuracy for EEG features. The analysis of the classification accuracy for EEG and peripheral features computed for different duration demonstrated that the EEG features are more robust to a decrease in the duration than the peripheral features, that confirms the importance of the EEG features for short-term emotion assessment.

## 8. Optogenetic brain interfaces

### 8.1. Basic principles

Along with precise detection of neural activity patterns in the brain, further development of BCIs requires the implementation of new ways for fast and targeted stimulation of brain cells. Among them, the most promising approach

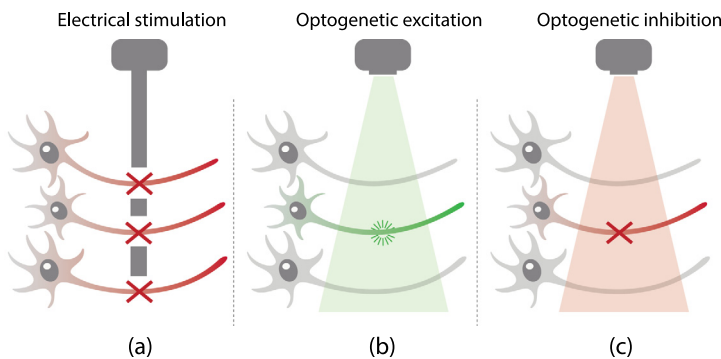


**Fig. 56.** Comparison between electrical and optogenetical stimulation. (a) Neural ensemble activity is blocked by electrical stimulation. (b–c) Different light colors activate the neurons which are modified with different types of the opsin-related protein and remains other neurons unaffected.

is the optogenetic brain stimulation. As the name implies, optogenetics combines optical and genetic methods and, by this, allows controlling excitation and inhibition properties of specific cells of living tissues.

Optogenetics implies the use of light to control activity of the neurons which have been genetically modified to express light-sensitive ion channels. This is achieved by using light-sensitive proteins. The role of these light-gated proteins in control of the flow of ions across the plasma membrane was known about 50 years ago. In particular, Stoeckenius and Oesterhelt [767] discovered that Halophilic bacteria has a purple membrane which acts as a photoreceptor and regulates the ion flow. It is possible due to a special protein (bacteriorhodopsin) which acts as an ion pump and can rapidly be activated by visible-light photons. The further studies [768] demonstrated that the purple membrane in *Halobacterium halobium* pumps protons outward under illumination, causing a proton gradient across the cell membrane. Some years later, the experiments with *Halobacterium* led to the discovery of another protein halorhodopsin [769] which acts as a light-gated ion pump, specific for chloride ions. In the next 40 years, many opsin-related proteins were discovered. In 2005, Boyden and colleagues [770,771] applied microbial opsin-related protein to *in vitro* control of neurons in mammalian brain.

Nowadays, the use of different opsin-related proteins, e.g., channelrhodopsin, bacteriorhodopsin and halorhodopsin provides possibility of turning neurons on or off, rapidly and safely, in response to diverse colors of light [772]. Unlike electrical stimulation, which affects all neurons in the vicinity of the recording electrode, optogenetic stimulation provides targeted control of the specific cell type by using appropriate opsin and light. The drawback of electrical stimulation is strong stimulation-induced electrical artifacts, that do not allow simultaneous recording of the brain activity during the stimulation. Therefore, optical stimulation is a very good alternative to electrical stimulation.

Fig. 56 represents the schematic comparison between electrical and optical stimulations. Red color indicates neurons whose activity is interrupted by the stimulation. Green color defines neurons which are excited by the stimulation and gray color corresponds to ones, which are not affected by the stimulation. One can see, that electrical stimulation affects all neurons in a similar way, e.g., turns them off (Fig. 56(a)). The optogenetical stimulation can either excite or inhibit a specific (target) type of cells by appropriate light and remain other cells unaffected (Figs. 56(b,c)).

## 8.2. Open-loop and closed-loop optogenetic interfaces

In 2007, Aravanis and colleagues from the Stanford University [773] proposed an optical neural interface allowing *in vivo* control of rodent motor cortex via optogenetic brain stimulation in real time. The authors explored channelrhodopsin adapted to mammalian neurons and delivered light through an optical fiber which was chronically implanted in the rat's brain during surgery (Fig. 57). They used the interface for controlling whisker movements of the rat by light activation of neurons in vibrissal motor cortex. The authors applied light anesthesia to keep animals in a lightly sedated state, where whisker deflections spontaneously occurred. They hypothesized that stimulation of this brain area could induce detectable whisker movements. In order to test their hypothesis, the authors used the setup shown in Fig. 57(c). To detect whisker movements, magnetic particles were attached to whiskers and a magnetic field sensor was used. As a result, the pulsed blue light delivered via the optical neural interface caused repeatedly evoked whisker deflections in the rat of up to 10°. Thus, they demonstrated the possibility to optically address specific cell types *in vivo* with millisecond temporal precision.

Along with control of motor neurons, Adamantidis et al. [774] also applied optogenetics to control transitions to wakefulness from either slow wave sleep or rapid eye movement sleep in freely moving mice. The optical neurointerface proposed by Aravanis and colleagues [773] is an open-loop control system which implies a one-way information transfer from a computer to brain without any feedback. At the same time, it provides high possibility to control brain activity by optogenetic stimulation in real time and causes a prospective application of optogenetic tools in BCIs.

The first optogenetical closed-loop interface was proposed in 2015 by Grosenick et al. [775], who applied a closed-loop control theory to optogenetic stimulation, inhibition, and modulation and defined it as “closed-loop optogenetics”.

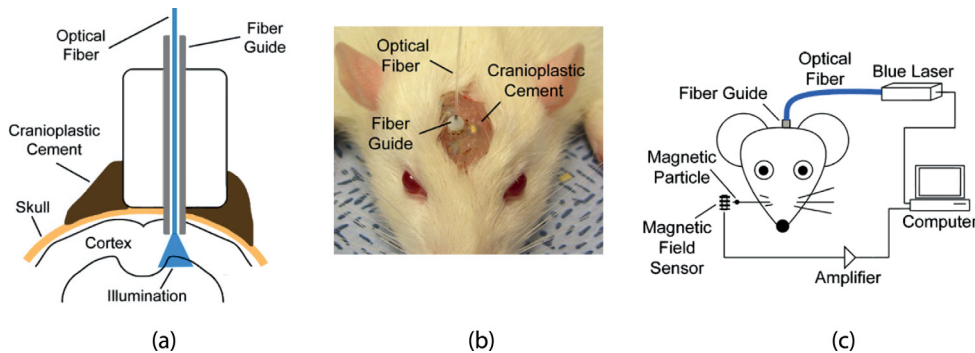


**Fig. 57.** Optical neural interface for *in vivo* control of neural activity in the motor cortex of rodents. (a) Schematic of optical neural interface mounted on the rat skull, showing optical fiber guide, optical fiber inserted and blue light transmitted to the cortex. (b) The rat with optical neural interface implanted. (c) Schematic of whisker movement measurement setup: optical neural interface used to activate the rat vibrissal motor cortex, a magnetic particle was attached to the contralateral C2 vibrissa and a magnetoresistive sensor was placed near the particle.  
Source: Reprinted from [773].

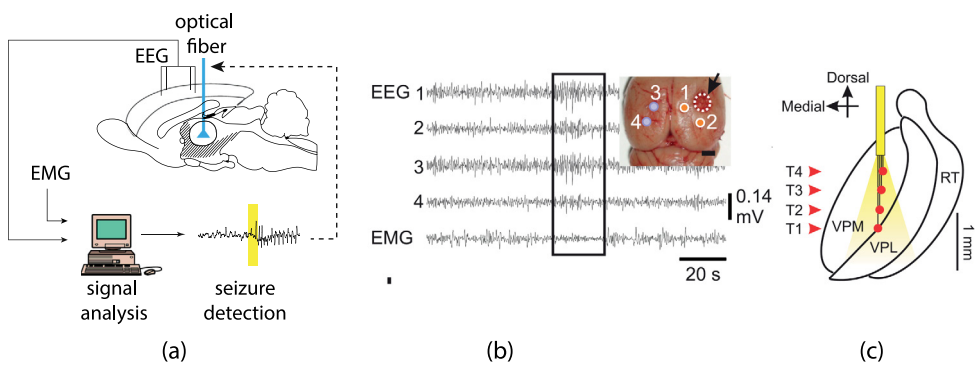


**Fig. 58.** (a) Schematic illustration of the experimental setup for optogenetic seizure control. (b) EEG signals are recorded with implanted electrodes and analyzed in real time. (c) Once a seizure is detected, yellow laser light is delivered into the thalamus via an optical fiber to inhibit thalamocortical neurons.  
Source: Reprinted from [776].

In closed-loop optogenetics, the control input is a structured, time-varying light stimulus that is automatically modulated based on the difference between desired and measured outputs, which may include behavioral, electrophysiological, or optical readouts of activity generated by the biological system.

One of the first applications of closed-loop optogenetics was the prediction and prevention of epileptic seizures occurring in rat's brain after cortical injury. The original paper was published by Paz et al. [776] in 2013. To provoke seizures, the authors induced a focal cortical stroke. Then, they analyzed mechanisms underlying the seizure development and found that the cortical stroke enhances excitability of thalamocortical cells, which made them to generate epileptiform oscillations. Thus, they hypothesized that targeting these neurons with a closed-loop optogenetic strategy could activate them in real-time and immediately interrupt seizures.

The closed-loop system is schematically illustrated in Fig. 58(a). The rats were implanted with a chronic device containing five EEG electrodes, one EMG wire to record electromyographic activity (Fig. 58(c)) and an optrode targeting the ventrobasal thalamus (Fig. 58(c)). The experiments were conducted in freely behaving animals. The EEG signals were acquired in real time with a 500-Hz sampling frequency and a 1–40 Hz bandpass filter. The seizures were detected in real time via a line length calculation [777]. After successful detection, the yellow laser's light was delivered into the thalamus via an optical fiber to inhibit thalamocortical neurons. An 11-s timeout was imposed after each detection event to prevent retriggering and allow the analysis of the brain response to the stimulation. As a result, the authors demonstrated that targeted inhibition of thalamocortical cells via optogenetics closed-loop control disrupted seizures at their onset. Finally, the authors highlighted that this type of control did not affect normal brain activity between seizures and became a promising potential therapeutic approach for otherwise untreatable epilepsy.

Along with post-stroke seizures, in 2013 Krook-Magnuson and his colleagues [687] from the Department of Anatomy and Neurobiology at the University of California demonstrated optogenetic control of spontaneous seizures in temporal lobe epilepsy. The authors built a closed-loop seizure-detection system to identify the seizures and rapidly suppress them. The seizures were detected in real-time by triggering light delivery. The schematic illustration of the closed-loop optical

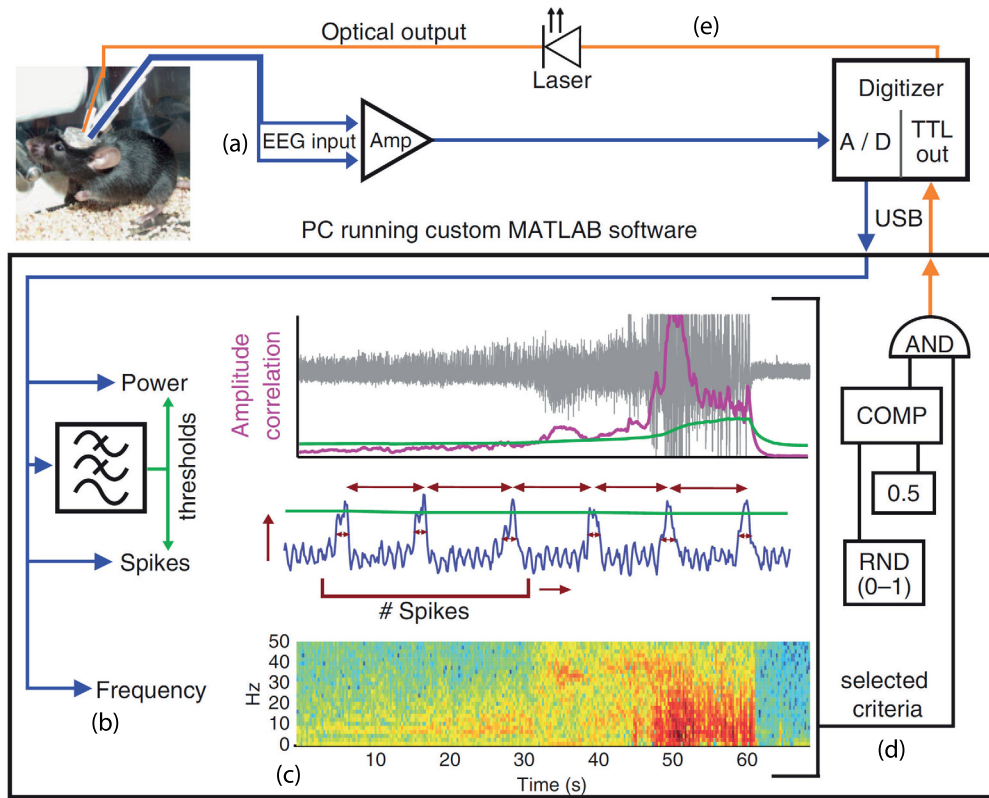


**Fig. 59.** Schematic illustration of a closed-loop optical interface for seizure control. (a) EEG input from the mouse hippocampus is amplified, digitized and relayed to a PC running a custom-designed real-time seizure detection software. (b) Structure of seizure detection software. The input signal is fed into a number of possible detection algorithms, which utilize features of signal power, spikes or frequency. Thresholds for power and spike properties (green) are determined using tunable leaky integrators acting as low-pass filters. (c) Calculated features of EEG. Top: Amplitude correlation (purple, during an example seizure, shown in gray); middle: spike characteristics (amplitude, rate, regularity and spike width, shown in red); bottom: power of the signal in specific frequency bands during the same seizure, with warmer colors representing higher energy. (d) Brain stimulation protocol. Light is delivered for 50% of the events in a random fashion. (e) Optical brain stimulation. The optical output (orange) delivered to the hippocampus of the mouse, via a TTLs from the digitizer to the laser.

Source: Reprinted from [687].

interface is given in Fig. 59. The mice were implanted with intrahippocampal depth electrodes and individual optical fibers (Fig. 59(a)). In order to induce temporal lobe epilepsy, kainate was injected unilaterally into the dorsal hippocampus. The EEG signals were sampled at 500 Hz and analyzed in real-time by a PC using a custom MATLAB seizure detection algorithm.

The algorithm estimated the signal time-frequency features and used thresholds to detect seizures (Fig. 59(b)). First, the EEG signal power was used to create inclusion or exclusion criteria and indirectly to determine amplitude thresholds for other criteria (for spike detection). Then, individual spikes were detected using the thresholds and interspike intervals were analyzed. Finally, frequency features of the EEG signals were considered. The relative contribution of the power of specific frequency bands was estimated based of the fast Fourier transform (Fig. 59(c)). Once a seizure has been detected using the selected criteria, for 50% of the events in a random fashion, the software activated the optical output (orange) delivered to the hippocampus of the mouse, via a transistor-transistor logic signal (TTLs) from the digitizer to the laser (Figs. 59(d,e)). All trigger events, however, were flagged for the later off-line analysis.

First, the authors made an attempt to stop seizures by direct inhibition of principal cells with halorhodopsin. They utilized a single optical fiber placed near the site of kainic acid injection to deliver light (amber, 589 nm) to a limited volume of tissue. This method allowed to stop 50% of seizures within 1 s of light delivery, while the seizure duration was reduced by 70%. The second cell-type specific strategy for stopping seizures was to activate a subpopulation of GABAergic cells. For cells activation the authors delivered light (blue, 473 nm) to the hippocampus ipsilateral to the kainic acid injection. As a result, a 43% reduction of the seizure duration was achieved, where about 59% seizures were stopping within 5 s of light delivery.

Thus, optogenetic neurointerfaces were shown to be an effective tool for controlling epileptic seizures. According to existence results, optogenetic stimulation needs several seconds to stop a seizure. Therefore, in order to prevent the seizure onset, it must be predicted for some seconds. Modern methods allow seizure prediction several seconds prior its onset in order to prevent its development by electrical brain stimulation.

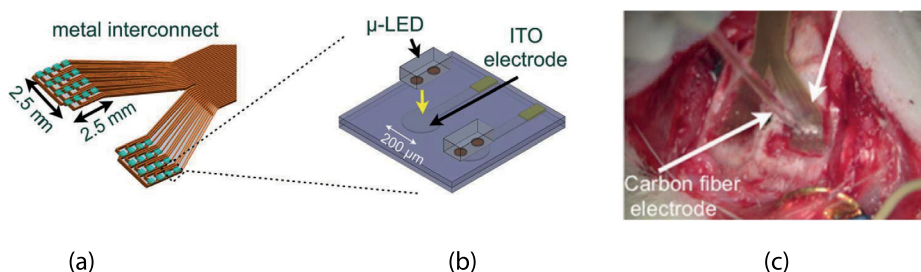


**Fig. 60.** (a) Concept illustration of the Opto- $\mu$ ECoG array. (b) Detailed illustration of a single channel containing an optically transparent ITO recording electrode and a LED light source. (c) Opto- $\mu$ ECoG array surgically implanted in the V1 area of the rat's cortex.  
Source: Reprinted from [778].

The closed-loop BCI epilepsy control requires permanent monitoring of neural activity. As mentioned above, unlike electrical brain stimulation, the optogenetical simulation does not produce artifacts in the brain activity signals. Therefore, the corresponding patterns of neural activity can be detected with the help of EEG and triggered by optical stimulation. At the same time, this approach requires a set of electrodes and optical fiber to be implanted in the brain.

An alternative approach was recently introduced by Kwon et al. [778]. The authors proposed combining optogenetic stimulation with electrophysiology recordings by using transparent electrodes with embedded light-emitting diodes (LEDs). They developed a BCI device, called the Opto- $\mu$ ECoG array, which combined ECoG recording and optogenetic stimulation to enable multichannel bidirectional interactions with neurons. The concept of the Opto- $\mu$ ECoG array is shown in Fig. 60. It has two sub-arrays, each contains 16 channels arranged to form a  $4 \times 4$  matrix and placed on a footprint designed to match the bilateral hemispherical area of the visual cortices in rats (Fig. 60(a)). Each channel was constructed by assembling a surface mounted micro-LED with a 460-nm peak wavelength on the top of a transparent electrode fabricated using indium tin oxide (ITO) (Fig. 60(b)). It allowed simultaneous optical stimulation and electrical recording. Parylene-C served as the main structural and packaging material, because of its flexibility, optical transparency, chemical inertness, and biocompatibility. These properties are favorable for implantable devices.

In order to demonstrate the efficiency of the proposed interface, the authors performed *in vivo* animal experiments, in which they applied the optointerface to simultaneously modulate and record neural activity in the visual cortex of the rat. Before the experiments, neurons in the primary visual cortex (V1) were transfected with channelrhodopsin to enable light sensitivity. Then, the Opto- $\mu$ ECoG array was surgically implanted in this area (see Fig. 60(c)).

As a result, the authors reported that the Opto- $\mu$ ECoG array allowed recording neural activity and simultaneous optical stimulation. Moreover, they found, that epidural LED light stimulation could evoke neural activity not only within the superficial cortical layers, but also in deeper cortical layers. Finally, the authors highlighted four unique features of their interface to address major challenges of existing optogenetics-based BCIs.

- LEDs allow a wireless untethered system, crucial for chronic implants.
- Optically transparent electrodes enable a maximum exposure of the target cortical area for optical stimulation.
- Recording electrodes and light sources are carefully arranged to avoid redundant neural recordings and overlapping light stimulation due to closely placed neighboring electrodes and LEDs, respectively.
- Polymer packaging and epidural placement of the device over the cortex enable long-term biocompatibility of the device and minimize the risk of potential tissue damage.

Two years later, Ramin Pashaie and colleagues [779] used a similar approach to build a closed-loop optogenetic interface. Similarly to Kwon et al. [778], they used micro-ECoG devices in which electrode arrays were embedded into an optically transparent biocompatible substrate that provided optical access to the brain tissue during electrophysiology recording. Thus, in the proposed closed-loop system, the feedback signal was taken from the micro-ECoG.

The proposed closed-loop interface is schematically shown in Fig. 61. The electrophysiology data recorded via the micro-ECoG array was continuously transferred to a computer and compared with some predefined spatio-temporal patterns of neural activity. The computer which processed the data also readjusted the duration and distribution of optogenetic stimulating pulses to minimize the difference between the recorded activity and the predefined setpoints. The interface was tested in sedated mice. The micro-ECoG device was placed over the sensorimotor cortex. The control protocol was evaluated via the following steps.

1. Reading the signals from micro-ECoG electrodes and processing the data in real-time. The output of this process is a variable that represents the area under the optically evoked potential curve for each site which is a robust feedback signal for the closed-loop algorithm.
2. Generating the error signal. The error is computed by taking the difference between the actual measured signal after processing and the corresponding temporal desired activity for each electrode site.

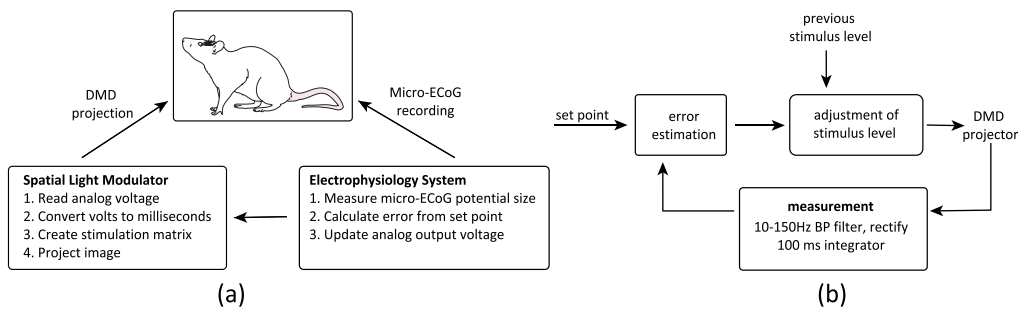


**Fig. 61.** (a,b) Micro-ECoG optogenetic closed-loop protocol. The system records the activity using the implanted micro-ECoG device. The recorded data is processed in real time and compared to predefined patterns (set of points) stored in the computer. Based on the difference between the recorded levels of activity on each electrode site and the set points, the computer updates the illumination pattern on the spatial light modulator to adjust the level of induced activity and minimize the error.

Source: Partly redrawn from [779].

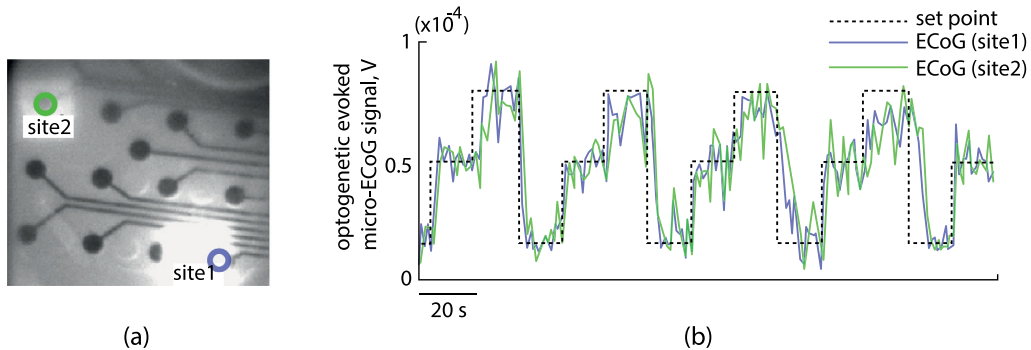


**Fig. 62.** Implementation of the single site closed-loop brain interface. The loop constants are measured and set for two separate sites marked as site-1 and site-2. Then, the closed-loop algorithm is conducted so that the signal from site-1 (blue signal) clamps to the user predefined setpoints (black curve), while the signal from site-2 (green signal) is clamped to the signal from site-1. In the other words, these two sites are connected by an optoelectronic bridge.

Source: Reprinted from [779].

3. Adjusting the duration of the exposure for the next round of optical stimulation. In this step, the computer adjusts the exposure time for the next round of stimulation to minimize the error signals for all electrode sites.

The results of the closed-loop control are presented in Fig. 62. The authors used two sites (Fig. 62(a)), where they tried to force the activity in site-1 to converge to the setpoints defined by a square wave, while lock the activity at site-2 to the activity at site-1. In the other words, the goal was to make a bridge between these two sites via electrophysiology recording and optogenetic stimulation. As shown in Fig. 62(b), the electrical activity signal from site-1 (blue curve) followed the setpoints (black square wave) with reasonable accuracy. Simultaneously, the signal from site-2 (green curve) is also tracing the activity of site-1. This method has potential application in compensating injuries that disrupt the horizontal connectivity among cortical circuitries [779].

The next step toward compact devices for optogenetic interfaces was made by Chen and his colleagues [780] from the Universities of Macau and Colorado. They developed a monolithic integrated circuit (IC) to record action potentials of cells and simultaneously control its activity using optogenetics. The proposed IC included a low-noise and high input impedance neural recording amplifier and a high current laser/light-emitting diode. Fig. 63(a) illustrates the fabricated IC, and Fig. 63(b) shows schematically the experimental setup for simultaneous optogenetic inhibition and electrophysiological recordings.

The experiments were performed *in vivo* with anaesthetized gerbil. An implantable “optrode” integrating a metal electrode and an optical fiber for simultaneous electrophysiology recording and optogenetic control was designed and fabricated. The optrode was intended to be used together with a custom IC as a complete package for animal neural recording experiments. The electrode was placed in the inferior colliculus, an auditory signal processing brain area. The animal was affected by a single frequency tone generated by an audio signal processor and played through two speakers, placed inside the ear canal of the gerbil. Since the inferior colliculus is a part of the auditory signal processing circuit in the brain, neurons within the inferior colliculus will only fire action potentials when the sound stimulus is played. According to this, the authors tested the possibility of the proposed system to monitor cells activity controlled by the

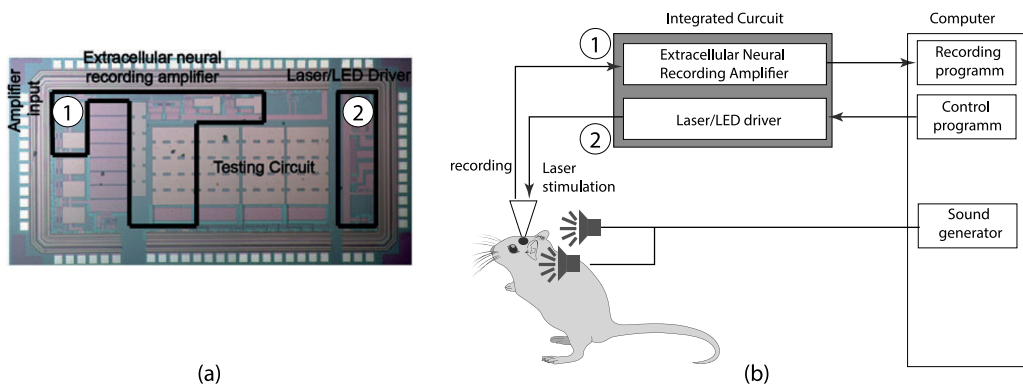


**Fig. 63.** (a) Picture of the fabricated IC with dimension of 2.9 mm×1.6 mm. (b) Experimental setup.  
Source: Reprinted from [780].

external audio stimuli. As a result, the obtained recordings of neural activity reflected the occurrence of the neural spikes that well correlated with the sound stimulation.

Along with the successful registration of auditory stimulated action potentials, the authors also demonstrated the possibility to simultaneously control neural firing by optogenetic stimulation, namely, to inhibit action potentials in neurons of the 5th nerve in the brainstem. In this experiment, the brainstem of the gerbil was injected with halorhodopsin to become sensitive to optogenetic stimulation. The optrode was positioned in the same area for optogenetic manipulation. The animal was anaesthetized, and the neural firing was confirmed through the IC output. Then, optical illuminations of a 3-s duration were delivered through the optical fiber of the optrode to the brainstem to activate optogenetic proteins and thereby inhibit the action potential firing. As a result, the firing rate of neural spiking was observed to be significantly reduced during the laser illumination epoch, and the action potential firing recovered after optical illumination was ceased.

The latest research in closed-loop optogenetic interfaces was focused on the more precise control of neural activity. To date, optogenetic stimulation was provided in either open-loop or discrete (on/off) closed-loop fashion, where a previously-determined stimulus was activated by an event (see, e.g., [687]). At the same time, according to the recent paper [781], neuronal responses elicited by stimulation can vary across individuals, cells, and even over time. According to this, a continuous use of feedback to update stimulation parameters in real-time is more effective. This type of feedback was implemented for the first time by Newman et al. [782] in *in vivo* experiments. The authors demonstrated the possibility to automatically adjust the light intensity to maintain a constant firing rate over time. Later, the same group used this approach to elicit sinusoidally modulated patterns of neural activity. Finally, they demonstrated that this procedure can be generalized to more complex, non-sinusoidal signals [781].

### 8.3. Approaches for hybrid optoelectronic interfaces

The development of hybrid systems allowing simultaneous monitoring and optogenetic stimulation of neural dynamics has become a hot topic attracting neuroscience researchers and engineers to invest great efforts in designing high precision *in vivo* implantable devices. These efforts have focused on the delivery of sufficient power to deep brain regions, while monitoring neural activity with high resolution and fidelity. The recent advances in the field of hybrid optoelectronic neural interfaces that combine optical stimulation with electrophysiological recordings were described in the review paper of Iseri and Kuzum [783]. The authors highlighted two main approaches for *in vivo* optogenetics studies: fiber and waveguide-based approaches and on-probe  $\mu$ LED-based approaches.

A *fiber or waveguide-based approach* was proposed by Gradinariu et al. [784], who designed a single optrode consisted of an extracellular tungsten electrode glued on an optical fiber (Fig. 64(a)). Their technique was able to deliver light to neurons and simultaneously record their electrical activity. A novel strategy for simultaneous electrophysiological recording and optical stimulation was introduced in 2012 by Anikeeva et al. [785]. Their device called “optetrode” contained an optical fiber-centric coaxial design and 16 microwires for multichannel electrophysiological recordings (Fig. 64(b)).

The further design improvements were aimed at increasing spatial resolution in both recording and stimulation. In this context, the multichannel version of the optrode, which consisted of a single optical fiber and multichannel electrodes (Fig. 64(c)) was proposed by Zhang et al. [786]. Their device enabled controlling and recording activity of multiple neurons. However, spatial resolution of light stimulation was relatively low, because only one optical channel was equipped. In order to increase spatial resolution, in 2012 Hayashi et al. [787] proposed a new optoelectronic probe consisting of multiple optical fibers and metal wire electrodes as a bundle enable to perform multichannel recordings (Fig. 64(d)).

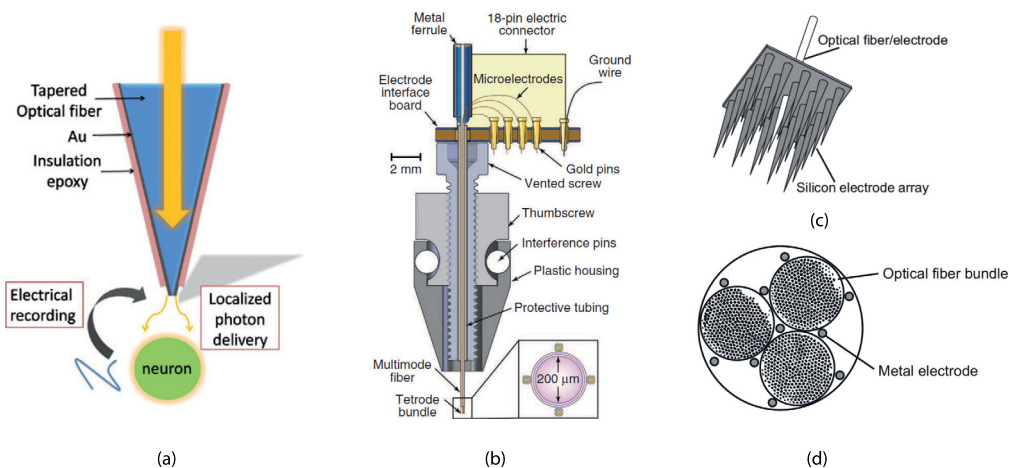


**Fig. 64.** (a) Optrode with dual stimulation and recording functions. Light is locally delivered through an aperture at the tip of the tapered optical fiber to nearby neurons. Neural activity is recorded through a thermally metallized gold tip of the optrode (reprinted from [786]). (b) Optrode design. The device body consists of a plastic housing and a thumbscrew, held tightly in place with two friction-fit plastic pins, mechanically driving a vented screw into which a protective tube containing 4 tetrodes and a multimode fiber is glued. The screw head is epoxied to both a metal ferrule optical connector at the end of the fiber and an electronic interface board, which connects tetrode microwires with an 18-pin electrical connector. Inset: Horizontal cross section of the optical fiber with 4 tetrode bundles affixed (reprinted from [785]). (c) Single optical fiber-multiple electrode combination. The multi-electrode array is combined with a tapered optical fiber (reprinted from [787]).

#### 8.4. On-probe $\mu$ LED-based approaches

An alternative approach for optical stimulation is the use of implanted  $\mu$ -LEDs inserted into the tissue. In this case, the light source is embedded in the inserted probe. It allows eliminating such limitations as insufficient power delivery to the target area and stringent design parameters for the waveguide. In addition, this approach can be used to design a wireless optoelectronic device that incorporates cellular-scale semiconductor components and inorganic light emitting diodes.

One of the earliest results in this direction was reported in 2013 by Kim and colleagues [788], who designed a multifunctional optoelectronic system mount on releasable injection needles for insertion into a soft tissue. The proposed device contained inorganic light-emitting diodes ( $\mu$ -ILEDs) to stimulate the brain and electrophysiological sensors to monitor electrical neuronal activity. Additional optical and thermal sensors were also implemented. The structure of the device is shown in Fig. 65(a)). The authors performed experiments with freely moving mice and demonstrated that the LED stimulation, on one hand, provided a sufficient power for activation of ion channels and, on the other hand, had a minimal heating effect on the brain tissue. Finally, the authors highlighted that LED caused smaller lesions than metal electrodes and fiber optics and was more appropriate for experiments with small freely moving animals.

Recently, Jia et al. [789] used  $\mu$ -LEDs in wireless optoelectronic BCIs in experiments with small freely behaving animals. A schematic representation of the proposed interface is shown in Fig. 65(b). The implantable device with two recording electrodes and four LEDs was placed over the primary visual cortex of adult rodents. A channelrhodopsin was injected to make the neurons sensitive to light.

The proposed interface was tested during *in vivo* animal experiments. At the first stage, the authors performed brain stimulation using 10-ms light pulses of about  $4 \text{ mW/mm}^2$  optical intensity. The ECoG activity was simultaneously recorded and analyzed. They demonstrated stable light-induced neural activity occurred simultaneously with optical stimulus flags. The effective detection of light-induced ECoG activity was possible with approximately 5-ms precision.

#### 8.5. From rodents to primates

Although, the first optogenetics interfaces were successfully implemented with small animals, the further development of this technology required transition to nonhuman primates (NHPs). The NHP optogenetics can bring advantages in studying a large-scale neural circuit function. At the same time, there are certain issues and challenges when applying optogenetics stimulation for NHPs. In particular, the adaptation of neural control tools to the primate brain is slow as compared with rapid adaptation of such tools for characterizing circuit functions in worms, flies, and mice [790]. Moreover, it is more difficult to target genes to genetically specified neuron types in primate brains [791]. From a technical point of view, the key challenges for designing optogenetic interfaces for NHPs are high levels of optogenetic expression across cortical areas that can span several square centimeters and perform combined optical stimulation and neurophysiological recordings across these large areas stably over long periods of time.

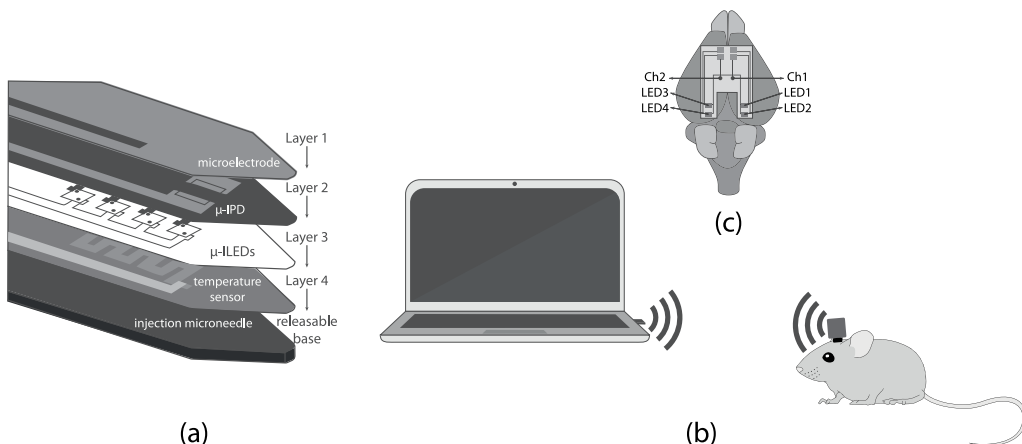


**Fig. 65.** (a) Multifunctional implantable optoelectronic device in the tilted exploded view layout illustrating various components. The system includes the layers for electrophysiological measurement (Layer 1: Pt contact pad, microelectrode), optical measurement (Layer 2: silicon  $\mu$ -IPD), optical stimulation (Layer 3:  $\mu$ -LED array), and temperature sensing (Layer 4: serpentine Pt resistor), all bonded to a releasable structural support for injection (microneedle) (reprinted from [788]). (b) Schematic representation of a wireless opto-electronic BCI. (1) Head-mounted headstage which includes a microfabricated opto-electronic interface with two recording electrodes Ch1 and Ch2 and four  $\mu$ LEDs. (2) Implanted custom-designed USB adapter for wireless data transfer. (3) PC running a custom-designed software.

Source: Reprinted from [789].

The possibility to affect the activity of genetically specified cells and neural pathways in the primate brain was demonstrated in 2006 by Tan et al. [792], who used the Drosophila allatostatin receptor. Three years later, Han et al. [791] used light-activated channel-rhodopsin-2 (ChR2) to control neurons of the macaque frontal cortex. Through an optical fiber they delivered optical stimulation to the neurons and simultaneously recorded neural activity using a microelectrode matrix. As a result, they managed to obtain good neural excitation and suppression by the optical stimulation of neocortical neural networks. Moreover, they demonstrated that channelrhodopsin was safely expressed and could mediate optical neuromodulation in primate neocortex over many months.

In 2011, Diester and colleagues [793] published the results of their study on the adaptation of optogenetical tools for a primate's brain using rhesus monkeys (*Macaca mulatta*). The authors addressed three main challenges of optogenetics. At the first step, they assessed the safety and efficiency of three relevant optogenetic agents: two viral vector systems (lentivirus and adeno-associated virus); two human promoters (human synapsin (hSyn) and human thymocyte-1 (hThy-1)) and three excitatory and inhibitory mammalian codon-optimized opsins (channelrhodopsin-2, enhanced natronomonas pharaonis halorhodopsin and the step-function opsin). At the second step, the reliability of the optogenetic stimulation and its effect on neural activity was analyzed. Finally, they determined expression levels *in vivo* with the help of fluorescence measurements.

The experimental setup and preparation process for this experiment are schematically illustrated in Fig. 66. Two monkeys were injected at 7 different sites with 4 different constructs. After 5 weeks, the optical stimulation and simultaneous neural activity recording were performed. The authors demonstrated a rapid reduction in firing rate when tissue was illuminated with green (561 nm) or yellow (594 nm) light. Then, they demonstrated the possibility to increase neuronal firing rates by blue-light illumination. Finally, the authors concluded that adeno-associated virus type 5 (AAV5) can be used as a safe and effective viral vector for delivering opsins into the brains of non-human primates. They found that 38%–50% of all neurons recorded at AAV5-injected sites were light-responsive. This level of expression might seem low, but is comparable with other (non-optogenetic) virus characterization studies [794]. Having in mind that AAVs are tolerated by the human immune system [795], the obtained results can be considered as a starting point for optogenetic studies in human brain.

In 2016, Yazdan-Shahmorad et al. [796] designed an interface for large-scale optogenetic stimulation and recording neural activity in NHPs. The authors carried out experiments with rhesus monkeys and examined circuit dynamics and large-scale connectivity in primary somatosensory (S1) and motor (M1) cortical areas. Using techniques developed by Bankiewicz and colleagues [797], they performed infusions of AAV5 viral vector to large cortical areas. The injections were verified with MRI images, and the expression was initially verified with the surface epifluorescence imaging. The expression was estimated across  $140 \text{ mm}^2$  of the cortical surface. The recordings were made using custom 96-channel  $\mu$  ECoG arrays. The stimulation was delivered via a fiber optic positioned on the top of the recording array. During the first experiment, the proposed interface was used to map the spatio-temporal response within cortical area to parametric changes in the stimulus. It was shown that the network response depended on the stimulus waveform shape. Then, during the second experiment, the authors demonstrated the possibility of using interface for studying circuit dynamics. They stimulated focally the S1 area, while recording from the whole array. Having analyzed the spatio-temporal features of the

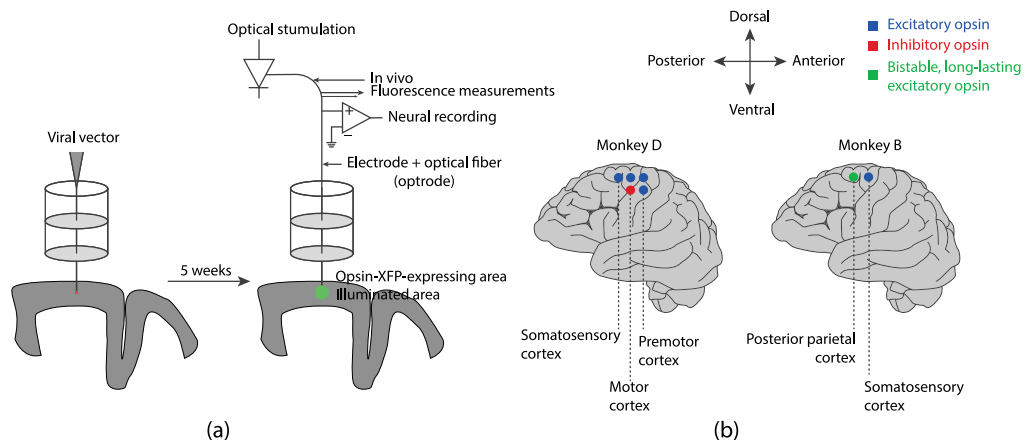


**Fig. 66.** Schematic overview of the optogenetic experiment with rhesus monkeys. (a) Left: injection device; right: stimulation, recording and *in vivo* fluorescence detector outline. The standard recording grid guides an injection needle to the desired location. Small quantities ( $1 \mu\text{L}$ ) of viral vectors carrying the opsin-fluorophore fusion gene were injected in the cortex at different depths and sites. Starting five weeks after injections, the injected sites were optically stimulated and electrical neural activity was simultaneously recorded using the combination of an optical fiber and an electrode (optrode) guided by the same grid as used for the injections. During the last week of the experiment, fluorescence was also measured *in vivo*. (b) Injection sites and viral vectors in monkeys D and B. Monkey D was injected at five different sites with three different constructs. Source: Reprinted from [793].

stimulus-evoked response in the high gamma-band (60–200 Hz), they found that while the S1 response was induced by direct illumination, the response at the M1 was the secondary response resulting from functional connectivity between S1 and M1.

According to the recent review of Delbeke et al. [798], optogenetics predominantly used as a research tool in animals, can be applied in humans in the nearest future. Nowadays, there are several patents on this topic. For example, Horsager et al. [799] invented methods for the selective silencing of neurons in pain pathway by using the combination of inhibitory light-sensitive protein gene transfer and wavelength specific illumination. Furthermore, Deisseroth [772] proposed approaches for optical stimulation of the peripheral nervous system. Finally, there are ongoing clinical trials using microbial opsins for vision restoration in patients affected by retinitis pigmentosa [800].

## 9. Brain-to-brain interfaces

Traditionally, BCIs imply the interaction between human's (or animal's) brain and a machine part (a computer or another external device). The main goal of the BCI is to repair and/or increase human performance in solving different tasks or enables paralyzed people to interact with the environment. In this particular case, a machine being controlled by human's brain activity, assumes a part of cognitive or physical human load. Similarly to the human-machine interaction, a human-human interaction can be improved by a special BCI enabling direct information transfer between brains. In this situation, the machine component of a traditional BCI can be replaced by another human. Such human-human interaction can be performed via a brain-to-brain interface (BBI).

### 9.1. Brain-to-brain interfaces for animal-animal interaction

The first BBI was performed in rats in 2013 by the researchers from the Duke University (USA) and the Institute for Neuroscience of Natal (Brasil) [801]. The proposed interface enabled a real-time transfer of information about sensorimotor neural activity between brains of two rats. In that BBI, one rat acted as *encoder* and performed sensorimotor tasks that consisted in selection one from two choices of the presented external stimuli. When the *encoder* performed the task, its cortical activity was recorded and transmitted to same cortical areas of a *decoder* using intracortical microstimulation (ICMS). As a result, the *decoder* learned to make similar behavioral selections, based just on the information coming from the *encoder*.

At the first stage, the animals were trained to take part in the experiments. The encoder was trained to respond to the presented external stimuli until the accuracy of its responses achieved 95%. The decoder, in its turn, was trained to correctly (up to 78%) respond to ICMS pulses. The main experiment was performed as follows.

1. The encoder identified a visual stimulus, signaled by a LED, and then pressed one of two levers to receive a small water reward.
2. Neural activity was recorded from the encoder and transmitted to the decoder by comparing the pattern of the encoder's activity with a template trial (previously built with the firing rate averaged over the trial sample).

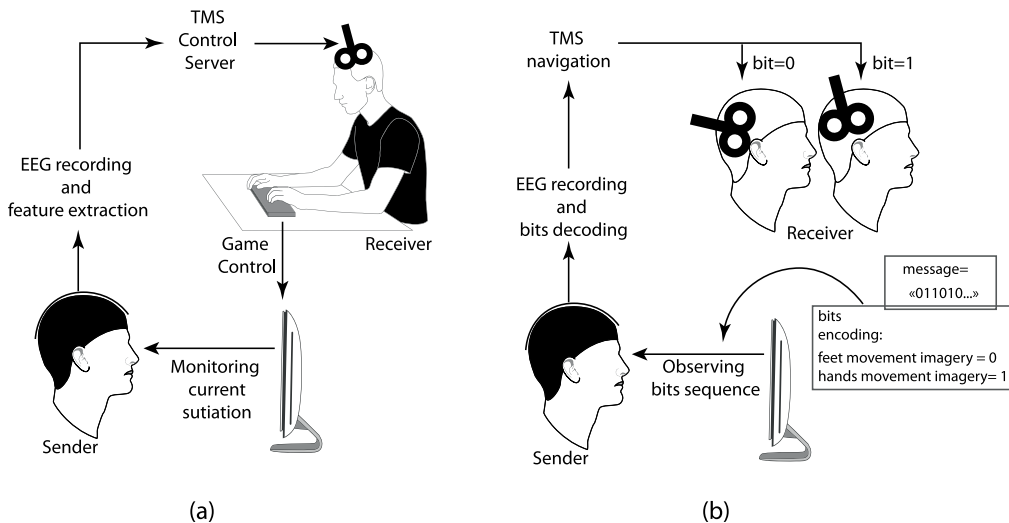


**Fig. 67.** (a) BBI proposed by Rao et al. [802]. The sender monitors the current situation on the game screen. In order to generate a control command, the sender tries to move a cursor to a target position with the help of motor imagery. When the command is generated, a corresponding motor-related pattern is translated to the receiver via tMS. The receiver presses a button to activate the game action. The receiver observes the result on the screen. (b) BBI for direct brain-to-brain communication [803]. The sender encodes bits by performing motor imagery of his/her hands. Control commands are translated to the receiver via tMS.

3. The difference between the number of spikes in a current trial and the template trial was used to calculate a Z-score.
4. Z-score was converted into an ICMS pattern through a sigmoid function. It allowed the ICMS patterns varied in real time, according to the number of spikes recorded from the encoder.
5. When ICMS was delivered to the decoder, it had to select the same lever pressed by the encoder.
6. Finally, if the decoder pressed the correct lever, both rats were rewarded.

Thus, when the cooperation between the rats was successful, the encoder received an additional reward that served as a feedback. As a result, the encoder performed task better than the decoder (95% vs 72%). In some experiments, the decoder's performance using the BBI was very close to the maximum performance obtained during the training (72% vs 78%).

## 9.2. Brain-to-brain interfaces for human-to-human interaction

In 2014, the researchers from the University of Washington implemented a direct BBI in humans [802]. This BBI detected motor imagery patterns in EEG signals recorded from one subject (sender) and transmitted this information to the motor cortex region of a second subject (receiver) via a transcranial magnetic stimulation (tMS). The schematic illustration of the BBI is presented in Fig. 67(a).

The subjects played together a computer game. The game purpose was to defend a city from enemy rockets which followed a trajectory, traversing the screen from the lower right to the upper left corner. In order to destroy the rocket, the subjects had to fire the cannon by pressing a touchpad. If the cannon was fired before the rocket passed the screen, the rocket was destroyed and the city was saved. In 50% of the trials, the rocket was replaced by a "supply airplane" and subjects had to avoid firing the cannon to let airplane reach the city.

The sender was able to see the game, but was not provided with any input device to control the cannon. The receiver could use right hand to press a touchpad, but could not see the game. The sender and the receiver could only communicate with each other through the brain-to-brain communication channel. In order to activate the cannon, the sender performed motor imagery to move a cursor up on the screen. In order to detect motor imagery patterns and translate them in the cursor control commands, the energy of the mu-band (8–12 Hz) was calculated. When the cursor reached the target position, a command was sent to the receiver through tMS.

In order to estimate the BBI efficiency, the pair's accuracy was compared during the experimental and control sessions. As a result, three pairs correctly identified and destroyed from 25% to 83% rockets in the experimental and 0% in the control sessions. Finally, the authors estimated the amount of information that was effectively transmitted between a sender and a receiver by calculating mutual information. It was shown that no information was transferred during the control sessions, while about 4–13 bits were transferred from one brain to another during each experimental session.

In the same year, the scientists from France, Spain and USA used EEG and tMS to implement a direct brain-to-brain interaction between humans [803]. In their research, one subject acted as a sender and three subjects were receivers. Fig. 67(b) demonstrates interaction between the sender and the receiver.

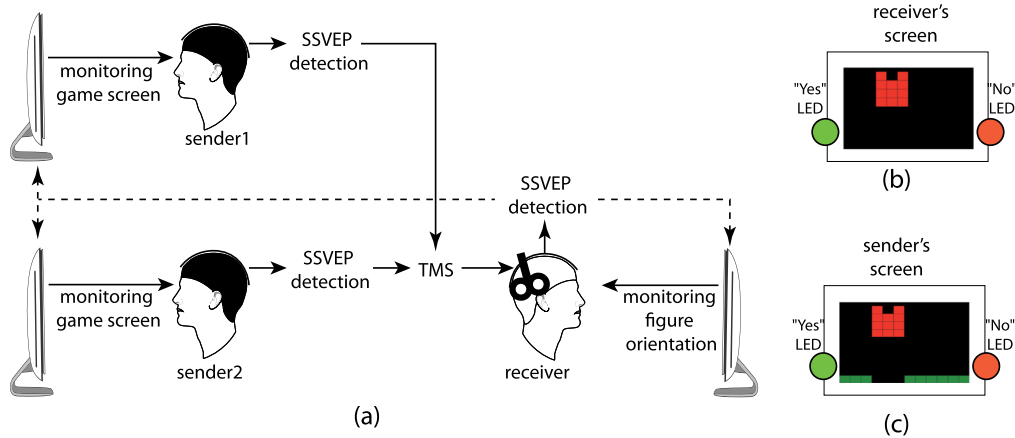


**Fig. 68.** Schematic illustration of BBI proposed by Jiang et al. [806]. Both sender 1 and sender 2 monitor the screen during a Tetris-like game. If one sender decides to rotate figure, he/she focuses on “Yes” LED, or on “No” LED otherwise. EEG signals are recorded to convey information about the brain state of each sender directly to the brain of the receiver. After consciously processing the two inputs from two senders, the receiver uses “Yes” LED or “No” LED to execute the action. The senders see the result of this action on the screen.

EEG signals were recorded from the emitter’s brain. Then, motor imagery patterns were detected in real time with the help of the algorithm described by Schalk et al. [804]. The sender sequentially showed on the screen the bits to be transmitted, each represented by either “1” or “0”. If it was “1”, the sender should encode it by performing motor imagery of his/her hands. On the contrary, bit “0” should be encoded by motor imagery of the feet. Similarly to Rao et al. [802], the emitter received information about motor imagery pattern formation in the brain. Motor imagery patterns produced by the sender’s brain controlled the vertical movement of a ball appearing on the screen. If the ball achieved the target position, the transmitted bit was correctly encoded. The bit transmission was performed with tMS. It is known [805] that a particular orientation of the tMS-induced electric field produced phosphene, while the orthogonal direction did not produce phosphene. Thus, bits “1” and “0” were associated with these orthogonal orientations of the TMS-induced electric field. Changes of TMS orientations in real time were implemented via a robotized tMS system.

This BBI was used to transmit pseudo-random sequences carrying encrypted messages encoding the words “hola” (experiment 1) and “ciao” (experiment 2). During experiment 1, the transmission error rates were of 6%, 5% and 11% for the brain–computer (BC) part, computer–brain (CB) part and the whole BBI, respectively. During experiment 2, error rates were of 2%, 1% and 4%, respectively. BC and CB transmission rates were equal to 3 and 2 bits per minute, respectively. The overall BBI transmission speed was equal to 2 bits per minute and limited by the CB branch.

Another BBI implemented in humans was described in a recent preprint [806]. Its schematic illustration is presented in Fig. 68(a). The BBI used EEG to record brain activity and tMS to deliver commands directly to the brain. The interface allowed three participants to collaborate while playing a Tetris-like game. Two subjects were senders and third subject was a receiver. Similarly to Rao et al. [802], the receiver did not see the whole game screen (see the example of the sender’s screen in Fig. 68(b)) and acted based on the commands delivered directly to his/her brain. Two senders played the same role in observing the current state of the game (see the example of the receiver’s screen in Fig. 68(c)) and conveyed their decisions to the receiver. The receiver had to integrate these two independent decisions and decided what to do.

The game consisted of independent trials, each of which involved deciding whether or not to rotate a single Tetris-like piece. Each trial included two rounds of interactions between the senders and the receiver. Each round offered a chance to rotate the piece. When the first round was finished, all three participants were able to see the current orientation of the piece. Based on this feedback, the senders got the possibility to send new suggestions to the receiver, allowing to correct a mistake made in the first round.

To generate a control command, SSVEPs were used. The senders were instructed to focus their attention on a “Yes” LED light flashing at 17 Hz placed on one side of their computer screens (to convey a “do rotate” decision) or “No” LED light flashing at 15 Hz placed on another side (to convey a “do not rotate” decision). The control command was then formed based on the estimation and comparison of the EEG signal energy at the corresponding frequencies.

The effectiveness of the human–human interaction was estimated via a different way. First, the authors measured the proportion of correct block rotations during a game. The accuracy was obtained to be 0.81 which was significantly higher than the performance expected by chance. Then, the performance was measured via EEG properties. It was shown that the average spectral power at the frequency corresponding to the correct answer in the trial was significantly larger than that of the frequency corresponding to the wrong answer. Finally, the authors calculated mutual information and demonstrated that the information transmitted was significantly greater compared to a chance performance.

Based on this multi-user BBI, the authors demonstrated that the receiver communicated better with one of the senders. According to this, the senders were classified as “good” and “bad” senders. The authors suggested that similarly to real social interactions the receiver successfully learned which of the two senders was a more reliable source of information.

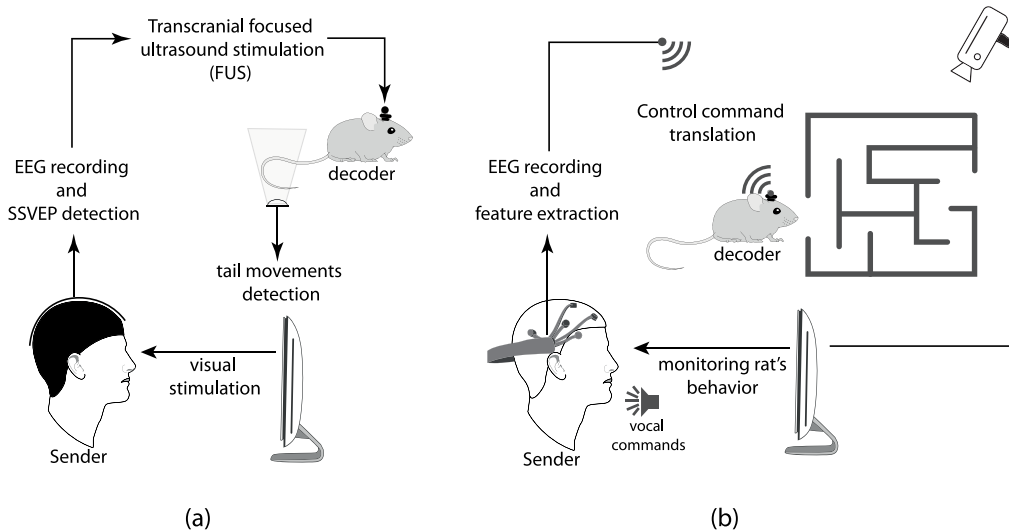


**Fig. 69.** (a) BBI proposed by Yoo et al. [808] for direct information transfer between human's and animal's brains. The sender is affected by visual stimulation at a certain frequency. SSVEP is detected from EEG signals and used as a command to activate rat's motor cortex. The successful stimulation of the rat's motor area causes detectable tail movement. (b) BBI proposed by Zhang et al. [809] enables to control the rat's brain during a navigation task. The sender receives vocal commands and performs motor imagery with the left or right arm. Corresponding patterns are detected in EEG and translated directly to the rat's brain to make it turn left or right. The sender has the possibility to follow the rat's behavior using video monitoring.

In the recent work [807], a BBI was supplemented by a muscle-to-muscle interface. The subject (sender) was instructed to perform right hand motor imagery with the help of a visual cue. The corresponding motor-related brain activity was reflected by ERD of the upper alpha-rhythm (10–13 Hz) in the vicinity of the C3 electrode over the contralateral hemispheric motor area of the right-hand side. When motor-related activity was detected in the sender's brain, tMS was applied to another subject (receiver) to induce his/her hand motion. When affecting the receiver's motor cortex, tMS induced a pronounced change of the motor evoked potentials (MEP) recorded by EMG of the receiver's arm. Finally, the recorded MEP triggered FES applied to the sender's arm and generated hand motion of the sender.

The system performance was estimated based on the ratio of the number of successful detections to the number of visual cues. Having considered six pairs, the authors demonstrated that the overall accuracy was  $69.7 \pm 8.55\%$  for the brain-to-brain part and  $87.37 \pm 9.7\%$  for the muscle-to-muscle part. The delays in BCI classification, EMG-triggered FES detection, and network data transfers were approximately 0.17, 0.35 and 0.1 s, respectively.

### 9.3. Brain-to-brain interfaces for human-animal interaction

The development of BBIs is one of the most actively progressing scientific directions at the intersection of physics and neuroscience. The main trends in the BBI research are aimed at providing people with a new way for communication directly from one brain to another, enabling control of the human's or animal's behavior and increasing working performance by using cognitive resources of multiple brains.

Along with the information transfer between human brains or between animal brains, some BBI were implemented to enable information transfer between human's brain and animal's brain. For instance, the researchers from the Korea Institute of Science and Technology and the Boston University implemented an interface for information transfer between human's and rat's brains [808]. The implementation was aimed to non-invasively translate the human volunteer's intention to stimulate a rat's brain motor area that is responsible for the tail movement. This BBI is schematically illustrated in Fig. 69(a).

In order to generate specific patterns of brain activity, the authors used SSVEPs. The volunteer was instructed to focus attention on a target area on the screen. This area represented itself as a circle which was displayed in the center of a gray background at different frequencies (5, 10, 15 and 20 Hz). As a result, a detected brain activity pattern manifested itself in the form of increased signal amplitude in the EEG bandwidth corresponding to the visual stimulation frequency. EEG signals were registered via surface electrodes. In order to deliver information to the rat's brain, the transcranial focused ultrasound (FUS) was used. The successful stimulation of the rat's motor area was examined using the corresponding tail movement detected by a motion sensor. The authors demonstrated high-degree of performance accuracy (up to 94%). The average response time between sender's intension and the FUS operation exhibited  $1.596 \pm 1.07$  s latency, while the latency between sonication initiations and the tail movement detection was  $40.246 \pm 0.05$  s.

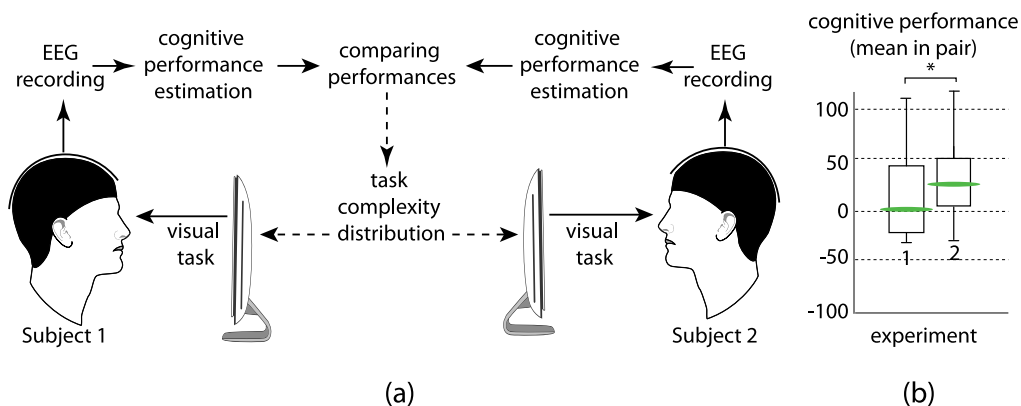


**Fig. 70.** Brain-to-brain interface for sharing cognitive load between two subjects in accordance with their current levels of cognitive performance estimated from EEG signals.

Source: Based on the data from [810].

Another way of the brain-to-brain interaction between a human and an animal was implemented in the recent paper of Zhang et al. [809], who utilized neural activity patterns recorded in the human's brain to directly control of the rat's brain during a navigation task in a complex environment. The schematic illustration of the proposed system is shown in Fig. 69(b). A human was instructed to perform motor imagery of the left or right arm after vocal instructions “turn left” or “turn right”, respectively. The EEG signals were acquired via the commercial EEG device (Emotiv EPOC, USA). Motor related patterns of neural activity were detected through a corresponding modulation of the sensorimotor rhythm amplitude in the 10–14 Hz frequency band using a CSP approach. As a result, the average accuracy in the EEG pattern recognition was  $77.86 \pm 12.4\%$ . Motor-related patterns recorded in the human's brain were transmitted to the rat's brain via ICMS. Finally, rat's movements were controlled by the human via a video recording in real time.

With the proposed interface, the authors compared two different control models for the BBI system, the thresholding model (TREM) and the gradient model (GRAM). In TREM, controlling commands were generated when the intensity of a corresponding motor-related EEG pattern exceeded a certain threshold. In GRAM, commands were generated when the gradient value between two decoding results transcended a threshold. Having compared these two strategies, the authors demonstrated that a longer time was taken to complete the same maze tasks with TREM.

In order to explain the different performances of the GRAM- and TREM-based strategies, the authors calculated delays occurred between EEG decoding and instructions generated by two different control models. The results demonstrated a 70% reduction of the instruction generation delay with GRAM ( $155.01 \pm 3.10$  ms) compared to TREM ( $494.70 \pm 47.22$  ms). Thus, control commands were generated much faster with the GRAM model, which ensured a less wrong turning behavior of the rat and better performance.

#### 9.4. Brain-to-brain interfaces for increasing human cognitive performance

Although the studies mentioned above provide an experimental evidence of the information transmission between brains, they have two main limitations. First, some of them use SSVEPs to produce control commands from EEG signals. This means that the sender does not generate control commands by himself, but uses an additional system producing visual or auditory stimuli. As it was described above in the review, this approach requires an additional setup for stimuli presentation, that takes time to produce a control command.

Other BBIs use motor imagery for command generation. In these systems, the sender can start generating a command voluntary at any moment of time by performing motor imagery. At the same time, a few are able to generate stable motor-related patterns of brain activity. Therefore, BBIs use a feedback to enable the sender to see the effectiveness of the motor attempt to produce control commands. This approach demonstrates a low speed of command generation, so that these interfaces are mostly valuable for paralyzed people as an alternative way of communication.

At the same, there exists a promising way to increase cognitive performance of healthy humans via a direct interaction between their brains. While a traditional BCI is aimed at increasing human performance by assistance of a computer, a BBI can use cognitive resource of one human to increase the performance of another human to solve cognitive tasks. This is of particular importance for people performing together a common working task which requires sustained attention and alertness. The first attempt to implement BBI for increasing human cognitive performance was made in 2018 [810]. The schematic illustration of the proposed BBI is shown in Fig. 70.

Two participants were subjected to a prolonged (approximately 40-min) task on classification of ambiguous visual stimuli with different degrees of ambiguity. The whole set of ambiguous stimuli was divided into two subsets: images with weak ambiguity and images with high ambiguity. The classification of weakly ambiguous images was judged as a

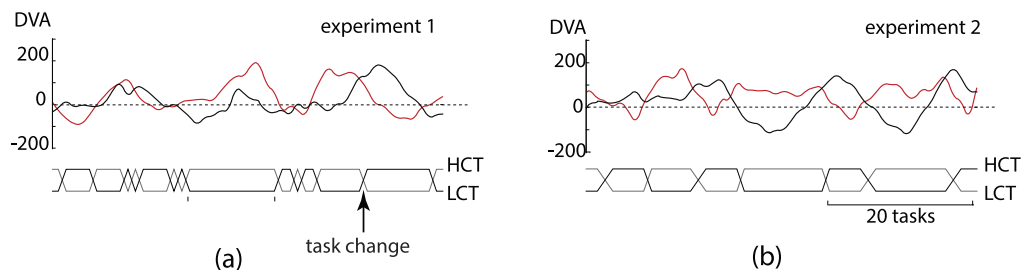


**Fig. 71.** Results of (a) experiment 1 and (b) experiment 2. (Upper traces) Evolution of DVA of each subject in pair. (Lower traces) Switches between two sets of visual stimuli (HCT and LCT). The arrow shows the single switch between HCT and LCT.

low complexity task (LCT), whereas the classification of highly ambiguous images was considered as a high complexity task (HCT).

During the session, the degree of visual attention (DVA) was estimated for each participant based on the EEG signal energy in the 8–12 Hz and 15–30 Hz frequency bands. DVA was considered as a factor which characterizes human performance during this classification task. The task was distributed between two partners depending on the individual DVA scores; the partner with higher DVA received a higher complexity part, while his/her partner received a lower complexity part.

With the proposed BBI, the authors carried out two experiments for six pairs. In the first experiment, the task was distributed based on the instantaneous DVA of the participants. In the second experiment, there was a delay in the coupling between the subjects, if the difference in DVA between subject 1 and subject 2 became higher than 10%, the partner with higher DVA received the higher complexity part.

In order to evaluate the effect of cognitive load distribution on the cognitive performance, the mean DVA was calculated by averaging over the whole experimental session. Fig. 70(b) demonstrates the comparison between the mean DVA in pair of two experiments. During experiment 1, the mean DVA was close to zero, while during experiment 2 the mean DVA was significantly increased in all pairs. To understand the changes in the DVA, the authors considered evolution of DVA in time for both experiments. The time series illustrating evolution of DVA are presented in Fig. 71 for two experiments. One can see that DVA evolves periodically. The intervals with high DVA are replaced by intervals with low DVA. The latter is associated with stages of cognitive fatigue, which require some time for restoring cognitive resource. In experiment 2 (Fig. 71(b)), where the mean DVA is increased, DVA of two participants are antiphase synchronized. DVA of one of the subjects achieves high values while another subject exhibits cognitive fatigue and vice versa. In experiment 1, DVA are not synchronized (Fig. 71(a)). Thus, a delay in experiment 2 led to an optimal mode of the task redistribution. The authors concluded that DVA oscillated with a certain period, which was determined by entire cognitive processes. Therefore, the performance of a common task by a working team can be improved if the task is distributed among the team members according to their brain rhythms. Otherwise, it caused a lot of extra switchings interfering synchronization between DVAs.

## 10. Brain–computer interface from past to future

The area of BCIs is one of few areas of knowledge in which the delay time between a scientific idea, the first experiment and application did not exceed several decades. As a result of the extensive research in the field of neurobiology and neurotechnology, it became possible not only to predict human's emotional and cognitive states, but also to control interactions between different humans. However, so far many new BCI technologies are at the stage of laboratory experiments and rarely implemented in clinical practice. One of few exceptions are cochlear implants [811,812], already successfully used in rehabilitation practice.

In order to fully realize a great potential of BCIs, the development of new BCI technologies in the forthcoming decades have to overcome a number of obstacles. For example, the amazing adaptation ability of people to dynamic complex tasks and environments impedes unambiguous classification of neurophysiological data according to their thoughts in real time. The difficulties may arise due to strong signal noise caused by environmental exposure, overlapping neural processes resulting from simultaneous multiple cognitive tasks, as well as changes in neural signatures in short and long terms resulted from adaptation and plasticity of neural ensembles, endogenous brain noise, etc. To understand future prospects of BCIs and overcome arising problems, it is worthwhile to dwell on the main stages of creating this neurotechnology, listed in Table 5.

It is clearly seen from the table that the main trend of the BCI technologies created in the last two decades, is the transition from invasive neurointerfaces to noninvasive ones (see Section 2.1.3). The quality of signals and the possibility of detailed control of external devices using implanted electrodes, even with fairly simple classification algorithms, allow effective control of external devices, such as a prosthesis or an anthropomorphic manipulator (see Section 5). This became possible because the excitation of neurons in the motor cortex sufficiently determines the position, acceleration and rotation angle of a primate's or human's hand. In the field of invasive interfaces, there is currently a tendency toward

**Table 5**  
Historical overview of BCI development and research.

Years	Refs.	Technology	Results
End 1950	[813] [814]	Implanted multielectrode arrays for recording bark potentials and electrical brain stimulation in monkeys.	Sensomotor cortex was activated when monkeys made movements, while electrical stimulation of the cortex, on the contrary, caused muscle contraction.
1957	[815]	Touch interface.	With the help of a single-channel electrode stimulated the auditory nerve, it was possible to cause sound sensations in the deaf.
1963	[816]	Implantation of electrodes in various areas of the cerebral cortex for medical reasons.	Patients were asked to switch slides by pressing a button and cortex area responsible for controlling movement was found. Then, the button was disconnected, but the slides continued to switch, i.e., the control was performed directly by the brain. Recorded neuron discharges were transformed into the hand movement trajectory using linear regression. The monkey learned to control a cursor position on the screen by activating neurons of the motor cortex.
End 1960	[642]	Implantation of electrodes to monkey's motor cortex to record potentials of several neurons during the brush movement.	Monkeys learned how to voluntarily control the activity of their cortical neurons, based on the firing rate of single neurons. Understanding "mirror neurons" activity and neurons involved in the empathy mechanism.
1960–1970	[55,817,818]	Implanted electrodes to monkeys. Biological feedback.	The cochlear neuroprosthesis was successfully introduced in clinical practice to compensate a hearing loss in patients with severe neurosensory (sensorineural) disorders.
1970	[819]	Cochlear implant containing a sound transducer and a multichannel electrode.	Visual sensations, peculiar neuroelectrophotopixels allowed blind people to learn how to recognize simple patterns. Electrical stimulation vision was introduced in clinical practice; a fairly complex image from a video camera (one or several) was transmitted to neuroimplants of eyes and visual cortex.
1960–1970	[820,821]	Implantation of the electrode matrix in visual cortex of blind patients.	Successful creation of BCIs for experiments with monkeys. Technology transfer to paralyzed people. In particular, patients with an amyotrophic lateral syndrome controlled a cursor [196] and a manipulator [91]. Controlling an anthropomorphic robotic arm with humans [825].
1990–2000	[54,555,635, 646,652, 822–824]	Invasive BCIs to control mechanical manipulators.	Optical neurointerface allowing <i>in vivo</i> control of rodent's motor cortex via optogenetic brain stimulation in real time. Control of neurons of the macaque's frontal cortex using a laser-coupled optical fiber to deliver optical stimulation and a recording microelectrode to monitor neural activity.
2007	[773]	First optogenetic BCI.	Neurorehabilitation and control of the operator's mental state, wheelchair management, communication, etc.
2009	[791]	Optical control of neural dynamics in the nonhuman primate brain.	
2000–2019	This review	Noninvasive BCIs based on EEG, MEG, and fNIRS.	

the use of optogenetic methods for controlling neural activity, mostly in rodents. Only the first experiments on primates have been made, but this method has not yet been implemented for humans (see Section 8). This technique allows, on one hand, to control a certain group of neurons, and on the other hand, to simultaneously register the neuronal activity. Unlike electrical stimulation, optogenetic impact does not cause artifacts in recorded signals. This makes it possible to register changes in neuron dynamics caused by the stimulation with a minimal delay, that allows controlling movements with high temporal resolution.

At the same time, invasive technologies, apart from obvious clinical indications, cannot go beyond the scope of research activities. Wide applications are only possible for noninvasive neurointerfaces that do not require neurosurgical intervention for implementation. However, since the accuracy in the command interpretation in noninvasive interfaces is currently much lower than in invasive ones, the application of noninvasive BCIs is limited to those areas where a large number of erroneous commands is uncritical.

Highlighting near-term prospects for noninvasive BCI technologies, we suppose that future developments will be devoted to those applications where neural signals provide us with information that is difficult or impossible to obtain using other methods (for example, instant concentration of attention or fatigue), where perfect accuracy is not required for successful BCI operation. Apparently, the efficiency of such BCIs will be higher if their calibration will be more accurate for an individual user, accounting for individual features of his/her brain activity.

Therefore, the increasing accuracy is a crucial problem for creating a perfect BCI. Currently, the classification of brain states with an accuracy of about 80% is the norm for classifiers used in noninvasive BCIs. Such accuracy can be considered acceptable, for example, in communication tasks, neurorehabilitation, or assessing the user's condition, but is clearly insufficient for controlling external devices (for example, a wheelchair, car, or prosthetic hand (orthosis)). Therefore, the important task is to improve processing accuracy brain signals in real time and, as a result, increase the accuracy in recognition of mental commands. One of the promising areas here could be the creation of multimodal HSC BCIs which would take into account several factors in the command formation. One of the variants of such systems are hybrid BCIs (HBCIs) that use several types of signals.

**Table 6**

Classification accuracy of 14 subjects of classical and type-1 BCIs.

Source: Reprinted from [828].

	ERD-BCI	SSVEP-BCI	HBCI
Mean accuracy, %	69.4	82.8	84.5
Standard deviation, %	8.6	12.2	10.2
Number of subjects	11	3	1

Another type of more effective BCIs are multimodal systems enable to estimate the operator's mental state. Such a BCI is a hybrid of active and passive BCIs when the command classification algorithm of the active BCI is dynamically modified depending on the operator's state diagnosed by the passive BCI. Following Choi et al. [826], 59% of created BCIs use only one type of physiological signals, mostly EEG. At the same time, one of the current trends of the BCI technology for improving the quality and effectiveness of the BCI is the combination of different approaches to create a "hybrid" BCI which takes advantages of different techniques [827,828]. In this context, we would like to highlight three types of BCIs.

- BCIs using various signals that reflect brain activity, for example, EEG together with optical NIRS signals, or the use of two types of control processes, such as, e.g., modulation of sensorimotor rhythm (ERD/ERS) and SSVEP.
- BCIs using various physiological signals, signals of brain activity simultaneously with EMG, EOG and electrocardiograms (ECG).
- BCIs using signals of brain activity in conjunction with external signals of different nature, such as, eye tracking, joystick, gyroscope, etc.

As an example, now we will show how such an approach can improve the BCI quality, in particular, a type-1 BCI with simultaneous use of ERD and SSVEP (simultaneous ERD/SSVEP BCI) [829]. Fourteen subjects participated in three experiments with the BCI which implemented two variants of the command. In all experiments, each test began with the demonstration of a "left" or "right" arrow on the screen. In the first experiment, the subject was asked to imagine the movement of his/her left or right hand. As a consequence, the subject's brain activity exhibited ERD in the somatosensory cortex. In the second experiment, the left arrow instructed the subject to focus his/her attention on the left LED which flickered with a 8-Hz frequency, whereas the right arrow indicated on the right LED flickering with a 13-Hz frequency. During this experiment, SSVEP was detected. In the third experiment (HBCI), the arrow "to the left" instructed the subject to imagine the movement of his/her left hand and follow the left LED, whereas the arrow "to the right" instructed the subject to imagine the movement of his/her right hand and follow the right LED. The BCI efficiency was estimated by (i) classification accuracy, i.e., whether or not the classifier could correctly distinguish EEG patterns associated with left-hand and right-hand motor imagery and (ii) subjective report based on the questionnaire. Table 6 summarizes the classification accuracy obtained, as well as the number of subjects whose classification accuracy was below 70%.

From the table we can draw the following main conclusions. First, the classification accuracy was the highest in the HBCI. Second, in terms of both ERD and SSVEP, some subjects could not achieve the classification accuracy required for effective communication. Some researchers named this problem "BCI illiteracy" [830]. However, when the subject showed a low accuracy with one type of signal (for example, in the case of the ERD detection), he/she usually demonstrated a higher accuracy with another type of control signal (in our example, with SSVEP). This result implies that people who cannot use a ERD-BCI or a SSVEP-BCI can effectively use a HBCI. Third, the responses to the questionnaire showed that the subjects usually did not consider the hybrid state more complex than the other two types of interaction. Consequently, the HBCI can give improved performance without imposing a more significant load on the user than the classical BCI.

Thus, the use of the HBCI which consists of a BCI and another system (which may be another BCI), will improve communication efficiency between humans and computers, achieving their goals better than classical BCIs. For example, the HBCI can more accurately determine user's intentions during the command registration based on motor imagery and/or visual attention, improve overall system performance, and reduce the number of false positives during rest periods. A HBCI can have more than one input, which are usually processed simultaneously (Fig. 72(a)), or work with two systems sequentially, when one of them acts as a "brain switch" (Fig. 72(b)) or a "selector" (Fig. 72(c)). Other types of sequential BCIs beyond this switch/selector concept, are also possible.

At the same time, one can speak of "simultaneous" and "sequential" BCI to designate these two types of BCIs. So, the above example of a hybrid ERD/SSVEP BCI is a simultaneous BCI. In both cases, as in any BCI, at least one of the input signals must be a signal recorded directly from the brain. The simultaneous HBCI can use two different brain signals, for instance, electrical and hemodynamic signals measured by fNIRS, as discussed in Section 2.2.6. Moreover, one of the brain signals (say, EEG) can be associated with two mental strategies, e.g., motor imagery and spatial visual attention. It is also possible of using together a brain signal and an external input. The latter can be either a physiological signal (for example, an ECG) or a signal from an external device (for example, a sight control system based on the eye-tracker [37]).

For sequential BCIs, a brain switch system is of particular interest. Such system is designed to detect one state (pattern) only in current brain activity which can be associated with various neurophysiological processes. Mason and Birch [831] were the first, who developed the EEG-based brain switching. They proposed the design of a low-frequency asynchronous switch, capable of automatically recognizing individual trials, voluntary motor potentials from the current

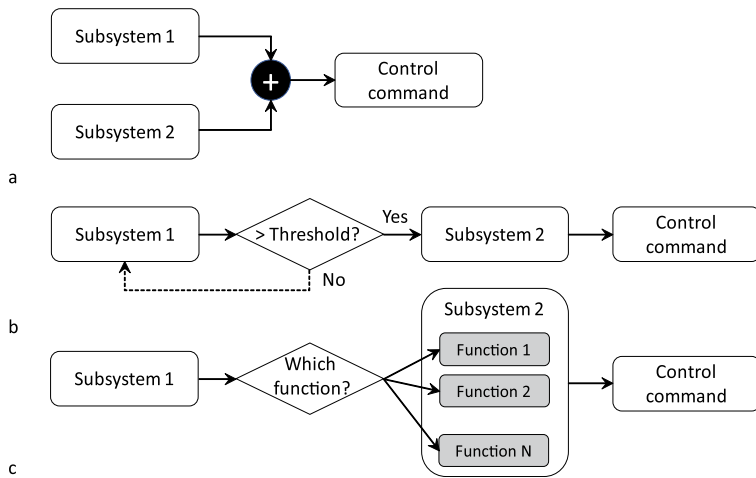


**Fig. 72.** HBCIs with (a) simultaneous, (b) sequential-switch, and (c) sequential-selector data processing.

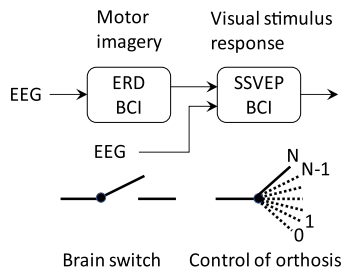


**Fig. 73.** Brain switch application in HBCI.

EEG activity in bipolar channels. Later, Pfurtscheller and colleagues [832,833] showed that it is possible to implement a single-channel brain switching when beta-ERS is detected in EEG during imagination of physical activity. The brain switching can also be detected by SSVEP with a high amplitude threshold [834] or by hemodynamic changes measured with fNIRS [132]. Fig. 73 illustrates the simplest use of the brain switch concept. In this example, the subsystem for detection of imaginary motions acts as the brain switch, and when turned on, activates an external device and control the second subsystem running on SSVEP and implementing a set of  $N$  commands, for example, to control an orthosis.

Although the efficiency and accuracy of HBCIs are very promising for the development of neurotechnology, certain problems still remain. In particular, current research on HBCIs is still largely based on visual stimulation or external devices that often cannot be used by certain target groups of users, especially, closed-minded people (group 1, see Section 2.4). However, for patients of group 2, with residual motor activity (movement of flashing of eyes, twitching of lips, etc.), HBCI technologies allow a significant increase in the speed of information transfer and the variety of commands for controlling external devices, as well as a reduction in a number of errors.

Another difficulty problem in the development of efficient BCIs is the variability of characteristics of neural activity among different subjects. This problem is well known in the context of the development of active neurointerfaces for the control of bioprostheses and anthropomorphic manipulators using neurophysiological biomarkers associated with motor imagery. Brain activity responsible for the imagination of movements has different structure in different untrained subjects, which characteristic biomarkers vary from one experimental session to another. Nevertheless, it is possible to divide subjects into two large groups, visual and kinesthetic, characterized by general laws. The presence of *a priori* information about which group the subject belongs to, allows an optimal configuration of the BCI and an increase of its efficiency [355].

When developing neural interfaces, it is also necessary to take into account that the structure of the electrical brain activity when solving cognitive tasks, essentially depends on the individual characteristics of a person. Among different features, one can distinguish psycho-physiological characteristics of the subject. According to the results of psychological and behavioral tests, personality traits affect the efficiency of solving cognitive tasks, and under certain conditions can be estimated from the recorded brain activity [835,836]. It was recently found that personality characteristics, such as intelligence and emotional stability, are directly related to attention and determine dynamics of neural activity while performing a simple cognitive task [379]. The obtained results make it possible to classify subjects into groups according to their psychophysiological brain activity. Moreover, the BCI operation is very sensitive to short-term changes

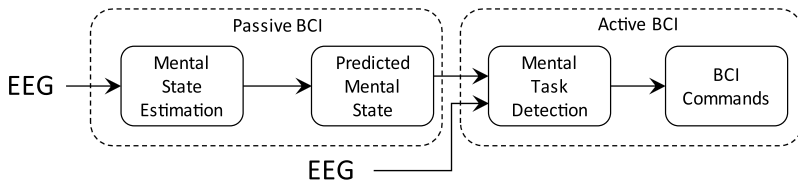


**Fig. 74.** General scheme of a psychologically adaptive hybrid active–passive BCI.

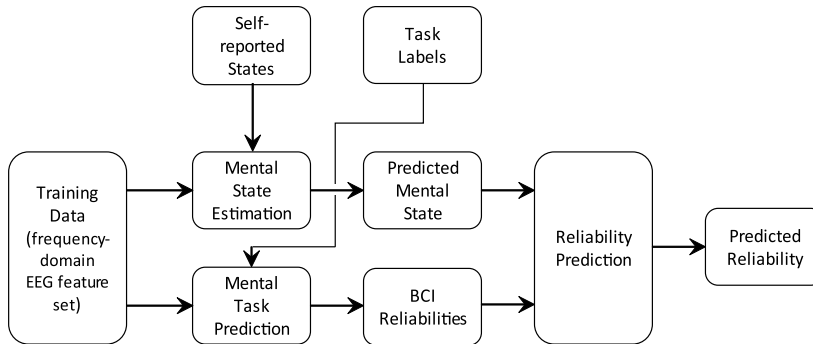


**Fig. 75.** General view of the scheme for training prediction algorithms. For each training set, the mental task to be performed for the command building is predicted using LDA, and the mental state is estimated using regularized regression. Predictions of a mental task and an estimated mental state are used to assess and predict BCI reliability.

in psychological states, such as fatigue, frustration and attention, that can be used for creation of a psychologically adaptive BCI [837–839].

A general scheme of such HBCI which combines active and passive neurointerfaces, is shown in Fig. 74. It includes, at the first stage, the assessment and prediction of the operator's mental state (passive BCI) and further adaptation of the active BCI classifier, taking into account the operator's current state (for example, attention or fatigue) to increase the accuracy in classification of commands. Based on this approach, Myrdan and Chau [837] developed an EEG-based BCI enabled to recognize two commands when performing user-specific mental tasks. In the subsystem of the active BCI, four options were considered as mental commands: mental arithmetic (addition/subtraction), motor imagery (imagination of the thumb movement), imaginary musical task (singing a song in mind), and imagination of words starting with a given letter. For each participant, two of these commands were selected, that exhibited the most pronounced differences from the background record (rest state) in terms of classification accuracy.

To determine the mental state, all participants in the experiment used the BCI during a long session of playing a simple navigational maze game, periodically reporting their perceived levels of fatigue, frustration and attention. The data from online sessions were analyzed offline to create a subsystem (passive BCI shown in Fig. 74), enable to automatically predict the perceived and previously noted levels of fatigue, disorder and attention based on the recorded EEG data using the regression method (see Section 4.4.6). This provided a continuous assessment of the mental state. The most important difference in the created scheme was the training scheme of the intellectual BCI system.

Fig. 75 illustrates the training scheme of prediction algorithms for the HBCI reliability. The amplitude of the Fourier component of the signal in the 1–30 Hz range was chosen as a feature vector, which amounted to 450 features (30 frequency components from each of the 15 EEG electrodes). This large feature set was further compressed by cross-validation using the feature clustering algorithm, which extracted significant frequency bands for each electrode [840]. The mental state is assessed using regularized regression and the results of the prediction were compared with self-reported states of fatigue, frustration, and attention (middle panels in Fig. 75). The BCI reliability prediction assumes (lower panels in Fig. 75) that the predicted mental state contains information regarding the success in the classification of the mental task that forms a management command. The LDA method was used to predict the class of the mental task (see Section 4.4.1). Since there exists a nonlinear relationship between a mental state and BCI indicators [839], the SVM classifier with the kernel in the form of RBF is used to predict the BCI reliability (see Eq. (36)).

To account for the mental state of the BCI user, this learning algorithm was modified by introducing an adaptive classification during the BCI operation. The essence of the method was as follows. It is assumed that the “separation” of the tasks used as commands for the active BCI and background activity (rest state) is preserved throughout the mental states space in the process of the feature classification. However, the distribution of the classes of each task propagates into the feature space as the BCI user changes his/her mental state. In fact, this means that in Fig. 25, the feature vector continuously moves in the feature space when the mental state changes, for example, due to increasing user's fatigue. Therefore, for each sample in the test set, a new classifier was trained using only training samples closest to this test

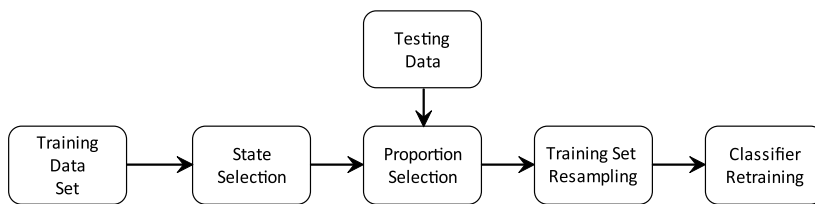


**Fig. 76.** Adaptive classification algorithm operating in real time. Optimal mental states and proportions are selected using inner cross-validation of the workout data, and then the workout data is recalculated for each test sample to train a new classifier.

sample in the three-dimensional space of the mental state “fatigue – disappointment – attention”, in which each EEG trial is located using the appropriate mental state predictions. For classification, an adaptive algorithm shown in Fig. 76 was used. On the basis of the predicted mental state, the optimal training set of EEG trials, closest to this mental state, was determined, and then the training data was recalculated for each test sample for training a new classifier.

The statistical analysis showed that there is a significant relationship between disappointment and BCI scores, while the relationship between fatigue and BCI scores is weak. The accuracy of the BCI classification was 7% lower than its average when the self-affirmation was low, and 7% higher than its average when the self-esteem was moderate. The multivariate analysis of the mental state revealed the presence of contiguous areas in the space of mental states, where BCI indicators were more accurate than their average, indicating the importance of moderate fatigue to achieve a slight focus on the BCI control, frustration as a potential motivator and attention as a compensatory mechanism for increasing disappointment. Taken together, these results show that the mental state is closely related to the BCI indices. Therefore, the development of a mentally adaptive hybrid active–passive BCI seems promising.

It is worth mentioning the technical side of the issue. One of the main obstacles in practical and mass usage of BCIs is the absence of convenient recording of brain activity [841]. When we talk about noninvasive registration neuroimaging methods, only the EEG record turns out to be a suitable cost and portable technology (see Table 2). Its disadvantage is the need to preinstall a large number of electrodes, as well as a low spatial resolution. Currently, in addition to wet classical electrodes, dry wireless electrodes with amplifiers have been developed. It can be expected that success in the field of intellectual technologies will lead to the appearance of “intelligent” electrodes for recording brain activity. We expect that such electrodes will automatically adapt their position and number depending on the user’s behavior and attitude. In the future, apparently, wireless electrodes will find a widespread use, that will make the BCI system more user-friendly in everyday activity. It is also expected that small-size electrodes will be developed with high capabilities for capturing very weak, including high-frequency, signals from brain regions we need, that will allow a high resolution, which at present can only be obtained with MEG. We hope that the combination of artificial intelligence and sensory technologies will lead to the creation of new advanced sensors for recording and primary processing of brain activity.

In the recent years, more and more research has looked at networks connecting individual brains, so-called *brain-net* (see Section 9). In general, the research task is formulated as the creation of networks that unite the efforts of several individuals in order to more effectively solve a common task. The first successful example is the creation of a BBI, in which a common routine task was divided between two operators depending on their attention, which was assessed independently in real time by the EEG signal of each of the partners [810].

In the long run, it seems promising a holistic approach that would combine information about the brain behavior, decision making, and the environment using multifunctional sensory and measurement technologies, including large-scale data collection of brain functionality (e.g., EEG, fMRI, fNIRS) (see Section 2.2) and brain structure (e.g., diffusion-weighted visualization [842]) on various scales, ranging from individual neurons to mapping the entire brain. The advances in computer networks, machine learning techniques and artificial intelligence, parallel data processing, and cloud computing technologies can provide a deep insight into brain functionality. This will help us to understand how differences and changes in the brain physical structure cause changes in its functional network, that can be detected in real time, thus providing much broader opportunities for the development of BCI technologies [843].

### Declaration of competing interest

The authors declare that they have no known competing financial interests or personal relationships that could have appeared to influence the work reported in this paper.

### Acknowledgments

This work was supported by the Russian Science Foundation through the grant 19-12-00050 in preparing Sections 5–9 and by President Program (NSh-2594.2020.2) in preparing Sections 3 and 4. A.N.P. acknowledges the Ministry of Economy and Competitiveness, (Spain) for support through the project SAF2016-80240-P for experimental MEG research. V.A.M. received personal support from the Russian Science Foundation (grant 20-72-00036) in reviewing machine learning methods and optimization techniques for brain signal analysis (Sections 4.5.1–4.5.3 and 4.5.5). The authors also thank Elena Pitsik for her assistance with figure preparation.

## References

- [1] J.R. Wolpaw, N. Birbaumer, D.J. McFarland, G. Pfurtscheller, T.M. Vaughan, Brain-computer interfaces for communication and control, *Clin. Neurophysiol.* 113 (6) (2002) 767–791, [http://dx.doi.org/10.1016/s1388-2457\(02\)00057-3](http://dx.doi.org/10.1016/s1388-2457(02)00057-3).
- [2] M.M. Moore, Real-world applications for brain-computer interface technology, *IEEE Trans. Neural Syst. Rehabil. Eng.* 11 (2003) 162–165, <http://dx.doi.org/10.1109/TNSRE.2003.814433>.
- [3] M.A. Lebedev, M.A.L. Nicolelis, Brain-machine interfaces: past, present and future, *Trends Neurosci.* 29 (9) (2006) 536–546, <http://dx.doi.org/10.1016/j.tins.2006.07.004>.
- [4] C. Guger, B. Allison, E.C. Leuthardt, *Brain-Computer Interface Research*, Springer, 2014.
- [5] X. Chen, Y. Wang, M. Nakanishi, X. Gao, T.P. Jung, S. Gao, High-speed spelling with a noninvasive brain-computer interface, *Proc. Natl. Acad. Sci. USA* 112 (44) (2015) E6058–E6067, <http://dx.doi.org/10.1073/pnas.1508080112>.
- [6] J.E. O'Doherty, M.A. Lebedev, P.J. Ifft, K.Z. Zhuang, S. Shokur, H. Bleuler, M.A.L. Nicolelis, Active tactile exploration using a brain-machine-brain interface, *Nature* 479 (7372) (2011) 228, <http://dx.doi.org/10.1038/nature10489>.
- [7] C.S. Nam, A. Nijholt, F. Lotte, *Brain-Computer Interfaces Handbook: Technological and Theoretical Advances*, CRC Press, 2018.
- [8] B. He, H. Yuan, J. Meng, S. Gao, *Brain-computer interfaces*, in: *Neural Engineering*, Springer, 2020, pp. 131–183.
- [9] J.J. Daly, J.R. Wolpaw, Brain-computer interfaces in neurological rehabilitation, *Lancet Neurol.* 7 (11) (2008) 1032–1043, [http://dx.doi.org/10.1016/S1474-4422\(08\)70223-0](http://dx.doi.org/10.1016/S1474-4422(08)70223-0).
- [10] U. Chaudhary, N. Birbaumer, A. Ramos-Murgialday, Brain-computer interfaces for communication and rehabilitation, *Nat. Rev. Neurol.* 12 (2016) 513–525, <http://dx.doi.org/10.1038/nrneurol.2016.113>.
- [11] K. Bowsher, E.F. Civillico, J. Coburn, J. Collinger, J.L. Contreras-Vidal, T. Denison, J. Donoghue, J. French, N. Getzoff, L.R. Hochberg, M. Hoffmann, J. Judy, N. Kleitman, G. Knaack, V. Krauthamer, K. Ludwig, M. Moynahan, J.J. Pancrazio, P.H. Peckham, C. Pena, V. Pinto, T. Ryan, D. Saha, H. Scharen, S. Shermer, K. Skodacek, P. Takmakov, D. Tyler, S. Vasudevan, K. Wachrathit, D. Weber, C.G. Welle, M. Ye, Brain-computer interface devices for patients with paralysis and amputation: a meeting report, *J. Neural Eng.* 13 (2) (2016) 23001, <http://dx.doi.org/10.1088/1741-2560/13/2/023001>.
- [12] A.B. Ajiboye, F.R. Willett, D.R. Young, W.D. Memberg, B.A. Murphy, J.P. Miller, B.L. Walter, J.A. Sweet, H.A. Hoyen, M.W. Keith, et al., Restoration of reaching and grasping movements through brain-controlled muscle stimulation in a person with tetraplegia: a proof-of-concept demonstration, *Lancet* 389 (10081) (2017) 1821–1830, [http://dx.doi.org/10.1016/S0140-6736\(17\)30601-3](http://dx.doi.org/10.1016/S0140-6736(17)30601-3).
- [13] T. Kawase, T. Sakurada, Y. Koike, K. Kansaku, A hybrid BMI-based exoskeleton for paresis: EMG control for assisting arm movements, *J. Neural Eng.* 14 (1) (2017) 16015, <http://dx.doi.org/10.1088/1741-2552/aa525f>.
- [14] W.C. Stacey, B. Litt, Technology insight: neuroengineering and epilepsy—designing devices for seizure control, *Nature Rev. Neurol.* 4 (4) (2008) 190, <http://dx.doi.org/10.1038/ncpneuro0750>.
- [15] S. Perrey, Brain activation associated with eccentric movement: A narrative review of the literature, *Eur. J. Sport Sci.* 18 (1) (2018) 75–82, <http://dx.doi.org/10.1080/17461391.2017.1391334>.
- [16] D. Hamacher, F. Herold, P. Wiegel, D. Hamacher, L. Schega, Brain activity during walking: A systematic review, *Neurosci. Biobehav. Rev.* 57 (2015) 310–327, <http://dx.doi.org/10.1016/j.neubiorev.2015.08.002>.
- [17] A. El-Madani, H.B.D. Sorensen, T.W. Kjær, C.E. Thomsen, S. Puthusserypady, Real-time brain computer interface using imaginary movements, *EPJ Nonlin. Biomed. Phys.* 3 (1) (2015) 9, <http://dx.doi.org/10.1140/epjnbp/s40366-015-0024-2>.
- [18] D.A. Rohani, W.S. Henning, C.E. Thomsen, T.W. Kjaer, S. Puthusserypady, H.B.D. Sorensen, BCI Using imaginary movements: The simulator, *Comput. Methods Programs Biomed.* 111 (2) (2013) 300–307, <http://dx.doi.org/10.1016/j.cmpb.2013.04.008>, <http://www.sciencedirect.com/science/article/pii/S0169260713001168>.
- [19] A. Frolov, D. Húsek, P. Bobrov, Comparison of four classification methods for brain-computer interface, *Neural Network World* 21 (2) (2011) 101.
- [20] F. Lotte, M. Congedo, A. Lécuyer, F. Lamarche, B. Arnaldi, A review of classification algorithms for EEG-based brain-computer interfaces, *J. Neural Eng.* 4 (2) (2007) R1, <http://stacks.iop.org/1741-2552/4/i=2/a=R01>.
- [21] F. Lotte, L. Bougrain, A. Cichocki, M. Clerc, M. Congedo, A. Rakotomamonjy, F. Yger, A review of classification algorithms for {EEG}-based brain-computer interfaces: a 10 year update, *J. Neural Eng.* 15 (3) (2018) 31005, <http://dx.doi.org/10.1088/1741-2552/aab2f2>.
- [22] J.J. Vidal, Toward direct brain-computer communication, *Annu. Rev. Biophys. Bioeng.* 2 (1) (1973) 157–180, <http://dx.doi.org/10.1146/annurev.bb.02.060173.001105>.
- [23] J.J. Vidal, Real-time detection of brain events in EEG, *Pros. IEEE* 65 (5) (1977) 633–641, <http://dx.doi.org/10.1109/PROC.1977.10542>.
- [24] J.R. Wolpaw, D.J. McFarland, Control of a two-dimensional movement signal by a noninvasive brain-computer interface in humans, *Proc. Natl. Acad. Sci. USA* 101 (51) (2004) 17849–17854.
- [25] N. Birbaumer, N. Ghanayim, T. Hinterberger, I. Iversen, B. Kotchoubey, A. Kübler, J. Perelmouter, E. Taub, H. Flor, A spelling device for the paralysed, *Nature* 398 (1999) 297–298, <http://dx.doi.org/10.1038/18581>.
- [26] T. Ma, H. Li, L. Deng, H. Yang, X. Lv, P. Li, F. Li, R. Zhang, T. Liu, D. Yao, et al., The hybrid BCI system for movement control by combining motor imagery and moving onset visual evoked potential, *J. Neural Eng.* 14 (2) (2017) 26015, <http://dx.doi.org/10.1088/1741-2552/aa5d5f>.
- [27] L. Peternek, T. Noda, T. Petric, A. Ude, J. Morimoto, J. Babic, Adaptive control of exoskeleton robots for periodic assistive behaviours based on EMG feedback minimisation, *PLoS One* 11 (2) (2016) 1–26, <http://dx.doi.org/10.1371/journal.pone.0148942>.
- [28] L.F. Nicolas-Alonso, J. Gomez-Gil, Brain computer interfaces, a review, *Sensors* 12 (2) (2012) 1211–1279, <http://dx.doi.org/10.3390/s120201211>, <http://www.mdpi.com/1424-8220/12/2/1211>.
- [29] Brain-machine interfaces, *Nature Web Focus* 442 (2006) 1211–1279.
- [30] Z. Huang, M. Li, Y. Ma, Parallel computing sparse wavelet feature extraction for P300 speller BCI, *Comput. Math. Methods Med.* 2018 (2018) <http://dx.doi.org/10.1155/2018/4089021>.
- [31] V.V. Grubov, V.O. Nedai佐夫, Stream processing of multichannel EEG data using parallel computing technology with NVIDIA CUDA graphics processors, *Tech. Phys. Lett.* 44 (5) (2018) 453–455, <http://dx.doi.org/10.1134/S1063785018050188>.
- [32] T.O. Zander, C. Kotche, Towards passive brain-computer interfaces: applying brain-computer interface technology to human-machine systems in general, *J. Neural Eng.* 8 (2) (2011) 25005, <http://stacks.iop.org/1741-2552/8/i=2/a=025005>.
- [33] E. Donchin, K.M. Spencer, R. Wijesinghe, The mental prosthesis: assessing the speed of a P300-based brain-computer interface, *IEEE Trans. Rehabil. Eng.* 8 (2) (2000) 174–179.
- [34] Z. Iscan, V.V. Nikulin, Steady state visual evoked potential (SSVEP) based brain-computer interface (BCI) performance under different perturbations, *PLoS One* 13 (1) (2018) 1–17, <https://doi.org/10.1371/journal.pone.0191673>.
- [35] E.C. Lalor, S.P. Kelly, C. Finucane, R. Burke, R. Smith, R.B. Reilly, G. Mcdarby, Steady-state VEP-based brain-computer interface control in an immersive 3D gaming environment, *EURASIP J. Adv. Signal Process.* 2005 (19) (2005) 706906, <http://dx.doi.org/10.1155/ASP.2005.3156>.
- [36] G.R. Müller-Putz, R. Scherer, C. Neuper, G. Pfurtscheller, Steady-state somatosensory evoked potentials: suitable brain signals for brain-computer interfaces?, *IEEE Trans. Neural Syst. Rehabil. Eng.* 14 (1) (2006) 30–37, <http://dx.doi.org/10.1109/TNSRE.2005.863842>.

- [37] T.O. Zander, C. Kothe, S. Jatzev, M. Gaertner, Enhancing human-computer interaction with input from active and passive brain-computer interfaces, in: *Brain-Computer Interfaces*, Springer, 2010, pp. 181–199.
- [38] T.O. Zander, Enhancing human-machine systems with secondary input from passive brain-computer interfaces, in: Proceeding of 4th International BCI Workshop, 2008, 2008, pp. 44–49.
- [39] T.O. Zander, S. Jatzev, Detecting affective covert user states with passive brain-computer interfaces, in: *Affective Computing and Intelligent Interaction and Workshops, 2009. ACII 2009. 3rd International Conference on*, IEEE, 2009, pp. 1–9, <http://dx.doi.org/10.1109/ACII.2009.5349456>.
- [40] K. Kingwell, Implantable device advises patients with epilepsy of seizure likelihood, *Nature Rev. Neurol.* 9 (2013) 297, <https://doi.org/10.1038/nrneurol.2013.94>.
- [41] V.A. Maksimenko, S. Heukelum van, V.V. Makarov, J. Kelderhuis, A. Lutjohann, A.A. Koronovskii, A.E. Hramov, G. Luijtelaar van, Absence seizure control by a brain computer interface, *Sci. Rep.* 7 (2017) 2487, <http://dx.doi.org/10.1038/s41598-017-02626-y>.
- [42] A.E. Hassaniyan, A.T. Azar, *Brain-Computer Interfaces: Current Trends and Applications*, Springer, 2015.
- [43] W.J. Freeman, M.D. Holmes, B.C. Burke, S. Vanhatalo, Spatial spectra of scalp EEG and EMG from awake humans, *Clin. Neurophysiol.* 114 (2003) 1053–1068, [http://dx.doi.org/10.1016/s1388-2457\(03\)00045-2](http://dx.doi.org/10.1016/s1388-2457(03)00045-2).
- [44] A.B. Schwartz, X.T. Cui, D.J. Weber, D.W. Moran, Brain-controlled interfaces: Movement restoration with neural prosthetics, *Neuron* 52 (2006) 205–220, <http://dx.doi.org/10.1016/j.neuron.2006.09.019>.
- [45] A.K. Shah, S. Mittal, Invasive electroencephalography monitoring: Indications and presurgical planning, *Ann. Indian Acad. Neurol.* 17 (Suppl S1) (2014) 89–94, <http://dx.doi.org/10.4103/0972-2327.128668>.
- [46] R.S. Fisher, A.L. Velasco, Electrical brain stimulation for epilepsy, *Nature Rev. Neurol.* 10 (2014) 261, <http://dx.doi.org/10.1038/nrneurol.2014.59>.
- [47] T.N. Lal, T. Hinterberger, G. Widman, M. Schröder, N.J. Hill, W. Rosenstiel, C.E. Elger, N. Birbaumer, B. Scholkopf, Methods towards invasive human brain computer interfaces, in: *Advances in Neural Information Processing Systems, 2005*, pp. 737–744.
- [48] E.C. Leuthardt, G. Schalk, J.R. Wolpaw, J.G. Ojemann, D.W. Moran, A brain-computer interface using electrocorticographic signals in humans, *J. Neural Eng.* 1 (2) (2004) 63, <http://stacks.iop.org/1741-2552/1/i=2/a=001>.
- [49] Z. Chao, Y. Nagasaka, N. Fujii, Long-term asynchronous decoding of arm motion using electrocorticographic signals in monkey, *Front. Neuroeng.* 3 (2010) 3, <http://dx.doi.org/10.3389/fneng.2010.00003>, <https://www.frontiersin.org/article/10.3389/fneng.2010.00003>.
- [50] J. Kubanek, K.J. Miller, J.G. Ojemann, J.R. Wolpaw, G. Schalk, Decoding flexion of individual fingers using electrocorticographic signals in humans, *J. Neural Eng.* 6 (6) (2009) 66001, <http://stacks.iop.org/1741-2552/6/i=6/a=066001>.
- [51] T. Pistoil, A. Schulze-Bonhage, A. Aertsen, C. Mehring, T. Ball, Decoding natural grasp types from human ecog, *NeuroImage* 59 (1) (2012) 248–260, <http://dx.doi.org/10.1016/j.neuroimage.2011.06.084>, <http://www.sciencedirect.com/science/article/pii/S105381191100749X>.
- [52] S. Waldert, Invasive vs. Non-invasive neuronal signals for brain-machine interfaces: Will one prevail? *Front. Neurosci.* 10 (2016) 295, <http://dx.doi.org/10.3389/fnins.2016.00295>.
- [53] D.A. Henze, Z. Borhegyi, J. Csicsvari, A. Mamiya, K.D. Harris, G. Buzsaki, Intracellular features predicted by extracellular recordings in the hippocampus in vivo, *Journal of neurophysiology* 84 (1) (2000) 390–400.
- [54] J.M. Carmena, M.A. Lebedev, R.E. Crist, J.E. O'Doherty, D.M. Santucci, D.F. Dimitrov, P.G. Patil, C.S. Henriquez, M.A.L. Nicolelis, Learning to control a brain-machine interface for reaching and grasping by primates, *PLoS Biol.* 1 (2) (2003) e42.
- [55] E.E. Fetz, Operant conditioning of cortical unit activity, *Science* 163 (3870) (1969) 955–958.
- [56] K. Ganguly, J.M. Carmena, Emergence of a stable cortical map for neuroprosthetic control, *PLoS Biol.* 7 (7) (2009) e1000153.
- [57] R.D. Flint, Z.A. Wright, M.R. Scheid, M.W. Slutsky, Long term, stable brain machine interface performance using local field potentials and multiunit spikes, *J. Neural Eng.* 10 (5) (2013) 56005.
- [58] J.A. Perge, S. Zhang, W.Q. Malik, M.L. Homer, S. Cash, G. Friehs, E.N. Eskandar, J.P. Donoghue, L.R. Hochberg, Reliability of directional information in unsorted spikes and local field potentials recorded in human motor cortex, *J. Neural Eng.* 11 (4) (2014) 46007.
- [59] Y.O. Okazaki, J.M. Horschig, L. Luther, R. Oostenveld, I. Murakami, O. Jensen, Real-time MEG neurofeedback training of posterior alpha activity modulates subsequent visual detection performance, *NeuroImage* 107 (2015) 323–332.
- [60] P. Zarjam, J. Epps, F. Chen, N.H. Lovell, Estimating cognitive workload using wavelet entropy-based features during an arithmetic task, *Comput. Biol. Med.* 43 (12) (2013) 2186–2195, <http://dx.doi.org/10.1016/j.combiomed.2013.08.021>, <http://www.sciencedirect.com/science/article/pii/S0010482513002369>.
- [61] R. Chai, M.R. Smith, T.N. Nguyen, S.H. Ling, A.J. Coutts, H.T. Nguyen, Comparing features extractors in EEG-based cognitive fatigue detection of demanding computer tasks, in: 2015 37th Annual International Conference of the IEEE Engineering in Medicine and Biology Society (EMBC), 2015, pp. 7594–7597, <http://dx.doi.org/10.1109/embc.2015.7320150>.
- [62] V.A. Maksimenko, A. Pavlov, A.E. Runnova, V. Nedavozov, V. Grubov, A.A. Koronovskii, S.V. Pchelintseva, E. Pitsik, A.N. Pisarchik, A.E. Hramov, Nonlinear analysis of brain activity, associated with motor action and motor imaginary in untrained subjects, *Nonlinear Dynam.* 91 (4) (2018) 2803–2817, <http://dx.doi.org/10.1007/s11071-018-4047-y>.
- [63] R.H.J. der Lubbe, I. Szumska, M. Fajkowska, Two sides of the same coin: ERP and wavelet analyses of visual potentials evoked and induced by task-relevant faces, *Adv. Cogn. Psychol.* 12 (2016) 154–168.
- [64] V.A. Maksimenko, A.E. Runnova, M.O. Zhuravlev, V. Nedavozov, V.V. Grubov, S.V. Pchelintseva, A.E. Hramov, A.N. Pisarchik, Visual perception affected by motivation and alertness controlled by a noninvasive brain-computer interface, *PLoS One* 12 (12) (2017) 1–20, <http://dx.doi.org/10.1371/journal.pone.0188700>, <https://doi.org/10.1371/journal.pone.0188700>.
- [65] L. Gao, J. Wang, L. Chen, Event-related desynchronization and synchronization quantification in motor-related EEG by Kolmogorov entropy, *J. Neural Eng.* 10 (3) (2013) 36023, <http://stacks.iop.org/1741-2552/10/i=3/a=036023>.
- [66] J.-R. Duan, J.-C. Chiou, A comparison of independent event-related desynchronization responses in motor-related brain areas to movement execution, movement imagery, and movement observation, *PLoS One* 11 (9) (2016) 1–16, <http://dx.doi.org/10.1371/journal.pone.0162546>, <https://doi.org/10.1371/journal.pone.0162546>.
- [67] L.M. McCane, S.M. Heckman, D.J. McFarland, G. Townsend, J.N. Mak, E.W. Sellers, D. Zeitlin, L.M. Tenteromano, J.R. Wolpaw, T.M. Vaughan, P300-based brain-computer interface (BCI) event-related potentials (ERPs): People with amyotrophic lateral sclerosis (ALS) vs. age-matched controls, *Clin. Neurophysiol.* 126 (2015) 2124–2131.
- [68] A. Onishi, K. Natsume, Multi-class ERP-based BCI data analysis using a discriminant space self-organizing map, in: 2014 36th Annual International Conference of the IEEE Engineering in Medicine and Biology Society, 2014, pp. 26–29, <http://dx.doi.org/10.1109/embc.2014.6943520>.
- [69] H.M. de Arruda Leite, S.N. de Carvalho, B. da Silva Costa, R. Attux, H.H. Hornung, D.S. Arantes, Analysis of user interaction with a brain-computer interface based on steady-state visually evoked potentials: Case study of a game, *Computational Intelligence and Neuroscience* 2018 (2018) 4920132.
- [70] J. Polich, P.C. Ellerson, J. Cohen, P300, stimulus intensity, modality, and probability, *Int. J. Psychophysiol.* 23 (1) (1996) 55–62, [http://dx.doi.org/10.1016/0167-8760\(96\)00028-1](http://dx.doi.org/10.1016/0167-8760(96)00028-1), <http://www.sciencedirect.com/science/article/pii/0167876096000281>.
- [71] J.N. Mak, Y. Arbel, J.W. Minett, L.M. McCane, B. Yuksel, D. Ryan, D. Thompson, L. Bianchi, D. Erdogmus, Optimizing the P300-based brain-computer interface: current status, limitations and future directions, *J. Neural Eng.* 8 (2) (2011) 25003, <http://stacks.iop.org/1741-2552/8/i=2/a=025003>.

- [72] I.P. Ganin, S.L. Shishkin, Kaplan, A P300-based brain-computer interface with stimuli on moving objects: Four-session single-trial and triple-trial tests with a game-like task design, *PLoS One* 8 (10) (2013) <http://dx.doi.org/10.1371/journal.pone.0077755>, <https://doi.org/10.1371/journal.pone.0077755>.
- [73] S.L. Shishkin, I.P. Ganin, A.Y. Kaplan, Event-related potentials in a moving matrix modification of the P300 brain-computer interface paradigm, *Neurosci. Lett.* 496 (2) (2011) 95–99, <http://dx.doi.org/10.1016/j.neulet.2011.03.089>, <http://www.sciencedirect.com/science/article/pii/S0304394011004241>.
- [74] C. Chernecky, B. Berger, *Laboratory Tests and Diagnostic Procedures*, sixth ed., Elsevier, 2013.
- [75] M.A. Lopez-Gordo, D. Sanchez-Morillo, P.F. Valle, Dry EEG electrodes, *Sensors* 14 (2014) 12847–12870.
- [76] E. Niedermeyer, F.L. da Silva, *Electroencephalography: Basic Principles, Clinical Applications, and Related Fields*, Lippincot Williams & Wilkins, 2004.
- [77] I. Choi, I. Rhiu, Lee, A systematic review of hybrid brain-computer interfaces: Taxonomy and usability perspectives, *PLoS One* 12 (4) (2017) 1–35, <http://dx.doi.org/10.1371/journal.pone.0176674>, <https://doi.org/10.1371/journal.pone.0176674>.
- [78] D.J. McFarland, W.A. Sarnacki, J.R. Wolpaw, Brain-computer interface (BCI) operation: optimizing information transfer rates, *Biological psychology* 63 (3) (2003) 237–251.
- [79] B. Obermaier, C. Neuper, C. Guger, G. Pfurtscheller, Information transfer rate in a five-classes brain-computer interface, *IEEE Trans. Neural Syst. Rehabil. Eng.* 9 (3) (2001) 283–288, <http://dx.doi.org/10.1109/3733.948456>.
- [80] M. Kolodziej, A. Majkowski, Ł. Oskwarek, R.J. Rak, P. Tarnowski, Processing and analysis of EEG signal for SSVEP detection, in: P. Augustyniak, R. Maniewski, R. Tadeusiewicz (Eds.), *Recent Developments and Achievements in Biocybernetics and Biomedical Engineering*, Springer International Publishing, Cham, 2018, pp. 3–21.
- [81] Y.-Y. Chien, F.-C. Lin, J.K. Zao, C.-C. Chou, Y.-P. Huang, H.-Y. Kuo, Y. Wang, T.-P. Jung, H.-P.D. Shieh, Polychromatic SSVEP stimuli with subtle flickering adapted to brain-display interactions, *J. Neural Eng.* 14 (1) (2017) 16018, <http://stacks.iop.org/1741-2552/14/i=1/a=016018>.
- [82] J.R. Wolpaw, D.J. McFarland, T.M. Vaughan, Brain-computer interface research at the wadsworth center, *IEEE Trans. Rehabil. Eng.* 8 (2) (2000) 222–226, <http://dx.doi.org/10.1109/86.847823>.
- [83] B. Blankertz, F. Losch, M. Krauledat, G. Dornhege, G. Curio, K.R. Muller, The berlin brain-computer interface: Accurate performance from first-session in BCI-naïve subjects, *IEEE Trans. Biomed. Eng.* 55 (10) (2008) 2452–2462, <http://dx.doi.org/10.1109/tbme.2008.923152>.
- [84] H. Yuan, B. He, Brain-computer interfaces using sensorimotor rhythms: Current state and future perspectives, *IEEE Trans. Biomed. Eng.* 61 (5) (2014) 1425–1435, <http://dx.doi.org/10.1109/tbme.2014.2312397>.
- [85] B. Rivet, A. Souloumiac, V. Attina, G. Gibert, xDAWN algorithm to enhance evoked potentials: Application to brain-computer interface, *IEEE Trans. Biomed. Eng.* 56 (8) (2009) 2035–2043, <http://dx.doi.org/10.1109/tbme.2009.2012869>.
- [86] A. Rakotomamonjy, V. Guigue, BCI Competition III: Dataset II- ensemble of SVMs for BCI P300 speller, *IEEE Trans. Biomed. Eng.* 55 (3) (2008) 1147–1154, <http://dx.doi.org/10.1109/tbme.2008.915728>.
- [87] J. Wessberg, C.R. Stambaugh, J.D. Kralik, P.D. Beck, M. Laubach, J.K. Chapin, J. Kim, S.J. Biggs, M.A. Srinivasan, M.A.L. Nicolelis, Real-time prediction of hand trajectory by ensembles of cortical neurons in primates, *Nature* 408 (2000) 361, <http://dx.doi.org/10.1038/35042582>.
- [88] D.M. Taylor, S.I.H. Tillery, A.B. Schwartz, Direct cortical control of 3D neuroprosthetic devices, *Science* 296 (5574) (2002) 1829–1832, <http://dx.doi.org/10.1126/science.1070291>, <http://science.sciencemag.org/content/296/5574/1829>.
- [89] M.L. Homer, A.V. Nurmikko, J.P. Donoghue, L.R. Hochberg, Implants and decoding for intracortical brain computer interfaces, *Annu. Rev. Biomed. Eng.* 15 (2013) 383–405.
- [90] E.K. Chadwick, D. Blana, J.D. Simmeral, J. Lambrecht, S.P. Kim, A.S. Cornwell, D.M. Taylor, L.R. Hochberg, J.P. Donoghue, R.F. Kirsch, Continuous neuronal ensemble control of simulated arm reaching by a human with tetraplegia, *J. Neural Eng.* 8 (3) (2011) 34003, <http://stacks.iop.org/1741-2552/8/i=3/a=034003>.
- [91] L.R. Hochberg, D. Bacher, B. Jarosiewicz, N.Y. Masse, J.D. Simmeral, J. Vogel, S. Haddadin, J. Liu, S.S. Cash, P. Van der, J.P. Donoghue, Reach and grasp by people with tetraplegia using a neurally controlled robotic arm, *Nature* 485 (2012) 372.
- [92] C. Pandarinath, P. Nuyujukian, C.H. Blabé, B.L. Sorice, J. Saab, F.R. Willett, L.R. Hochberg, K.V. Shenoy, J.M. Henderson, High performance communication by people with paralysis using an intracortical brain-computer interface, in: S. Kastner (Ed.), *eLife* 6 (2017) e18554, <http://dx.doi.org/10.7554/elife.18554>, <https://doi.org/10.7554/elife.18554>.
- [93] J.D. Simmeral, S.-P. Kim, M.J. Black, J.P. Donoghue, L.R. Hochberg, Neural control of cursor trajectory and click by a human with tetraplegia 1000 days after implant of an intracortical microelectrode array, *J. Neural Eng.* 8 (2) (2011) 25027, <http://stacks.iop.org/1741-2552/8/i=2/a=025027>.
- [94] R.T. Lauer, P.H. Peckham, K.L. Kilgore, W.J. Heetderks, Applications of cortical signals to neuroprosthetic control: a critical review, *IEEE Trans. Rehabil. Eng.* 8 (2) (2000) 205–208, <http://dx.doi.org/10.1109/86.847817>.
- [95] E. Musk, et al., An integrated brain-machine interface platform with thousands of channels, *J. Med. Internet Res.* 21 (10) (2019) e16194.
- [96] J.E. Zimmerman, P. Thiene, J.T. Harding, Design and operation of stable rf-biased superconducting point-contact quantum devices, and a note on the properties of perfectly clean metal contacts, *J. Appl. Phys.* 41 (4) (1993) 1572–1580.
- [97] B.J. Schwartz, Magnetic source imaging as a clinical tool in functional brain mapping, *GEC Review* 14 (2) (1999) 124–143.
- [98] C.L. Reed, D.J. Hagler Jr, K. Marinovic, A. Dale, E. Halgren, Sequences of cortical activation for tactile pattern discrimination using magnetoencephalography, *Neuroreport* 20 (10) (2009) 941–945.
- [99] O. Hauk, D.G. Wakeman, R. Henson, Comparison of noise-normalized minimum norm estimates for MEG analysis using multiple resolution metrics, *Neuroimage* 54 (3) (2011) 1966–1974.
- [100] A.E. Hramov, N.S. Frolov, V.A. Maksimenko, V.V. Makarov, A.A. Koronovskii, J. Garcia-Prieto, L.F. Antón-Toro, F. Maestú, A.N. Pisarchik, Artificial neural network detects human uncertainty, *Chaos* 28 (3) (2018) 33607, <http://dx.doi.org/10.1063/1.5002892>.
- [101] S.I. Dimitriadis, M.E. López, R. Brufa, P. Cuesta, A. Marcos, F. Maestú, E. Pereda, How to build a functional connectomic biomarker for mild cognitive impairment from source reconstructed MEG resting-state activity: The combination of ROI representation and connectivity estimator matters, *Front. Neurosci.* 12 (2018).
- [102] S. Baillet, J.C. Mosher, R.M. Leahy, Electromagnetic brain mapping, *IEEE Signal Process. Mag.* 18 (6) (2001) 14–30, <http://dx.doi.org/10.1109/79.962275>.
- [103] J. Mellinger, G. Schalk, C. Braun, H. Preissl, W. Rosenstiel, N. Birbaumer, A. Kubler, An {MEG}-based brain-computer interface (BCI), *NeuroImage* 36 (3) (2007) 581–593, <http://dx.doi.org/10.1016/j.neuroimage.2007.03.019>, <http://www.sciencedirect.com/science/article/pii/S1053811907002261>.
- [104] J.N. Mak, J.R. Wolpaw, Clinical applications of brain-computer interfaces: current state and future prospects, *IEEE Rev. Biomed. Eng.* 2 (2009) 187.
- [105] D. Cohen, Magnetoencephalography: detection of the brain's electrical activity with a superconducting magnetometer, *Science* 175 (4022) (1972) 664–666.
- [106] R. Hari, O.V. Lounasmaa, Recording and interpretation of cerebral magnetic fields, *Science* 244 (4903) (1989) 432–436.
- [107] T. Lal, M. Schröder, J. Hill, H. Preissl, T. Hinterberger, J. Mellinger, M. Bogdan, W. Rosenstiel, T. Hofmann, N. Birbaumer, B. Schölkopf, A brain computer interface with online feedback based on magneto-encephalography, in: L. De Raedt, S. Wrobel (Eds.), *Proceedings of the 22nd International Conference on Machine Learning*, 2005, pp. 465–472.

- [108] V. Shah, R.T. Wakai, A compact, high performance atomic magnetometer for biomedical applications, *Phys. Med. Biol.*..
- [109] C. Lin, T. Tierney, N. Holmes, E. Boto, J. Leggett, S. Bestmann, R. Bowtell, G. Brookes, R. Miall, Using optically pumped magnetometers to measure magnetoencephalographic signals in the human cerebellum, *J. Physiol.*..
- [110] E. Boto, N. Holmes, J. Leggett, G. Roberts, V. Shah, S. Meyer, L. Munoz, K. Mullinger, T. Tierney, S. Bestmann, G. Barnes, R. Bowtell, M. Brookes, Moving magnetoencephalography towards real-world applications with a wearable system, *Nature* 555 (7698) (2018) 657–661, <http://dx.doi.org/10.1038/nature26147>.
- [111] N. Holmes, J. Leggett, E. Boto, G. Roberts, R.M. Hill, T.M. Tierney, V. Shah, G.R. Barnes, M.J. Brookes, R. Bowtell, A bi-planar coil system for nulling background magnetic fields in scalp mounted magnetoencephalography, *NeuroImage* 181 (2018) 760–774, <http://dx.doi.org/10.1016/j.neuroimage.2018.07.028>.
- [112] D. Barry, T. Tierney, N. Holmes, E. Boto, G. Roberts, J. Leggett, R. Bowtell, M. Brookes, G. Barnes, E. Maguire, Imaging the human hippocampus with optically-pumped magnetometers, *NeuroImage* 203 (2019) 116192, <http://dx.doi.org/10.1016/j.neuroimage.2019.116192>.
- [113] E. Boto, S.S. Meyer, V. Shah, O. Alem, S. Knappe, P. Kruger, T.M. Fromhold, M. Lim, P.M. Glover, P.G. Morris, R. Bowtell, G.R. Barnes, M.J. Brookes, A new generation of magnetoencephalography: Room temperature measurements using optically-pumped magnetometers, *NeuroImage* 149 (2017) 404–414, <http://dx.doi.org/10.1016/j.neuroimage.2017.01.034>.
- [114] T. Tierney, N. Holmes, S. Meyer, E. Boto, G. Roberts, J. Leggett, S. Buck, L. Duque-Muñoz, V. Litvak, S. Bestmann, T. Baldeweg, R. Bowtell, M. Brookes, G. Barnes, Cognitive neuroscience using wearable magnetometer arrays: Non-invasive assessment of language function, *NeuroImage* 149 (2017) 404–414, <http://dx.doi.org/10.1016/j.neuroimage.2017.01.034>.
- [115] A. Paek, A. Kilicarslan, B. Korenko, V. Gerginov, S. Knappe, J. Contreras-Vidal, Towards a portable magnetoencephalography based brain computer interface with optically-pumped magnetometers, *Annu. Int. Conf. IEEE Eng. Med. Biol. Soc.* 2020 Jul. (2020) 3420–3423, <http://dx.doi.org/10.1109/EMBC4109.2020.9176159>.
- [116] A. Borna, T. Carter, J. Goldberg, A. Colombo, Y. Jau, C. Berry, J. McKay, J. Stephen, M. Weisend, P. Schwindt, A 20-channel magnetoencephalography system based on optically pumped magnetometers, *Phys. Med. Biol.* 62 (23) (2017) 8909–8923, <http://dx.doi.org/10.1088/1361-6560/aa93d1>.
- [117] J. Iivaniainen, R. Zetter, K. Hakkariinen, L. Parkkonen, On-scalp MEG system utilizing an actively shielded array of optically-pumped magnetometers, *NeuroImage* 194 (23) (2019) 244–258, <http://dx.doi.org/10.1016/j.neuroimage.2019.03.022>.
- [118] M.S.M. Chow, S.L. Wu, S.E. Webb, K. Gluskin, D.T. Yew, Functional magnetic resonance imaging and the brain: A brief review, *World J. Radiol.* 9 (2017) 5–9.
- [119] G.H. Glover, Overview of functional magnetic resonance imaging, *Neurosurgery Clin. North America* 22 (2) (2011) 133–139, <http://dx.doi.org/10.1016/j.nec.2010.11.001>, <http://www.sciencedirect.com/science/article/pii/S1042368010001129>.
- [120] G. Deshpande, D. Rangaprakash, L. Oeding, A. Cichocki, X.P. Hu, A new generation of brain-computer interfaces driven by discovery of latent EEG-fMRI linkages using tensor decomposition, *Front. Neurosci.* 11 (2017) 246, <http://dx.doi.org/10.3389/fnins.2017.00246>, <https://www.frontiersin.org/article/10.3389/fnins.2017.00246>.
- [121] N. Weiskopf, R. Sitaran, O. Josephs, R. Veit, F. Scharnowski, R. Goebel, N. Birbaumer, R. Deichmann, K. Mathiak, Real-time functional magnetic resonance imaging: methods and applications, *Magn. Reson. Imag.* 25 (6) (2007) 989–1003, <http://dx.doi.org/10.1016/j.mri.2007.02.007>, <http://www.sciencedirect.com/science/article/pii/S0730725X07001725>.
- [122] R. Christopher deCharms, Applications of real-time fMRI, *Nat. Rev. Neurosci.* 9 (2008) 720, <http://dx.doi.org/10.1038/nrn2414>.
- [123] B.D. Ward, Y. Mazaheri, Information transfer rate in fMRI experiments measured using mutual information theory, *J. Neurosci. Methods* 167 (1) (2008) 22–30, <http://dx.doi.org/10.1016/j.jneumeth.2007.06.027>, <http://www.sciencedirect.com/science/article/pii/S0165027007003081>.
- [124] A. Villringer, J. Planck, C. Hock, L. Schleinkofer, U. Dirnagl, Near infrared spectroscopy (NIRS): A new tool to study hemodynamic changes during activation of brain function in human adults, *Neurosci. Lett.* 154 (1) (1993) 101–104, [http://dx.doi.org/10.1016/0304-3940\(93\)90181-j](http://dx.doi.org/10.1016/0304-3940(93)90181-j), <http://www.sciencedirect.com/science/article/pii/030439409390181j>.
- [125] G. Taga, F. Homae, H. Watanabe, Effects of source-detector distance of near infrared spectroscopy on the measurement of the cortical hemodynamic response in infants, *NeuroImage* 38 (3) (2007) 452–460, <http://dx.doi.org/10.1016/j.neuroimage.2007.07.050>, <https://doi.org/10.1016/j.neuroimage.2007.07.050>.
- [126] J. Shin, S. Kang, M. Sung, J. Kim, Y. Kim, J. Jeong, A study on information transfer rate by brain-computer interface (BCI) using functional near-infrared spectroscopy (fNIRS), in: 2013 International Winter Workshop on Brain-Computer Interface (BCI), 2013, pp. 32–33, <http://dx.doi.org/10.1109/iww-bci.2013.6506620>.
- [127] S.D. Power, A. Kushki, T. Chau, Towards a system-paced near-infrared spectroscopy brain-computer interface: differentiating prefrontal activity due to mental arithmetic and mental singing from the no-control state, *J. Neural Eng.* 8 (6) (2011) 66004, <http://stacks.iop.org/1741-2552/8/i=6/a=066004>.
- [128] G. Gratton, C.R. Brumback, B.A. Gordon, M.A. Pearson, K.A. Low, M. Fabiani, Effects of measurement method, wavelength, and source-detector distance on the fast optical signal, *NeuroImage* 32 (4) (2006) 1576–1590.
- [129] X.-S. Hu, K.-S. Hong, S.S. Ge, Recognition of stimulus-evoked neuronal optical response by identifying chaos levels of near-infrared spectroscopy time series, *Neurosci. Lett.* 504 (2) (2011) 115–120.
- [130] A. Akin, D. Bilensoy, U.E. Emir, M. Gülsöy, S. Candansayar, H. Bolay, Cerebrovascular dynamics in patients with migraine: near-infrared spectroscopy study, *Neurosci. Lett.* 400 (1–2) (2006) 86–91.
- [131] K. Yoshino, T. Kato, Vector-based phase classification of initial dips during word listening using near-infrared spectroscopy, *NeuroReport* 23 (16) (2012) 947–951.
- [132] S.M. Coyle, T.E. Ward, C.M. Markham, Brain-computer interface using a simplified functional near-infrared spectroscopy system, *J. Neural Eng.* 4 (3) (2007) 219.
- [133] N. Naseer, K.-S. Hong, fNIRS-based brain-computer interfaces: a review, *Front. Hum. Neurosci.* 9 (2015) 3.
- [134] P.W. McCormick, M. Stewart, G. Lewis, M. Dujovny, J.I. Ausman, Intracerebral penetration of infrared light, *J. Neurosurg.* 76 (2) (1992) 315–318.
- [135] L. Gagnon, M.A. Yücel, M. Dehaes, R.J. Cooper, K.L. Perdue, J. Selb, T.J. Huppert, R.D. Hoge, D.A. Boas, Quantification of the cortical contribution to the NIRS signal over the motor cortex using concurrent NIRS-fMRI measurements, *NeuroImage* 59 (4) (2012) 3933–3940.
- [136] S. Luu, T. Chau, Decoding subjective preference from single-trial near-infrared spectroscopy signals, *J. Neural Eng.* 6 (1) (2008) 16003.
- [137] S.D. Power, A. Kushki, T. Chau, Towards a system-paced near-infrared spectroscopy brain-computer interface: differentiating prefrontal activity due to mental arithmetic and mental singing from the no-control state, *J. Neural Eng.* 8 (6) (2011) 66004.
- [138] S.D. Power, A. Kushki, T. Chau, Automatic single-trial discrimination of mental arithmetic, mental singing and the no-control state from prefrontal activity: toward a three-state {NIRS-BCI}, *BMC Res. notes* 5 (1) (2012) 141.
- [139] S.D. Power, A. Kushki, T. Chau, Intersession consistency of single-trial classification of the prefrontal response to mental arithmetic and the no-control state by NIRS, *PLoS One* 7 (7) (2012) e37791.
- [140] N. Naseer, M.J. Hong, K.-S. Hong, Online binary decision decoding using functional near-infrared spectroscopy for the development of brain-computer interface, *Exp. Brain Res.* 232 (2) (2014) 555–564.
- [141] M.J. Khan, M.J. Hong, K.-S. Hong, Decoding of four movement directions using hybrid NIRS-eeg brain-computer interface, *Front. Hum. Neurosci.* 8 (2014) 244.

- [142] R. Sitaram, H. Zhang, C. Guan, M. Thulasidas, Y. Hoshi, A. Ishikawa, K. Shimizu, N. Birbaumer, Temporal classification of multichannel near-infrared spectroscopy signals of motor imagery for developing a brain-computer interface, *NeuroImage* 34 (4) (2007) 1416–1427.
- [143] N. Naseer, K.-S. Hong, Classification of functional near-infrared spectroscopy signals corresponding to the right-and left-wrist motor imagery for development of a brain-computer interface, *Neurosci. Lett.* 553 (2013) 84–89.
- [144] A. Vuckovic, F. Sepulveda, A two-stage four-class BCI based on imaginary movements of the left and the right wrist, *Med. Eng. Phys.* 34 (7) (2012) 964–971.
- [145] V.A. Maksimenko, S.A. Kurkin, E.N. Pitsik, V.Y. Musatov, A.E. Runnova, T.Y. Efremova, A.E. Hramov, A.N. Pisarchik, Artificial neural network classification of motor-related EEG: An increase in classification accuracy by reducing signal complexity, *Complexity* 2018 (2018) <http://dx.doi.org/10.1155/2018/9385947>.
- [146] Y. Tran, A. Craig, P. Boord, D. Craig, Using independent component analysis to remove artifact from electroencephalographic measured during stuttered speech, *Med. Biol. Eng. Comput.* 42 (2004) 627–633.
- [147] U. Elena, I. Jorge, A. Manuel, V. Miguel, V. César, A. Julio, Independent component analysis removing artifacts in ictal recordings, *Epilepsia* 45 (9) (2004) 1071–1078.
- [148] V.A. Maksimenko, V.V. Grubov, D.V. Kirsanov, Use of parallel computing for analyzing big data in EEG studies of ambiguous perception, in: *Dynamics and Fluctuations in Biomedical Photonics XV*, 10493, International Society for Optics and Photonics, 2018, p. 104931H.
- [149] M.M. Botvinick, T.S. Braver, D.M. Barch, C.S. Carter, J.D. Cohen, Conflict monitoring and cognitive control, *Psychol. Rev.* 108 (3) (2001) 624.
- [150] J.M. Nunez, B.J. Casey, T. Egner, T. Hare, J. Hirsch, Intentional false responding shares neural substrates with response conflict and cognitive control, *NeuroImage* 25 (1) (2005) 267–277.
- [151] C.D. Von Gunten, H.I. Volpert-Esmond, B.D. Bartholow, Temporal dynamics of reactive cognitive control as revealed by event-related brain potentials, *Psychophysiology* 55 (3) (2018) e13007.
- [152] V.A. Maksimenko, A.E. Hramov, V.V. Grubov, V.O. Nedaivozov, V.V. Makarov, A.N. Pisarchik, Nonlinear effect of biological feedback on brain attentional state, *Nonlinear Dynam.* 95 (3) (2019) 1923–1939, <http://dx.doi.org/10.1007/s11071-018-4668-1>.
- [153] C. Jeunet, F. Lotte, J.-M. Batail, P. Philip, J.-A.M. Franchi, Using recent BCI literature to deepen our understanding of clinical neurofeedback: A short review, *Neuroscience* 378 (2018) 225–233.
- [154] N. Omejc, B. Rojc, P.P. Battaglini, U. Marusic, Review of the therapeutic neurofeedback method using electroencephalography: EEG neurofeedback, *Bosn. J. Basic Med. Sci.* (2018) <http://dx.doi.org/10.17305/bjbjms.2018.3785>.
- [155] V. Maksimenko, A. Badarin, V. Nedaivozov, D. Kirsanov, A. Hramov, Brain-computer interface on the basis of EEG system encephalan, in: Saratov Fall Meeting 2017: Laser Physics and Photonics XVIII; and Computational Biophysics and Analysis of Biomedical Data IV, 10717, International Society for Optics and Photonics, 2018, p. 107171R, <http://dx.doi.org/10.1117/12.2314651>.
- [156] S. Koganemaru, Y. Mikami, H. Maezawa, S. Ikeda, K. Ikoma, T. Mima, Neurofeedback control of the human gabaergic system using non-invasive brain stimulation, *Neuroscience* 380 (2018) 38–48.
- [157] E.T. Erdogan, S.S. Saydam, A. Kurt, S. Karamursel, Anodal transcranial direct current stimulation of the motor cortex in healthy volunteers, *Neurophysiology* 50 (2) (2018) 124–130.
- [158] F. Galán, M.R. Baker, K. Alter, S.N. Baker, Degraded EEG decoding of wrist movements in absence of kinaesthetic feedback, *Hum. Brain map* 36 (2) (2015) 643–654.
- [159] F. Galán, S.N. Baker, Deafferented controllers: a fundamental failure mechanism in cortical neuroprosthetic systems, *Front. Behav. Neurosci.* 9 (2015) 186.
- [160] C. Klaes, Y. Shi, S. Kellis, J. Minxha, B. Revechkis, R.A. Andersen, A cognitive neuroprosthetic that uses cortical stimulation for somatosensory feedback, *J. Neural Eng.* 11 (5) (2014) 56024.
- [161] T. Callier, E.W. Schluter, G.A. Tabot, L.E. Miller, F.V. Tenore, S.J. Bensmaia, Long-term stability of sensitivity to intracortical microstimulation of somatosensory cortex, *J. Neural Eng.* 12 (5) (2015) 56010.
- [162] M.S. Treder, B. Blankertz, (C)overt attention and visual speller design in an ERP-based brain-computer interface, *Behav. Brain Funct.* 6 (1) (2010) 28, <https://doi.org/10.1186/1744-9081-6-28>.
- [163] G. Pfurtscheller, B. Allison, G. Bauernfeind, C. Brunner, T. Solis Escalante, R. Scherer, T.O. Zander, G. Mueller-Putz, C. Neuper, N. Birbaumer, The hybrid BCI, *Front. Neurosci.* 4 (2010) 3, <http://dx.doi.org/10.3389/fnpro.2010.00003>, <https://www.frontiersin.org/article/10.3389/fnpro.2010.00003>.
- [164] C. Kubler, N. Birbaumer, Brain-computer interfaces and communication in paralysis: Extinction of goal directed thinking in completely paralysed patients?, *Clin. Neurophysiol.* 119 (11) (2018) 2658–2666, <http://dx.doi.org/10.1016/j.clinph.2008.06.019>.
- [165] W. Deng, I. Papavasileiou, Z. Qiao, W. Zhang, K.-Y. Lam, H. Song, Advances in automation technologies for lower-extremity neurorehabilitation: A review and future challenges, *IEEE Rev. Biomed. Eng.* (2018).
- [166] M. Mihara, I. Miyai, N. Hattori, M. Hatakenaka, H. Yagura, T. Kawano, M. Okibayashi, N. Danjo, A. Ishikawa, Y. Inoue, et al., Neurofeedback using real-time near-infrared spectroscopy enhances motor imagery related cortical activation, *PLoS One* 7 (3) (2012) e32234.
- [167] J.H. Gruzelier, EEG-Neurofeedback for optimising performance. I: A review of cognitive and affective outcome in healthy participants, *Neurosci. Biobehav. Rev.* 44 (2014) 124–141.
- [168] F. Pichiorri, F.D.V. Fallani, F. Cincotti, F. Babiloni, M. Molinari, S.C. Kleih, C. Neuper, A. Kübler, D. Mattia, Sensorimotor rhythm-based brain-computer interface training: the impact on motor cortical responsiveness, *J. Neural Eng.* 8 (2) (2011) 25020.
- [169] F. Taya, Y. Sun, F. Babiloni, N. Thakor, A. Bezerianos, Brain enhancement through cognitive training: a new insight from brain connectome, *Front. Syst. Neurosci.* 9 (2015) 44, <http://dx.doi.org/10.3389/fnsys.2015.00044>, <https://www.frontiersin.org/article/10.3389/fnsys.2015.00044>.
- [170] E.W. Sellers, T.M. Vaughan, J.R. Wolpaw, A brain-computer interface for long-term independent home use, *Amyotroph. Lateral Scler.* 11 (5) (2010) 449–455, <http://dx.doi.org/10.3109/17482961003777470>.
- [171] J.R. Wolpaw, E. Wolpaw, Brain-computer interfaces: Principles and practice, Oxford University Press, 2012.
- [172] H. Ramoser, J. Müller-Gerking, G. Pfurtscheller, Optimal spatial filtering of single trial EEG during imagined hand movement, *IEEE Trans. Rehabil. Eng.* 8 (2000) 441–446.
- [173] M. Grosse-Wentrup, M. Buss, Multiclass common spatial patterns and information theoretic feature extraction, *IEEE Trans. Biomed. Eng.* 55 (8) (2008) 1991–2000, <http://dx.doi.org/10.1109/tbme.2008.921154>.
- [174] S. Lemm, B. Blankertz, G. Curio, K. Müller, Spatio-spectral filters for improving the classification of single trial EEG, *IEEE Trans. Biomed. Eng.* 52 (9) (2005) 1541–1548, <http://dx.doi.org/10.1109/tbme.2005.851521>.
- [175] H. Park, J. Kim, B. Min, B. Lee, Motor imagery EEG classification with optimal subset of wavelet based common spatial pattern and kernel extreme learning machine, in: 2017 39th Annual International Conference of the IEEE Engineering in Medicine and Biology Society, EMBC, 2017, pp. 2863–2866, <http://dx.doi.org/10.1109/embc.2017.8037454>.
- [176] E.A. Mousavi, J.J. Maller, P.B. Fitzgerald, B.J. Lithgow, Wavelet common spatial pattern in asynchronous offline brain computer interfaces, *Biomed. Signal Process Control* 6 (2) (2011) 121–128, <http://dx.doi.org/10.1016/j.bspc.2010.08.003>.
- [177] T. Hinterberger, S. Schmidt, N. Neumann, J. Mellinger, B. Blankertz, G. Curio, N. Birbaumer, Brain-computer communication and slow cortical potentials, *IEEE Trans. Biomed. Eng.* 51 (6) (2004) 1011–1018, <http://dx.doi.org/10.1109/tbme.2004.827067>.

- [178] B. Obermaier, G.R. Muller, G. Pfurtscheller, "virtual keyboard" controlled by spontaneous EEG activity, *IEEE Trans. Neural Syst. Rehab. Eng.* 11 (4) (2003) 422–426, <http://dx.doi.org/10.1109/tnsre.2003.816866>.
- [179] L.A. Farwell, E. Donchin, Talking off the top of your head: toward a mental prosthesis utilizing event related brain potentials, *EEG Clin. Neurophysiol.* 70 (1988) 510.
- [180] S. Silvoni, C. Volpato, M. Cavinato, M. Marchetti, K. Priftis, A. Merico, P. Tonin, K. Koutsikos, F. Beverina, F. Piccione, P300-based brain-computer interface communication: evaluation and follow-up in amyotrophic lateral sclerosis, *Front. Neurosci.* 3 (2009) 1, <http://dx.doi.org/10.3389/neuro.20.001.2009>.
- [181] Intendix. Available online: <http://www.intendix.com/> (Accessed on 13 November 2018).
- [182] Neurochat. Available online: <http://neurochat.pro/> (Accessed on 26 March 2021).
- [183] R. Fazel-Rezai, K. Abhari, A region-based P300 speller for brain-computer interface, *Canad. J. Electr. Comput. Eng.* 34 (3) (2009) 81–85.
- [184] A. Furdea, S. Halder, D.J. Krusinski, D. Gross, F. Nijboer, N. Birbaumer, A. Kubler, An auditory oddball (P300) spelling system for brain-computer interfaces, *Psychophysiology* 46 (3) (2009) 617–625.
- [185] A. Kubler, A. Furdea, S. Halder, E.M. Hammer, F. Nijboer, B. Kotchoubey, A brain–computer interface controlled auditory event-related potential (P300) spelling system for locked-in patients, *Ann. New York Acad. Sci.* 1157 (1) (2009) 90–100.
- [186] M. Schreuder, T. Rost, M. Tangermann, Listen, you are writing! speeding up online spelling with a dynamic auditory BCI, *Front. Neurosci.* 5 (2011) 112.
- [187] M.J. Vansteensel, E.G. Pels, M.G. Bleichner, M.P. Branco, T. Denison, Z.V. Freudenburg, P. Gosselaar, S. Leinders, T.H. Ottens, M.A. Van Den Boom, et al., Fully implanted brain–computer interface in a locked-in patient with ALS, *N. Engl. J. Med.* 375 (21) (2016) 2060–2066.
- [188] M. Naito, Y. Michioka, K. Ozawa, Y. Ito, M. Kiguchi, T. Kanazawa, A communication means for totally locked-in ALS patients based on changes in cerebral blood volume measured with near-infrared light, *IEICE Trans. Inform. Syst.* 90 (7) (2007) 1028–1037.
- [189] V. Martínez-Cagigal, J. Gómez-Pilar, D. Álvarez, R. Hornero, An asynchronous P300-based brain-computer interface web browser for severely disabled people, *IEEE Trans. Neural Syst. Rehabil. Eng.* 25 (8) (2017) 1332–1342, <http://dx.doi.org/10.1109/tnsre.2016.2623381>.
- [190] A.G. Yehia, S. Eldawlatly, M. Taher, Webb: A brain-computer interface web browser based on steady-state visual evoked potentials, in: 2017 12th International Conference on Computer Engineering and Systems, ICICES 2017, pp. 52–57, <http://dx.doi.org/10.1109/icces.2017.8275277>.
- [191] A.A. Karim, T. Hinterberger, J. Richter, J. Mellinger, N. Neumann, H. Flor, A. Kubler, N. Birbaumer, Neural internet: Web surfing with brain potentials for the completely paralyzed, *Neurorehab. Neural Repair* 20 (4) (2006) 508–515, <https://doi.org/10.1177/1545968306290661>.
- [192] M. Bensch, A.A. Karim, J. Mellinger, T. Hinterberger, M. Tangermann, M. Bogdan, W. Rosenstiel, N. Birbaumer, Nessi: an EEG-controlled web browser for severely paralyzed patients, *Comput. Intell. Neurosci.* 2007 (2007) 71863, <https://www.ncbi.nlm.nih.gov/pubmed/18350132>.
- [193] J. Yin, D. Jiang, J. Hu, Design and application of brain-computer interface web browser based on VEP, in: 2009 International Conference on Future BioMedical Information Engineering, FBIE, 2009, pp. 77–80, <http://dx.doi.org/10.1109/fbie.2009.5405788>.
- [194] E.M. Mugler, C.A. Ruf, S. Halder, M. Bensch, A. Kubler, Design and implementation of a P300-based brain-computer interface for controlling an internet browser, *IEEE Trans. Neural Syst. Rehabil. Eng.* 18 (6) (2010) 599–609, <http://dx.doi.org/10.1109/tnsre.2010.2068059>.
- [195] F. Cincotti, D. Mattia, F. Aloise, S. Bufalari, G. Schalk, G. Oriolo, A. Cherubini, M.G. Marciani, F. Babiloni, Non-invasive brain–computer interface system: towards its application as assistive technology, *Brain Res. Bull.* 75 (6) (2008) 796–803.
- [196] L.R. Hochberg, M.D. Serruya, G.M. Friehs, J.A. Mukand, M. Saleh, A.H. Caplan, A. Branner, D. Chen, R.D. Penn, J.P. Donoghue, Neuronal ensemble control of prosthetic devices by a human with tetraplegia, *Nature* 442 (2006) 164–171.
- [197] S. Halder, K. Takano, K. Kansaku, Comparison of four control methods for a five-choice assistive technology, *Front. Hum. Neurosci.* 12 (2018).
- [198] A.A. for the Advancement of Science, et al., Human performance in space: Advancing astronautics research in China, *Science* 345 (6203) (2014) 1522–1522.
- [199] M.D. Serruya, N.G. Hatsopoulos, L. Paninski, M.R. Fellows, J.P. Donoghue, Instant neural control of a movement signal, *Nature* 416 (2002) 141, <https://doi.org/10.1038/416141a>.
- [200] K. Tanaka, K. Matsunaga, H.O. Wang, Electroencephalogram-based control of an electric wheelchair, *IEEE Trans. Robot.* 21 (4) (2005) 762–766, <http://dx.doi.org/10.1109/tro.2004.842350>.
- [201] B. Rebsamen, C. Guan, H. Zhang, C. Wang, C. Teo, M.H. Ang, E. Burdet, A brain controlled wheelchair to navigate in familiar environments, *IEEE Trans. Neural Syst. Rehabil. Eng.* 18 (6) (2010) 590–598.
- [202] I. Iturrate, J.M. Antelis, A. Kubler, J. Minguez, A noninvasive brain-actuated wheelchair based on a P300 neurophysiological protocol and automated navigation, *IEEE Trans. Robot.* 25 (3) (2009) 614–627.
- [203] Y. Li, J. Pan, F. Wang, Z. Yu, A hybrid BCI system combining P300 and SSVEP and its application to wheelchair control, *IEEE Trans. Biomed. Eng.* 60 (11) (2013) 3156–3166.
- [204] D. De Venuto, V.F. Annese, G. Mezzina, Real-time P300-based BCI in mechatronic control by using a multi-dimensional approach, *IET Software* 12 (5) (2018) 418–424.
- [205] F. Quandt, F.C. Hummel, The influence of functional electrical stimulation on hand motor recovery in stroke patients: a review, *Exp. Transl. Stroke Med.* 6 (1) (2014) 9.
- [206] G.P. Braz, M. Russold, G.M. Davis, Functional electrical stimulation control of standing and stepping after spinal cord injury: A review of technical characteristics, *Neuromodulation: Technology at the Neural Interface* 12(3) 180–190, <http://dx.doi.org/10.1111/j.1525-1403.2009.00213.x>, <https://onlinelibrary.wiley.com/doi/abs/10.1111/j.1525-1403.2009.00213.x>.
- [207] R.T. Lauer, P.H. Peckham, K.L. Kilgore, EEG-Based control of a hand grasp neuroprosthesis, *Neuroreport* 10 (8) (1999) 1767–1771.
- [208] G. Pfurtscheller, G.R. Müller, J. Pfurtscheller, H.J. Gerner, R. Rupp, 'Thought'-control of functional electrical stimulation to restore hand grasp in a patient with tetraplegia, *Neurosci. Lett.* 351 (1) (2003) 33–36.
- [209] G. Pfurtscheller, C. Guger, G. Müller, G. Krausz, C. Neuper, Brain oscillations control hand orthosis in a tetraplegic, *Neurosci. Lett.* 292 (3) (2000) 211–214.
- [210] G.R. Muller-Putz, R. Scherer, G. Pfurtscheller, R. Rupp, EEG-based neuroprosthesis control: A step towards clinical practice, *Neurosci. Lett.* 382 (1) (2005) 169–174, <http://dx.doi.org/10.1016/j.neulet.2005.03.021>.
- [211] J. Gutiérrez-Martínez, Neuroprostheses: Significance in gait rehabilitation, in: *Advanced Technologies for the Rehabilitation of Gait and Balance Disorders*, Springer, 2018, pp. 427–446.
- [212] K.K. Ang, C. Guan, K.S. Phua, C. Wang, L. Zhou, K.Y. Tang, E. Joseph, J. Gopal, C.W.K. Kuah, K.S.G. Chua, Brain-computer interface-based robotic end effector system for wrist and hand rehabilitation: results of a three-armed randomized controlled trial for chronic stroke, *Front. Neuroeng.* 7 (2014) 30.
- [213] A.A. Frolov, O. Mokienko, R. Lyukmanov, E. Biryukova, S. Kotov, L. Turbina, G. Nadareyshvily, Y. Bushkova, Post-stroke rehabilitation training with a motor-imagery-based brain-computer interface (BCI)-controlled hand exoskeleton: a randomized controlled multicenter trial, *Front. Neurosci.* 11 (2017) 400.
- [214] A.A. Frolov, D. Húsek, E. Biryukova, P.D. Bobrov, O. Mokienko, A.V. Alexandrov, Principles of motor recovery in post-stroke patients using hand exoskeleton controlled by the brain-computer interface based on motor imagery, *Neural Network World* 27 (1) (2017) 107.
- [215] Z.O. Khokhar, Z.G. Xiao, C. Menon, Surface EMG pattern recognition for real-time control of a wrist exoskeleton, *Biomed. Eng. Online* 9 (1) (2010) 41.

- [216] T. Lenzi, S.M.M. De Rossi, N. Vitiello, M.C. Carrozza, Intention-based EMG control for powered exoskeletons, *IEEE Trans. Biomed. Eng.* 59 (8) (2012) 2180–2190.
- [217] M. Mulas, M. Folgheraiter, G. Gini, An EMG-controlled exoskeleton for hand rehabilitation, in: 9th International Conference on Rehabilitation Robotics, 2005. ICORR 2005., IEEE, 2005, pp. 371–374.
- [218] S. Silvoni, A. Ramos-Murguialday, M. Cavinato, C. Volpato, G. Cisotto, A. Turolla, F. Piccione, N. Birbaumer, Brain-computer interface in stroke: a review of progress, *Clin. EEG Neurosci.* 42 (4) (2011) 245–252.
- [219] J.E. Huggins, P.A. Wren, K.L. Gruis, What would brain-computer interface users want? Opinions and priorities of potential users with amyotrophic lateral sclerosis, *Amyotroph. Lateral Scler.* 12 (5) (2011) 318–324.
- [220] World Health Organization, et al., *World health statistics 2018: monitoring health for the SDGs, sustainable development goals*, World Health Organization, 2018.
- [221] S. Paolucci, M. Bragoni, P. Coiro, D. De Angelis, F.R. Fusco, D. Morelli, V. Venturiero, L. Pratesi, Quantification of the probability of reaching mobility independence at discharge from a rehabilitation hospital in nonwalking early ischemic stroke patients: a multivariate study, *Cerebrovasc. Dis.* 26 (1) (2008) 16–22.
- [222] I.V. Orlov, Y.K. Stolbkov, Y.P. Gerasimenko, Vestibular prosthesis: concept, approaches, results, *Russ. Physiol. J.* 103 (3) (2017) 250–267.
- [223] S.M. LaConte, Decoding fMRI brain states in real-time, *Neuroimage* 56 (2) (2011) 440–454.
- [224] N. Weiskopf, Real-time fMRI and its application to neurofeedback, *Neuroimage* 62 (2) (2012) 682–692.
- [225] M. Mihara, N. Hattori, M. Hatakenaka, H. Yagura, T. Kawano, T. Hino, I. Miyai, Near-infrared spectroscopy-mediated neurofeedback enhances efficacy of motor imagery-based training in poststroke victims: a pilot study, *Stroke* 44 (4) (2013) 1091–1098.
- [226] C.M. Sinclair, M.C. Gasper, A.S. Blum, Basic electronics in clinical neurophysiology, in: *The Clinical Neurophysiology Primer*, Springer, 2007, pp. 3–18.
- [227] J.B. Caplan, J.R. Madsen, S. Raghavachari, M.J. Kahana, Distinct patterns of brain oscillations underlie two basic parameters of human maze learning, *J. Neurophysiol.* 86 (1) (2001) 368–380.
- [228] A. Berenyi, M. Belluscio, D. Mao, G. Buzsaki, Closed-loop control of epilepsy by transcranial electrical stimulation, *Science* 337 (6095) (2012) 735–737.
- [229] R.N. Roy, J. Frey, Neurophysiological markers for passive brain–computer interfaces, *Brain–Computer Interfaces 1: Foundations and Methods* (2016) 85–100.
- [230] G. Borghini, P. Aricò, L. Astolfi, J. Toppi, F. Cincotti, D. Mattia, P. Cherubino, G. Vecchiato, A.G. Maglione, I. Graziani, et al., Frontal EEG theta changes assess the training improvements of novices in flight simulation tasks, in: 2013 35th Annual International Conference of the IEEE Engineering in Medicine and Biology Society, EMBC, IEEE, 2013, pp. 6619–6622.
- [231] S.H. Fairclough, Fundamentals of physiological computing, *Interact. Comput.* 21 (1–2) (2009) 133–145.
- [232] A.-M. Brouwer, A. Snelteling, M. Jaswa, O. Flascher, L. Krol, T.O. Zander, Physiological effects of adaptive cruise control behaviour in real driving, in: Proceedings of the 2017 ACM Workshop on an Application-Oriented Approach To BCI Out of the Laboratory, ACM, 2017, pp. 15–19.
- [233] L. Krol, T. Zander, M. Jaswa, O. Flascher, A. Brouwer, Online-capable cleaning of highly artefactual EEG data recorded during real driving, in: Proceedings of the 7th Graz Brain-Computer Interface Conference, 2017, pp. 254–259.
- [234] C. Herff, F. Putze, T. Schultz, Evaluating fNIRS-based workload discrimination in a realistic driving scenario, in: The First Biannual Neuroadaptive Technology Conference, 2017, p. 69.
- [235] A. Reyes-Muñoz, M. Domingo, M. López-Trinidad, J. Delgado, Integration of body sensor networks and vehicular ad-hoc networks for traffic safety, *Sensors* 16 (1) (2016) 107.
- [236] J. Perrier, S. Jongen, E. Vuurman, M.L. Bocca, J.G. Ramaekers, A. Vermeeren, Driving performance and EEG fluctuations during on-the-road driving following sleep deprivation, *Biolog. Psychol.* 121 (2016) 1–11.
- [237] F. Dehais, A. Duprè, G. Di Flumeri, K.J. Verdière, G. Borghini, F. Babiloni, R.N. Roy, Monitoring pilot's cognitive fatigue with engagement features in simulated and actual flight conditions using an hybrid fNIRS-EEG passive BCI, *IEEE SMC* (2018).
- [238] D. Dasari, G. Shou, L. Ding, ICA-Derived EEG correlates to mental fatigue, effort, and workload in a realistically simulated air traffic control task, *Front. Neurosci.* 11 (2017) 297.
- [239] L.-W. Ko, O. Komarov, W.D. Hairston, T.-P. Jung, C.-T. Lin, Sustained attention in real classroom settings: An EEG study, *Front. Hum. Neurosci.* 11 (2017) 388.
- [240] A. Al-Nafjan, M. Hosny, Y. Al-Ohali, A. Al-Wabil, Review and classification of emotion recognition based on EEG brain-computer interface system research: a systematic review, *Appl. Sci.* 7 (12) (2017) 1239.
- [241] I. Daly, L. Chen, S. Zhou, J. Jin, An investigation into the use of six facially encoded emotions in brain-computer interfacing, *Brain-Comput. Interfaces* 3 (1) (2016) 59–73.
- [242] N. Jatupaiboon, S. Pan-ngum, P. Israsena, Real-time EEG-based happiness detection system, *Sci. World J.* 2013 (2013).
- [243] R. Yuvaraj, M. Murugappan, N.M. Ibrahim, K. Sundaraj, M.I. Omar, K. Mohamad, R. Palaniappan, Detection of emotions in Parkinson's disease using higher order spectral features from brain's electrical activity, *Biomed. Signal Process. Control* 14 (2014) 108–116.
- [244] G. Csukly, G. Stefanics, S. Komlósi, I. Czigler, P. Czobor, Event-related theta synchronization predicts deficit in facial affect recognition in schizophrenia., *J. Abnormal Psychol.* 123 (1) (2014) 178.
- [245] U.R. Acharya, V.K. Sudarshan, H. Adeli, J. Santhosh, J.E.W. Koh, A. Adeli, Computer-aided diagnosis of depression using EEG signals, *Eur. Neurol.* 73 (5–6) (2015) 329–336.
- [246] G.M. Bairy, S. Bhat, L.W.J. Eugene, U.C. Niranjan, S.D. Puthankattil, P.K. Joseph, Automated classification of depression electroencephalographic signals using discrete cosine transform and nonlinear dynamics, *J. Med. Imag. Health Inform.* 5 (3) (2015) 635–640.
- [247] M. Akbarfahimi, M. Tehrani-Doost, F. Ghassemi, Emotional face perception in patients with schizophrenia: an event-related potential study, *Neurophysiology* 45 (3) (2013) 249–257.
- [248] C.A. Brenner, S.P. Rumak, A.M.N. Burns, Facial emotion memory in schizophrenia: From encoding to maintenance-related EEG, *Clin. Neurophysiol.* 127 (2) (2016) 1366–1373.
- [249] R. Yuvaraj, M. Murugappan, N.M. Ibrahim, M.I. Omar, K. Sundaraj, K. Mohamad, R. Palaniappan, M. Satiyan, Emotion classification in Parkinson's disease by higher-order spectra and power spectrum features using EEG signals: A comparative study, *J. Integr. Neurosci.* 13 (01) (2014) 89–120.
- [250] A. Schaefer, C.L. Pottage, A.J. Rickart, Electrophysiological correlates of remembering emotional pictures, *Neuroimage* 54 (1) (2011) 714–724.
- [251] I. Daly, D. Williams, A. Kirke, J. Weaver, A. Malik, F. Hwang, E. Miranda, S.J. Nasuto, Affective brain-computer music interfacing, *J. Neural Eng.* 13 (4) (2016) 46022.
- [252] Y.-P. Lin, Y.-H. Yang, T.-P. Jung, Fusion of electroencephalographic dynamics and musical contents for estimating emotional responses in music listening, *Front. Neurosci.* 8 (2014) 94.
- [253] G. Chanel, C. Rebetez, M. Bétrancourt, T. Pun, Emotion assessment from physiological signals for adaptation of game difficulty, *IEEE Trans. Syst. Man Cybern.-A: Syst. Hum.* 41 (6) (2011) 1052–1063.
- [254] F. Taya, Y. Sun, F. Babiloni, N. Thakor, A. Bezerianos, Brain enhancement through cognitive training: a new insight from brain connectome, *Front. Syst. Neurosci.* 9 (2015) 44, <http://dx.doi.org/10.3389/fnsys.2015.00044>.

- [255] V. Grubov, A. Runnova, A. Koronovskii, A. Hramov, Adaptive filtering of electroencephalogram signals using the empirical-modes method, *Tech. Phys. Lett.* 43 (7) (2017) 619–622, <http://dx.doi.org/10.1134/S1063785017070070>.
- [256] S. Makeig, A. Bell, T. Jung, T.J. Sejnowski, Independent component analysis of electroencephalographic data, *Adv. Neural Inf. Process. Syst.* 8 (1996) 145–151.
- [257] C. Joyce, I. Gorodnitsky, M. Kutas, Automatic removal of eye movement and blink artifacts from EEG data using blind component separation, *Psychophysiology* 41 (2004) 313–325.
- [258] A.N. Pavlov, A.E. Hramov, A.A. Koronovskii, E.Y. Sitnikova, V.A. Makarov, A.A. Ovchinnikov, Wavelet analysis in neurodynamics, *Phys.-Usp.* 55 (9) (2012) 845–875, <http://dx.doi.org/10.3367/UFNe.0182.201209a.0905>.
- [259] G. Gratton, M. Coles, E. Donchin, A new method for off-line removal of ocular artifact, *Electroencephalogr. Clin. Neurophysiol.* 55 (1983) 468–484.
- [260] V.V. Grubov, E. Sitnikova, A.N. Pavlov, A.A. Koronovskii, A.E. Hramov, Recognizing of stereotypic patterns in epileptic {EEG} using empirical modes and wavelets, *Physica A* 486 (2017) 206–217, <http://dx.doi.org/10.1016/j.physa.2017.05.091>.
- [261] T. Jung, S. Makeig, M. Westerfield, J. Townsend, E. Courchesne, T. Sejnowski, Removal of eye activity artifacts from visual event-related potentials in normal and clinical subjects, *Clin. Neurophys.* 11 (2000) 1745–1758.
- [262] C. James, C. Hesse, Independent component analysis for biomedical signals, *Physiol. Meas.* 26 (2005) 15–39.
- [263] A. Bell, T. Sejnowski, An information-maximization approach to blind separation and blind deconvolution, *Neural Comput.* 7 (1995) 1129–1159.
- [264] C. James, O. Gibson, Temporally constrained ICA: an application to artifact rejection in electromagnetic brain signal analysis, *IEEE Trans. Biomed. Eng.* 41 (2003) 1108–1116.
- [265] A. Flexer, H. Bauer, J. Pripfl, G. Dorffner, Using {ICA} for removal of ocular artifacts in {EEG} recorded from blind subjects, *Neural Netw.* 18 (2005) 998–1005.
- [266] S. Tong, A. Bezerianos, J. Paul, Y. Zhu, N. Thakor, Removal of {ECG} interference from the {EEG} recordings in small animals using independent component analysis, *J. Neurosci. Methods* 108 (2001) 11–17.
- [267] A. Amari S. Cichocki, H. Yang, A new learning algorithm for blind source separation, *Adv. Neural Inf. Process. Syst.* 8 (1996) 757–763.
- [268] T. Lee, M. Girolami, T. Sejnowski, Independent component analysis using an extended infomax algorithm for mixed subgaussian and supergaussian sources, *Neural Comput.* 11 (1999) 417–441.
- [269] T. Jung, C. Humphries, T. Lee, M. McKeown, V. Iragui, S. Makeig, Removing electroencephalographic artifacts by blind source separation, *Psychophysiology* 37 (2000) 163–178.
- [270] K. Friston, Modes or models: a critique on independent component analysis for fMRI, *Trends Cogn. Sci.* 2 (1998) 373–375.
- [271] A.E. Hramov, A.A. Koronovskii, V.A. Makarov, A.N. Pavlov, E. Sitnikova, *Wavelets in Neuroscience*, Springer Series in Synergetics, Springer, Heidelberg, New York, Dordrecht, London, 2015.
- [272] A.E. Hramov, A.A. Koronovskii, O.I. Moskalenko, M.O. Zhuravlev, R. Jaimes-Reategui, A.N. Pisarchik, Separation of coexisting dynamical regimes in multistate intermittency based on wavelet spectrum energies in an erbium-doped fiber laser, *Phys. Rev. E* 93 (5) (2016) 52218, <http://dx.doi.org/10.1103/physreve.93.052218>.
- [273] E.B. Postnikov, E.A. Lebedeva, Decomposition of strong nonlinear oscillations via modified continuous wavelet transform, *Phys. Rev. E* 82 (5) (2010) 57201.
- [274] I.M. Dremin, O.V. Ivanov, V.A. Nechitailo, Wavelets and their uses, *Phys.-Usp.* 44 (5) (2001) 447–478.
- [275] S. Jaffard, Y. Meyer, R. Ryan, *Wavelets: Tools for Science and Technology*, Philadelphia, SIAM, 2001.
- [276] J.S. Walker, *A Primer on Wavelets and Their Scientific Applications*, Boca Raton, CRC Press, 1999.
- [277] A. Aldroubi, M. Unser, *Wavelets in Medicine and Biology*, CRC-Press, 1996.
- [278] P. Fryzlewicz, S. Van Bellegem, R. Von Sachs, Forecasting non-stationary time series by wavelet process modelling, *Ann. Inst. Statist. Math.* 55 (4) (2003) 737–764.
- [279] A.E. Hramov, A.A. Koronovskii, V.I. Ponomarenko, M.D. Prokhorov, Detection of synchronization from univariate data using wavelet transform, *Phys. Rev. E* 75 (5) (2007) 56207, <http://dx.doi.org/10.1103/PhysRevE.75.056207>.
- [280] T. Kreuz, F. Mormann, R.G. Andrzejak, A. Kraskov, K. Lehnhertz, P. Grassberger, Measuring synchronization in coupled model systems: A comparison of different approaches, *Physica D* 225 (1) (2007) 29–42.
- [281] E. Sitnikova, A.E. Hramov, A.A. Koronovskii, E.L. Luijtelaar, Sleep spindles and spike-wave discharges in EEG: Their generic features, similarities and distinctions disclosed with fourier transform and continuous wavelet analysis, *J. Neurosci. Methods* 180 (2009) 304–316, <http://dx.doi.org/10.1016/j.jneumeth.2009.04.006>.
- [282] E. Sitnikova, A.E. Hramov, V. Grubov, A.A. Koronovsky, Time-frequency characteristics and dynamics of sleep spindles in WAG/Rij rats with absence epilepsy, *Brain Res.* 1543 (2014) 290–299, <http://dx.doi.org/10.1016/j.brainres.2013.11.001>.
- [283] J. Morlet, G. Arens, E. Fourgeau, D. Glard, Wave propagation and sampling theory—Part I: Complex signal and scattering in multilayered media, *Geophysics* 47 (2) (1982) 203–221.
- [284] D.E. Newland, *An Introduction to Random Vibrations, Spectral and Wavelet Analysis*, N. Y.: John Wiley, 1993.
- [285] D.L. Donoho, I.M. Johnstone, G. Kerkyacharian, D. Picardi, Wavelet shrinkage: asymptopia?, *J. R. Stat. Soc. B* 57 (1995) 301–369.
- [286] L. Debnath, *Wavelet Transforms and Their Applications*, Birkhauser, 2002.
- [287] N.P. Castellanos, V.A. Makarov, Recovering EEG brain signals: Artifact suppression with wavelet enhanced independent component analysis, *J. Neurosci. Methods* 158 (2) (2006) 300–312, <http://dx.doi.org/10.1016/j.jneumeth.2006.05.033>, <http://www.sciencedirect.com/science/article/pii/S0165027006002834>.
- [288] A.E. Hramov, V.A. Maksimenko, S.V. Pchelintseva, A.E. Runnova, V.V. Grubov, V.Y. Musatov, M.O. Zhuravlev, A.A. Koronovskii, A.N. Pisarchik, Classifying the perceptual interpretations of a bistable image using EEG and artificial neural networks, *Front. Neurosci.* 11 (2017) 674, <http://dx.doi.org/10.3389/fnins.2017.00674>.
- [289] A.E. Runnova, M.O. Zhuravlev, E.Y. Sitnikova, A. Koronovskii, A.E. Hramov, Removing oculomotor artifacts in human EEG during ambiguous image recognition, *Inform. Control Syst.* 90 (5) (2017) 105–112.
- [290] M. Corbetta, G. Patel, G.L. Shulman, The reorienting system of the human brain: from environment to theory of mind, *Neuron* 58(3) (2008) 306–324.
- [291] N. Ille, P. Berg, M. Scherg, Artifact correction of the ongoing {EEG} using spatial filters based on artifact and brain signal topographies, *J. Clin. Neurophysiol.* 19 (113–124) (2002).
- [292] S. Hoffmann, M. Falkenstein, The correction of eye blink artefacts in the EEG: A comparison of two prominent methods, *PLoS One* 3 (8) (2008) 1–11.
- [293] N. Ille, P. Berg, M. Scherg, Automatic artifact rejection for eeg data using high-order statistics and independent component analysis, in: *Proceedings of the Third International ICA Conference*, December 9–13, 2001, San Diego, USA, 2001, pp. 9–12.
- [294] W. Cheney, D. Kincaid, *Linear Algebra: Theory and Applications*, Sudbury, Jones and Bartlett, 2009.
- [295] A.A. Koronovskii, A.E. Hramov, O.I. Moskalenko, V.V. Grubov, Method for Eye Motor Artifacts Removal on Electroencephalogram, Patent for Invention No 25560388, Official bulletin of the Federal Service for Intellectual Property, Patents and Trademarks. Moscow: FIPS., 2015.

- [296] A. Runnova, M. Zhuravlev, A. Koronovskiy, A. Hramov, Mathematical approach to recover EEG brain signals with artifacts by means of Gram-Schmidt transform, in: Saratov Fall Meeting 2016: Laser Physics and Photonics XVII; and Computational Biophysics and Analysis of Biomedical Data III, 10337, International Society for Optics and Photonics, 2017, p. 103370Y, <http://dx.doi.org/10.1117/12.2267828>.
- [297] N.E. Huang, Z. Shen, *Hilbert-Huang Transform and Its Applications*, Singapore: World Scientific, 2005.
- [298] A. Pavlov, A. Filatova, A. Hramov, Digital filtering and time-and-frequency analysis of nonstationary signals on the basis of wavelets and empirical modes, *J. Commun. Technol. Electron.* 56 (9) (2011) 1098.
- [299] P. Flandrin, G. Rilling, P. Goncalves, Empirical mode decomposition as a filterbank, *IEEE Signal Proc. Lett.* 11 (2003) 112–114.
- [300] V. Grubov, E. Sitnikova, A. Pavlov, M. Khamrova, A. Koronovskii, A. Hramov, Time-frequency analysis of epileptic EEG patterns by means of empirical modes and wavelets, *Proc. SPIE* 9448 (2015) 9448, <http://dx.doi.org/10.1117/12.2178898>.
- [301] G. Pfurtscheller, C. Neuper, Motor imagery activates primary sensorimotor area in humans, *Neurosci. Lett.* 239 (2) (1997) 65–68, [http://dx.doi.org/10.1016/S0304-3940\(97\)00889-6](http://dx.doi.org/10.1016/S0304-3940(97)00889-6), <http://www.sciencedirect.com/science/article/pii/S0304394097008896>.
- [302] V.A. Maksimenko, A. Lüttjohann, V.V. Makarov, M.V. Goremyko, A.A. Koronovskii, V. Nedairov, A.E. Runnova, G. Luijtelaar van, A.E. Hramov, S. Boccaletti, Macroscopic and microscopic spectral properties of brain networks during local and global synchronization, *Phys. Rev. E* 96 (1) (2017) 12316, <http://dx.doi.org/10.1103/PhysRevE.96.012316>.
- [303] T. Yu, J. Xiao, F. Wang, R. Zhang, Z. Gu, A. Cichocki, Y. Li, Enhanced motor imagery training using a hybrid BCI with feedback, *IEEE Trans. Biomed. Eng.* 62 (7) (2015) 1706–1717.
- [304] C. Vidaurre, B. Blankertz, Towards a cure for BCI illiteracy, *Brain Topograph.* 23 (2) (2010) 194–198.
- [305] C. Neuper, G.R. Müller-Putz, R. Scherer, G. Pfurtscheller, Motor imagery and EEG-based control of spelling devices and neuroprostheses, *Prog. Brain Res.* 159 (2006) 393–409.
- [306] S.D. Power, T.H. Falk, T. Chau, Classification of prefrontal activity due to mental arithmetic and music imagery using hidden Markov models and frequency domain near-infrared spectroscopy, *J. Neural Eng.* 7 (2) (2010) 26002.
- [307] T.W. Picton, S. Bentin, P. Berg, E. Donchin, S.A. Hillyard, R. Johnson, G.A. Miller, W. Ritter, D.S. Ruchkin, M.D. Rugg, et al., Guidelines for using human event-related potentials to study cognition: recording standards and publication criteria, *Psychophysiology* 37 (2) (2000) 127–152.
- [308] M.D. Rugg, M.G.H. Coles, *Electrophysiology of Mind: event-Related Brain Potentials and Cognition*, Oxford University Press, 1995.
- [309] G. Hajcak, A. MacNamara, D.M. Olvet, Event-related potentials, emotion, and emotion regulation: an integrative review, *Develop. Neuropsychol.* 35 (2) (2010) 129–155.
- [310] A. Kok, Event-related-potential (ERP) reflections of mental resources: a review and synthesis, *Biol. Psychol.* 45 (1–3) (1997) 19–56.
- [311] A. Verrotti, S. Matricardi, V.E. Rinaldi, G. Prezioso, G. Coppola, Neuropsychological impairment in childhood absence epilepsy: review of the literature, *J. Neurol. Sci.* 359 (1–2) (2015) 59–66.
- [312] R.J. Barry, S.J. Johnstone, A.R. Clarke, A review of electrophysiology in attention-deficit/hyperactivity disorder: II. Event-related potentials, *Clin. Neurophysiol.* 114 (2) (2003) 184–198.
- [313] N. Birbaumer, T. Elbert, A.G. Canavan, B. Rockstroh, Slow potentials of the cerebral cortex and behavior, *Physiol. Rev.* 70 (1990) 1–41.
- [314] A. Kubler, B. Kotchoubey, T. Hinterberger, N. Ghanayim, J. Perelmouter, M. Schauer, C. Fritsch, E. Taub, N. Birbaumer, The thought translation device: A neurophysiological approach to communication in total motor paralysis, *Exp. Brain Res.* 124 (1999) 223–232.
- [315] N. Birbaumer, T. Hinterberger, A. Kubler, N. Neumann, The thought-translation device (TTD): Neurobehavioral mechanisms and clinical outcome, *IEEE Trans. Neural Syst. Rehab. Eng.* 11 (2003) 120–123.
- [316] I.H. Iversen, N. Ghanayim, A. Kubler, N. Neumann, N. Birbaumer, J. Kaiser, A brain-computer interface tool to assess cognitive functions in completely paralyzed patients with amyotrophic lateral sclerosis, *Clin. Neurophys.* 119 (2008) 2214–2223.
- [317] B. He, *Neural Engineering*, Springer publisher, New York, 2013.
- [318] D. Regan, *Human Brain Electrophysiology: Evoked Potentials and Evoked Magnetic Fields in Science and Medicine*, Elsevier, New York, USA, 1989.
- [319] W. Yijun, W. Ruiping, G. Xiaorong, H. Bo, G. Shangkai, A brain-computer interface tool to assess cognitive functions in completely paralyzed patients with amyotrophic lateral sclerosis, *IEEE Trans. Neural Syst. Rehab. Eng.* 14 (2006) 234–240.
- [320] M. Middendorf, G. Mcmillan, G. Calhoun, K.S. Jones, Brain computer interfaces based on steady state visual evoked response, *IEEE Trans. Rehabil. Eng.* 8 (2000) 211–214, <http://dx.doi.org/10.1109/86.847819>.
- [321] G. Xiaorong, X. Dingfeng, C. Ming, G. Shangkai, A BCI-based environmental controller for the motion-disabled, *IEEE Trans. Neural Syst. Rehabil. Eng.* 11 (2003) 137–140, <http://dx.doi.org/10.1109/TNSRE.2003.814449>.
- [322] J.V.. Odom, M. Bach, C. Barber, M. Brigell, M.F. Marmor, A.P. Tormene, G.E. Holder, Visual evoked potentials standard, *Doc. Ophthalmol.* 108 (2004) 1115–1123.
- [323] N. Birbaumer, T. Hinterberger, A. Kubler, N. Neumann, I.H. Iversen, N. Ghanayim, A. Kubler, N. Neumann, N. Birbaumer, J. Kaiser, W. Yijun, W. Ruiping, G. Xiaorong, H. Bo, G. Shangkai, N. Galloway, N. Birbaumer, T. Elbert, A.G. Canavan, B. Rockstroh, B. He, J.V.. Odom, M. Bach, C. Barber, M. Brigell, M.F. Marmor, A.P. Tormene, G.E. Holder, D. Zhu, J. Bieger, G. Garcia Molina, R.M. Aarts, W.M. Perlstein, M.A. Cole, M. Larson, K. Kelly, P. Seignourel, A. Keil, B. Tamara, J. Howard, D. Regan, F. Lotte, L. Bougrain, A. Cichocki, M. Clerc, M. Congedo, A. Rakotomamonjy, F. Yger, G. Xiaorong, X. Dingfeng, C. Ming, G. Shangkai, M. Middendorf, G. Mcmillan, G. Calhoun, K.S. Jones, B. Guragain, A. Haider, R. Fazel-Rezai, M. Gray, A.H. Kemp, R.B. Silberstein, P.J. Nathan, A brain-computer interface tool to assess cognitive functions in completely paralyzed patients with amyotrophic lateral sclerosis, *IEEE Trans. Neural Syst. Rehab. Eng.* 11 (3) (2003) 120–123.
- [324] A. Pisarchik, P. Chholak, A. Hramov, Brain noise estimation from MEG response to flickering visual stimulation, *Chaos, Solit. Fract.*: X 1 (2019) 100005, <http://dx.doi.org/10.1016/j.csfx.2019.100005>.
- [325] P. Szendro, Pink-noise behaviour of biosystems, *Eur. Biophys. J.* 30 (2001) 227–231.
- [326] N. Galloway, Human brain electrophysiology: Evoked potentials and evoked magnetic fields in science and medicine, *Br. J. Ophthalmol.* 74 (1990) 255.
- [327] W.M. Perlstein, M.A. Cole, M. Larson, K. Kelly, P. Seignourel, A. Keil, Steady-state visual evoked potentials reveal frontally-mediated working memory activity in humans, *Neurosci. Lett.* 342 (2003) 191–195.
- [328] M. Gray, A.H. Kemp, R.B. Silberstein, P.J. Nathan, Cortical neurophysiology of anticipatory anxiety: An investigation utilizing steady state probe topography ((SSPT)), *Neuroimage* 20 (2003) 975–986.
- [329] Y. Wang, R. Wang, X. Gao, B. Hong, S. Gao, A practical VEP-based brain-computer interface, *IEEE Trans. Neural Syst. Rehabil. Eng.* 14 (2) (2006) 234–240, <http://dx.doi.org/10.1109/TNSRE.2006.875576>.
- [330] N.R. Waytowich, Y. Yamani, D.J. Krusinski, Optimization of checkerboard spatial frequencies for steady-state visual evoked potential brain-computer interfaces, *IEEE Trans. Neural Syst. Rehabil. Eng.* 25 (6) (2017) 557–565.
- [331] C. Han, G. Xu, J. Xie, C. Chen, S. Zhang, Highly interactive brain-computer interface based on flicker-free steady-state motion visual evoked potential, *Sci. Rep.* 8 (1) (2018) 5835.
- [332] B. Tamara, J. Howard, Privacy by design in brain-computer interfaces, University of Washington, UWEE, technical report number UWEETR-2013-0001, 2013.
- [333] S.M.M. Martens, N.J. Hill, J. Farquhar, B. Schölkopf, Overlap and refractory effects in a brain-computer interface speller based on the visual P300 event-related potential, *J. Neural Eng.* 6 (2009) 26003.

- [334] K. Takano, T. Komatsu, N. Hata, Y. Nakajima, K. Kansaku, Visual stimuli for the P300 brain-computer interface: A comparison of white/gray and green/blue flicker matrices, *Clin. Neurophys.* 120 (2009) 1562–1566.
- [335] S. Ikegami, K. Takano, N. Saeki, K. Kansaku, Operation of a P300-based brain-computer interface by individuals with cervical spinal cord injury, *Clin. Neurophys.* 122 (2011) 991–996.
- [336] J. Hill, J. Farquhar, S. Martens, F. Bießmann, B. Scholkopf, Effects of stimulus type and of error-correcting code design on bci speller performance, in: *Advances in Neural Information Processing Systems*, 2009, pp. 665–672.
- [337] E. Yin, Z. Zhou, J. Jiang, F. Chen, Y. Liu, D. Hu, A speedy hybrid BCI spelling approach combining P300 and SSVEP, *IEEE Trans. Biomed. Eng.* 61 (2) (2014) 473–483.
- [338] G. Townsend, B.K. LaPallo, C.B. Boulay, D.J. Krusinski, G.E. Frye, C.K. Hauser, N.E. Schwartz, T.M. Vaughan, J.R. Wolpaw, E.W. Sellers, A novel {P300}-based brain-computer interface stimulus presentation paradigm: Moving beyond rows and columns, *Clin. Neurophys.* 121 (2010) 1109–1120.
- [339] P. Chholak, V.A. Maksimenko, A.E. Hramov, A.N. Pisarchik, Voluntary and involuntary attention in bistable visual perception: A MEG study, *Front. Hum. Neurosci.* 14 (2020) 555, <http://dx.doi.org/10.3389/fnhum.2020.597895>.
- [340] S. Halder, M. Rea, R. Andreoni, F. Nijboer, E.M. Hammer, S.C. Kleih, N. Birbaumer, A. Kübler, An auditory oddball brain-computer interface for binary choices, *Clin. Neurophysiol.* 121 (4) (2010) 516–523.
- [341] T. Harmony, The functional significance of delta oscillations in cognitive processing, *Front. Integr. Neurosci.* 7 (2013) 83.
- [342] J.P. Donoghue, J.N. Sanes, Motor areas of the cerebral cortex., *J. Clin. Neurophysiol.* 11 (4) (1994) 382–396.
- [343] J.I. Todor, T. Doane, Handedness and hemispheric asymmetry in the control of movements, *J. Mot. Behav.* 10 (4) (1978) 295–300.
- [344] A. Pavlov, A. Runnova, V. Maksimenko, O. Pavlova, D. Grishina, A. Hramov, Detrended fluctuation analysis of EEG patterns associated with real and imaginary arm movements, *Physica A* 509 (2018) 777–782, <http://dx.doi.org/10.1016/j.physa.2018.06.096>.
- [345] D.S. Grishina, A.E. Runnova, O.N. Pavlova, A.N. Pavlov, A.E. Hramov, Recognizing human movements by processing EEG-signals using multiresolution analysis, in: *Dynamics and Fluctuations in Biomedical Photonics XVI*, vol. 10877, International Society for Optics and Photonics, 2019, 1087710, <http://dx.doi.org/10.1117/12.2511406>.
- [346] A. Butfield, P.W. Ferrez, J.R. Millán, Towards a robust BCI: error potentials and online learning, *IEEE Trans. Neural Syst. Rehab. Eng.* 14 (2006) 146–148.
- [347] S. Arroyo, R.P. Lesser, B. Gordon, S. Uematsu, D. Jackson, R. Webber, Functional significance of the mu rhythm of human cortex: an electrophysiologic study with subdural electrodes, *Electroencephalograph. Clin. Neurophysiol.* 87 (3) (1993) 76–87.
- [348] C.I. Penalosa, M. Alimardani, S. Nishio, Android feedback-based training modulates sensorimotor rhythms during motor imagery, *IEEE Trans. Neural Syst. Rehab. Eng.* 26 (3) (2018) 666–674.
- [349] G. Tacchino, M. Gandolla, S. Coelli, R. Barbieri, A. Pedrocchi, A.M. Bianchi, EEG Analysis during active and assisted repetitive movements: evidence for differences in neural engagement, *IEEE Trans. Neural Syst. Rehab. Eng.* 25 (6) (2017) 761–771.
- [350] G. Pfurtscheller, C. Neuper, G.R. Muller, B. Obermaier, G. Krausz, A. Schlogl, R. Scherer, B. Graimann, C. Keinrath, D. Skliris, et al., Graz-BCI: state of the art and clinical applications, *IEEE Trans. Neural Syst. Rehab. Eng.* 11 (2) (2003) 1–4, <http://dx.doi.org/10.1109/TNSRE.2003.814454>.
- [351] A. Ferreira, W.C. Celeste, F.A. Cheein, T.F. Bastos-Filho, M. Sarcinelli-Filho, R. Carelli, Human-machine interfaces based on EMG and EEG applied to robotic systems, *J. NeuroEng. Rehab.* 5 (1) (2008) 10.
- [352] G.N. Ranky, S. Adamovich, Analysis of a commercial EEG device for the control of a robot arm, in: *Proceedings of the 2010 IEEE 36th Annual Northeast Bioengineering Conference (NEBEC)*, IEEE, 2010, pp. 1–2.
- [353] D.P. Murphy, O. Bai, A.S. Gorgey, J. Fox, W.T. Lovegreen, B.W. Burkhardt, R. Atri, J.S. Marquez, Q. Li, D.-Y. Fei, Electroencephalogram-based brain-computer interface and lower-limb prosthesis control: A case study, *Front. Neurol.* 8 (2017) 696.
- [354] P. Chholak, G. Niso, V. Maksimenko, N. Frolov, S. Kurkin, E. Pitsik, A.E. Hramov, A.N. Pisarchik, Visual and kinesthetic modes affect motor imagery classification in untrained subjects, *Sci. Rep.* (2019) 9838.
- [355] H. Hanna-Leena, P. Lauri, Across-subject offline decoding of motor imagery from MEG and EEG, *Sci. Rep.* 8 (1) (2018) 10087.
- [356] G. Borghini, P. Aricò, G. Di Flumeri, G. Cartocci, A. Colosimo, S. Bonelli, A. Golfteti, J.P. Imbert, G. Granger, R. Benhacene, et al., EEG-Based cognitive control behaviour assessment: an ecological study with professional air traffic controllers, *Sci. Rep.* 7 (1) (2017) 547.
- [357] C.G. Lim, T.S. Lee, C. Guan, D.S.S. Fung, Y. Zhao, S.S.W. Teng, H. Zhang, K.R.R. Krishnan, A brain-computer interface based attention training program for treating attention deficit hyperactivity disorder, *PLoS One* 7 (10) (2012) e46692.
- [358] B. Hillard, A.S. El-Baz, L. Sears, A. Tasman, E.M. Sokhadze, Neurofeedback training aimed to improve focused attention and alertness in children with ADHD: a study of relative power of EEG rhythms using custom-made software application, *Clin. EEG Neurosci.* 44 (3) (2013) 193–202.
- [359] Z. Zhang, K.K. Parhi, Low-complexity seizure prediction from iEEG/sEEG using spectral power and ratios of spectral power, *IEEE Trans. Biomed. Circuit. Syst.* 10 (3) (2016) 693–706.
- [360] A. Pitkänen, W. Löscher, A. Vezzani, A.J. Becker, M. Simonato, K. Lukasiuk, O. Gröhn, J.P. Bankstahl, A. Friedman, E. Aronica, et al., Advances in the development of biomarkers for epilepsy, *Lancet Neurol.* 15 (8) (2016) 843–856.
- [361] G. Luijtelaar van, A. Lutjeh Johann, V.V. Makarow, V.A. Maksimenko, A.A. Koronovskii, A.E. Hramov, Methods of automated absence seizure detection, interference by stimulation, and possibilities for prediction in genetic absence models, *J. Neurosci. Methods* 260 (2016) 144–158.
- [362] M. Pais-Vieira, A.P. Yadav, D. Moreira, D. Guggenmos, A. Santos, M. Lebedev, M.A.L. Nicolelis, A closed loop brain-machine interface for epilepsy control using dorsal column electrical stimulation, *Sci. Rep.* 6 (2016) 32814, <http://dx.doi.org/10.1038/srep32814>.
- [363] F. Tang, A. Hartz, B. Bauer, Drug-resistant epilepsy: multiple hypotheses, few answers, *Front. Neurol.* 8 (2017) 301.
- [364] V. Salanova, T. Witt, R. Worth, T.R. Henry, R.E. Gross, J.M. Nazzaro, D. Labar, M.R. Sperling, A. Sharan, E. Sandok, et al., Long-term efficacy and safety of thalamic stimulation for drug-resistant partial epilepsy, *Neurology* 84 (10) (2015) 1017–1025.
- [365] S.W.S. MacDonald, L. Nyberg, L. Bäckman, Intra-individual variability in behavior: links to brain structure, neurotransmission and neuronal activity, *Trends Neurosci.* 29 (8) (2006) 474–480.
- [366] S. Mueller, D. Wang, M.D. Fox, B.T.T. Yeo, J. Sepulcre, M.R. Sabuncu, R. Shafee, J. Lu, H. Liu, Individual variability in functional connectivity architecture of the human brain, *Neuron* 77 (3) (2013) 586–595.
- [367] B. Luna, K.R. Thulborn, D.P. Munoz, E.P. Merriam, K.E. Garver, N.J. Minshew, M.S. Keshavan, C.R. Genovese, W.F. Eddy, J.A. Sweeney, Maturation of widely distributed brain function subserves cognitive development, *Neuroimage* 13 (5) (2001) 786–793.
- [368] J. Gläscher, C. Büchel, Formal learning theory dissociates brain regions with different temporal integration, *Neuron* 47 (2) (2005) 295–306.
- [369] T.H.B. Fitzgerald, K.J. Friston, R.J. Dolan, Action-specific value signals in reward-related regions of the human brain, *J. Neurosci.* 32 (46) (2012) 16417–16423.
- [370] K.J. Friston, Functional and effective connectivity in neuroimaging: a synthesis, *Hum. Brain Mapp.* 2 (1–2) (1994) 56–78.
- [371] G. Tononi, G.M. Edelman, Consciousness and complexity, *Science* 282 (5395) (1998) 1846–1851.
- [372] C. Büchel, J.T. Coull, K.J. Friston, The predictive value of changes in effective connectivity for human learning, *Science* 283 (5407) (1999) 1538–1541.
- [373] E. Salinas, T.J. Sejnowski, Correlated neuronal activity and the flow of neural information, *Nat. Rev. Neurosci.* 2 (8) (2001) 539.
- [374] S. Chennu, P. Finoia, E. Kamau, J. Allanson, G.B. Williams, M.M. Monti, V. Noreika, A. Arnatkeviciute, A. Canales-Johnson, F. Olivares, et al., Spectral signatures of reorganised brain networks in disorders of consciousness, *PLoS Comput. Biol.* 10 (10) (2014) e1003887.

- [375] B. Voytek, R.T. Knight, Dynamic network communication as a unifying neural basis for cognition, development, aging, and disease, *Biol. Psych.* 77 (12) (2015) 1089–1097.
- [376] B. Voytek, A.S. Kayser, D. Badre, D. Fegen, E.F. Chang, N.E. Crone, J. Parvizi, R.T. Knight, M. D'esposito, Oscillatory dynamics coordinating human frontal networks in support of goal maintenance, *Nature Neurosci.* 18 (9) (2015) 1318.
- [377] V.P. Buch, A.G. Richardson, C. Brandon, J. Stiso, M.N. Khattak, D.S. Bassett, T.H. Lucas, Network brain-computer interface (nBCI): An alternative approach for cognitive prosthetics, *Front. Neurosci.* 12 (2018) 790.
- [378] V.A. Maksimenko, A.E. Runnova, N.S. Frolov, V.V. Makarov, V.O. Nedaiwozov, A.A. Koronovskii, A.N. Pisarchik, A.E. Hramov, Multiscale neural connectivity during human sensory processing in the brain, *Phys. Rev. E* 97 (2018) <http://dx.doi.org/10.1103/PhysRevE.97.052405>.
- [379] V.A. Maksimenko, A.E. Runnova, M.O. Zhuravlev, P. Protasov, R. Kulanin, M.V. Khamanova, A.N. Pisarchik, A.E. Hramov, Human personality reflects spatio-temporal and time-frequency eeg structure, *PLoS One* 13 (9) (2018) e0197642, <http://dx.doi.org/10.1371/journal.pone.0197642>.
- [380] S. Boccaletti, V. Latora, V. Moreno, M. Chavez, D.U. Hwang, Complex networks: Structure and dynamics, *Phys. Rep.* 424 (2006) 175–308, <http://dx.doi.org/10.1016/j.physrep.2005.10.009>.
- [381] M. Rubinov, O. Sporns, Complex network measures of brain connectivity: uses and interpretations, *Neuroimage* 52 (3) (2010) 1059–1069.
- [382] H.-J. Park, K. Friston, Structural and functional brain networks: from connections to cognition, *Science* 342 (6158) (2013) 1238411.
- [383] Z. Dai, J. De Souza, J. Lim, P.M. Ho, Y. Chen, J. Li, N. Thakor, A. Bezerianos, Y. Sun, Eeg cortical connectivity analysis of working memory reveals topological reorganization in theta and alpha bands, *Front. Hum. Neurosci.* 11 (2017) 237.
- [384] N.A. Crossley, A. Micheli, P.E. Vértes, T.T. Winton-Brown, A.X. Patel, C.E. Ginestet, P. McGuire, E.T. Bullmore, Cognitive relevance of the community structure of the human brain functional coactivation network, *Proc. Natl. Acad. Sci. USA* 110 (28) (2013) 11583–11588.
- [385] U. Braun, A. Schäfer, H. Walter, S. Erk, N. Romanczuk-Seiferth, L. Haddad, J.I. Schweiger, O. Grimm, A. Heinz, H. Tost, et al., Dynamic reconfiguration of frontal brain networks during executive cognition in humans, *Proc. Natl. Acad. Sci. USA* 112 (37) (2015) 11678–11683.
- [386] V.V. Makarov, M.O. Zhuravlev, A.E. Runnova, P. Protasov, V.A. Maksimenko, N.S. Frolov, A.N. Pisarchik, A.E. Hramov, Betweenness centrality in multiplex brain network during mental task evaluation, *Phys. Rev. E* 98 (6) (2018) 62413, <http://dx.doi.org/10.1103/PhysRevE.98.062413>.
- [387] F. Varela, J.-P. Lachaux, E. Rodriguez, J. Martinerie, The brainweb: phase synchronization and large-scale integration, *Nat. Rev. Neurosci.* 2 (4) (2001) 229.
- [388] J.M. Shine, P.G. Bissett, P.T. Bell, O. Koyejo, J.H. Balsters, K.J. Gorgolewski, C.A. Moodie, R.A. Poldrack, The dynamics of functional brain networks: integrated network states during cognitive task performance, *Neuron* 92 (2) (2016) 544–554.
- [389] B.J. Baars, In the theatre of consciousness. Global workspace theory, a rigorous scientific theory of consciousness, *J. Conscious. Stud.* 4 (4) (1997) 292–309.
- [390] S. Dehaene, M. Kerszberg, J.-P. Changeux, A neuronal model of a global workspace in effortful cognitive tasks, *Proc. Natl. Acad. Sci. USA* 95 (24) (1998) 14529–14534.
- [391] P. Fries, A mechanism for cognitive dynamics: neuronal communication through neuronal coherence, *Trends Cogn. Sci.* 9 (10) (2005) 474–480.
- [392] G.G. Gregoriou, S.J. Gotts, H. Zhou, R. Desimone, High-frequency, long-range coupling between prefrontal and visual cortex during attention, *Science* 324 (5931) (2009) 1207–1210.
- [393] J.E. Lisman, O. Jensen, The theta-gamma neural code, *Neuron* 77 (6) (2013) 1002–1016.
- [394] P. Fries, Rhythms for cognition: communication through coherence, *Neuron* 88 (1) (2015) 220–235.
- [395] M. Bamdad, H. Zarshenas, M.A. Auais, Application of {BCI} systems in neurorehabilitation: a scoping review, *Disab. Rehab.: Assistive Technol.* 10 (5) (2015) 355–364.
- [396] J. Luauté, D. Morlet, J. Mattout, {BCI} In patients with disorders of consciousness: clinical perspectives, *Ann. Phys. Rehabil. Med.* 58 (1) (2015) 29–34.
- [397] Y. Ezzyat, J.E. Kragel, J.F. Burke, D.F. Levy, A. Lyalenko, P. Wanda, L. O'Sullivan, K.B. Hurley, S. Busygin, I. Pedisich, et al., Direct brain stimulation modulates encoding states and memory performance in humans, *Curr. Biol.* 27 (9) (2017) 1251–1258.
- [398] Y. Jiang, R. Abiri, X. Zhao, Tuning up the old brain with new tricks: attention training via neurofeedback, *Front. Aging Neurosci.* 9 (2017) 52.
- [399] Y. Ezzyat, P.A. Wanda, D.F. Levy, A. Kadel, A. Aka, I. Pedisich, M.R. Sperling, A.D. Sharan, B.C. Lega, A. Burks, et al., Closed-loop stimulation of temporal cortex rescues functional networks and improves memory, *Nat. Commun.* 9 (1) (2018) 365.
- [400] H. Wang, A.R. McIntosh, N. Kovacevic, M. Karachalias, A.B. Protzner, Age-related multiscale changes in brain signal variability in pre-task versus post-task resting-state EEG, *J. Cogn. Neurosci.* 28 (7) (2016) 971–984.
- [401] M. Gosak, R. Markovič, J. Dolenšek, M.S. Rupnik, M. Marhl, A. Stožer, M. Perc, Network science of biological systems at different scales: a review, *Phys. Life Rev.* 24 (2018) 118–135.
- [402] R. Sala-Llonch, D. Bartrés-Faz, C. Junqué, Reorganization of brain networks in aging: a review of functional connectivity studies, *Front. Psychol.* 6 (2015) 663.
- [403] A. Avena-Koenigsberger, B. Misic, O. Sporns, Communication dynamics in complex brain networks, *Nat. Rev. Neurosci.* 19 (1) (2018) 17.
- [404] A.M. Bastos, J.-M. Schoffelen, A tutorial review of functional connectivity analysis methods and their interpretation pitfalls, *Front. Syst. Neurosci.* 9 (2016) 175.
- [405] X. Li, D. Li, L.J. Voss, J.W. Sleigh, The comodulation measure of neuronal oscillations with general harmonic wavelet bicoherence and application to sleep analysis, *NeuroImage* 48 (3) (2009) 501–514.
- [406] R.E. Greenblatt, M.E. Pflieger, A.E. Ossadtchi, Connectivity measures applied to human brain electrophysiological data, *J. Neurosci. Methods* 207 (1) (2012) 1–16.
- [407] F. Wendling, K. Ansari-Asl, F. Bartolomei, L. Senhadji, From EEG signals to brain connectivity: a model-based evaluation of interdependence measures, *J. Neurosci. Methods* 183 (1) (2009) 9–18.
- [408] V. Sakkalis, Review of advanced techniques for the estimation of brain connectivity measured with EEG/MEG, *Comput. Biol. Med.* 41 (12) (2011) 1110–1117.
- [409] S. Nobukawa, M. Kikuchi, T. Takahashi, Changes in functional connectivity dynamics with aging: A dynamical phase synchronization approach, *NeuroImage* 188 (2019) 357–368.
- [410] D. Ibáñez-Soria, J. García-Ojalvo, A. Soria-Frisch, G. Ruffini, Detection of generalized synchronization using echo state networks, *Chaos* 28 (3) (2018) 033118.
- [411] N. Frolov, V. Maksimenko, A. Lüttjohann, A. Koronovskii, A. Hramov, Feed-forward artificial neural network provides data-driven inference of functional connectivity, *Chaos* 29 (9) (2019) 091101.
- [412] K. Friston, R. Moran, A.K. Seth, Analysing connectivity with granger causality and dynamic causal modelling, *Curr. Opin. Neurobiol.* 23 (2) (2013) 172–178.
- [413] N. Marwan, C.M. Romano, M. Thiel, J. Kurths, Recurrence plots for the analysis of complex systems, *Phys. Rep.* 438 (5–6) (2007) 237–329.
- [414] N. Frolov, V. Maksimenko, A. Hramov, Revealing a multiplex brain network through the analysis of recurrences, *Chaos* 30 (12) (2020) 121108, <http://dx.doi.org/10.1063/5.0028053>.
- [415] J.M. Fletcher, T. Wennekers, From structure to activity: Using centrality measures to predict neuronal activity, *Int. J. Neural Syst.* 28 (02) (2018) 1750013.
- [416] O. Sporns, Graph theory methods: applications in brain networks, *Dialogues Clin. Neurosci.* 20 (2) (2018) 111.

- [417] K. Shen, R.M. Hutchison, G. Bezin, S. Everling, A.R. McIntosh, Network structure shapes spontaneous functional connectivity dynamics, *J. Neurosci.* 35 (14) (2015) 5579–5588.
- [418] V.V. Makarov, D.V. Kirsanov, N.S. Frolov, V.A. Maksimenko, X. Li, Z. Wang, A.E. Hramov, S. Boccaletti, Assortative mixing in spatially-extended networks, *Sci. Rep.* 8 (1) (2018) 13825, <http://dx.doi.org/10.1038/s41598-018-32160-4>.
- [419] E. Bullmore, O. Sporns, Complex brain networks: graph theoretical analysis of structural and functional systems, *Nat. Rev. Neurosci.* 10 (3) (2009) 186.
- [420] G. Tononi, O. Sporns, G.M. Edelman, A measure for brain complexity: relating functional segregation and integration in the nervous system, *Proc. Natl. Acad. Sci. USA* 91 (11) (1994) 5033–5037.
- [421] O. Sporns, Network analysis, complexity, and brain function, *Complexity* 8 (1) (2002) 56–60.
- [422] K.J. Miller, E.C. Leuthardt, G. Schalk, R.P.N. Rao, N.R. Anderson, D.W. Moran, J.W. Miller, J.G. Ojemann, Spectral changes in cortical surface potentials during motor movement, *J. Neurosci.* 27 (9) (2007) 2424–2432.
- [423] D.S. Bassett, M. Yang, N.F. Wymbs, S.T. Grafton, Learning-induced autonomy of sensorimotor systems, *Nature Neurosci.* 18 (5) (2015) 744.
- [424] I.-E. Nicolae, L. Acqualagna, B. Blankertz, Assessing the depth of cognitive processing as the basis for potential user-state adaptation, *Front. Neurosci.* 11 (2017) 548.
- [425] H.R. McGregor, P.L. Gribble, Functional connectivity between somatosensory and motor brain areas predicts individual differences in motor learning by observing, *J. Neurophysiol.* 118 (2) (2017) 1235–1243.
- [426] M. Alimardani, S. Nishio, H. Ishiguro, The importance of visual feedback design in BCIs; from embodiment to motor imagery learning, *PLoS One* 11 (9) (2016) e0161945.
- [427] J.H.K. Friedman, On bias, variance, 0/1-loss, and the curse-of-dimensionality, *Data Min. Knowl. Discov.* 1 (1997) 1.
- [428] A.K. Jain, R.P.W. Duin, J. Mao, Statistical pattern recognition: A review, *IEEE Trans. Pattern Anal. Mach. Intell.* 22 (2000) 4–37.
- [429] S.J. Raudys, A.K. Jain, Small sample size effects in statistical pattern recognition: Recommendations for practitioners, *IEEE Trans. Pattern Anal. Mach. Intell.* 13 (1991) 252–264.
- [430] A.K. Jain, B. Chandrasekaran, Dimensionality and sample size considerations in pattern recognition practice, *Handbook of Statistics*, 1982.
- [431] L. Breiman, Arcing classifiers, *Ann. Statist.* 26 (1998) 801–849.
- [432] V.N. Vapnik, An overview of statistical learning theory, *IEEE Trans. Neural Netw.* 10 (1999) 988–999.
- [433] H. Bashashati, R. Ward, G. Birch, A. Bashashati, Comparing different classifiers in sensory motor brain computer interfaces, *PLoS One* 10 (2015) e0129435.
- [434] R.O. Duda, P.E. Hart, D.G. Stork, *Pattern Recognition*, second edition, Wiley–Interscience, 2001.
- [435] J.R. Millan, On the need for on-line learning in brain-computer interfaces, in: *Proceedings of 2004 IEEE International Joint Conference on Neural Networks*, 2004, 4, IEEE, 2004, pp. 2877–2882.
- [436] P. Shenoy, M. Krauledat, B. Blankertz, R.P. Rao, K.-R. Müller, Towards adaptive classification for BCI, *J. Neural Eng.* 3 (1) (2006) R13.
- [437] D.J. Krusinski, M. Grosse-Wentrup, F. Galán, D. Coyle, K.J. Miller, E. Forney, C.W. Anderson, Critical issues in state-of-the-art brain-computer interface signal processing, *J. Neural Eng.* 8 (2) (2011) 25002.
- [438] F. Lotte, C. Jeunet, Online classification accuracy is a poor metric to study mental imagery-based bci user learning: an experimental demonstration and new metrics, in: *7th International BCI Conference*, 2017.
- [439] D.J. McFarland, J.R. Wolpaw, (EEG)-based brain–computer interfaces, *Curr. Opin. Biomed. Eng.* 4 (2017) 194–200.
- [440] M. Kaper, P. Meinicke, U. Grosseskather, T. Lingner, H. Ritter, BCI Competition 2003-data set IIb: support vector machines for the P300 speller paradigm, *IEEE Trans. Biomed. Eng.* 51 (6) (2004) 1073–1076.
- [441] J.R. Millan, J. Mourinjo, Asynchronous BCI and local neural classifiers: an overview of the adaptive brain interface project, *IEEE Trans. Neural Syst. Rehabil. Eng.* 11 (2) (2003) 159–161.
- [442] G. Pfurtscheller, C. Neuper, A. Schlogl, K. Lügger, Separability of EEG signals recorded during right and left motor imagery using adaptive autoregressive parameters, *IEEE Trans. Rehabil. Eng.* 6 (3) (1998) 316–325.
- [443] W.D. Penny, A. Et, EEG-Based communication: A pattern recognition approach, *IEEE Trans. Rehabil. Eng.* 8 (2000) 214–215.
- [444] W. Ting, Y. Guo-zheng, Y. Bang-hua, S. Hong, EEG Feature extraction based on wavelet packet decomposition for brain computer interface, *Measurement* 41 (6) (2008) 618–625.
- [445] A.A. Ovchinnikov, A. Lutjehann, A.E. Hramov, G. Luijtelaar van, An algorithm for real-time detection of spike-wave discharges in rodents, *J. Neurosci. Meth.* 194 (2010) 172–178, <http://dx.doi.org/10.1016/j.jneumeth.2010.09.017>.
- [446] V.A. Maksimenko, A.A. Harchenko, A. Lutjehann, Automated system for epileptic seizures prediction based on multi-channel recordings of electrical brain activity, *Inf. Control. Syst.* 4 (2018) 115–122.
- [447] A. Frolov, D. Húsek, P. Bobrov, O. Mokienko, J. Tintera, Sources of electrical brain activity most relevant to performance of brain-computer interface based on motor imagery, in: *Brain-Computer Interface Systems-Recent Progress and Future Prospects*, IntechOpen, 2013.
- [448] A. Zaitcev, G. Cook, W. Liu, M. Paley, E. Milne, Source localization for brain-computer interfaces, in: *Brain-Computer Interfaces*, Springer, 2015, pp. 125–153.
- [449] I. Daly, S.J. Nasuto, K. Warwick, Brain computer interface control via functional connectivity dynamics, *Pattern Recognit.* 45 (6) (2012) 2123–2136.
- [450] A. Gonzalez-Moreno, S. Arunetxeta, M.-E. Lopez-Garcia, F. del Pozo, F. Maestú, A. Nevado, Signal-to-noise ratio of the MEG signal after preprocessing, *J. Neurosci. Methods* 222 (2014) 56–61.
- [451] J. Gross, S. Baillet, G.R. Barnes, R.N. Henson, A. Hillebrand, O. Jensen, K. Jerbi, V. Litvak, B. Maess, R. Oostenveld, et al., Good practice for conducting and reporting MEG research, *Neuroimage* 65 (2013) 349–363.
- [452] M. Spüler, A high-speed brain-computer interface (BCI) using dry EEG electrodes, *PLoS One* 12 (2) (2017) e0172400.
- [453] J.W.Y. Kam, S. Griffin, A. Shen, S. Patel, H. Hinrichs, H.-J. Heinze, L.Y. Deouell, R.T. Knight, Systematic comparison between a wireless EEG system with dry electrodes and a wired EEG system with wet electrodes, *NeuroImage* 184 (2019) 119–129.
- [454] K.R. Müller, M. Tangermann, G. Dornhege, M. Krauledat, F. Losch, G. Curio, B. Blankertz, Machine learning for real-time single-trial EEG-analysis: From brain-computer interfacing to mental state monitoring, *J. Neurosci. Methods* 167 (2008) 82–90.
- [455] G. Dornhege, B. Blankertz, M. Krauledat, F. Losch, G. Curio, K.-R. Müller, Combined optimization of spatial and temporal filters for improving brain-computer interfacing, *IEEE Trans. Biomed. Eng.* 53 (11) (2006) 2274–2281.
- [456] A. Runnova, Mathematical model of pattern selection for complex multichannel data in EEG processing., *Inf. Control. Syst./Informazionno-Upravlyayushie Sistemy* 95 (4) (2018).
- [457] A.E. Runnova, M.O. Zhuravlev, A.N. Pisarchik, M.V. Khramova, V.V. Grubov, The study of cognitive processes in the brain EEG during the perception of bistable images using wavelet skeleton, in: *Dynamics and Fluctuations in Biomedical Photonics XIV*, 10063, International Society for Optics and Photonics, 2017, 1006319.
- [458] L. Montefusco, L. Puccio, *Wavelets: Theory, Algorithms, and Applications*, Volume 5, Elsevier, 2014.
- [459] W.J. Staszewski, Identification of non-linear systems using multi-scale ridges and skeletons of the wavelet transform, *J. Sound Vib.* 214 (4) (1998) 639–658.

- [460] P. Cavalier, D. O'Hagan, Maximum wavelet coefficient points for potential field analysis and inversion, in: International Conference on Engineering Geophysics, Al Ain, United Arab Emirates, 9–12 October 2017, Society of Exploration Geophysicists, 2017, pp. 128–131.
- [461] S.T. Klein, T.C. Serebro, D. Shapira, Optimal skeleton huffman trees, in: International Symposium on String Processing and Information Retrieval, Springer, 2017, pp. 241–253.
- [462] V.V. Grubov, A.E. Runnova, M.O. Zhuravlev, V.A. Maksimenko, S.V. Pchelintseva, A.N. Pisarchik, Perception of multistable images: EEG studies, *Cybern. Phys.* 6 (2017) 108–113.
- [463] A.N. Pisarchik, R. Jaimes-Reategui, C.D.A. Magallón-Garcia, C.O. Castillo-Morales, Critical slowing down and noise-induced intermittency in bistable perception: bifurcation analysis, *Biol. Cybernet.* 108 (4) (2014) 397–404, <http://dx.doi.org/10.1007/s00422-014-0607-5>.
- [464] A.E. Runnova, A.E. Hramov, V.V. Grubov, A.A. Koronovskii, M.K. Kurovskaya, A.N. Pisarchik, Theoretical background and experimental measurements of human brain noise intensity in perception of ambiguous images, *Chaos Solitons Fractals* 93 (2016) 201–206, <http://dx.doi.org/10.1016/j.chaos.2016.11.001>.
- [465] H. Laufs, J.L. Holt, R. Elfont, M. Kramps, J.S. Paul, K. Krakow, A. Kleinschmidt, Where the BOLD signal goes when alpha EEG leaves, *Neuroimage* 31 (2006) 1408–1418, <http://dx.doi.org/10.1016/j.neuroimage.2006.02.002>.
- [466] G. Michalareas, J. Vezoli, S. van Pelt, J.M. Schoffelen, H. Kennedy, P. Fries, Alpha-beta and gamma rhythms subserve feedback and feedforward influences among human visual cortical areas, *Neuron* 384 (2016) 384–397, <http://dx.doi.org/10.1016/j.neuron.2015.12.018>.
- [467] E.A. Buffalo, P. Fries, R. Landman, T.J. Buschman, R. Desimone, Laminar differences in gamma and alpha coherence in the ventral stream, *Proc. Natl. Acad. Sci. USA* 108 (2011) 11262–11267, <http://dx.doi.org/10.1073/pnas.1011284108>.
- [468] A.M. Coenen, E.L.J.M. Luijtenaar van, Genetic animal models for absence epilepsy: a review of the WAG/Rij strain of rats, *Behav. Genet.* 33 (2003) 635–655.
- [469] G. Van Luijtelaar, A. Hramov, E. Sitnikova, A. Koronovskii, Spike-wave discharges in WAG/Rij rats are preceded by delta and theta precursor activity in cortex and thalamus, *Clin. Neurophysiol.* 122 (4) (2011) 687–695.
- [470] J.A. Wilson, Using general-purpose graphic processing units for BCI systems, in: Engineering in Medicine and Biology Society, EMBC, 2011 Annual International Conference of the IEEE, IEEE, 2011, pp. 4625–4628.
- [471] R.P.N. Rao, Brain-Computer Interfacing. An Introduction, Cambridge University Press, 2013.
- [472] A.N. Pavlov, V.A. Makarov, I. Makarova, F. Panetsos, Sorting of neural spikes: when wavelet based methods outperform principal component analysis, *Nat. Comput.* 6 (2007) 269–281.
- [473] E.S. Nurse, P.J. Karoly, D.B. Grayden, D.R. Freestone, A generalizable brain-computer interface (bci) using machine learning for feature discovery, *PLoS One* 10 (6) (2015) 131328.
- [474] L. Gao, W. Cheng, J. Zhang, J. Wang, {EEG} classification for motor imagery and resting state in BCI applications using multi-class {Adaboost} extreme learning machine, *Rev. Sci. Instrum.* 87 (8) (2016) 85110.
- [475] M.R. Hasan, M.I. Ibrahimy, S.M.A. Motakabber, S. Shahid, Classification of multichannel EEG signal by linear discriminant analysis, in: Progress in Systems Engineering, Springer, 2015, pp. 279–282.
- [476] D. Garrett, D.A. Peterson, C.W. Anderson, M.H. Thaut, Comparison of linear, nonlinear, and feature selection methods for eeg signal classification, *IEEE Trans. Neural Syst. Rehabil. Eng.* 11 (2) (2003) 141–144.
- [477] P. Xu, P. Yang, X. Lei, D. Yao, An enhanced probabilistic LDA for multi-class brain computer interface, *PLoS One* 6 (1) (2011) e14634.
- [478] B. Blankertz, G. Curio, K.-R. Müller, Classifying single trial {EEG}: Towards brain computer interfacing, in: Advances in Neural Information Processing Systems, 2002, pp. 157–164.
- [479] K.-R. Müller, M. Krauledat, G. Dornhege, G. Curio, B. Blankertz, Machine learning techniques for brain-computer interfaces, Citeseer, 2004.
- [480] R. Fukunaga, Statistical Pattern Recognition, Academic Press., 1990.
- [481] S. Lemm, C. Schafer, G. Curio, {BCI} competition 2003-data set {III}: probabilistic modeling of sensorimotor/spl mu/rhythms for classification of imaginary hand movements, *IEEE Trans. Biomed. Eng.* 51 (6) (2004) 1077–1080.
- [482] G.A. Barreto, R.A. Frotta, F.N.S. de Medeiros, On the classification of mental tasks: a performance comparison of neural and statistical approaches, in: Proceedings of the 2004 14th IEEE Signal Processing Society Workshop Machine Learning for Signal Processing, 2004., IEEE, 2004, pp. 529–538.
- [483] C.M. Bishop, Pattern Recognition and Machine Learning, Springer, 2006.
- [484] B. Obermaier, C. Guger, C. Neuper, G. Pfurtscheller, Hidden Markov models for online classification of single trial EEG data, *Pattern Recognit. Lett.* 22 (12) (2001) 1299–1309.
- [485] D. Lederman, J. Tabrikian, Classification of multichannel EEG patterns using parallel hidden Markov models, *Med. Biol. Eng. Comput.* 50 (4) (2012) 319–328.
- [486] S. Solhjoo, A.M. Nasrabadi, M.R.H. Golpayegani, Classification of chaotic signals using {HMM} classifiers: {EEG}-based mental task classification, in: 13th European Signal Processing Conference, IEEE, 2005, pp. 1–4.
- [487] B.V. Dasarathy, NN Concepts and techniques. an introductory survey, *Nearest Neighb. Norms: NN Pattern Classif. Tech.* (1991) 1–30.
- [488] A. Schlägl, F. Lee, H. Bischof, G. Pfurtscheller, Characterization of four-class motor imagery EEG data for the BCI-competition 2005, *J. Neural Eng.* 2 (4) (2005) L14.
- [489] M.Z. Ilyas, P. Saad, M.I. Ahmad, A.R.I. Ghani, Classification of EEG signals for brain-computer interface applications: Performance comparison, in: 2016 International Conference on Robotics, Automation and Sciences (ICORAS), IEEE, 2016, pp. 1–4.
- [490] J.F. Borisoff, S.G. Mason, A. Bashashati, G.E. Birch, Brain-computer interface design for asynchronous control applications: improvements to the {LF-ASD} asynchronous brain switch, *IEEE Trans. Biomed. Eng.* 51 (6) (2004) 985–992.
- [491] J. Kevric, A. Subasi, Comparison of signal decomposition methods in classification of EEG signals for motor-imagery BCI system, *Biomed. Signal Process. Control.* 31 (2017) 398–406.
- [492] F. Cincotti, A. Scipione, A. Timperi, D. Mattia, A.G. Marciani, J. Millan, S. Salinari, L. Bianchi, F. Bablioni, Comparison of different feature classifiers for brain computer interfaces, in: First International IEEE EMBS Conference on Neural Engineering, 2003. Conference Proceedings., IEEE, 2003, pp. 645–647.
- [493] S. Xiang, F. Nie, C. Zhang, Learning a Mahalanobis distance metric for data clustering and classification, *Pattern Recognit.* 41 (12) (2008) 3600–3612.
- [494] V. Vapnik, The Nature of Statistical Learning Theory, Springer-Verlag, New York, 1995.
- [495] L. Quigadamo, F. Cavrini, L. Sbernini, F. Riillo, L. Bianchi, S. Seri, G. Saggio, Support vector machines to detect physiological patterns for EEG and EMG-based human-computer interaction: a review, *J. Neural Eng.* 14 (1) (2017) 011001.
- [496] S.R. Gunn, Support vector machines for classification and regression, *ISIS Tech. Rep.* 14 (1) (1998) 5–16.
- [497] D. De Massari, T. Matuz, A. Furdea, C.A. Ruf, S. Halder, N. Birbaumer, Brain-computer interface and semantic classical conditioning of communication in paralysis, *Biolog. Psychol.* 92 (2) (2013) 267–274.
- [498] S. Deepajothi, S. Selvarajan, Performance evaluation of SVM-RBF kernel for classifying ECoG motor imagery, *Int. J. Comput. Sci. Telecommun.* 4 (5) (2013) 44–48.
- [499] A.M. Chiarelli, P. Croce, A. Merla, F. Zappasodi, Deep learning for hybrid EEG-fNIRS brain-computer interface: application to motor imagery classification, *J. Neural Eng.* 15 (3) (2018) 36028.

- [500] L. Breiman, Random forests, *Mach. Learn.* 45 (1) (2001) 5–32.
- [501] S.R. Safavian, D. Landgrebe, A survey of decision tree classifier methodology, *IEEE Trans. Syst. Man Cybern.* 21 (3) (1991) 660–674.
- [502] M. Bentlemsan, E.-T. Zemouri, D. Bouchaffra, B. Yahya-Zoubir, K. Ferroudji, Random forest and filter bank common spatial patterns for EEG-based motor imagery classification, in: 2014 5th International Conference on Intelligent Systems, Modelling and Simulation, IEEE, 2014, pp. 235–238.
- [503] F. Akram, S.M. Han, T.-S. Kim, An efficient word typing P300-BCI system using a modified T9 interface and random forest classifier, *Comput. Biol. Med.* 56 (2015) 30–36.
- [504] J.-C. Zhang, Y.-Q. Xu, L. Yao, P300 detection using boosting neural networks with application to BCI, in: 2007 IEEE/ICME International Conference on Complex Medical Engineering, IEEE, 2007, pp. 1526–1530.
- [505] R. Boostani, M.H. Moradi, A new approach in the BCI research based on fractal dimension as feature and adaboost as classifier, *J. Neural Eng.* 1 (4) (2004) 212.
- [506] U. Hoffmann, G. Garcia, J.-M. Vesin, K. Diserens, T. Ebrahimi, A boosting approach to P300 detection with application to brain-computer interfaces, in: Conference Proceedings. 2nd International IEEE EMBS Conference on Neural Engineering, 2005., IEEE, 2005, pp. 97–100.
- [507] Y. Liu, H. Zhang, M. Chen, L. Zhang, A boosting-based spatial-spectral model for stroke patients? EEG analysis in rehabilitation training, *IEEE Trans. Neural Syst. Rehabil. Eng.* 24 (1) (2016) 169–179.
- [508] R. Penrose, A generalized inverse for matrices, in: Mathematical Proceedings of the Cambridge Philosophical Society, 51, (3) Cambridge University Press, 1955, pp. 406–413.
- [509] A. Luckow, M. Cook, N. Ashcraft, E. Weill, E. Djerekarov, B. Vorster, Deep learning in the automotive industry: Applications and tools, in: 2016 IEEE International Conference on Big Data (Big Data), IEEE, 2016, pp. 3759–3768.
- [510] N.F. Rulkov, M.M. Sushchik, L.S. Tsimring, H.D. Abarbanel, Generalized synchronization of chaos in directionally coupled chaotic systems, *Phys. Rev. E* 51 (2) (1995) 980.
- [511] O.I. Moskalenko, A.A. Koronovskii, A.E. Hramov, S. Boccaletti, Generalized synchronization in mutually coupled oscillators and complex networks, *Phys. Rev. E* 86 (3) (2012) 036216, <http://dx.doi.org/10.1103/PhysRevE.86.036216>.
- [512] Y. LeCun, Y. Bengio, G. Hinton, Deep learning, *Nature* 521 (7553) (2015) 436–444.
- [513] I. Goodfellow, Y. Bengio, A. Courville, Y. Bengio, Deep Learning, 1, MIT Press Cambridge, 2016.
- [514] K.G. Kim, Book review: Deep learning, *Healthc. Inform. Res.* 22 (4) (2016) 351–354.
- [515] Y. Roy, H. Banville, I. Albuquerque, A. Gramfort, T.H. Falk, J. Faubert, Deep learning-based electroencephalography analysis: a systematic review, *J. Neural Eng.* 16 (5) (2019) 051001.
- [516] D.E. Rumelhart, J.L. McClelland, P.D.P.R. Group, Parallel Distributed Processing: Exploration in the Microstructure of Cognition, Vol. 1, Cambridge, MA: MIT Press, 1986.
- [517] J.L. McClelland, D.E. Rumelhart, A distributed model of human learning and memory, in: Parallel Distributed Processing: Explorations in the Microstructure of Cognition, Vol. 2, Mit Press, 1986, pp. 170–215.
- [518] X. Yao, Evolving artificial neural networks, *Proc. IEEE* 87 (9) (1999) 1423–1447.
- [519] I.A. Basheer, M. Hajmeer, Artificial neural networks: fundamentals, computing, design, and application, *J. Microbiol. Meth.* 43 (1) (2000) 3–31.
- [520] Y. Wang, Z. Zhang, Y. Li, X. Gao, S. Gao, F. Yang, BCI Competition 2003-data set IV: an algorithm based on CSSD and FDA for classifying single-trial EEG, *IEEE Trans. Biomed. Eng.* 51 (6) (2004) 1081–1086.
- [521] M. Congedo, F. Lotte, A. Lécuyer, Classification of movement intention by spatially filtered electromagnetic inverse solutions, *Phys. Med. Biol.* 51 (8) (2006) 1971.
- [522] J. del R Millan, J. Mourão, M. Franzé, F. Cincotti, M. Varsta, J. Heikkonen, F. Babiloni, A local neural classifier for the recognition of EEG patterns associated to mental tasks, *IEEE Trans. Neural Netw.* 13 (3) (2002) 678–686.
- [523] K. Nakayama, K. Inagaki, A brain computer interface based on neural network with efficient pre-processing, in: 2006 International Symposium on Intelligent Signal Processing and Communications, IEEE, 2006, pp. 673–676.
- [524] E. Haselsteiner, G. Pfurtscheller, Using time-dependent neural networks for EEG classification, *IEEE Trans. Rehabil. Eng.* 8 (4) (2000) 457–463.
- [525] H.U. Amin, W. Mumtaz, A.R. Subhani, M.N.M. Saad, A.S. Malik, Classification of EEG signals based on pattern recognition approach, *Front. Comput. Neurosci.* 11 (2017) 103.
- [526] I.T. Hettiarachchi, T. Babaei, T. Nguyen, C.P. Lim, S. Nahavandi, A fresh look at functional link neural network for motor imagery-based brain-computer interface, *J. Neurosci. Methods* 305 (2018) 28–35.
- [527] E.B. Assi, L. Gagliano, S. Rihana, D.K. Nguyen, M. Sawan, Bispectrum features and multilayer perceptron classifier to enhance seizure prediction, *Sci. Rep.* 8 (1) (2018) 1–8.
- [528] J.J. Bird, D.R. Faria, L.J. Manso, A. Ekárt, C.D. Buckingham, A deep evolutionary approach to bioinspired classifier optimisation for brain-machine interaction, *Complexity* 2019 (2019).
- [529] A.E. Hramov, V. Maksimenko, A. Koronovskii, A.E. Runnova, M. Zhuravlev, A.N. Pisarchik, J. Kurths, Percept-related EEG classification using machine learning approach and features of functional brain connectivity, *Chaos* 29 (9) (2019) 093110, <http://dx.doi.org/10.1063/1.5113844>.
- [530] X. Zhang, D. Wu, On the vulnerability of CNN classifiers in EEG-based BCIs, *IEEE Trans. Neural Syst. Rehabil. Eng.* 27 (5) (2019) 814–825.
- [531] V.J. Lawhern, A.J. Solon, N.R. Waytowich, S.M. Gordon, C.P. Hung, B.J. Lance, Eegnet: a compact convolutional neural network for EEG-based brain-computer interfaces, *J. Neural Eng.* 15 (5) (2018) 056013.
- [532] Z. Gao, X. Wang, Y. Yang, C. Mu, Q. Cai, W. Dang, S. Zuo, EEG-Based spatio-temporal convolutional neural network for driver fatigue evaluation, *IEEE Trans. Neural Netw. Learn. Syst.* 30 (9) (2019) 2755–2763.
- [533] Z. Gao, Y. Li, Y. Yang, N. Dong, X. Yang, C. Grebogi, A coincidence filtering-based approach for CNNs in EEG-based recognition, *IEEE Trans. Ind. Inf.* (2019).
- [534] R.T. Schirrmeister, J.T. Springenberg, L.D.J. Fiederer, M. Glasstetter, K. Eggensperger, M. Tangermann, F. Hutter, W. Burgard, T. Ball, Deep learning with convolutional neural networks for EEG decoding and visualization, *Hum. Brain Mapp.* 38 (11) (2017) 5391–5420.
- [535] K. Greff, R.K. Srivastava, J. Koutník, B.R. Steunebrink, J. Schmidhuber, LSTM: A search space odyssey, *IEEE Trans. Neural Netw. Learn. Syst.* 28 (10) (2016) 2222–2232.
- [536] S. Hochreiter, J. Schmidhuber, Long short-term memory, *Neural Comput.* 9 (8) (1997) 1735–1780.
- [537] F.A. Gers, J. Schmidhuber, F. Cummins, Learning to forget: Continual prediction with LSTM, *IET*, 1999.
- [538] F.A. Gers, J. Schmidhuber, Recurrent nets that time and count, in: Proceedings of the IEEE-INNS-ENNS International Joint Conference on Neural Networks. IJCNN 2000. Neural Computing: New Challenges and Perspectives for the New Millennium, 3, IEEE, 2000, pp. 189–194.
- [539] K. Cho, B. Van Merriënboer, C. Gulcehre, D. Bahdanau, F. Bougares, H. Schwenk, Y. Bengio, Learning phrase representations using RNN encoder-decoder for statistical machine translation, 2014, arXiv preprint [arXiv:1406.1078](https://arxiv.org/abs/1406.1078).
- [540] Y. Yu, X. Si, C. Hu, J. Zhang, A review of recurrent neural networks: LSTM cells and network architectures, *Neural Comput.* 31 (7) (2019) 1235–1270.
- [541] G. Bouallegue, R. Djemal, S.A. Alshebeili, H. Aldhalaan, A dynamic filtering DF-RNN deep-learning-based approach for EEG-based neurological disorders diagnosis, *IEEE Access* 8 (2020) 206992–207007.

- [542] W. Lu, Y. Wei, J. Yuan, Y. Deng, A. Song, Tractor assistant driving control method based on EEG combined with RNN-TL deep learning algorithm, *IEEE Access* 8 (2020) 163269–163279.
- [543] O. Tal, D. Friedman, Recurrent neural networks for P300-based BCI, 2019, arXiv preprint [arXiv:1901.10798](https://arxiv.org/abs/1901.10798).
- [544] P. Wang, A. Jiang, X. Liu, J. Shang, L. Zhang, LSTM-Based EEG classification in motor imagery tasks, *IEEE Trans. Neural Syst. Rehabil. Eng.* 26 (11) (2018) 2086–2095.
- [545] S. Tortora, S. Ghidoni, C. Chisari, S. Micera, F. Artoni, Deep learning-based BCI for gait decoding from EEG with LSTM recurrent neural network, *J. Neural Eng.* (2020).
- [546] H.G. Yeom, J.S. Kim, C.K. Chung, LSTM Improves accuracy of reaching trajectory prediction from magnetoencephalography signals, *IEEE Access* 8 (2020) 20146–20150.
- [547] G. Tanaka, T. Yamane, J.B. Héroux, R. Nakane, N. Kanazawa, S. Takeda, H. Numata, D. Nakano, A. Hirose, Recent advances in physical reservoir computing: A review, *Neural Netw.* 115 (2019) 100–123.
- [548] D. Ibanez-Soria, A. Soria-Frisch, J. Garcia-Ojalvo, G. Ruffini, Echo state networks ensemble for SSVEP dynamical online detection, *bioRxiv* (2018) 268581.
- [549] D. Ibáñez-Soria, A. Soria-Frisch, J. García-Ojalvo, G. Ruffini, Characterization of the non-stationary nature of steady-state visual evoked potentials using echo state networks, *PLoS One* 14 (7) (2019) e0218771.
- [550] M. Sugiyama, M. Krauledat, K.-R. Määrä, Covariate shift adaptation by importance weighted cross validation, *J. Mach. Learn. Res.* 8 (May) (2007) 985–1005.
- [551] S. Lu, C. Guan, H. Zhang, Unsupervised brain computer interface based on intersubject information and online adaptation, *IEEE Trans. Neural Syst. Rehabil. Eng.* 17 (2) (2009) 135–145.
- [552] C. Vidaurre, C. Sannelli, K.-R. Müller, B. Blankertz, Machine-learning-based coadaptive calibration for brain-computer interfaces, *Neural Comput.* 23 (3) (2011) 791–816.
- [553] J. Wolpaw, E.W. Wolpaw, Brain-Computer Interfaces: Principles and Practice, OUP USA, 2012.
- [554] D. Huebner, T. Verhoeven, K.-R. Mueller, P.-J. Kindermans, M. Tangermann, Unsupervised learning for brain-computer interfaces based on event-related potentials: Review and online comparison [research frontier], *IEEE Comput. Intell. Mag.* 13 (2) (2018) 66–77.
- [555] M.A. Lebedev, J.M. Carmena, J.E. O'Doherty, M. Zacksenhouse, C.S. Henriquez, J.C. Principe, M.A. Nicolelis, Cortical ensemble adaptation to represent velocity of an artificial actuator controlled by a brain-machine interface, *J. Neurosci.* 25 (19) (2005) 4681–4693.
- [556] E.A. Pohlmeier, B. Mahmoudi, S. Geng, N.W. Prins, J.C. Sanchez, Using reinforcement learning to provide stable brain-machine interface control despite neural input reorganization, *PLoS One* 9 (1) (2014) e87253.
- [557] L.R. Hochberg, D. Bacher, B. Jarosiewicz, N.Y. Masse, J.D. Simeral, J. Vogel, S. Haddadin, J. Liu, S.S. Cash, P. Van Der Smagt, et al., Reach and grasp by people with tetraplegia using a neurally controlled robotic arm, *Nature* 485 (7398) (2012) 372–375.
- [558] J. Simeral, S.-P. Kim, M. Black, J. Donoghue, L. Hochberg, Neural control of cursor trajectory and click by a human with tetraplegia 1000 days after implant of an intracortical microelectrode array, *J. Neural Eng.* 8 (2) (2011) 025027.
- [559] A.L. Orsborn, S. Dangi, H.G. Moorman, J.M. Carmena, Closed-loop decoder adaptation on intermediate time-scales facilitates rapid BMI performance improvements independent of decoder initialization conditions, *IEEE Trans. Neural Syst. Rehabil. Eng.* 20 (4) (2012) 468–477.
- [560] B. Mahmoudi, E.A. Pohlmeier, N.W. Prins, S. Geng, J.C. Sanchez, Towards autonomous neuroprosthetic control using hebbian reinforcement learning, *J. Neural Eng.* 10 (6) (2013) 066005.
- [561] R.S. Sutton, A.G. Barto, Reinforcement learning: an introduction, Cambridge, MA: MIT Press., 1998.
- [562] B.T. Marsh, V.S.A. Tarigopula, C. Chen, J.T. Francis, Toward an autonomous brain machine interface: integrating sensorimotor reward modulation and reinforcement learning, *J. Neurosci.* 35 (19) (2015) 7374–7387.
- [563] N.W. Prins, J.C. Sanchez, A. Prasad, Feedback for reinforcement learning based brain-machine interfaces using confidence metrics, *J. Neural Eng.* 14 (3) (2017) 036016.
- [564] C. Wirth, P. Dockree, S. Harty, E. Lacey, M. Arvaneh, Towards error categorisation in BCI: single-trial EEG classification between different errors, *J. Neural Eng.* 17 (1) (2019) 016008.
- [565] T.L. Carroll, Using reservoir computers to distinguish chaotic signals, *Phys. Rev. E* 98 (5) (2018) 052209.
- [566] H. Jaeger, H. Haas, Harnessing nonlinearity: Predicting chaotic systems and saving energy in wireless communication, *Science* 304 (5667) (2004) 78–80.
- [567] W. Maass, T. Natschläger, H. Markram, Real-time computing without stable states: A new framework for neural computation based on perturbations, *Neural Comput.* 14 (11) (2002) 2531–2560.
- [568] M. Lukoševičius, H. Jaeger, Reservoir computing approaches to recurrent neural network training, *Comp. Sci. Rev.* 3 (3) (2009) 127–149.
- [569] Z. Lu, J. Pathak, B. Hunt, M. Girvan, R. Brockett, E. Ott, Reservoir observers: Model-free inference of unmeasured variables in chaotic systems, *Chaos* 27 (4) (2017) 041102.
- [570] J. Pathak, Z. Lu, B.R. Hunt, M. Girvan, E. Ott, Using machine learning to replicate chaotic attractors and calculate Lyapunov exponents from data, *Chaos* 27 (12) (2017) 121102.
- [571] Z. Lu, B.R. Hunt, E. Ott, Attractor reconstruction by machine learning, *Chaos* 28 (6) (2018) 061104.
- [572] J. Pathak, B. Hunt, M. Girvan, Z. Lu, E. Ott, Model-free prediction of large spatiotemporally chaotic systems from data: A reservoir computing approach, *Phys. Rev. Lett.* 120 (2) (2018) 024102.
- [573] J. Pathak, A. Wikner, R. Fussell, S. Chandra, B.R. Hunt, M. Girvan, E. Ott, Hybrid forecasting of chaotic processes: Using machine learning in conjunction with a knowledge-based model, *Chaos* 28 (4) (2018) 041101.
- [574] A. Griffith, A. Pomerance, D.J. Gauthier, Forecasting chaotic systems with very low connectivity reservoir computers, *Chaos* 29 (12) (2019) 123108.
- [575] J. Jiang, Y.-C. Lai, Model-free prediction of spatiotemporal dynamical systems with recurrent neural networks: Role of network spectral radius, *Phys. Rev. Res.* 1 (3) (2019) 033056.
- [576] R.S. Zimmermann, U. Parlitz, Observing spatio-temporal dynamics of excitable media using reservoir computing, *Chaos* 28 (4) (2018) 043118.
- [577] P.R. Vlachas, J. Pathak, B.R. Hunt, T.P. Sapsis, M. Girvan, E. Ott, P. Koumoutsakos, Backpropagation algorithms and reservoir computing in recurrent neural networks for the forecasting of complex spatiotemporal dynamics, *Neural Netw.* (2020).
- [578] H. Fan, J. Jiang, C. Zhang, X. Wang, Y.-C. Lai, Long-term prediction of chaotic systems with machine learning, *Phys. Rev. Res.* 2 (1) (2020) 012080.
- [579] F. Wyffels, B. Schrauwen, A comparative study of reservoir computing strategies for monthly time series prediction, *Neurocomputing* 73 (10–12) (2010) 1958–1964.
- [580] K. Nakai, Y. Saiki, Machine-learning inference of fluid variables from data using reservoir computing, *Phys. Rev. E* 98 (2) (2018) 023111.
- [581] L. Kocarev, U. Parlitz, Generalized synchronization, predictability, and equivalence of unidirectionally coupled dynamical systems, *Phys. Rev. Lett.* 76 (11) (1996) 1816.
- [582] K. Pyragas, Conditional Lyapunov exponents from time series, *Phys. Rev. E* 56 (5) (1997) 5183.
- [583] T. Weng, H. Yang, C. Gu, J. Zhang, M. Small, Synchronization of chaotic systems and their machine-learning models, *Phys. Rev. E* 99 (4) (2019) 042203.

- [584] M. Lukoševičius, H. Jaeger, Reservoir computing approaches to recurrent neural network training, *Comp. Sci. Rev.* 3 (3) (2009) 127–149.
- [585] K. Vandoorne, J. Dambre, D. Verstraeten, B. Schrauwen, P. Bienstman, Parallel reservoir computing using optical amplifiers, *IEEE Trans. Neural Netw.* 22 (9) (2011) 1469–1481.
- [586] M.A.A. Fiers, T. Van Vaerenbergh, F. Wyffels, D. Verstraeten, B. Schrauwen, J. Dambre, P. Bienstman, Nanophotonic reservoir computing with photonic crystal cavities to generate periodic patterns, *IEEE Trans. Neural Netw. Learn. Syst.* 25 (2) (2013) 344–355.
- [587] D. Brunner, M.C. Soriano, C.R. Mirasso, I. Fischer, Parallel photonic information processing at gigabyte per second data rates using transient states, *Nat. Commun.* 4 (1) (2013) 1–7.
- [588] L. Larger, A. Baylón-Fuentes, R. Martinenghi, V.S. Udal'tsov, Y.K. Chembo, M. Jacquot, High-speed photonic reservoir computing using a time-delay-based architecture: Million words per second classification, *Phys. Rev. X* 7 (1) (2017) 011015.
- [589] N.D. Haynes, M.C. Soriano, D.P. Rosin, I. Fischer, D.J. Gauthier, Reservoir computing with a single time-delay autonomous boolean node, *Phys. Rev. E* 91 (2) (2015) 020801.
- [590] K. Hornik, M. Stinchcombe, H. White, Multilayer feedforward networks are universal approximators, *Neural Netw.* 2 (5) (1989) 359–366.
- [591] G. Cybenko, Approximation by superpositions of a sigmoidal function, *Math. Control Signals Syst.* 2 (4) (1989) 303–314.
- [592] H.D. Abarbanel, N.F. Rulkov, M.M. Sushchik, Generalized synchronization of chaos: The auxiliary system approach, *Phys. Rev. E* 53 (5) (1996) 4528.
- [593] A.E. Hramov, A.A. Koronovskii, Generalized synchronization: a modified system approach, *Phys. Rev. E* 71 (6) (2005) 067201, <http://dx.doi.org/10.1103/PhysRevE.71.067201>.
- [594] N. Birbaumer, A.R. Murgia, C. Weber, P. Montoya, Neurofeedback and brain–computer interface: clinical applications, *Int. Rev. Neurobiol.* 86 (2009) 107–117.
- [595] W.C. Stacey, B. Litt, Technology insight: neuroengineering and epilepsy-designing devices for seizure control, *Nat. Clin. Pract. Neurol.* 4 (4) (2008) 190–201.
- [596] A. Coenen, E. Van Luijtelaar, Genetic animal models for absence epilepsy: a review of the WAG/Rij strain of rats, *Behav. Genet.* 33 (6) (2003) 635–655.
- [597] W.-X. Wang, Y.-C. Lai, C. Grebogi, Data based identification and prediction of nonlinear and complex dynamical systems, *Phys. Rep.* 644 (2016) 1–76.
- [598] D. Gurve, D. Delisle-Rodriguez, T. Bastos-Filho, S. Krishnan, Trends in compressive sensing for EEG signal processing applications, *Sensors* 20 (13) (2020) 3703.
- [599] M.M. de Oliveira, M. Khosravy, H.L. Monteiro, T.W. Cabral, F.M. Dias, M.A. Lima, L.R.M. Silva, C.A. Duque, Compressive sensing of electroencephalogram: a review, in: *Compressive Sensing in Healthcare*, Elsevier, 2020, pp. 247–268.
- [600] T. Ma, H. Li, H. Yang, X. Lv, P. Li, T. Liu, D. Yao, P. Xu, The extraction of motion-onset VEP BCI features based on deep learning and compressed sensing, *J. Neurosci. Methods* 275 (2017) 80–92.
- [601] H. Lee, J. Choi, S. Kim, S.C. Jun, B.-G. Lee, A compressive sensing-based automatic sleep-stage classification system with radial basis function neural network, *IEEE Access* 7 (2019) 186499–186509.
- [602] K. Zeng, J. Yan, Y. Wang, A. Sik, G. Ouyang, X. Li, Automatic detection of absence seizures with compressive sensing EEG, *Neurocomputing* 171 (2016) 497–502.
- [603] H. Lin, J. Mairal, Z. Harchaoui, A universal catalyst for first-order optimization, *Adv. Neural Inf. Process. Syst.* 28 (2015) 3384–3392.
- [604] P. Xu, F. Roosta, M.W. Mahoney, Second-order optimization for non-convex machine learning: An empirical study, in: *Proceedings of the 2020 SIAM International Conference on Data Mining*, SIAM, 2020, pp. 199–207.
- [605] E. Mezura-Montes, C.A.C. Coello, A simple multimembered evolution strategy to solve constrained optimization problems, *IEEE Trans. Evol. Comput.* 9 (1) (2005) 1–17.
- [606] P.-T. De Boer, D.P. Kroese, S. Mannor, R.Y. Rubinstein, A tutorial on the cross-entropy method, *Ann. Oper. Res.* 134 (1) (2005) 19–67.
- [607] D.E. Goldberg, *Genetic Algorithms*, Pearson Education India, 2006.
- [608] D. Whitley, A genetic algorithm tutorial, *Stat. Comput.* 4 (2) (1994) 65–85.
- [609] F.M. Noori, N. Naseer, N.K. Qureshi, H. Nazeer, R.A. Khan, Optimal feature selection from fNIRS signals using genetic algorithms for BCI, *Neurosci. Lett.* 647 (2017) 61–66.
- [610] R. Boostani, B. Graimann, M.H. Moradi, G. Pfurtscheller, A comparison approach toward finding the best feature and classifier in cue-based BCI, *Med. Biol. Eng. Comput.* 45 (4) (2007) 403.
- [611] J. Kennedy, R. Eberhart, Particle swarm optimization, in: *Proceedings of ICNN'95-International Conference on Neural Networks*, 4, IEEE, 1995, pp. 1942–1948.
- [612] H. Garg, A hybrid PSO-GA algorithm for constrained optimization problems, *Appl. Math. Comput.* 274 (2016) 292–305.
- [613] Y. Qi, F. Ding, F. Xu, J. Yang, Channel and feature selection for a motor imagery-based BCI system using multilevel particle swarm optimization, *Comput. Intell. Neurosci.* 2020 (2020).
- [614] Z. Li, L. Qiu, R. Li, Z. He, J. Xiao, Y. Liang, F. Wang, J. Pan, Enhancing BCI-based emotion recognition using an improved particle swarm optimization for feature selection, *Sensors* 20 (11) (2020) 3028.
- [615] E. Mezura-Montes, C.A.C. Coello, Constraint-handling in nature-inspired numerical optimization: past, present and future, *Swarm Evol. Comput.* 1 (4) (2011) 173–194.
- [616] H.-M. Gutmann, A radial basis function method for global optimization, *J. Global Optim.* 19 (3) (2001) 201–227.
- [617] P.I. Frazier, A tutorial on bayesian optimization, 2018, arXiv preprint [arXiv:1807.02811](https://arxiv.org/abs/1807.02811).
- [618] J. Snoek, H. Larochelle, R.P. Adams, Practical bayesian optimization of machine learning algorithms, *Adv. Neural Inf. Process. Syst.* 25 (2012) 2951–2959.
- [619] M.A. Gelbart, J. Snoek, R.P. Adams, Bayesian Optimization with unknown constraints, 2014, arXiv preprint [arXiv:1403.5607](https://arxiv.org/abs/1403.5607).
- [620] H. Ke, D. Chen, B. Shi, J. Zhang, X. Liu, X. Zhang, X. Li, Improving brain E-health services via high-performance eeg classification with grouping Bayesian optimization, *IEEE Trans. Serv. Comput.* (2019).
- [621] R. Lorenz, A. Hampshire, R. Leech, Neuroadaptive Bayesian optimization and hypothesis testing, *Trends Cogn. Sci.* 21 (3) (2017) 155–167.
- [622] H. Bashashati, R.K. Ward, A. Bashashati, User-customized brain computer interfaces using Bayesian optimization, *J. Neural Eng.* 13 (2) (2016) 026001.
- [623] S. Shah talebi, A. Mohammadi, Bayesian Optimized spectral filters coupled with ternary ECOC for single-trial EEG classification, *IEEE Trans. Neural Syst. Rehabil. Eng.* 26 (12) (2018) 2249–2259.
- [624] B. He, B. Baxter, B.J. Edelman, C.C. Cline, W.Y. Wenjing, Noninvasive brain-computer interfaces based on sensorimotor rhythms, *Pros. IEEE* 103 (6) (2015) 907–925.
- [625] K.K. Ang, C. Guan, Brain–computer interface for neurorehabilitation of upper limb after stroke, *Pros. IEEE* 103 (6) (2015) 944–953.
- [626] G. Müller-Putz, P. Ofner, A. Schwarz, J. Pereira, G. Luzhnica, C. di Sciascio, E. Veas, S. Stein, J. Williamson, R. Murray-Smith, et al., Moregrasp: Restoration of upper limb function in individuals with high spinal cord injury by multimodal neurom prostheses for interaction in daily activities, 2017.

- [627] K. Tanaka, K. Matsunaga, H.O. Wang, Electroencephalogram-based control of an electric wheelchair, *IEEE Trans. Robot. Autom.* 21 (4) (2005) 762–766.
- [628] J. Meng, S. Zhang, A. Bekyo, J. Olsoe, B. Baxter, B. He, Noninvasive electroencephalogram based control of a robotic arm for reach and grasp tasks, *Sci. Rep.* 6 (2016) 38565.
- [629] M. AL-Quraishi, I. Elamvazuthi, S. Daud, S. Parasuraman, A. Borboni, EEG-based control for upper and lower limb exoskeletons and prostheses: A systematic review, *Sensors* 18 (10) (2018) 3342.
- [630] D. Delisle-Rodriguez, V. Cardoso, D. Gurve, F. Loterio, M.A. Romero-Laiseca, S. Krishnan, T. Bastos Filho, System based on subject-specific bands to recognize pedaling motor imagery: Towards a BCI for lower-limb rehabilitation, *J. Neural Eng.* (2019).
- [631] E.C. Leuthardt, Z. Freudenberg, D. Bundy, J. Roland, Microscale recording from human motor cortex: implications for minimally invasive electrocorticographic brain-computer interfaces, *Neurosurg. Focus* 27 (1) (2009) E10.
- [632] M. Velliste, S. Perel, M.C. Spalding, A.S. Whitford, A.B. Schwartz, Cortical control of a prosthetic arm for self-feeding, *Nature* 453 (7198) (2008) 1098.
- [633] X. Ma, C. Ma, J. Huang, P. Zhang, J. Xu, J. He, Decoding lower limb muscle activity and kinematics from cortical neural spike trains during monkey performing stand and squat movements, *Front. Neurosci.* 11 (2017) 44.
- [634] S. Rajangam, P.-H. Tseng, A. Yin, G. Lehew, D. Schwarz, M.A. Lebedev, M.A.L. Nicolelis, Wireless cortical brain-machine interface for whole-body navigation in primates, *Sci. Rep.* 6 (2016) 22170.
- [635] P.J. Ifft, S. Shokur, Z. Li, M.A. Lebedev, M.A.L. Nicolelis, A brain-machine interface enables bimanual arm movements in monkeys, *Sci. Transl. Med.* 5 (210) (2013) 210ra154.
- [636] J.R. Wolpaw, N. Birbaumer, D.J. McFarland, G. Pfurtscheller, T.M. Vaughan, Brain-computer interfaces for communication and control, *Clin. Neurophysiol.* 113 (6) (2002) 767–791.
- [637] J. Kilmarx, R. Abiri, S. Borhani, Y. Jiang, X. Zhao, Sequence-based manipulation of robotic arm control in brain machine interface, *Int. J. Intell. Robotics Appl.* 2 (2) (2018) 149–160.
- [638] R.A. Khan, N. Naseer, N.K. Qureshi, F.M. Noori, H. Nazeer, M.U. Khan, fNIRS-based neurorobotic interface for gait rehabilitation, *J. Neuroeng. Rehabil.* 15 (1) (2018) 7.
- [639] C. Klaes, Invasive brain-computer interfaces and neural recordings from humans, in: *Handbook of Behavioral Neuroscience*, 28, Elsevier, 2019, pp. 527–539.
- [640] M.Z. Baig, N. Aslam, H.P. Shum, Filtering techniques for channel selection in motor imagery eeg applications: a survey, *Artif. Intell. Rev.* (2019) 1–26.
- [641] S.N. Flesher, J.L. Collinger, S.T. Foldes, J.M. Weiss, J.E. Downey, E.C. Tyler-Kabara, S.J. Bensmaia, A.B. Schwartz, M.L. Boninger, R.A. Gaunt, Intracortical microstimulation of human somatosensory cortex, *Sci. Transl. Med.* 8 (361) (2016) 361–141.
- [642] E.V. Evarts, Pyramidal tract activity associated with a conditioned hand movement in the monkey., *J. Neurophysiol.* 29 (6) (1966) 1011–1027.
- [643] E. Marg, J.E. Adams, Indwelling multiple micro-electrodes in the brain, *Electroencephalogr. Clin. Neurophysiol.* 23 (3) (1967) 277–280.
- [644] J.P. Donoghue, Connecting cortex to machines: recent advances in brain interfaces, *Nature Neurosci.* 5 (11s) (2002) 1085.
- [645] M.D. Serruya, N.G. Hatsopoulos, L. Paninski, M.R. Fellows, J.P. Donoghue, Brain-machine interface: Instant neural control of a movement signal, *Nature* 416 (6877) (2002) 141.
- [646] J.K. Chapin, K.A. Moxon, R.S. Markowitz, M.A. Nicolelis, Real-time control of a robot arm using simultaneously recorded neurons in the motor cortex, *Nature Neurosci.* 2 (7) (1999) 664.
- [647] T. Vouga, K. Zhuang, J. Olivier, M. Lebedev, M. Nicolelis, M. Bouri, H. Bleuler, EXiO-A brain-controlled lower limb exoskeleton for rhesus macaques, *IEEE Trans. Neural Syst. Rehabil. Eng.* 25 (2) (2017) 131–141.
- [648] S.H. Tillery, D. Taylor, A. Schwartz, The general utility of a neuromprosthetic device under direct cortical control, in: *Proceedings of the 25th Annual International Conference of the IEEE Engineering in Medicine and Biology Society (IEEE Cat. No. 03CH37439)*, 3, IEEE, 2003, pp. 2043–2046.
- [649] A.B. Schwartz, D.M. Taylor, S.I.H. Tillery, Extraction algorithms for cortical control of arm prosthetics, *Curr. Opin. Neurobiol.* 11 (6) (2001) 701–708.
- [650] U. Rokni, O. Steinberg, E. Vaadia, H. Sompolinsky, Cortical representation of bimanual movements, *J. Neurosci.* 23 (37) (2003) 11577–11586.
- [651] O. Donchin, A. Gribova, O. Steinberg, H. Bergman, E. Vaadia, Primary motor cortex is involved in bimanual coordination, *Nature* 395 (6699) (1998) 274.
- [652] N. Fitzsimmons, M. Lebedev, I. Peikon, M.A.L. Nicolelis, Extracting kinematic parameters for monkey bipedal walking from cortical neuronal ensemble activity, *Front. Integr. Neurosci.* 3 (2009) 3.
- [653] M. Capogrosso, T. Milekovic, D. Borton, F. Wagner, E.M. Moraud, J.-B. Mignardot, N. Buse, J. Gandar, Q. Barraud, D. Xing, et al., A brain-spine interface alleviating gait deficits after spinal cord injury in primates, *Nature* 539 (7628) (2016) 284–288.
- [654] C. Ethier, E.R. Oby, M.J. Bauman, L.E. Miller, Restoration of grasp following paralysis through brain-controlled stimulation of muscles, *Nature* 485 (7398) (2012) 368–371.
- [655] C.E. Bouton, A. Shaikhouni, N.V. Annetta, M.A. Bockbrader, D.A. Friedenberg, D.M. Nielson, G. Sharma, P.B. Sederberg, B.C. Glenn, W.J. Mysiw, et al., Restoring cortical control of functional movement in a human with quadriplegia, *Nature* 533 (7602) (2016) 247–250.
- [656] C.H. Ho, R.J. Triolo, A.L. Elias, K.L. Kilgore, A.F. DiMarco, K. Bogie, A.H. Vette, M.L. Aduu, R. Kobetic, S.R. Chang, et al., Functional electrical stimulation and spinal cord injury, *Phys. Med. Rehabil. Clin.* 25 (3) (2014) 631–654.
- [657] N. Kapadia, K. Masani, B. Catharine Craven, L.M. Giangregorio, S.L. Hitzig, K. Richards, M.R. Popovic, A randomized trial of functional electrical stimulation for walking in incomplete spinal cord injury: effects on walking competency, *J. Spinal Cord Med.* 37 (5) (2014) 511–524.
- [658] N. Wenger, E.M. Moraud, S. Raspopovic, M. Bonizzato, J. DiGiovanna, P. Musienko, M. Morari, S. Micera, G. Courtine, Closed-loop neuromodulation of spinal sensorimotor circuits controls refined locomotion after complete spinal cord injury, *Sci. Transl. Med.* 6 (255) (2014) 255ra133.
- [659] D.A. Schwarz, M.A. Lebedev, T.L. Hanson, D.F. Dimitrov, G. Lehew, J. Meloy, S. Rajangam, V. Subramanian, P.J. Ifft, Z. Li, et al., Chronic, wireless recordings of large-scale brain activity in freely moving rhesus monkeys, *Nature Methods* 11 (6) (2014) 670.
- [660] K. Hu, M. Jamali, Z.B. Moses, C.A. Ortega, G.N. Friedman, W. Xu, Z.M. Williams, Decoding unconstrained arm movements in primates using high-density electrocorticography signals for brain-machine interface use, *Sci. Rep.* 8 (1) (2018) 10583.
- [661] B. Wittevrongel, E. Khachatrian, M. Fahimi Hnazaee, F. Camarrone, E. Carrette, L. De Taeye, A. Meurs, P. Boon, D. Van Roost, M.M. Van Hulle, Decoding steady-state visual evoked potentials from electrocorticography, *Front. Neuroinform.* 12 (2018) 65.
- [662] D.J. McFarland, A.T. Lefkowicz, J.R. Wolpaw, Design and operation of an EEG-based brain-computer interface with digital signal processing technology, *Behav. Res. Methods Instrum. Comput.* 29 (3) (1997) 337–345, <http://dx.doi.org/10.3758/BF03200585>.
- [663] D. Bacher, B. Jarosiewicz, N.Y. Masse, S.D. Stavisky, J.D. Simeral, K. Newell, E.M. Oakley, S.S. Cash, G. Fries, L.R. Hochberg, Neural point-and-click communication by a person with incomplete locked-in syndrome, *Neurorehabil. Neural Repair* 29 (5) (2015) 462–471.
- [664] R. Abiri, G. Heise, F. Schwartz, X. Zhao, EEG-Based control of a unidimensional computer cursor using imagined body kinematics, in: *Biomedical Engineering Society Annual Meeting (BMES 2015)*, 2015.

- [665] T.J. Bradberry, R.J. Gentili, J.L. Contreras-Vidal, Fast attainment of computer cursor control with noninvasively acquired brain signals, *J. Neural Eng.* 8 (3) (2011) 036010.
- [666] S. Perrey, Non-invasive NIR spectroscopy of human brain function during exercise, *Methods* 45 (4) (2008) 289–299.
- [667] S.K. Piper, A. Krueger, S.P. Koch, J. Mehnert, C. Habermehl, J. Steinbrink, H. Obrig, C.H. Schmitz, A wearable multi-channel fNIRS system for brain imaging in freely moving subjects, *Neuroimage* 85 (2014) 64–71.
- [668] E. García-Cossío, M. Severens, B. Nienhuis, J. Duysens, P. Desain, N. Keijser, J. Farquhar, Decoding sensorimotor rhythms during robotic-assisted treadmill walking for brain computer interface (BCI) applications, *PLoS One* 10 (12) (2015) e0137910.
- [669] A.I. Sburlea, L. Montesano, R.C. de la Cuerda, I.M.A. Diego, J.C. Miangolarra-Page, J. Minguez, Detecting intention to walk in stroke patients from pre-movement eeg correlates, *J. Neuroeng. Rehabil.* 12 (1) (2015) 113.
- [670] L. Clemmensen, T. Hastie, D. Witten, B. Ersbøll, Sparse discriminant analysis, *Technometrics* 53 (4) (2011) 406–413.
- [671] I. Miyai, H.C. Tanabe, I. Sase, H. Eda, I. Oda, I. Konishi, Y. Tsunazawa, T. Suzuki, T. Yanagida, K. Kubota, Cortical mapping of gait in humans: a near-infrared spectroscopic topography study, *Neuroimage* 14 (5) (2001) 1186–1192.
- [672] M. Suzuki, I. Miyai, T. Ono, I. Oda, I. Konishi, T. Kochiyama, K. Kubota, Prefrontal and premotor cortices are involved in adapting walking and running speed on the treadmill: an optical imaging study, *Neuroimage* 23 (3) (2004) 1020–1026.
- [673] M. Mihara, I. Miyai, M. Hatakenaka, K. Kubota, S. Sakoda, Sustained prefrontal activation during ataxic gait: a compensatory mechanism for ataxic stroke?, *Neuroimage* 37 (4) (2007) 1338–1345.
- [674] M.J. Kurz, T.W. Wilson, D.J. Arpin, Stride-time variability and sensorimotor cortical activation during walking, *Neuroimage* 59 (2) (2012) 1602–1607.
- [675] S. Perrey, Possibilities for examining the neural control of gait in humans with fNIRS, *Front. Physiol.* 5 (2014) 204.
- [676] M. Rea, M. Rana, N. Lugato, P. Terekhin, L. Gizzi, D. Brötz, A. Fallgatter, N. Birbaumer, R. Sitaram, A. Caria, Lower limb movement preparation in chronic stroke: a pilot study toward an fNIRS-BCI for gait rehabilitation, *Neurorehabil. Neural Repair* 28 (6) (2014) 564–575.
- [677] A. Vilringer, J. Planck, C. Hock, L. Schleinkofer, U. Dirnagl, Near infrared spectroscopy (NIRS): a new tool to study hemodynamic changes during activation of brain function in human adults, *Neurosci. Lett.* 154 (1–2) (1993) 101–104.
- [678] A.E. Hramov, V. Grubov, A. Badarin, V.A. Maksimenko, A.N. Pisarchik, Functional near-infrared spectroscopy for the classification of motor-related brain activity on the sensor-level, *Sensors* 20 (8) (2020) 2362.
- [679] B. Blankertz, G. Dornhege, M. Krauledat, K.R. Müller, G. Curio, The non-invasive Berlin brain-computer interface: fast acquisition of effective performance in untrained subjects, *NeuroImage* 37 (2) (2007) 539–550.
- [680] C. Neuper, R. Scherer, M. Reiner, G. Pfurtscheller, Imagery of motor actions: Differential effects of kinesthetic and visual-motor mode of imagery in single-trial EEG, *Cogn. Brain Res.* 25 (3) (2005) 668–677.
- [681] N. Mizuguchi, H. Nakata, Y. Uchida, K. Kanosue, Motor imagery and sport performance, *J. Phys. Fit. Sports Med.* 1 (1) (2012) 103–111.
- [682] N. Tomida, T. Tanaka, S. Ono, M. Yamagishi, H. Higashi, Active data selection for motor imagery EEG classification, *IEEE Trans. Biomed. Eng.* 62 (2) (2015) 458–467.
- [683] J. Yang, H. Singh, E.L. Hines, F. Schlaghecken, D.D. Iliescu, M.S. Leeson, N.G. Stocks, Channel selection and classification of electroencephalogram signals: an artificial neural network and genetic algorithm-based approach, *Artif. Intell. Med.* 55 (2) (2012) 117–126.
- [684] M.C. Åberg, J. Wessberg, Evolutionary optimization of classifiers and features for single-trial EEG discrimination, *Biomed. Eng. online* 6 (1) (2007) 32.
- [685] A.L. Velasco, M. Velasco, F. Velasco, D. Menes, F. Gordon, L. Rocha, M. Briones, I. Márquez, Subacute and chronic electrical stimulation of the hippocampus on intractable temporal lobe seizures: preliminary report, *Arch. Med. Res.* 31 (3) (2000) 316–328.
- [686] V.K. Kimiskidis, D. Kugiumtzis, S. Papagiannopoulos, N. Vlaikidis, Transcranial magnetic stimulation (TMS) modulates epileptiform discharges in patients with frontal lobe epilepsy: a preliminary EEG-tms study, *Int. J. Neural Syst.* 23 (01) (2013) 1250035.
- [687] E. Krook-Magnuson, C. Armstrong, M. Ojala, I. Soltesz, On-demand optogenetic control of spontaneous seizures in temporal lobe epilepsy, *Nat. Commun.* 4 (2013) 1376.
- [688] R.S. Fisher, G.L. Krauss, E. Ramsay, K. Laxer, J. Gates, Assessment of vagus nerve stimulation for epilepsy: report of the therapeutics and technology assessment subcommittee of the American academy of neurology, *Neurology* 49 (1) (1997) 293–297.
- [689] M. Hodaie, R.A. Wennberg, J.O. Dostrovsky, A.M. Lozano, Chronic anterior thalamus stimulation for intractable epilepsy, *Epilepsia* 43 (6) (2002) 603–608.
- [690] E.H. Kossoff, E.K. Ritzl, J.M. Politsky, A.M. Murro, J.R. Smith, R.B. Duckrow, D.D. Spencer, G.K. Bergey, Effect of an external responsive neurostimulator on seizures and electrographic discharges during subdural electrode monitoring, *Epilepsia* 45 (12) (2004) 1560–1567.
- [691] A. Berényi, M. Belluscio, D. Mao, G. Buzsáki, Closed-loop control of epilepsy by transcranial electrical stimulation, *Science* 337 (6095) (2012) 735–737.
- [692] A.E. Hramov, A.A. Koronovskii, I.S. Midyanovskaya, E. Sitnikova, C.M. Rijn, On-off intermittency in time series of spontaneous paroxysmal activity in rats with genetic absence epilepsy, *Chaos* 16 (2006) 43111, <http://dx.doi.org/10.1063/1.2360505>.
- [693] E. Sitnikova, A.E. Hramov, V.V. Grubov, A.A. Ovchinnikov, A.A. Koronovsky, On-off intermittency of thalamo-cortical oscillations in the electroencephalogram of rats with genetic predisposition to absence epilepsy, *Brain Res.* 1436 (2012) 147–156, <http://dx.doi.org/10.1016/j.brainres.2011.12.006>.
- [694] A.A. Koronovskii, A.E. Hramov, V.V. Grubov, O.I. Moskalenko, E. Sitnikova, A.N. Pavlov, Coexistence of intermittencies in the neuronal network of the epileptic brain, *Phys. Rev. E* 93 (3) (2016) 32220, <http://dx.doi.org/10.1103/physreve.93.032220>.
- [695] D. Gupta, P. Ossenkopp, G. van Luijtelaar, Space-time network connectivity and cortical activations preceding spike wave discharges in human absence epilepsy: a MEG study, *Med. Biol. Eng. Comput.* 49 (5) (2011) 555–565.
- [696] V.V. Makarov, V.A. Maximenko, G. van Luijtelaar, A. Lüttjohann, A.E. Hramov, Control of epileptic seizures in WAG/Rij rats by means of brain-computer interface, in: Dynamics and Fluctuations in Biomedical Photonics XV, 10493, International Society for Optics and Photonics, 2018, 1049311, <http://dx.doi.org/10.1117/12.2291696>.
- [697] D.R. Freestone, P.J. Karoly, M.J. Cook, A forward-looking review of seizure prediction, *Curr. Opin. Neurol.* 30 (2) (2017) 167–173.
- [698] M.J. Cook, P.J. Karoly, D.R. Freestone, D. Himes, K. Leyde, S. Berkovic, T. O'Brien, D.B. Grayden, R. Boston, Human focal seizures are characterized by populations of fixed duration and interval, *Epilepsia* 57 (3) (2016) 359–368.
- [699] E. Nurse, B.S. Mashford, A.J. Yip, I. Kiral-Kornek, S. Harrer, D.R. Freestone, Decoding EEG and LFP signals using deep learning: heading truenorth, in: Proceedings of the ACM International Conference on Computing Frontiers, ACM, 2016, pp. 259–266.
- [700] P.A. Merolla, J.V. Arthur, R. Alvarez-Icaza, A.S. Cassidy, J. Sawada, F. Akopyan, B.L. Jackson, N. Imam, C. Guo, Y. Nakamura, et al., A million spiking-neuron integrated circuit with a scalable communication network and interface, *Science* 345 (6197) (2014) 668–673.
- [701] N.D. Truong, A.D. Nguyen, L. Kuhlmann, M.R. Bonyadi, J. Yang, S. Ippolito, O. Kavehei, Convolutional neural networks for seizure prediction using intracranial and scalp electroencephalogram, *Neural Netw.* 105 (2018) 104–111.
- [702] I. Kiral-Kornek, S. Roy, E. Nurse, B. Mashford, P. Karoly, T. Carroll, D. Payne, S. Saha, S. Baldassano, T. O'Brien, et al., Epileptic seizure prediction using big data and deep learning: toward a mobile system, *EBioMedicine* 27 (2018) 103–111.

- [703] M.J. Cook, T.J. O'Brien, S.F. Berkovic, M. Murphy, A. Morokoff, G. Fabinyi, W. D'Souza, R. Yerra, J. Archer, L. Litewka, et al., Prediction of seizure likelihood with a long-term, implanted seizure advisory system in patients with drug-resistant epilepsy: a first-in-man study, *Lancet Neurol.* 12 (6) (2013) 563–571.
- [704] L. Kuhlmann, K. Lehnhertz, M.P. Richardson, B. Schelter, H.P. Zaveri, Seizure prediction—ready for a new era, *Nature Rev. Neurol.* (2018) 1.
- [705] B. Direito, C.A. Teixeira, F. Sales, M. Castelo-Branco, A. Dourado, A realistic seizure prediction study based on multiclass SVM, *Int. J. Neural Syst.* 27 (03) (2017) 1750006.
- [706] C. Xiao, S. Wang, L. Iasemidis, S. Wong, W.A. Chaovallitwongse, An adaptive pattern learning framework to personalize online seizure prediction, *IEEE Trans. Big Data* (2017).
- [707] N.A. Aleksandrova, T.N. Chernyaeva, M.V. Khramova, A.E. Hramov, The implementation of the innovation platform "educational potential of hardware-software complexes based on the study and interpretation of brain activity patterns", in: 2018 IEEE International Conference "Quality Management, Transport and Information Security, Information Technologies"(IT&QM&IS), IEEE, 2018, pp. 533–535.
- [708] R.d.O. Heidrich, M.A. Branco, J.B. Mossmann, A.R. Schuh, E. Jensen, Development of BCI based softwares to assist people with mobility limitations in the school inclusion process, in: Proceedings of the 17th International ACM SIGACCESS Conference on Computers & Accessibility, ACM, 2015, pp. 397–398.
- [709] G. Di Flumeri, F. De Crescenzo, B. Berberian, O. Ohneiser, J. Kramer, P. Aricò, G. Borghini, F. Babiloni, S. Bagassi, S. Piastra, Brain-computer interface-based adaptive automation to prevent out-of-the-loop phenomenon in air traffic controllers dealing with highly automated systems, *Front. Hum. Neurosci.* 13 (2019).
- [710] N.H. Mackworth, The breakdown of vigilance during prolonged visual search, *Q. J. Exp. Psychol.* 1 (1) (1948) 6–21, arXiv:<https://doi.org/10.1080/17470214808416738>, DOI: 10.1080/17470214808416738.
- [711] S. Makeig, F.S. Elliott, M. Postal, First demonstration of an alertness monitoring management system, *Nav. Health Res. Cent. (Report No. 93-36)* (1994) 21.
- [712] A. Vuckovic, V. Radivojevic, A.C. Chen, D. Popovic, Automatic recognition of alertness and drowsiness from EEG by an artificial neural network, *Med. Eng. Phys.* 24 (5) (2002) 349–360.
- [713] T. Kohonen, The self-organizing map, in: *Neural Networks*, IEEE Press, New York, 1992, pp. 74–90.
- [714] P. Wasserman, *Neural Computing: Theory and Practice*, ANZA Research, New York, 1989.
- [715] M.J. Khan, M.J. Hong, K.-S. Hong, Decoding of four movement directions using hybrid NIRS-eeg braincomputer interface, *Front. Hum. Neurosci.* 8 (2014) 244.
- [716] S. Fazli, J. Mehnert, J. Steinbrink, G. Curio, A. Villringer, K.-R. Müller, B. Blankertz, Enhanced performance by a hybrid NIRS-EEG brain computer interface, *Neuroimage* 59 (1) (2012) 519–529.
- [717] A. von Lühmann, H. Wabnitz, T. Sander, K.-R. Müller, M3BA: a mobile, modular, multimodal biosignal acquisition architecture for miniaturized EEG-NIRS-based hybrid BCI and monitoring, *IEEE Trans. Biomed. Eng.* 64 (6) (2017) 1199–1210.
- [718] M.J. Khan, K.-S. Hong, Passive BCI based on drowsiness detection: an fNIRS study, *Biomed. Opt. Express* 6 (10) (2015) 4063–4078.
- [719] W.B. Baker, A.B. Parthasarathy, D.R. Busch, R.C. Mesquita, J.H. Greenberg, A.G. Yodh, Modified beer-lambert law for blood flow, *Biomed. Opt. Express* 5 (11) (2014) 4053–4075.
- [720] N.R. Pal, C.Y. Chuang, L.W. Ko, T.P. Chao, S.F. Liang, C.T. Lin, EEG-based subject- and session-independent drowsiness detection: an unsupervised approach, *EURASIP Journal on Advances in Signal Processing* 2008(519480):192, <http://dx.doi.org/10.1155/2008/519480>.
- [721] C.T. Lin, R.C. Wu, S.F. Liang, W.H. Chao, Y.J. Chen, T.P. Jung, EEG-Based drowsiness estimation for safety driving using independent component analysis, *IEEE Trans. Circuits Syst. I: Regular Papers* 52 (12) (2005) 2726–2738, <http://dx.doi.org/10.1109/TCSI.2005.857555>.
- [722] S.H. Hsu, T.P. Jung, Monitoring alert and drowsy states by modeling EEG source nonstationarity, *J. Neural Eng.* 14 (5) (2017) 056012.
- [723] P.C. Mahalanobis, On the generalized distance in statistics, *Proc. Natl. Inst. Sci. (India)* 2 (1) (1936) 49–55.
- [724] N. Bigdely-Shamlo, T. Mullen, K.M. Kothe, K.A. Robbins, The PREP pipeline: standardized preprocessing for large-scale eeg analysis, *Front. Neuroinform.* 9 (2015) 16.
- [725] L.W. Ko, O. Komarov, T.P. Hairston W D and, C.T. Lin, Sustained attention in real classroom settings: An EEG study, *Front. Hum. Neurosci.* 11 (2017) 388.
- [726] B.H. Kantowitz, P.A. Caper, Human workload in aviation, in: *Human Factors in Aviation*, Academic Press, New York, 1988, pp. 157–187.
- [727] B.H. Kantowitz, Attention and mental workload, *Proc. Hum. Factors Ergon. Soc. Annu. Meet.* 44 (21) (2000) 3–456–3–459.
- [728] A. Chaudhuri, P.O. Behan, Fatigue and basal ganglia, *J. Neurol. Sci.* 179 (1–2) (2000) 34–42.
- [729] K. Mizuno, M. Tanaka, K. Yamaguti, O. Kajimoto, H. Kuratsune, Y. Watanabe, Mental fatigue caused by prolonged cognitive load associated with sympathetic hyperactivity, *Behav. Brain Fun.* 7 (1) (2011) 17.
- [730] A. Bonnefond, N. Doignon-Camus, P. Touzalin-Chretien, A. Dufour, Vigilance and intrinsic maintenance of alert state: an ERP study, *Behav. Brain Res.* 211 (2) (2010) 185–190.
- [731] M.A. Boksem, T.F. Meijman, M.M. Lorist, Effects of mental fatigue on attention: an ERP study, *Behav. Brain Res.* 25 (1) (2005) 107–116.
- [732] Y. Kato, H. Endo, T. Kizuka, Mental fatigue and impaired response processes: event-related brain potentials in a go/no-go task, *Int. J. Psychophysiol.* 72 (2) (2009) 204–211.
- [733] B.F. Gore, S.M. Casner, W.C. D, Workload measurement and management in system development, in: *Space Safety and Human Performance*, Elsevier, Butteworth-Heinemann, Oxford, 2018, pp. 54–69.
- [734] C. Berka, D.J. Levendowski, M.N. Lumicao, A. Yau, G. Davis, V.T. Zivkovic, R.E. Olmstead, P.D. Tremoulet, P.L. Craven, EEG Correlates of task engagement and mental workload in vigilance, learning, and memory tasks, *Aviat. Space Environ. Med.* 78 (5 Suppl) (2007) B231–B244.
- [735] G. Borghini, R. Isabella, G. Vecchiato, J. Toppi, L. Astolfi, C. Caltagirone, F. Babiloni, Brainshield: HREEG study of perceived pilot mental workload, *Italian J. Aerosp. Med.* 5 (2011) 34–41.
- [736] S.H. Fairclough, L. Tattersall, The influence of task demand and learning on the psychophysiological response, *Int. J. Psychophysiol.* 56 (2) (2005) 171–184.
- [737] G. Borghini, G. Vecchiato, J. Toppi, L. Astolfi, A. Maglione, R. Isabella, C. Caltagirone, W. Kong, D. Wei, Z. Zhou, L. Polidori, S. Vitiello, F. Babiloni, Assessment of mental fatigue during car driving by using high resolution EEG activity and neurophysiologic indices, *Conf. Proc. IEEE Eng. Med. Biol. Soc.* 2012 (2) (2012) 6442–6445.
- [738] S.K. Lal, A. Craig, Driver fatigue: Psychophysiological effects, in: *International Conference on Fatigue and Transportation*, 4th, 2000, Fremantle, Western Australia, 2000.
- [739] S. Lal, A. Craig, Psychophysiological effects associated with drowsiness: driver fatigue and electroencephalography, *Int. J. Psychophysiol.* 35 (1) (2000) 39.
- [740] C. Babiloni, F. Babiloni, F. Carducci, F. Cincotti, F. Vecchio, B. Cola, S. Rossi, M. C., P.M. Rossini, Functional frontoparietal connectivity during short-term memory as revealed by high-resolution EEG coherence analysis, *Behav. Neurosci.* 118 (4) (2004) 687–697.
- [741] L. Astolfi, F. Cincotti, C. Babiloni, F. Carducci, A. Basilisco, P.M. Rossini, S. Salinari, D. Mattia, S. Cerutti, D.B. Dayan, L. Ding, Y. Ni, B. He, F. Babiloni, Estimation of the cortical connectivity by high-resolution EEG and structural equation modeling: simulations and application to finger tapping data, *IEEE Trans. Biomed. Eng.* 52 (5) (2005) 757–768.

- [742] G.D. Di Flumeri, G. Borghini, P. Aricó, N. Sciaraffa, P. Lanzi, S. Pozzi, V. Vignal, C. Lantieri, A. Bichicchi, A. Simone, F. Babiloni, EEG-Based mental workload assessment during real driving: a taxonomic tool for neuroergonomics in highly automated environments, in: *Neuroergonomics: The Brain At Work and in Everyday Life*, Elsevier, London, 2019, pp. 121–126.
- [743] F. Dehais, A. Duprés, G. Di Flumeri, K.J. Verdiére, G. Borghini, F. Babiloni, R.N. Roy, Monitoring pilot's cognitive fatigue with engagement features in simulated and actual flight conditions using an hybrid fNIRS-EEG passive BCI, in: *IEEE Systems, Man, and Cybernetics Society (SMC 2018)*, 2018.
- [744] P. Aricó, G. Borghini, G. Di Flumeri, A. Colosimo, S. Bonelli, A. Galfetti, F. Babiloni, Adaptive automation triggered by EEG-based mental workload index: a passive brain-computer interface application in realistic air traffic control environment, *Front. Human Neurosci.* 2016 (10) (2016) 539.
- [745] J.C.F. de Winter, R. Happee, M.H. Martens, N.A. Stanton, Effects of adaptive cruise control and highly automated driving on workload and situation awareness: a review of the empirical evidence, *Transp. Res. F: Traffic Psychol. Behav.* 27 (2014) 196–217.
- [746] T. Fawcett, Introduction to ROC analysis, *Pattern Recogn. Lett.* 27 (8) (2006) 861–874.
- [747] J. Min, P. Wang, J. Hu, Driver fatigue detection through multiple entropy fusion analysis in an EEG-based system, *PLoS One* 12 (12) (2017) e0188756.
- [748] K.A. Lee, G. Hicks, G. Nino-Murcia, Validity and reliability of a scale to assess fatigue, *Psychiatry Res.* 36 (3) (1991) 291–298.
- [749] G. Borg, Psychophysical scaling with applications in physical work and the perception of exertion, *Scand. J. Work Environ. Health* 16 (Suppl. 1) (1990) 55–58.
- [750] N. Kannathal, M.L. Choo, U.R. Acharya, P. Sadasivan, Entropies for detection of epilepsy in EEG, *Comput. Methods Programs Biomed.* 80 (3) (2005) 187–194.
- [751] S.M. Pincus, Approximate entropy as a measure of system complexity, *Proc. Natl. Acad. Sci. USA* 88 (6) (1991) 2297–2301.
- [752] J.S. Richman, J.R. Moorman, Physiological time-series analysis using approximate entropy and sample entropy, *Am. J. Physiol. Circ. Physiol.* 278 (6) (2000) H2039–H2049.
- [753] J. Xiang, C. Li, H. Li, R. Cao, B. Wang, X. Han, J. Chen, The detection of epileptic seizure signals based on fuzzy entropy, *J. Neurosci. Methods* 243 (2015) 18–25.
- [754] J. Han, J. Pei, M. Kamber, *Data Mining: Concepts and Techniques*, Elsevier, Amsterdam, 2011.
- [755] H.B. Demuth, M.H. Beale, O. De Jess, M.T. Hagan, *Neural Network Design*, Martin Hagan, Oklahoma, 2014.
- [756] A.L. Boulesteix, S. Janitza, J. Kruppa, I.R. Kónig, Overview of random forest methodology and practical guidance with emphasis on computational biology and bioinformatics, *Wiley Interdiscip. Rev.: Data Min. Knowl. Discov.* 2 (6) (2012) 493–507.
- [757] X. Cui, D.M. Bryant, L.A. Reiss, NIRS-Based hyperscanning reveals increased interpersonal coherence in superior frontal cortex during cooperation, *Neuroimage* 59 (3) (2012) 24302437.
- [758] A. Delorme, S. Makeig, EEGLAB: an open source toolbox for analysis of single-trial EEG dynamics including independent component analysis, *J. Neurosci. Methods* 134 (1) (2004) 9–21.
- [759] P. Aricó, G. Borghini, G. Di Flumeri, A. Colosimo, S. Pozzi, F. Babiloni, A passive brain-computer interface (p-BCI) application for the mental workload assessment on professional air traffic controllers (ATCOs) during realistic ATC tasks, *Prog. Brain Res.* 228 (2016) 295–328.
- [760] A. Al-Nafjan, M. Hosny, Y. Al-Ohal, A. Al-Wabil, Review and classification of emotion recognition based on EEG brain-computer interface system research: a systematic review, *Appl. Sci.* 17 (12) (2017) 1239.
- [761] Y.J. Liu, M. Yu, G. Zhao, J. Song, Y. Ge, Y. Shi, Real-time movie-induced discrete emotion recognition from EEG signals, *IEEE Trans. Affect. Comput.* 9 (4) (2018) 550–562.
- [762] G. Chanel, C. Rebetez, M. Bétrancourt, T. Pun, Emotion assessment from physiological signals for adaptation of game difficulty, *IEEE Trans. Syst. Man Cybern.* 41 (6) (2011) 1052–1063.
- [763] D.J. McFarland, L.M. McCane, S.V. David, J.R. Wolpaw, Spatial filter selection for EEG-based communication, *Electroencephalogr. Clin. Neurophysiol.* 103 (3) (1997) 386–394.
- [764] L.I. Aftanas, N.V. Reva, S.V. Varlamov, V.P. Makhnev, Analysis of evoked EEG synchronization and desynchronization in conditions of emotional activation in humans: Temporal and topographic characteristics, *Neurosci. Behav. Physiol.* 34 (8) (2004) 859–867.
- [765] L. Yu, H. Liu, Efficient feature selection via analysis of relevance and redundancy, *J. Mach. Learn. Res.* 5 (Oct) (2004) 1205–1224.
- [766] P. Pudil, F.J. Ferri, J. Novovicova, J. Kittler, Floating search methods for feature selection with nonmonotonic criterion functions, in: *Proceedings of the 12th IAPR International Conference on Pattern Recognition*, Vol. 3 – Conference C: Signal Processing (Cat. No.94CH3440-5), 2, 1994, pp. 279–283, <http://dx.doi.org/10.1109/ICPR.1994.576920>.
- [767] D. Oesterhelt, W. Stoeckenius, Rhodopsin-like protein from the purple membrane of halobacterium halobium, *Nature New Biol.* 233 (39) (1971) 149.
- [768] D. Oesterhelt, W. Stoeckenius, Functions of a new photoreceptor membrane, *Proc. Natl. Acad. Sci. USA* 70 (10) (1973) 2853–2857.
- [769] A. Matsuno-Yagi, Y. Mukohata, Two possible roles of bacteriorhodopsin; a comparative study of strains of halobacterium halobium differing in pigmentation, *Biochem. Biophys. Res. Commun.* 78 (1) (1977) 237–243.
- [770] E.S. Boyden, F. Zhang, E. Bamberg, G. Nagel, K. Deisseroth, Millisecond-timescale, genetically targeted optical control of neural activity, *Nature Neurosci.* 8 (9) (2005) 1263.
- [771] F. Zhang, L.-P. Wang, E.S. Boyden, K. Deisseroth, Channelrhodopsin-2 and optical control of excitable cells, *Nature Methods* 3 (10) (2006) 785.
- [772] K. Deisseroth, Optogenetics, *Nature Methods* 8 (1) (2011) 26.
- [773] A.M. Aravanis, L.-P. Wang, F. Zhang, L.A. Meltzer, M.Z. Mogri, M.B. Schneider, K. Deisseroth, An optical neural interface: in vivo control of rodent motor cortex with integrated fiberoptic and optogenetic technology, *J. Neural Eng.* 4 (3) (2007) S143.
- [774] A.R. Adamantidis, F. Zhang, A.M. Aravanis, K. Deisseroth, L. De Lecea, Neural substrates of awakening probed with optogenetic control of hypocretin neurons, *Nature* 450 (7168) (2007) 420.
- [775] L. Grosenick, J.H. Marshel, K. Deisseroth, Closed-loop and activity-guided optogenetic control, *Neuron* 86 (1) (2015) 106–139.
- [776] J.T. Paz, T.J. Davidson, E.S. Frechette, B. Delord, I. Parada, K. Peng, K. Deisseroth, J.R. Huguenard, Closed-loop optogenetic control of thalamus as a tool for interrupting seizures after cortical injury, *Nature Neurosci.* 16 (1) (2013) 64.
- [777] R. Esteller, J. Echauz, T. Tcheng, B. Litt, B. Pless, Line length: an efficient feature for seizure onset detection, in: *Engineering in Medicine and Biology Society, 2001. Proceedings of the 23rd Annual International Conference of the IEEE*, 2, IEEE, 2001, pp. 1707–1710.
- [778] K.Y. Kwon, B. Sirowatka, A. Weber, W. Li, Opto-uecog array: A hybrid neural interface with transparent uecog electrode array and integrated LEDs for optogenetics, *IEEE Trans. Biomed. Circuits Syst.* 7 (5) (2013) 593–600.
- [779] R. Pashaei, R. Baumgartner, T.J. Richner, S.K. Brodnick, M. Azimipour, K.W. Elceiri, J.C. Williams, Closed-loop optogenetic brain interface, *IEEE Trans. Biomed. Eng.* 62 (10) (2015) 2327–2337.
- [780] C.H. Chen, E.A. McCullagh, S.H. Pun, P.U. Mak, M.I. Vai, P.I. Mak, A. Klug, T.C. Lei, An integrated circuit for simultaneous extracellular electrophysiology recording and optogenetic neural manipulation, *IEEE Trans. Biomed. Eng.* 64 (3) (2017) 557–568.
- [781] M.F. Bolus, A.A. Willats, C.J. Whitmire, C.J. Rozell, G.B. Stanley, Design strategies for dynamic closed-loop optogenetic neurocontrol in vivo, *J. Neural Eng.* 15 (2) (2018) 26011.

- [782] J.P. Newman, M.-f. Fong, D.C. Millard, C.J. Whitmire, G.B. Stanley, S.M. Potter, Optogenetic feedback control of neural activity, *Elife* 4 (2015) e07192.
- [783] E. Iseri, D. Kuzum, Implantable optoelectronic probes for in vivo optogenetics, *J. Neural Eng.* 14 (3) (2017) 31001.
- [784] V. Gradinariu, K.R. Thompson, F. Zhang, M. Mogri, K. Kay, M.B. Schneider, K. Deisseroth, Targeting and readout strategies for fast optical neural control in vitro and in vivo, *J. Neurosci.* 27 (52) (2007) 14231–14238.
- [785] P. Anikeeva, A.S. Andelman, I. Witten, M. Warden, I. Goshen, L. Grosenick, L.A. Gunaydin, L.M. Frank, K. Deisseroth, Optetrode: a multichannel readout for optogenetic control in freely moving mice, *Nature Neurosci.* 15 (1) (2012) 163.
- [786] J. Zhang, F. Laiwalla, J.A. Kim, H. Urabe, R.V. Wagenen, Y.-K. Song, B.W. Connors, F. Zhang, K. Deisseroth, A.V. Nurmikko, Integrated device for optical stimulation and spatiotemporal electrical recording of neural activity in light-sensitized brain tissue, *J. Neural Eng.* 6 (5) (2009) 55007, <http://dx.doi.org/10.1088/1741-2560/6/5/055007>.
- [787] Y. Hayashi, Y. Tagawa, S. Yawata, S. Nakanishi, K. Funabiki, Spatio-temporal control of neural activity in vivo using fluorescence microendoscopy, *Eur. J. Neurosci.* 36 (6) (2012) 2722–2732.
- [788] T.-i. Kim, J.G. McCall, Y.H. Jung, X. Huang, E.R. Siuda, Y. Li, J. Song, Y.M. Song, H.A. Pao, R.-H. Kim, et al., Injectable, cellular-scale optoelectronics with applications for wireless optogenetics, *Science* 340 (6129) (2013) 211–216.
- [789] Y. Jia, W. Khan, B. Lee, B. Fan, F. Madi, A. Weber, W. Li, M. Ghovanloo, Wireless opto-electro neural interface for experiments with small freely behaving animals, *J. Neural Eng.* (2018).
- [790] L. Luo, E.M. Callaway, K. Svoboda, Genetic dissection of neural circuits, *Neuron* 57 (5) (2008) 634–660.
- [791] X. Han, X. Qian, J.G. Bernstein, H.-h. Zhou, G.T. Franzesi, P. Stern, R.T. Bronson, A.M. Graybiel, R. Desimone, E.S. Boyden, Millisecond-timescale optical control of neural dynamics in the nonhuman primate brain, *Neuron* 62 (2) (2009) 191–198.
- [792] E.M. Tan, Y. Yamaguchi, G.D. Horwitz, S. Gosgnach, E.S. Lein, M. Goulding, T.D. Albright, E.M. Callaway, Selective and quickly reversible inactivation of mammalian neurons in vivo using the drosophila allatostatin receptor, *Neuron* 51 (2) (2006) 157–170.
- [793] I. Diester, M.T. Kaufman, M. Mogri, R. Pashaie, W. Goo, O. Yizhar, C. Ramakrishnan, K. Deisseroth, K.V. Shenoy, An optogenetic toolbox designed for primates, *Nature Neurosci.* 14 (3) (2011) 387.
- [794] J.L. Nathanson, Y. Yanagawa, K. Obata, E.M. Callaway, Preferential labeling of inhibitory and excitatory cortical neurons by endogenous tropism of adeno-associated virus and lentivirus vectors, *Neuroscience* 161 (2) (2009) 441–450.
- [795] M.G. Kaplitt, A. Feigin, C. Tang, H.L. Fitzsimons, P. Mattis, P.A. Lawlor, R.J. Bland, D. Young, K. Strybing, D. Eidelberg, et al., Safety and tolerability of gene therapy with an adeno-associated virus (AAV) borne GAD gene for parkinson's disease: an open label, phase i trial, *Lancet* 369 (9579) (2007) 2097–2105.
- [796] A. Yazdan-Shahmorad, C. Diaz-Botia, T.L. Hanson, V. Kharazia, P. Ledochowitsch, M.M. Maharbiz, P.N. Sabes, A large-scale interface for optogenetic stimulation and recording in nonhuman primates, *Neuron* 89 (5) (2016) 927–939.
- [797] A.P. Kells, P. Hadaczek, D. Yin, J. Bringas, V. Varenika, J. Forsayeth, K.S. Bankiewicz, Efficient gene therapy-based method for the delivery of therapeutics to primate cortex, *Proc. Natl. Acad. Sci. USA* 106 (7) (2009) 2407–2411.
- [798] J. Delbeke, L. Hoffman, K. Mols, D. Braeken, D. Prodanov, And then there was light: perspectives of optogenetics for deep brain stimulation and neuromodulation, *Front. Neurosci.* 11 (2017) 663.
- [799] A. Horsager, K. Greenberg, B.C. Matteo, E.S. Boyden, D.G. Ririe, J.C. Eisenach, C. Wentz, Methods and compositions for decreasing chronic pain, Google Patents, 2013.
- [800] M. GARITA HERNANDEZ, L. Guibbal, L. Toualbi, F. Routet, A. Chaffiol, C. Winckler, M. Harinquet, C. Robert, S. Fouquet, S. Bellow, et al., Optogenetic light sensors in human retinal organoids, *Front. Neurosci.* 12 (2018) 789.
- [801] M. Pais-Vieira, M. Lebedev, C. Kunicki, J. Wang, M.A.L. Nicolelis, A brain-to-brain interface for real-time sharing of sensorimotor information, *Sci. Rep.* 3 (2013) 1319 EP, <http://dx.doi.org/10.1038/srep01319>.
- [802] R.P.N. Rao, A. Stocco, M. Bryan, D. Sarma, T.M. Youngquist, J. Wu, C.S. Prat, A direct brain-to-brain interface in humans, *PLoS One* 9 (11) (2014) e111332.
- [803] C. Grau, R. Ginhoux, A. Riera, T.L. Nguyen, H. Chauvat, M. Berg, J.L. Amengual, A. Pascual-Leone, G. Ruffini, Conscious brain-to-brain communication in humans using non-invasive technologies, *PLoS One* 9 (8) (2014) e105225.
- [804] G. Schalk, J. Mellinger, A practical guide to brain-computer interfacing with BCI2000: General-purpose software for brain-computer interface research, data acquisition, stimulus presentation, and brain monitoring, Springer Science & Business Media, 2010.
- [805] P.C. Taylor, V. Walsh, M. Eimer, The neural signature of phosphene perception, *Hum. Brain Map* 31 (9) (2010) 1408–1417.
- [806] L. Jiang, A. Stocco, D.M. Losey, J.A. Abernethy, C.S. Prat, R.P.N. Rao, Brainnet: a multi-person brain-to-brain interface for direct collaboration between brains, 2018, arXiv preprint [arXiv:1809.08632](https://arxiv.org/abs/1809.08632).
- [807] M.E.M. Mashat, G. Li, D. Zhang, Human-to-human closed-loop control based on brain-to-brain interface and muscle-to-muscle interface, *Sci. Rep.* 7 (1) (2017) 11001.
- [808] S.-S. Yoo, H. Kim, E. Filandrianos, S.J. Taghados, S. Park, Non-invasive brain-to-brain interface (BBI): establishing functional links between two brains, *PLoS One* 8 (4) (2013) e60410.
- [809] S. Zhang, S. Yuan, L. Huang, X. Zheng, Z. Wu, K. Xu, G. Pan, Human mind control of rat cyborg's continuous locomotion with wireless brain-to-brain interface, *Sci. Rep.* 9 (1) (2019) 1321.
- [810] V.A. Maksimenko, A.E. Hramov, N.S. Frolov, A. Lüttjohann, V.O. Nedavozov, V.V. Grubov, A.E. Runnova, V.V. Makarov, J. Kurths, A.N. Pisarchik, Increasing human performance by sharing cognitive load using brain-to-brain interface, *Front. Neurosci.* 12 (2018) <http://dx.doi.org/10.3389/fnins.2018.00049>.
- [811] R.V. Shannon, Advances in auditory prostheses, *Curr. Opin. Neurol.* 25 (1) (2012) 61.
- [812] B.S. Wilson, M.F. Dorman, Cochlear implants: a remarkable past and a brilliant future, *Hear. Res.* 242 (1–2) (2008) 3–21.
- [813] J.C. Lilly, Distribution of motor functions in the cerebral cortex in the conscious intact monkey, *Science* 124 (3228) (1956) 937.
- [814] J.C. Lilly, Instantaneous relations between the activities of closely spaced zones on the cerebral cortex: electrical figures during responses and spontaneous activity, *Am. J. Physiol. Content* 176 (3) (1954) 493–504.
- [815] A. Djourno, C. Eyries, Auditory prosthesis by remote electrical excitation of the sensory nerve with the aid of a permanently implanted coil, *Presse Med.* 65 (1957) 1417.
- [816] D.C. Dennett, *Consciousness explained*, Penguin UK, 1993.
- [817] E.E. Fetz, D.V. Finocchio, Operant conditioning of specific patterns of neural and muscular activity, *Science* 174 (4007) (1971) 431–435.
- [818] E. Fetz, D. Finocchio, Correlations between activity of motor cortex cells and arm muscles during operantly conditioned response patterns, *Exp. Brain Res.* 23 (3) (1975) 217–240.
- [819] W.F. House, J. Urban, Long term results of electrode implantation and electronic stimulation of the cochlea in man, *Ann. Otol. Rhinol. Laryngol.* 82 (4) (1973) 504–517.
- [820] G.S. Brindley, W. Lewin, The sensations produced by electrical stimulation of the visual cortex, *J. Physiol.* 196 (2) (1968) 479–493.
- [821] W.H. Dobelle, M. Mladejovsky, J. Girvin, Artificial vision for the blind: electrical stimulation of visual cortex offers hope for a functional prosthesis, *Science* 183 (4123) (1974) 440–444.

- [822] J. Wessberg, C.R. Stambaugh, J.D. Kralik, P.D. Beck, M. Laubach, J.K. Chapin, J. Kim, S.J. Biggs, M.A. Srinivasan, M.A. Nicolelis, Real-time prediction of hand trajectory by ensembles of cortical neurons in primates, *Nature* 408 (6810) (2000) 361.
- [823] P.R. Kennedy, R.A.E. Bakay, Restoration of neural output from a paralyzed patient by a direct brain connection, *Neuroreport* 9 (8) (1998) 1707–1711.
- [824] D.M. Taylor, S.I.H. Tillery, A.B. Schwartz, Direct cortical control of 3D neuroprosthetic devices, *Science* 296 (5574) (2002) 1829–1832.
- [825] J.L. Collinger, B. Wodlinger, J.E. Downey, W. Wang, E.C. Tyler-Kabara, D.J. Weber, A.J.C. McMorland, M. Velliste, M.L. Boninger, A.B. Schwartz, High-performance neuroprosthetic control by an individual with tetraplegia, *Lancet* 381 (9866) (2013) 557–564.
- [826] I. Choi, I. Rhiu, Y. Lee, M.H. Yun, C.S. Nam, A systematic review of hybrid brain-computer interfaces: Taxonomy and usability perspectives, *PLoS One* 12 (4) (2017) e0176674.
- [827] C.S. Nam, A. Nijholt, F. Lotte, Brain-computer interfaces handbook: technological and theoretical advances. Chapter 27: Hybrid Brain-Computer Interfaces and Their Applications, orgname = crc press., 2018.
- [828] G. Pfurtscheller, B.Z. Allison, G. Bauernfeind, C. Brunner, T. Solis Escalante, R. Scherer, T.O. Zander, G. Mueller-Putz, C. Neuper, N. Birbaumer, The hybrid BCI, *Front. Neurosci.* 4 (2010) 3.
- [829] B.Z. Allison, C. Brunner, V. Kaiser, G.R. Müller-Putz, C. Neuper, G. Pfurtscheller, Toward a hybrid brain-computer interface based on imagined movement and visual attention, *J. Neural Eng.* 7 (2) (2010) 026007.
- [830] A. Nijholt, D. Tan, G. Pfurtscheller, C. Brunner, J.d.R. Millán, B. Allison, B. Graimann, F. Popescu, B. Blankertz, K.-R. Müller, Brain-computer interfacing for intelligent systems, *IEEE Intell. Syst.* 23 (3) (2008) 72–79.
- [831] S.G. Mason, G.E. Birch, A brain-controlled switch for asynchronous control applications, *IEEE Trans. Biomed. Eng.* 47 (10) (2000) 1297–1307.
- [832] G. Pfurtscheller, C. Neuper, C. Brunner, F.L. Da Silva, Beta rebound after different types of motor imagery in man, *Neurosci. Lett.* 378 (3) (2005) 156–159, <http://dx.doi.org/10.1016/j.neulet.2004.12.034>.
- [833] T. Solis-Escalante, G. Müller-Putz, C. Brunner, V. Kaiser, G. Pfurtscheller, Analysis of sensorimotor rhythms for the implementation of a brain switch for healthy subjects, *Biomed. Signal Process. Control.* 5 (1) (2010) 15–20.
- [834] M. Cheng, X. Gao, S. Gao, D. Xu, Design and implementation of a brain-computer interface with high transfer rates, *IEEE Trans. Biomed. Eng.* 49 (2002) 1181–1186.
- [835] M.J. Euler, T.L. McKinney, H.M. Schryver, H. Okabe, ERP Correlates of the decision time-IQ relationship: The role of complexity in task-and brain-IQ effects, *Intelligence* 65 (2017) 1–10.
- [836] N.S. Roslan, L.I. Izhar, I. Faye, M.N.M. Saad, S. Sivapalan, M.A. Rahman, Review of EEG and ERP studies of extraversion personality for baseline and cognitive tasks, *Pers. Individ. Dif.* 119 (2017) 323–332.
- [837] A. Myrden, T. Chau, Towards psychologically adaptive brain-computer interfaces, *J. Neural Eng.* 13 (6) (2016) 066022.
- [838] A. Myrden, T. Chau, A passive EEG-BCI for single-trial detection of changes in mental state, *IEEE Trans. Neural Syst. Rehabil. Eng.* 25 (4) (2017) 345–356.
- [839] A. Myrden, T. Chau, Effects of user mental state on EEG-BCI performance, *Front. Human Neurosci.* 9 (2015) 308.
- [840] A. Myrden, T. Chau, Feature clustering for robust frequency-domain classification of EEG activity, *J. Neurosci. Methods* 262 (2016) 77–84.
- [841] R.A. Ramadan, A.V. Vasilakos, Brain computer interface: control signals review, *Neurocomputing* 223 (2017) 26–44.
- [842] R. Bammer, Basic principles of diffusion-weighted imaging, *Eur. J. Radiol.* 45 (3) (2003) 169–184.
- [843] B.J. Lance, S.E. Kerick, A.J. Ries, K.S. Oie, K. McDowell, Brain-computer interface technologies in the coming decades, *Proc. IEEE* 100 (Special Centennial Issue) (2012) 1585–1599.